Dynamic Modelling of a Fixed Bed Reactor to Study the First Instants of Gas Phase Ethylene Polymerisation

Barbara Hazard Browning

N° d'ordre 109-2013 Année 2013

THESE DE L'UNIVERSITE DE LYON

Délivrée par

L'UNIVERSITE CLAUDE BERNARD LYON 1

Ecole Doctorale de Chimie

DIPLOME DE DOCTORAT

Spécialité GENIE DES PROCEDES

(arrêté du 7 août 2006)

soutenue publiquement le 09 Juillet 2013

par

Mme. HAZARD BROWNING Barbara

Dynamic Modelling of a Fixed Bed Reactor to Study the First Instants of Gas Phase Ethylene Polymerisation

Directeur de thèse: M. McKENNA Timothy

JURY: Mme. TAYAKOUT Melaz (President)
M. LATIFI Abderrazak (rapporteur)
M. EDOUARD David (rapporteur)
M. JOLY Jean-François
M. McKENNA Timothy
Mme. PITAULT Isabelle

UNIVERSITE CLAUDE BERNARD - LYON 1

Président de l'Université	**M. François-Noël GILLY**
Vice-président du Conseil d'Administration	M. le Professeur Hamda BEN HADID
Vice-président du Conseil des Etudes et de la Vie Universitaire	M. le Professeur Philippe LALLE
Vice-président du Conseil Scientifique	M. le Professeur Germain GILLET
Directeur Général des Services	M. Alain HELLEU

COMPOSANTES SANTE

Faculté de Médecine Lyon Est – Claude Bernard	Directeur : M. le Professeur J. ETIENNE
Faculté de Médecine et de Maïeutique Lyon Sud – Charles Mérieux	Directeur : Mme la Professeure C. BURILLON
Faculté d'Odontologie	Directeur : M. le Professeur D. BOURGEOIS
Institut des Sciences Pharmaceutiques et Biologiques	Directeur : Mme la Professeure C. VINCIGUERRA
Institut des Sciences et Techniques de la Réadaptation	Directeur : M. le Professeur Y. MATILLON
Département de formation et Centre de Recherche en Biologie Humaine	Directeur : M. le Professeur P. FARGE

COMPOSANTES ET DEPARTEMENTS DE SCIENCES ET TECHNOLOGIE

Faculté des Sciences et Technologies	Directeur : M. le Professeur F. DE MARCHI
Département Biologie	Directeur : M. le Professeur F. FLEURY
Département Chimie Biochimie	Directeur : Mme le Professeur H. PARROT
Département GEP	Directeur : M. N. SIAUVE
Département Informatique	Directeur : M. le Professeur S. AKKOUCHE
Département Mathématiques	Directeur : M. le Professeur A. GOLDMAN
Département Mécanique	Directeur : M. le Professeur H. BEN HADID
Département Physique	Directeur : Mme S. FLECK
Département Sciences de la Terre	Directeur : Mme la Professeure I. DANIEL
UFR Sciences et Techniques des Activités Physiques et Sportives	Directeur : M. C. COLLIGNON
Observatoire des Sciences de l'Univers de Lyon	Directeur : M. B. GUIDERDONI
Polytech Lyon	Directeur : M. P. FOURNIER
Ecole Supérieure de Chimie Physique Electronique	Directeur : M. G. PIGNAULT
Institut Universitaire de Technologie de Lyon 1	Directeur : M. C. VITON
Institut Universitaire de Formation des Maîtres	Directeur : M. A. MOUGNIOTTE
Institut de Science Financière et d'Assurances	Administrateur provisoire : M. N. LEBOISNE

A joke in a verse

“A rose coloured swan,” I heard him say,
I raised my eyes and looked away,
"But there it is for you to see
Look, floating past that willow tree!"
"That swan is white my friend," I said,
He looked at me and shook his head,
"Maybe what you say is true,
But roses are white, I've seen them too!"

Reginald Henry Barnes (1920 – 2006)

The purpose of science is not to analyze or describe, but to make useful models of the world.
Edward de Bono (1933 -)

Nature is written in mathematical language.
Galileo Galilei (1564 – 1642)

This thesis was prepared at

Laboratoire de Génie des Procédés Catalytiques Université de Lyon, CNRS-CPE Lyon

in collaboration with

Laboratoire Chimie, Catalyse, Polymères et Procédés, Université de Lyon, CNRS-CPE Lyon-UCBL
Laboratoire d'Automatique et de Génie de Procédés, Université de Lyon, CNRS-UCBL, CPE Lyon

Université de Lyon, 43 bd du 11 novembre 1918, 69616 Villeurbanne, France

Acknowledgements

There are certain people without whom this thesis would never have been written. In particular, it has been my privilege to work with my thesis directors, Isabelle Pitault and Timothy McKenna, who have given me unwavering support and invested both their time and energy in this project. Thank you Isabelle, for having confidence in me and offering me the chance to model this reactor, and also for your expertise, clear thinking and ability to always see the whole picture. Thank you Tim, for having offered to extend the modelling project into a thesis and for you own expertise, ideas, encouragement and for speaking to me in English! Many thanks must also go to Claude de Bellefon, LGPC laboratory director, for your support, for being so flexible about the working week and, especially, for arranging a 'baptême de plongée' for my daughter, Isabelle!

Particular thanks also to Nida Othman for your skill, help and tuition and to Estevan Tioni, without whom there would have been no experiments to model! Thanks to other members of C2P2 who have been involved in and supported my work. Vincent Monteil has brought his wide polymerization knowledge and background to discussions regarding the model and Jean-Pierre Broyer has given endless practical help with the experimental set-up.

Significant contributions to this project have also been made by Frederic Bornette, who has always been on hand to help in any way, and Fabrice Campoli, whose welding abilities are second to none, many thanks to both of you. Thanks also to all the other members of LGPC, who have helped me in various ways, work related and not. Stephanie, Jean-Noel, Fred, Ahmed gave my son, Thomas, a cool work experience week. Laurent, thank you for letting me share your office …and for the good hiking ideas …and for tutoring my daughter in maths …and for making the office such a pleasant place to be!

Last but not least, thanks must go to all those people outside the workplace who have given me encouragement and support. Thanks to my Dad, who used to 'make molecules' and walk us up and down mountains at every opportunity and to my brilliant, caring and funny sister. Thanks to my all friends and to my children, Thomas, Isabelle, Marianne and Emily for being yourselves and to my husband, Peter, thanks for supporting me throughout this thesis and in life!

Résumé

La polymérisation des oléfines à l'aide de catalyseurs metallocène est une réaction développée au niveau industriel. Bien que les premiers instants de la réaction aient une importance déterminante pour le procédé, ils n'ont fait l'objet que de très peu de travaux de recherche. Dernièrement, le l'équipe du prof. Mc Kenna a conçu un réacteur de type lit fixe pour étudier en détail ces premiers instants de la réaction. Néanmoins, face à la complexité de la réaction étudiée, un travail de modélisation s'avérait nécessaire afin de mieux appréhender l'ensemble des phénomènes influant sur les résultats et ainsi proposer des améliorations à ce montage expérimental. C'est ce travail qui est présenté dans ce manuscrit.

Le premier modèle considère le réacteur comme un calorimètre semi-ouvert sur la matière en entrée, et utilise des lois cinétiques simplifiées. Il a ainsi était démontré que l'augmentation de la température dans le réacteur était un paramètre particulièrement important. Le design a ainsi été modifié en conséquence afin de contrôler l'exothermie de la réaction.

Dans un second temps, une étude fine sur les mesures de pression récupérées dans le réacteur a été réalisée mettant en avant que le régime transitoire de montée en pression avait un rôle clef sur cette réaction. L'intégration de ces données a permis d'améliorer le modèle utilisé. Contrairement aux résultats obtenus sur des temps de réaction longs, il a été démontré que la désactivation était plus rapide à basse température lors des premiers instants de la réaction.

Mots Clés: modélisation de réacteur; polymérisation d'oléfines; transfert de chaleur; début de polymérisation

Abstract

The behaviour of silica supported metallocene catalyst in the early moments of olefin polymerization is not well understood. The complexity, rapidity and high exothermicity of the reaction impede observation of the kinetics and morphological changes. The fixed bed reactor constructed by McKenna's group is designed to study these first instants of gas phase olefin polymerisation. The purpose of the modelling work presented is to gain understanding and improve the set-up through better knowledge of the reactor conditions.

After a literature survey, the existing set-up was reviewed and analysed. A reactor model was constructed and programmed with polymerisation kinetics represented by a simple relation. The model was validated for individual experiments under optimised conditions. Use of the reactor as a calorimeter was evaluated and a state observer for the polymerisation rate was tested. The model was also used to show that very high temperatures are possible in the reactor bed and to simulate effects of changes to reactor construction and operating conditions.

The reactor pressurisation profile is non negligible for experiments of shorter duration. New kinetics based on this were incorporated into the model: these were able to represent series of experiments and take account of the deactivation reaction. Contrary to results from longer duration experiments, our model finds initial deactivation does not appear to be controlled by temperature.

Keywords: reactor modeling; olefin polymerization; heat transfer; nascent polymerization

Table of Contents

Introduction

The gas phase polymerisation of ethylene is of great economic importance, with several tens of millions of tonnes produced annually. This is a heterogeneously catalysed process, with different types of active sites dispersed on a highly porous solid support; Ziegler-Natta catalysts, $TiCl_4$ dispersed on $MgCl_2$, and chromium catalysts, CrO_x dispersed on silica are the two most common examples. The reaction is rapid and highly exothermic and the polymer accumulates as a solid at the active sites on the catalyst support. This leads to particle growth and also to rapid changes in the physical structure of the catalyst support and the environment of the active sites. The catalyst and polymerisation behaviour during the first instants is critical to the success of the polymerisation and quality of the final product. It could be said to lay the foundations for the whole polymerisation.

The first moments of the polymerisation are particularly complex because catalyst particles must undergo a transition period where the physical properties of the polymer and catalyst support are changing rapidly. The catalyst support must break up in a controlled way to allow the developing polymer particle to grow. The reaction is also at its most intense, just when the particle surface area for heat transfer is at a minimum, so overheating is a risk. The polymerisation is typically carried out at 353K. The melting point of polyethylene (PE) is about 400K and forms an upper limit for the permissible reaction temperature. Above this, the polymer softens and melts, becoming sticky and blocking catalyst pores.

For industrial gas phase polyethylene processes, the first moments of the reaction are particularly problematic because introducing fresh catalyst particles to monomer under normal reaction conditions can result in overheating. This can lead to reactor fouling or catalyst disintegration, producing fines. The step is usually carried out as a separate pre-polymerisation stage before the catalyst particles are fed to the main reactor. Improved understanding of the effects of the initial contact between the catalyst and monomer could lead to more resilient catalysts or better control methods and is therefore of great industrial interest.

From a research point of view, the interest is to gain understanding of this initial period which is so complex and difficult to observe. The main factors to be overcome in studying heterogeneous gas phase olefin polymerisation are the rapidity and exothermicity of the reaction and the short duration of the critical period. Also, in industry the gas phase process for polyethylene production is carried out in fluidised bed reactors, which are difficult to represent on the laboratory scale, and metallocene catalysts are sensitive to oxygen and

must be handled under an inert atmosphere. Finally, this is a period of flux for the physical properties of the polymer and growing catalyst particle, which adds complexity to the meaning of measured data. A reactor to study the first instants of gas phase olefin polymerisation must therefore meet challenging criteria.

McKenna's group [1,2] developed a fixed bed reactor for this purpose. The reactor is designed to operate close to industrial conditions and is constructed with a cartridge to contain the catalyst. This allows the fixed bed to be prepared and manipulated in the glove box. The mass of catalyst used is about 40 mg, diluted to 3-5wt% of the fixed bed by mixing with a chemically inert solid. Computer controlled solenoid valves with a minimum time of 100 milliseconds between subsequent actions were fitted to the gas supply and outlet to allow experiments of very short duration to be carried out. Temperature control was via a hot water bath. Temperature measurement at the reactor inlet and outlet was used to monitor the reaction. This fixed bed reactor is not isothermal and the polymerisation kinetics and catalyst behaviour are temperature dependent so a clear understanding of the reaction conditions is needed.

Experiments showed that, despite the hot water bath, overheating could occur in the fixed bed reactor. The measured reactor outlet temperatures were high and the polymer in the reactor showed visible signs of melting, forming a solid block of polymer in the hotter areas of the bed rather than free flowing grains. Tioni [3] made improvements to the reactor system and its operation to moderate the reaction temperature. The ethylene gas was diluted with helium in a molar ration of 2:1, alternative seedbeds were tested for dilution of the solid catalyst and the gas velocity through the fixed bed was maximised. However, a good estimate of temperature and concentration profiles within the reactor bed was still needed. The data available to calculate this was the reactor inlet and outlet temperatures measured externally to the bed supports, the masses of catalyst used and polymer formed and the reaction gas flowrate.

This thesis focuses on the dynamic modelling of a fixed bed reactor for the study of the first instants of gas phase ethylene polymerisation with silica supported metallocene catalyst based on the experiments carried out by Tioni [3]. Following a literature review on olefin polymerisation, polymerisation reactors used in industry and modelling of catalytic reactors, I will present my work to model this reactor using a simple relation to represent the reaction kinetics. Thermal phenomena aside from the main reaction are identified to occur in the fixed bed and significant axial temperature gradients were found. Modelling work using a state observer to estimate the reaction rate will then be presented and modifications to

improve the reactor and set-up will be proposed. Finally, I will present an improved kinetic model which provides a closer fit with the series of experimental data.

---

[1] Olalla B., Broyer J.P. & McKenna T.F.L., Heat Transfer and Nascent Polymerisation of Olefins on Supported Catalysts. Macromol. Symp. 271 (2008) 1-7

[2]Tioni E., Broyer J.P., Spitz R., Monteil V. & McKenna T.F.L., Heat Transfer in Gas Phase Olefin Polymerisation, Macromol. Symp. 285 (2009) 58-63

[3] Tioni E., Optimisation of a Tool to Study the Start-up of the Gas Phase Olefin Polymerisation, Ph.D. Thesis UCBL1 338-2011

Chapter 1

Literature Review

1 Literature Review

1.1 Introduction

The main work presented in this thesis is the modelling of a laboratory scale reactor to study the kinetics of gas phase olefin polymerisation, and in this case, used for ethylene polymerisation. This chapter consists of a literature review divided into three sections.

The first section introduces the subject with some background and history about PE and its importance. A brief review of the different chemical processes and catalysts used in PE manufacture is given along with a description of the main types of catalyst support used. This is followed by a description of the reactors used for ethylene polymerisation in industry. The focus is directed towards supported metallocene catalysts as this is the type used in the experiments modelled in this work.

The second part of the literature review covers the different types of reactors and experimental methods which have been used to investigate the first instants of olefin polymerisation using coordination catalysts. Both on-line methods, which follow the polymerisation in real time, and off-line studies, which give a snapshot view of the process, are considered.

Finally, the subject of the third section is modelling at each of the various scales of the polymerisation. Data found in the literature regarding the reaction kinetics of ethylene polymerisation with metallocene catalyst is reported. Particle scale and fixed bed reactor modelling are also reviewed.

1.1.1 Polyethylene and Polypropylene

PE molecules are chains formed with ethylene as monomer; the properties are dependent upon the chain length distribution, and the amount and type of branching which occurs during the polymerisation process. Less branching tends to increase polymer crystallinity and therefore density, resulting in a stronger but less flexible product [1]. PE is often classified by density with the following ranges and terminology:

- ULDPE/VLDPE, Ultra/Very low density polyethylene, <0.915 g.cm^{-3}
- LDPE, Low density polyethylene, 0.915 - 0.94 g.cm^{-3}
- HDPE, High density polyethylene, 0.94 – 0.97 g.cm^{-3}
- UHMWPE, Ultra high molecular weight polyethylene, > 0.97 g.cm^{-3}

Whilst the chemistry of the catalysts used can differ, ethylene and propylene polymerisation share many similarities from the point of view of the fundamental issues surrounding heat and mass transfer, as well as particle growth in catalysed processes. In this thesis we are concerned with ethylene polymerisation. However, in general, conclusions drawn from either process can be applied to both PE and polypropylene (PP) systems.

1.1.1.1 Low Density Polyethylene

The first PE to be manufactured on a commercial basis was low density polyethylene (LDPE) introduced by Imperial Chemical Industries in 1938 [2]. LDPE is made by free radical polymerisation at very high pressures (up to 2750 bar [2]) and high temperatures (up to 350°C) in tubular or autoclave reactors. The product is a highly branched, partly crystalline material. The branching results from the free radical polymerisation mechanism that includes back-biting, which creates short chain branches, and transfer to polymer which causes long chain branches. This is the only means of making LDPE with long chain branches which confer rheological properties to the material useful for downstream processing. Some uses are packaging films, plastic bags and cable insulation [1].

Catalysed processes were originally intended as a means to circumvent the rather extreme reaction conditions used to make LDPE. However, 75 years after LDPE entered into production, a cost-effective means of making PE with long chain branches via a catalytic process remains elusive. LDPE thus remains a commercially important material despite the process-related challenges of operating at high pressures. Nevertheless, we will not treat this type of polymer in the current thesis, focusing instead on catalysed polymerisations.

1.1.1.2 Polyethylene from Co-ordination Catalysis

PE formed by catalysis is different from that produced by free radical polymerisation because the transfer reactions which cause long and short chain branches do not occur at the active site of the catalyst, and the polymer chains grow only by inserting one monomer unit after another. In these processes, different amounts of α-olefins are used to create short chain branches on the main PE chain, and thus control the density of the final product. High density polyethylene (HDPE) has few branches (i.e. only very low levels of α-olefin comonomers are used) resulting in a more crystalline, stronger, stiffer material than LDPE. When more short chain branches on the polymer chain are created by co-polymerisation, the resulting polymer is a linear low density polyethylene (LLDPE).

It is possible to change process conditions and concentrations midway through the polymerisation and create a final polymer which comprises chains with a wider range of

branching than could be produced under fixed conditions. This is important because in industry two reactors are often used in series as a means of changing the conditions mid-polymerisation to control polymer properties.

1.1.2 Catalyst Types

Table 1-1, taken from Polyolefin Reaction Engineering by Soares & McKenna [3], gives a summary of the main catalyst groups used in olefin polymerisation. Two types of polymer are distinguished: uniform and non-uniform. This is because supporting the catalyst can lead to different effects. Uniform polymer is produced when there is no interaction between the catalyst molecule and the support, so only one type of active site is present and polymer is formed with a narrow molecular weight distribution and a polydispersity index (PDI) of 2. The PDI is the ratio of the polymer weight average molecular weight to the number average molecular weight and gives a measure of the spread of molecular weights in a given polymer sample. Alternatively, the active metal centres can be affected by the supporting processes, leading to different centres that behave in different ways under the same conditions. This means polymer chains of different lengths are produced at different rates on the various active centres, leading to a broad, non-uniform, molecular weight distribution.

Type	Physical State	Examples	Polymer Type
Ziegler-Natta	Heterogeneous	$TiCl_3$, $TiCl_4/MgCl_2$	Non-uniform
	Homogeneous	VCl_4, $VOCl_3$	Uniform
Chromium Oxide	Heterogeneous	CrO_3/SiO_2	Non-uniform
Metallocene	Homogeneous	Cp_2ZrCl_2	Uniform
	Heterogeneous	Cp_2ZrCl_2/SiO_2	Uniform
Late Transition Metal	Homogeneous	Ni, Pd, Co, Fe with diimine and other ligands	Uniform

Table 1-1. Main characteristics of coordination catalysts for olefin polymerization [3].

1.1.2.1 Chromium Oxide Catalyst

In the early 1950's, Phillips discovered and commercialised chromium catalyst for the manufacture of HDPE. In the initial Phillips manufacturing method, the PE was formed directly in solution using an unsupported (molecular) catalyst. In 1961, a slurry process was commercialised using a 'loop' reactor to maximise heat transfer area for cooling. Later, in an attempt to mimic the properties of LDPE, α-olefin comonomers such as 1-butene or 1-hexene were added to the reaction to create short chain branches. This led to the introduction of a process to produce LLDPE. However, whilst this new polymer had

commercially useful properties and could be employed in some of the same markets as LDPE, it could not replace LDPE in many areas. Chromium oxide catalyst is specific to PE and cannot be used to make PP.

Typical modern chromium oxide catalysts are supported on silica and do not require activation with a co-catalyst. They are still extremely important in the global market place [2].

1.1.2.2 Ziegler-Natta Catalyst

The Nobel Prize in Chemistry 1963 was awarded jointly to Karl Ziegler and Giulio Natta *"for their discoveries in the field of the chemistry and technology of high polymers"* [4]. In 1953 Karl Ziegler's research led him to discover that in the presence of aluminium compounds zirconium and titanium were both catalysts for ethylene polymerisation. The material produced was HDPE as for the Phillips catalyst. Giulio Natta broadened the work to allow isotactic propylene [1] to be made.

Ziegler-Natta (ZN) catalyst systems comprise a transition metal salt catalyst (groups IV-VIII) with a metal alkyl co-catalyst (groups I-III). In industry the most usual combinations are a titanium salt with an aluminium alkyl [5]. Since the early discoveries of Ziegler and Natta these catalysts have been greatly developed and improved. In particular, by using a $MgCl_2$ catalyst support in combination with $TiCl_4$, which facilitates monomer access to the active sites, and by selectively modifying or poisoning some active sites with electron donors which gives a more uniform polymer. These changes have led from relatively low activity catalysts to systems which produce such high yields that catalyst residues in the final product are only trace quantities which need not be removed [6].

1.1.2.3 Metallocenes

Metallocenes are compounds with a π- bonded transition metal atom 'sandwiched' between two cyclopentadienyl rings, which can include substituted groups. During the 1970s, Sinn & Kaminsky investigated zirconium and titanium metallocenes for olefin catalysis. Their work led to the discovery of the co-catalyst methylaluminoxane (MAO). The metallocene/MAO catalyst system is extremely active for the polymerisation of olefins, with a monomer insertion time of the order 10^{-5} seconds. MAO is required in very large ratio (>1000:1) to the quantity of metallocene and is now known to act as a scavenger and an alkylating agent to the catalyst as well as to contribute to the formation of active sites and help prevent their deactivation [5].

Sinn & Kaminsky [7] studied the metallocene/MAO catalyst system in solution polymerisation and found the molecular weight distribution of the polymer formed to be very narrow, giving a

PDI of about two. This is what would be expected for 'single site' catalysts as opposed to the higher PDI observed with ZN and CrO_x catalysts and associated with more than one type of active catalyst site. Also, for propylene polymerisation some metallocenes can produce highly isotactic polypropylene. These findings led to a good understanding of the function of the catalyst at a molecular level and fine control of the microstructure of the polymer that could be produced. The main strengths of metallocene catalyst systems are, therefore, their high activity combined with control of molecular structure, particularly for polypropylene and in co-polymerisation whilst their main disadvantage is cost. For ethylene polymerisation in solution, metallocene systems have been shown to be sensitive to the ratio of co-catalyst quantity to active metal centres; to structural changes in the catalyst [8] and to temperature [9].

Kaminsky & Laban [10,11] list the activities of different metallocene compounds for solution polymerisation. The range of values given for ethylene polymerisation is very wide, varying from 890 to 111900 $kg_{polymer}.h^{-1}.mol^{-1}{}_{metallocene}.(mol^{-1}.L)_{monomer}$ for the same experimental conditions (30°C, 2.5 bar, $6.25.10^{-6}$ $mol.L^{-1}$ metallocene, metallocene:MAO molar ratio of 1:250).

In industry a metallocene catalyst is often supported (but can be used directly in solution processes). The benefits of supporting the catalyst are: easier handling, better polymer morphology control, increased average polymer molecular weight, the possibility of combining catalysts to control polymer properties and finally, that the MAO can be used in reduced quantity or replaced by a less expensive co-catalyst [3]. Amorphous silica is the most commonly used support for metallocene catalysts [12]. Generally a supported catalyst is less active than its homogeneous equivalent and the polymer formed has a broader molecular weight distribution. On the molecular scale this could be due to the active site experiencing steric or electronic effects from the silica surface [13]. At the scale of the catalyst support particle, mass and heat transfer effects can also affect activity [12].

1.1.3 Catalyst Supports

Catalyst activity and polymer properties are both dependent on having an effective catalyst support. As well as the generally required properties of high porosity and surface area, the mechanical properties of the support must be designed for the structure to disintegrate during the very early stages of the polymerisation, yet be robust enough to survive handling, transfer and injection into the reactor. ZN catalyst is usually supported on $MgCl_2$ and metallocene catalysts are commonly supported on silica. Much experimental work evaluating modified silicas and other supports for olefin polymerisation is reported in the

literature. Examples are: alumina [14], polymers [15], silica-alumina & aluminophosphate [16], silica gel [17], mesoporous silicate MCM-41 [18] and POSS modified silica [19].

1.1.3.1 Magnesium Chloride ($MgCl_2$)

$MgCl_2$ is the preferred catalyst support for olefin polymerisation using ZN catalysts. It is a loose agglomeration of primary particles, which are ionic crystallites, formed in irregularly stacked layers [20] and has the required properties of high porosity, surface area and friability. The $TiCl_4$ active sites are actually incorporated into the structure of certain crystal faces which means they are extremely well distributed on the surface of the catalyst support. This discovery was one of the advances in ZN catalyst which allowed activity to be dramatically increased. $MgCl_2$ supports are more friable than their silica counterparts with the fragmentation step being complete in the first second of polymerisation. They can be used to produce spherical polymer pellets directly from the reactor and can be designed with controlled morphologies to further improve their properties [21].

1.1.3.2 Amorphous Silica

Amorphous silica is usually used as the catalyst support for chromium oxides and for metallocene. Silica is particularly interesting for grafting metallocene catalyst because of the hydroxyl or silanol groups which form part of its surface chemistry. These allow the co-catalyst to bond with the surface. The concentration of hydroxyl groups is a physico-chemical constant dependent only on calcination temperature [22]. Amorphous silica is preferred because it has high surface area, porosity and particle friability which can be controlled during the manufacturing process. It is also relatively inexpensive [3].

Descriptions of the manufacturing route to precipitated silica are given by Unger [23], Bergna [24] and by Severn & Chadwick [25]. The pH of a sodium silicate solution is adjusted to produce a suspension of discrete, spherical, non-porous and amorphous particles. For Grace Davison precipitated silicas these particles are of size greater than 4-5 nm [26]. The process conditions are then controlled for a coagulation and precipitation stage which will give final particles with the desired pore structure and pore size distribution. Fractal methods [27], developed by Mandelbrot to describe structures which are self replicating at different length scales, have been used to study this step of silica production [28,29,30]. During this stage, small particles are dissolving and re-precipitating, cementing and strengthening the links between adjoining spheres. Finally, spray drying of the particles leads to two significant effects: shrinkage with the pore volume decreasing dramatically from about 4-5 $mL.g^{-1}$ to 1-2 $mL.g^{-1}$ [25] and agglomeration to form final particles which can include cavities and be quite heterogeneous in structure.

The main methods of characterisation for silica particles are imaging and nitrogen adsorption which allows the surface area and pore size distribution to be determined. Several studies include images of the section of whole silica catalyst supports showing the heterogeneity between individual particles, in particular in the quantity and distribution of the internal cavities formed during spray drying. [31, 32, 33] Tisse et al. [34] used laser diffraction particle size analysis to measure the particle size distribution of Grace proprietary silica 948. Although the distribution is quite symmetrical, there is a tail representing a significant quantity of smaller particles.

Niegisch et al. [35] used electron microscopy to produce images of the surface of Grace Davison proprietary silica at magnifications of x30000 and x72000. The substructure is seen to consist of small nodular clusters of size 200 to 500nm. These are formed, in turn, from smaller clusters of 50 to 100nm. They also embedded particles in resin and used microtomy and electron microscopy to reveal the internal structure of aggregated sub-particles and pores. Fink et al. [36] produced similar electron microscopy images at higher magnification where the primary particle diameter seems to be about 10nm. These images are very similar to those showing the aggregation stage of amorphous silica production [30].

Silveira et al. [37] characterised several silicas for olefin polymerisation, including three Grace Davison industrial silicas by atomic force microscopy (AFM) and by small angle X-ray scattering (SAXS). AFM images showed nodular particle surface features of around 300 to 400nm. SAXS allowed the authors to describe two of the silicas as mass fractals and the other as surface fractal. A mass fractal is a quite open structure which could be produced by cluster-cluster agglomeration with the particles joining together at about the same rate and units of the same size agglomerating. The sub-units of a surface fractal are more densely packed. The calculated values for the radius of gyration of the secondary particles ranged from 8.3nm to 8.8nm (ie primary particle diameter of around 17nm).

1.1.3.3 Supporting Metallocene Catalyst and MAO on Silica

A number of procedures for supporting the metallocene catalyst on silica are reported in the literature. The method described in patents by Welborn [38] and Takahashi [39] is well known and was used by Tioni et al. [40] to prepare the catalyst used in the experiments modelled in this work. In this method, the silica support is first impregnated with the co-catalyst, MAO, and then the metallocene is added. The form adopted by the supported MAO molecule is not certain and several ideas have been put forward including cage structures which can surround the metallocene catalyst active sites[41].

In their detailed review, Severn et al. [42] discuss the interactions between the catalyst, MAO and the silica surface. In particular they note that activity depends on the conditions used for catalyst preparation and that grafting the catalyst to the surface produces more than one type of attached species. It also reduces catalyst activity and can result in a catalyst which produces polypropylene of different stereo-specificity than the same molecule used in solution polymerisation. Garcia-Orozco et al. [19] clearly demonstrate this reduction in catalyst activity in experiments using the same metallocene molecule in solution and supported on silica. They measured activity of the supported catalyst to be 30% of the unsupported value. Also, as with homogeneous olefin polymerisation, the molecular ratio of MAO to metallocene affects the catalyst activity [40].

Catalyst and co-catalyst need to be distributed evenly on the support. Tisse et al. [43] and Steinmetz et al. [33] both used energy dispersive X-ray analysis (EDX) to measure the distribution of aluminium in their catalyst particles and showed that this was uniform. However, the concentration of zirconium was too low to be measured by EDX.

The pore size distribution of the catalyst support is another important factor. Steinmetz et al. [33] and Silveira et al. [44] both used adsorption methods to measure the effect of catalyst deposition on catalyst specific surface and pore size distribution. Steinmetz et al. reported that the addition of the catalyst/MAO to the silica did not produce an additional pore structure or change the specific surface of the support. On the other hand, in their later work, Silveira et al. were able to measure a reduction in both specific surface and pore diameter after catalyst deposition, with the greatest decreases being for the smallest pores.

1.1.4 Industrial Scale Reactors

In industry, continuous solution, slurry and gas phase catalytic processes are all used for polyolefin production by coordination catalysis. Heat removal is a major limiting factor in reactor design for all these processes due to the high exothermicity of the polymerisation reaction.

Autoclave reactors are used for solution and slurry phase processes (Figure 1-1). Different arrangements are used depending on the desired final product. Possible configurations are a single reactor or multiple reactors in series or parallel. Loop reactors are also used for slurry processes as, in combination with a very high duty pump, they can provide a large surface for heat transfer and sufficient circulation and agitation. However, while loops might offer higher production rates due to better heat transfer, the ease of operation and

robustness of stirred autoclaves makes these reactors attractive for lower production rates [3].

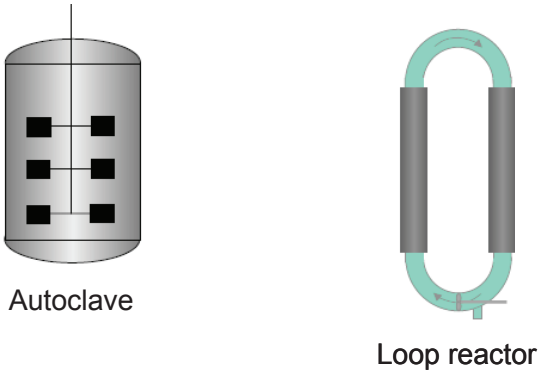

Figure 1-1 Reactors used in solution and slurry phase polymerisation [3]

Figure 1-2 shows the different types of gas phase reactors which exist for polyolefin production, including horizontal and vertical stirred beds, riser-downer and fluidised bed reactors. PP can be made in any type of reactor, depending on the quantity and type of polymer desired, however in the case of PE only fluidised bed reactors (FBRs) offer the large heat transfer capacities required for economical production.

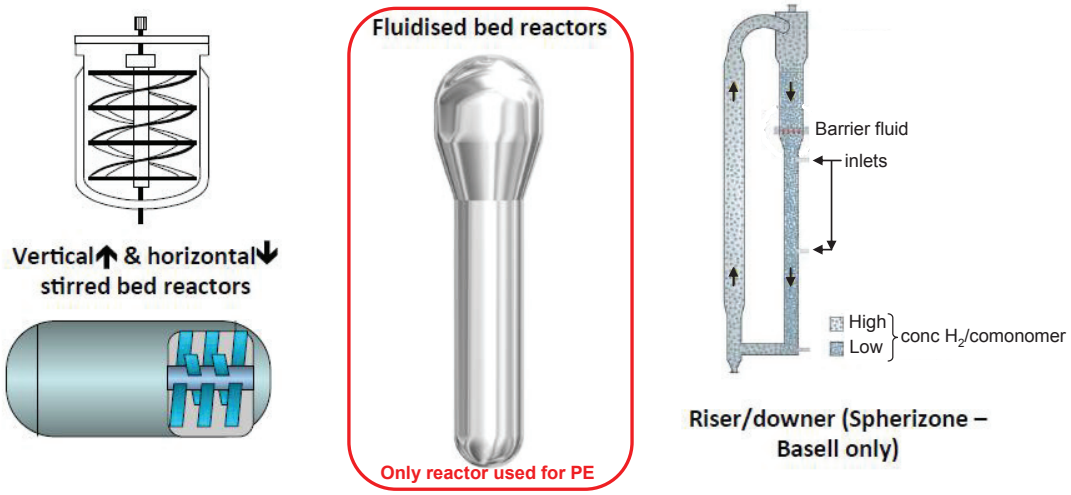

Figure 1-2 Reactors used in gas phase polymerisation [3]

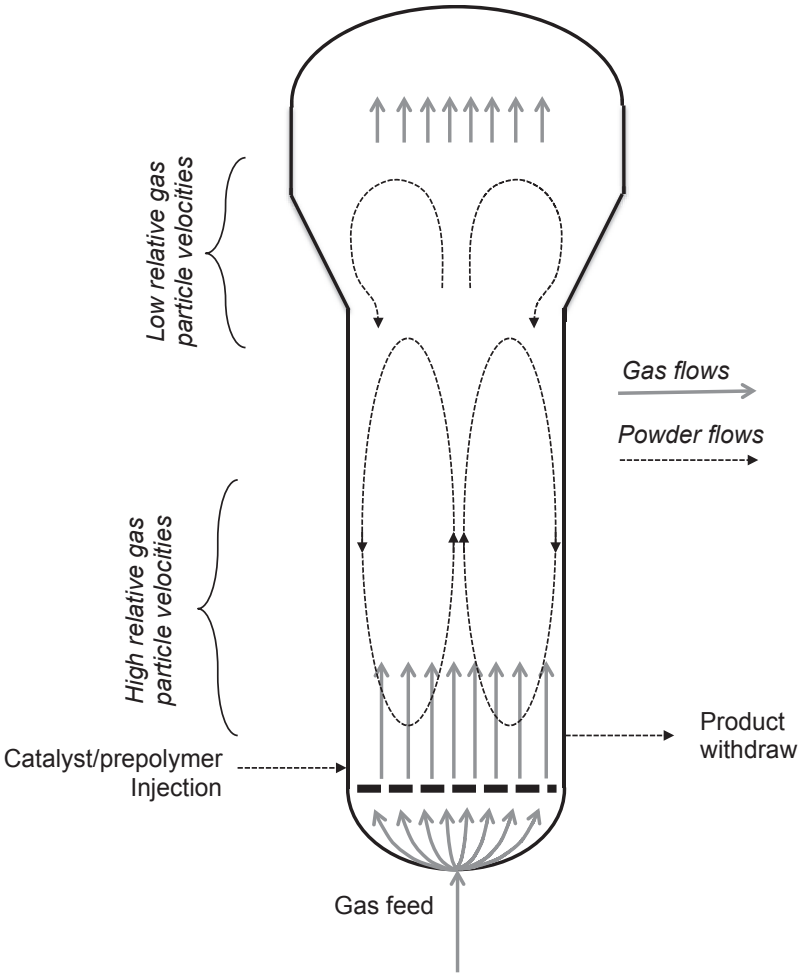

Figure 1-3 Diagram of an industrial scale FBR for olefin polymerisation [3]

Gas phase PE polymerisation processes are then carried out in large scale FBRs (Figure 1-3) operating around 70-110°C and 20-40 bar. The reactor bed, contains particles at every stage of growth, and therefore has a wide particle size distribution. The bed is divided into a lower reaction zone where the polymerisation is taking place and upper freeboard zone which is mostly empty. Above the bed is a disengagement zone where increased reactor diameter is used to decrease gas velocity causing entrained particles to fall back down into the bed. The transition between zones of different diameter means this is a section of the reactor where particles can roll down the wall so, here, there is increased risk of fouling. The diameter of the disengagement zone is at least twice that of the reactor bed and so gas velocity drops to around 0.25 times that in the main reactor. This raises the point that particles in the different zones of an industrial FBR are experiencing different flow conditions with different associated heat transfer coefficients. As such, it would be useful to have sufficient flexibility in a laboratory scale reactor to simulate this range of relative flowrates and to be able to consider them separately. The reactor proposed by Olalla et al. [45] and modified by Tioni et al. [46,47] appears to be one potentially useful tool for this and this is discussed below in Section 1.2.2.4.3.

The reaction zone of an industrial scale FBR is 10-15m high and the bed height to diameter ratio is 2-2.5m. The superficial gas velocity in the reactor bed is 0.5-1m.s^{-1} and the gas-particle relative velocity is 2-8 times the minimum fluidising velocity. The gas recycle ratio is generally >50 and the gas conversion per pass is in the range 2-30%. The catalyst addition and product withdrawal to and from the bed are pulsed, as opposed to completely continuous, and the catalyst has usually been pre-polymerised. Pre-polymerisation (the production of small amounts of polymer under mild conditions in a reactor placed just in front of the main reactor train) can help to reduce fines and also narrows the range of particle sizes in the bed making fluidisation easier. Some olefin polymerisation FBRs operate in 'condensed mode' where a compound such as iso-pentane is injected into the base of the reactor in liquid form; the heat of vaporisation and heat capacity of the pentane absorb some of the heat of reaction, helping with temperature control. Potential problems with these reactors are explosion, due to static, and fouling, caused by softened polymer sticking to the sides of the reactor [3, 48].

So, PE is not a single material but a range of materials with different properties, applications and methods of fabrication. The three main catalyst systems used for olefin polymerisation are CrO_x, ZN and metallocenes the latter two of which require a co-catalyst to be active. The classification as ZN or metallocene relates to a set of similar molecules so there are a variety of ZN and metallocene catalysts.

To improve handling, and for gas phase processes, ZN catalysts are usually supported on $MgCl_2$, and metallocene and CrO_x catalysts on amorphous silica. In both cases it is not only the physical properties of the support which are important but also the chemical properties of the support surface. The production process and physical properties of amorphous silica are well known, as are the methods of supporting metallocene catalyst which can reduce activity by as much as a factor of 10.

Industrial routes to polyolefin products are carried out in solution, slurry and gas phase with different reactor types and designs adapted to the particular case in question. For gas phase PE production the only reactor type with sufficient heat transfer capacity to match the rapidity and exothermicity of the early stages of the polymerisation is the FBR. The variability of the flow regimes inside these large reactors can make it difficult to understand (and optimise) heat transfer, and quantify the impact of changing relative gas-particle velocities on polymer properties at the laboratory scale.

1.2 Polymerisation and Experimental Investigations

This section begins with an overview of what happens to the catalyst particles upon injection to the reactor, and then moves on to look at the different techniques that have been used to date to investigate polymerisations and, in particular, the crucial initial stages.

1.2.1 The Study of Fragmentation and the Origin of Particle Morphology

For polymerisation reactions using supported catalysts, the first instants are critical to the success of the polymerisation as they define the particle morphology, and it is here that the metal atoms are activated by the presence of monomer for the first time. Perhaps the most crucial step in the "life" of a catalyst particle is fragmentation, which occurs during the first fractions of a second to first few tens of seconds. This is very rapid compared to the residence time of a commercial reactor, which is on the order of hours. The catalyst support must 'fragment' to allow the newly forming polymer particles to grow and monomer to continue to access the active sites and the overall catalyst/support/polymer particle must remain intact because if particles shatter and break up this leads to problems with fines.

Because the fragmentation of the catalyst support is a necessary step in the polymerisation process it has been studied since the early days of heterogeneous olefin catalysis. McKenna et al. [49] describe the process in their recent review of fragmentation and nascent polymer structures. Fragmentation is the transition of the catalyst support from its initial condition, as a unit of aggregated primary particles or micrograins, to a set of separate subparticles or fragments distributed within a continuous, porous polymer matrix. This is achieved because the polymer accumulating at the active sites asserts enough force to break the catalyst support and, at the same time, entanglements form between the growing polymer chains which make them stick together and prevent the whole unit from disintegrating. Fragmentation can only occur if the balance between the strength of the catalyst support; the hydraulic forces of the polymer and the reaction rate are right. If the support is not friable enough, fragmentation does not occur and the polymerisation rate falls to zero. At the other extreme, polymerisation can cause the support to break up too soon, before enough polymer has been formed to hold the unit together. Although this fragmentation process must occur for all olefin catalyst supports, it is not identical between them. Silica supports have been observed to break up progressively, from the outside in, with a gradually disappearing silica core. $MgCl_2$ catalyst support fragments much more rapidly and uniformly [50].

The condition of the newly active polymer particle at any given moment is the result of several interacting phenomena: chemical kinetics; monomer diffusion; catalyst break up and

heat transfer. In a review of their work on the kinetics of ethylene polymerisation with silica supported CrO_x catalyst, Webb et al. [51] emphasise the difference between the conditions of particles undergoing the initial reaction and later when the particle has accumulated polymer. Particle growth dilutes the catalyst and increases the surface area for heat transfer and thus the capacity to evacuate heat from the particle. The same conditions which lead to unstable heat and mass transfer dynamics in fresh catalyst can result in steady growth and controlled temperatures for larger, more mature particles.

In their recent review, McKenna et al. [52] show that study of the first instants of polymerisation is not straightforward and specially adapted reactors are necessary for this purpose. Various methods have been used to study the first instants of olefin polymerisation and research focuses on both kinetic and morphological aspects. Experiments for this purpose are often done under low monomer concentrations or at reduced temperature. Stopped flow reactors, which are well known for carrying out very short duration liquid phase reactions, have also been used. Apart from the traditional stirred tank reactors, other equipment used to study gas phase polymerisation includes chromatography columns, fluidised beds, microscopy and video microscopy set-ups and fixed bed reactors designed for short duration experiments.

The most obvious way to study the fragmentation stage of ethylene polymerisation is visually and quite a lot of work using microscopy is reported. In order to 'catch' the fragmentation most workers have slowed the reaction by using mild slurry phase reaction conditions. There are potential problems with this method. One is that fragmentation behaviour varies according to the reaction conditions so what is observed for one case may not be true for others and one aim of the fixed bed reactor developed in our group [53, 45, 46] is to observe gas phase fragmentation under realistic conditions. Another problem is that the few particles that are chosen for study may not be statistically significant so as to give a true representation of the whole.

1.2.2 Reactors for Laboratory Scale Investigation

The section briefly considers laboratory scale reactors used to study olefin polymerisation before describing why the first instants of the process are so important. Experimental work to observe the catalyst support and its fragmentation is reviewed along with how the catalyst is supported and the effects of changing process conditions or catalyst properties. Finally, the use of stopped-flow reactors to study olefin polymerisation is reported.

1.2.2.1 Conventional Stirred Bed Reactors

In the laboratory, solution, slurry and gas phase catalytic olefin polymerisations are all found carried out in semi-batch stirred tank reactors. CSTRs have also been used in kinetic studies of solution polymerisation [9,54,55,56,57]. Gas phase olefin polymerisation is generally carried out in stirred reactors and seedbeds are commonly used to prevent growing polymer particles from sticking to one another and to the reactor wall [58,59,60,61]. Such systems have the advantage of flexibility and simplicity, as well as the capacity to produce useful amounts of polymer for characterisation and are in wide-spread use in industrial and academic laboratories around the world. However, they have the disadvantage of being closed systems. It is therefore difficult to study the effect of varying gas phase compositions, catalyst concentration or imposed temperature profiles in these reactors. In addition, because of the way they are designed and set up to study the polymerisation over longer durations, the system dynamics make it very difficult to run precise experiments on time scales associated with the initial stages of particle growth and fragmentation (see this chapter, section 1.2.1).

Other reactor configurations with growing use in the development of catalysts for olefin polymerisation include high-throughput experimentation (HTE) systems. HTEs are used to evaluate new potential catalysts for olefin polymerisation [62] and other applications [63]. These systems are suited to soluble catalysts, or catalysts used in slurry phase, and consist of a number of mini-reactors operating in parallel and monitoring reaction parameters such as temperature, pressure and monomer uptake. However, to the best of our knowledge there are no such platforms available for the study of gas phase systems, nor are they adapted for continual gas flow.

The electro-thermal micro-reactor, developed by Chrisman et al. [64] for olefin polymerisation, which uses the resistance of the reactor walls to monitor temperature is another example of how innovative reactors are being used in this area. This reactor is constructed from LC-type stainless steel tubing with preheat and reaction sections. In the preheat zone the reactor contents are heated by applying current from a precisely controlled power supply to generate electrical resistance in the reactor wall. In the reaction zone a series of voltage taps at the reactor wall allow a temperature profile to be determined, which can then be correlated with the mass of PE produced.

1.2.2.2 Fluidised Bed Systems

FBRs are the reactors of choice for gas phase ethylene polymerisation in industry. However, they are difficult to use in laboratory investigations because their behaviour is extremely

sensitive to scale. Small, laboratory scale, reactors can have problems with electrostatic effects but they also have different dynamics to larger reactors, leading to problems with particle mixing and segregation. Industrial FBRs operate in a bubbling regime where there is a central up-flow which induces particle circulation and mixing. When the reactor size is reduced, the flow pattern is different and the ratio between bubble size and reactor diameter is much greater, so slugging flow occurs at relatively low fluidisation velocity. The result is that small FBRs have much reduced axial mixing and increased vertical gradients. It is possible to bring the behaviour of a small FBR closer to that found on the industrial scale by the addition of a draft tube and conical mixing zone [65].

Another fluidised bed system which has been used in the laboratory to study gas phase olefin polymerisation is a gas phase riser-downer reactor for polypropylene. This reactor is designed to simulate the fluidisation behaviour of an industrial riser-downer reactor. However, whilst these reactors can be used in place of an FBR, they operate in a transporting slugging mode with completely different hydrodynamics. So, although FBRs are used in industry for polyolefin manufacture, they do not translate easily to the laboratory scale [66].

1.2.2.3 On-line Microreactors Coupled With Microscopy

An on-line microreactor with microscopy consists of a small gas phase reactor fitted with a transparent window and microscope. Some catalyst particles are set on a support in view of the microscope, monomer is supplied to the reactor chamber and temperature and visual changes to the particles are recorded. The main benefit of this system is that morphological changes to the catalyst particles can be observed directly as they happen. It also allows many particles to be observed at once and is very responsive for control of temperature and feed gas composition.

Early versions of this set-up used mild conditions and a thermocouple to measure the gas phase temperature inside the reactor chamber. More recently infra-red microscopy has been used to follow the surface temperature of the particles and temperatures and pressures close to industrial values have been used [67].

Hamilton et al. [68] used both optical and infrared cameras to observe the growth and temperature change during the first few minutes of reaction for silica supported, metallocene catalyst particles. Heat transfer by conduction from the catalyst particles to the metal support plate was identified as significant and minimised by replacing the plate with nylon mesh. An immediate initial maximum temperature was seen which then decays as the particle grows.

The temperature peak was greater at higher experimental temperatures and also greater for clusters than for individual particles. An unusual pattern in the particle growth rate was observed with a local minimum after the early burst of growth followed by a second shallow maximum.

The main drawback of this set-up is that the high gas flowrates found in an FBR, which are important in determining the particle heat transfer coefficient, can not be simulated. The polymerisation is carried out in a stagnant gas phase and so one would expect to see different surface temperature profiles to those found in a typical industrial situation.

1.2.2.4 Stopped Flow Reactors

In their review, Gomez-Hens and Perez-Bendito [69] describe the design and applications of a stopped-flow reactor. The reactor provides rapid efficient mixing of reagents, contact for a short controlled time and abrupt stopping of the reaction and can be designed to operate under a wide range of conditions. Figure 1-4 (a) shows the basic scheme of a typical stopped-flow reactor. Two syringes (A) force two reactant streams to be rapidly merged in a mixing chamber (C). A third syringe (B) stops the flow and the extent of the reaction in the mixing chamber is measured. This form of stopped-flow reactor has been used in combination with various detector types and other techniques including calorimetry. They provide kinetic data for fast reaction mechanisms and are also used for analysis in many scientific areas.

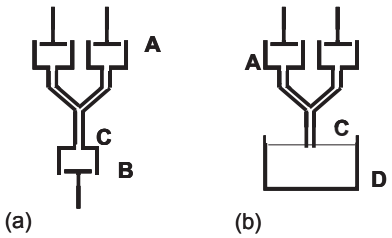

Figure 1-4: (a) stopped-flow reactor (b) stopped-flow reactor for olefin polymerisation

Figure 1-4 (b) shows the arrangement generally described as a stopped-flow reactor for olefin polymerisation. The stopping syringe (B) is replaced by a quench pot (D) containing a catalyst poison which stops the reaction immediately on contact.

Di Martino et al. [70] describe the design of a stopped-flow reactor for olefin polymerisation and include a detailed list of their design criteria. It would thus appear that, while not solving all of the problems associated with the study of the first instants of the polymerisation on supported catalysts, stopped flow systems offer inherent advantages over the reactor systems discussed above.

A brief review of stopped-flow studies for olefin polymerisation is given, classified into systems with soluble catalyst followed by slurry phase ZN/$MgCl_2$ catalyst systems with PP and then PE.

1.2.2.4.1 Homogeneous Olefin Polymerisation

Fink's group [71,72] were the first to use the stopped flow technique for kinetic studies of olefin polymerisations. They studied titanium based homogeneous metallocene catalysts under mild conditions. Later, Shiono et al. [73] carried out experiments of duration 33-200ms with a mild catalyst at atmospheric pressure and 20°C. They found the PE yield increased almost linearly over this period after a very short induction time.

The experiments of Busico et al. [74] used a more active catalyst and were of duration 50-460ms at 0.4 bar gauge and 20-60°C. They also found PE yield increasing linearly with time and calculated that only about 5-25% of the Zr atoms became active sites. They noted that their reaction rate was around 100 times greater than reported for the same catalyst in a conventional reactor and suggested this was because some precipitation of solid polymer could occur. They cited the work of Janiak et al. [75] who had previously observed precipitation with very active soluble systems in conventional reactors leading to mass transfer limitation of polymerisation rates.

Song et al. [76] considered two types of catalyst systems for propylene polymerisation using the metallocene/MAO system as a reference. They observed a similar pattern to Busico et al. with polymer yield increasing linearly after a short induction period.

1.2.2.4.2 Slurry Phase ZN/$MgCl_2$ Catalyst Systems

In the case of stopped flow experiments with heterogeneous catalysts most workers have studied olefin polymerisation with a ZN/$MgCl_2$ catalyst.

Keii's group [77] were the first to use a stopped-flow reactor to investigate the kinetics of heterogeneous propylene polymerisation over ZN/$MgCl_2$ catalyst. Lui et al. [78] summarise much of the group's work with the stopped-flow reactor and its subsequent modifications. They carried out reactions of precise durations of the order 0.2s (20°C, 1 bar) and analysed yields and polymer properties. The reaction duration was less than the average lifetime of a polymer chain which meant the polymer under analysis was a 'quasi-living population' without the influence of time dependent changes such as deactivation. They demonstrated

that ZN catalyst must have several types of active site, measured intrinsic kinetic parameters and were able to compare catalyst systems and evaluate numerous effects including the roles of co-catalyst and hydrogen.

Soga et al. [79] carried out similar experiments for slurry polymerisation of ethylene at 20°C over a ZN/$MgCl_2$ catalyst. They found that, as opposed to experiments with PP, the polymer yield was not proportional to reaction time with the reaction rate decreasing rapidly in the first 100ms. They estimated that PE formed under these conditions would be 83% crystalline and attributed the decreasing reaction rate to mass transfer resistance through a highly crystalline polymer film. This could be similar to the polypropylene layer formed under mild conditions and observed visually by Zechlin et al. [80] using scanning electron microscopy (SEM). A brief summary of the different microscopy techniques used to observe the early stages of heterogeneous polymerisation is given later in this chapter, in section 1.2.3.

Di Martino et al. [50, 81] designed a stopped-flow reactor for slurry phase olefin polymerisation at 8 bar and 80°C which allowed reactions to be carried out on timescales of 40ms to 1.6s (Figure 1-4(b)). The reactor was used to study the first instants of ethylene slurry polymerisation over a ZN/$MgCl_2$ catalyst, particularly with regard to the morphology of the polymer and particles produced. Evolution of polymer molecular weight, crystallinity and melting point were also measured and all were found to be increasing with ongoing reaction. The initial activity of the catalyst was several times higher than normal, decaying rapidly to stabilise at the expected value after about one second. These experiments were at higher temperatures than those of Soga et al. [79] and measured polymer crystallinity was low, particularly for the shortest duration reactions, so a crystalline film seems unlikely. On the other hand, polymer at the particle surface may be more crystalline than polymer within the pores of the catalyst. However, mass transfer limitation was ruled out as an explanation for the decreasing reaction rate because polymer molecular weight is not decreasing with time. The authors experimented with mixing the catalyst and co-catalyst prior to injection into the stopped-flow reactor and in-situ. Without pre-contact between catalyst and co-catalyst, the reaction rate was limited by diffusion of the co-catalyst and hollow particles were formed. The reaction rate was lower in this case but maintained a profile of fast decay to a stable rate. In terms of particle morphology, polymer particles were observed to replicate the shape of the initial catalyst. Early polymer ‘nodules’ and ‘worms’ were generated before the support particle began to break up, possibly caused by high local concentrations of active sites. During the break-up, cracks in the support structure were seen with fibrils of polymer stretched across them, but also in early stages some cracks with no polymer fibrils were found. The melting temperature of the polymer produced after 40ms showed two peaks

which the authors suggest could be due to two 'types' of polymer having been produced. Soga & Shiono [6] had similar results with long duration experiments when they formed polypropylene with two melting points using metallocene/MAO/SiO_2 catalyst and they attributed this to two types of active site-support surface bonding.

Terano's group [21, 82] carried out a stopped-flow study of slurry phase propylene polymerisation at 1 bar and 30°C using ZN/$MgCl_2$ catalyst. The catalyst was particular in that it was synthesised from $Mg(OEt)_2$ and SEM showed the particles to have a thin dense outer shell, a porous layer and a compact core. The authors observed polymer build up and fragmentation first in the porous middle layer then the outermost shell and compact core. They note that the layered architecture of the catalyst prevents disintegration which is usually achieved by use of a pre-polymerisation step. They also used a stopped-flow reactor to investigate the cause of the co-monomer effect, where addition of a small amount of co-monomer increases polymerisation rate. They found the effect to be much more significant after accumulation of some polymer and concluded that it is mainly due to physical effects. These could be either increased monomer diffusion rate through the polymer or a more uniform fragmentation.

1.2.2.4.3 Gas Phase Systems

McKenna's group [83,53] developed a 'short stop' fixed bed reactor for the gas phase polymerisation of olefins. The aim was to be able to perform very short duration gas phase experiments close to industrial conditions and, also, to recover the polymer intact and in sufficient quantity to carry out useful analysis. The initial reactor design used a seedbed of 75 µm glass beads; the bed volume was 1 cm^3 (exterior reactor dimensions were 4 cm long by 1.5 cm diameter) and the catalyst represented 2-6 wt% of the bed. This reactor was used to study ethylene homo-polymerisations using ZN/$MgCl_2$ and ZN/SiO_2 catalysts. Experimental temperatures were 60°C and 75°C, pressures ranged from 1.5 - 8 bar and reaction duration from 0.1s to 6s. Computer controlled solenoid valves were programmed to allow monomer flow through the reactor bed for the duration required, followed by a quench gas. From the polymer yields (about 0.2 to 2 $g_{PE}.g_{catalyst}^{-1}$) it could be seen that the polymerisation rate decreases very rapidly from its initial value. This result is similar to the findings of both Di Martino et al. [50] and Soga et al. [79] for slurry phase ethylene polymerisation with a ZN catalyst. Analysis of the polymer produced in these experiments indicated that the crystallinity, melting temperature, molecular weight and PDI of the polymer were changing during the reaction period with both crystallinity and melting temperature increasing. This was taken to indicate that the polymerisation has not yet reached a pseudo-steady state for the reactions of very short duration. SEM images of the catalyst/polymer

particles were used to observe the early changes in morphology and the authors also studied the effect of hydrogen on the polymerisation kinetics. Experimental results with very good reproducibility were obtained in this reactor. Due to the initial rapidity and exothermicity of the polymerisation and in light of the work which follows, there is a risk that temperature gradients existed in the reactor bed. The main drawback observed was a lack of flow control which led to backflow at low experimental pressures. Silva et al. used this reactor to show that the morphology of a growing polypropylene particle after 2 seconds is quite different for reaction temperatures of 20°C, 40°C and 60°C when all other conditions are kept the same. This leads to the conclusion that fragmentation studies are only valid for the conditions in which they are carried out.

A second version of the reactor set-up was proposed to overcome some of the initial challenges [45,46,47]. The new reactor was larger, with a bed volume of 3.14 cm^3, and was fitted with a flow controller on the gas outlet line and thermocouples at the reactor inlet and outlet. The continuous temperature measurement provides real time data on the activity in the reactor. This reactor has been used to study ethylene homo-polymerisation with both $ZN/MgCl_2$ and silica supported metallocene catalysts. Longer duration experiments of up to 75 seconds were carried out and evidence showed that the combination of increased reactor volume and reaction time led to overheating; the polymer formed was sometimes a solid block rather than a free flowing powder. Methods to optimise the reactor and reduce temperature excursions were investigated and resulted in:

- an alternative seedbed of very fine, agglomerated 5μm NaCl particles
- addition of helium to the reaction
- increased reaction gas flowrate.

Tioni [40] also used this reactor to investigate the effects on start-up behaviour of parameters other than those used to optimise the reactor. In particular:

- use of a co-monomer
- polymerisation temperature
- alternative metallocene catalyst
- co-catalyst concentration
- catalyst/co-catalyst concentration ratio
- co-catalyst impregnation time
- catalyst particle size
- catalyst pore size

Polymerisation of ethylene over metallocene catalyst was chosen for the study because this system gives less dispersion in polymer properties, so changes can be observed more easily. The work shows a clear transition from unsteady to steady state behaviour for these catalysts and that the early behaviour is sensitive to almost all the parameters listed above.

The activity profiles in this reactor did not conform to the pattern of initial maximum activity decaying to a stable reactor rate. The maximum activity was measured after approximately one second of reaction. The authors also used a simplified energy balance to show that the particle temperatures were often much higher than the temperature of the outlet gas. This last observation led us to believe that calorimetric techniques (e.g. an adaption of the approach used by Tisse et al. [84] might be a practical means of following the reaction rate in real time. Part of the work in this thesis will thus be focused on using state estimation techniques in an attempt at following the polymerisation, and at developing models for this type of reactor.

To sum up this section, semi-batch stirred tank reactors are most commonly used for the investigation of olefin polymerisation but novel reactors and a range of other more traditional set-ups have also been tried. The behaviour of an FBR is highly dependent on scale so they cannot easily be used to simulate industrial conditions in the laboratory. The first instants of heterogeneous olefin polymerisation are critical to the ongoing reaction and this is a time where physical properties are changing rapidly. Work with microreactors and video-microscopy has allowed real-time observation of thermal and morphological changes during this period. The use of stopped-flow reactors has revealed that both homogeneous and heterogeneous initial reaction rates in ethylene polymerisation are much higher than during the later stages of the reaction. It has also provided insight into the morphological development of the particles; the reaction kinetics and the physical effects surrounding polymerisation.

1.2.3 Off-line studies of the initial moments of polymerisation

This section covers findings from analysis of partially polymerised catalyst particles after the reaction and outside the reactor environment. As for the catalyst support, common methods of studying the early polymerisation are by imaging of partially polymerised particles and by using nitrogen adsorption to measure specific surface and pore size distribution. More information can be gained from changes in catalyst activity and in the properties of the polymer formed. The initial catalyst support structure is very important for the early polymerisation and its impact continues to be seen throughout the polymerisation, well after the initial fragmentation has taken place [2]. The characteristics of amorphous silica catalyst

support which can be adjusted during manufacture (although not independently) are primary particle size, pore size distribution, specific surface and particle size.

1.2.3.1 Microscopy and Tomography

Figure 1-5 shows partially polymerised catalyst particles taken from the laboratory scale fixed bed reactor developed by McKenna's group after an experiment of duration 30s [40] . These images were produced using X-ray tomography and are very typical of other images of partially polymerised silica supported catalyst particles found in the literature.

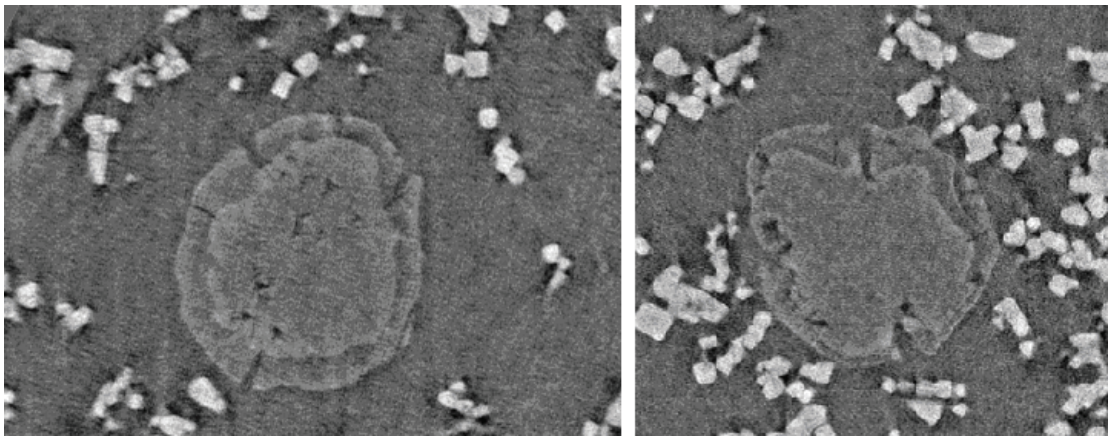

Figure 1-5: Images of partially polymerised catalyst particles after 30s reaction time, 80°C, 6 bar ethylene + 3 bar helium, nominal gas/particle velocity 0.11 m.s^{-1} [40]

Microscopy and tomography have often been used together in the same study to examine both the surface and internal features of silica supported olefin catalysts and partially polymerised particles. For observation of internal changes to the particles an early method was to combine microscopy with tomography. More recently, X-ray methods have been used with computers to build a precise 3D picture. A summary of the conditions and methods used to produce the images reported in this section is given in Table 1-2 and Table 1-3.

Year	Catalyst	Phase	Polymer	T (°C)	P(bar)	Method	Ref
1990	CrO_x/SiO_2	Gas	PE			XRM/μCT	86
1992	CrO_x/SiO_2	Gas	PE			SEM/EDS	35
1997	CrO_x/SiO_2	Gas	PE	110	1.013	AFM	85
1997	$Met/MAO/SiO_2$	Slurry	PP	40-	2	SEM/EDX	33*
1999	$Met/MAO/SiO_2$	Slurry	PP	60	2	SEM/EDX	80*
2001	$Met/MAO/SiO_2$	Slurry	PP	40	2	SEM/TEM	31*
		Bulk	PP	40	21	SEM/TEM	
2003	$Met/MAO/SiO_2$	Bulk	PP	50	21	SEM/TEM/EDX	32*
2005	$Met/MAO/SiO_2$	Slurry	PE	50	40	LSCFM	87
	Met/MAO/PS	Slurry	PE	70	40	LSCFM	
2006	$Met/MAO/SiO_2$	Slurry	Copolymer	70	1.013	SEM/XMT	88
			(C_2H_4/C_6H_{12})	80			89
2008	ZN/SiO_2	Gas	PP	70	20	XMT	90
2008						XMT	* Fink's group

Table 1-2 Conditions used to provide partially fragmented silica supported catalyst particles for microscopy analysis

Neigisch et al. [35] show SEM images of partially fragmented CrO_x catalyst particles and microtomed sections where a polymer rich exterior and silica interior of the fragmenting particle are clearly visible.

Ruddick et al. [85] used AFM to observe changes to the particle surface during the early stages of gas phase ethylene polymerisation with a CrO_x catalyst. They measured 0.27 μm spheroid catalyst sub-particles before the polymerisation and smaller, 0.12 μm, sub-particles after a short reaction period which they attributed to the larger spheroids having begun to break up as part of the fragmentation process. Trough-like features were also formed in the particle surface.

Surface observation methods		
SEM	Scanning electron microscopy	Electron beam scans particle surface
AFM	Atomic force microscopy	Cantilevered probe scans particle surface
EDS/EDX	X-ray spectometry	Surface composition analysis
Methods of observing the internal structure of the particles		
LSCFM	Laser scanning confocal fluorescence microscopy	Laser beam scans particle surface Fine resolution. 3D reconstruction possible.
XRM	X-ray microscopy	X-ray + enlargement Gives a 2D image of whole 3D particle
TEM	Transmission electron microscopy	Electron beam passes through ultra-thin particle slice
µCT/XMT	X-ray computed microtomography	Synchrotron generated X-rays give images of transverse slices. 3D reconstruction possible.
	X-ray holotomography	As X-ray computed microtomography with 4 sets of data for each particle measured with the light source at different distances from the target. Better phase contrast

Table 1-3 Summary of microscopy and tomography methods

Fink's group carried out research into the fragmentation behaviour of silica supported metallocene/MAO catalysts for slurry phase propylene polymerisation and also for bulk phase polymerisations where liquid propylene is both the solvent and monomer. Steinmetz et al. [33] carried out polymerisations at mild conditions (40-60°C, 2 bar) with two similar metallocene/MAO catalysts. They used microtomography with SEM and EDX to compare the early behaviour of the two catalysts. Zechlin et al. [80] also used the same methods with polymerisation experiments of increasing duration to show the fragmentation process for slurry phase polypropylene polymerisation with silica supported metallocene catalyst at 40°C and 2 bar. Their images are almost identical to that of Neigisch et al. [35] for gas phase CrO_x catalyst polymerisation. An initial layer of highly crystalline polypropylene was formed on the outside of the catalyst particles causing mass transfer resistance which was gradually overcome as polymer continued to form inside the particle leading to its fragmentation from the outside in. This is coherent with the reaction rate profile observed by Hamilton et al. [68]. The final polymer particles replicated the shape of the initial catalyst. Fink et al. [31] and Knoke et al. [32] found this description of the fragmentation process was also applicable to

bulk phase propylene polymerisations but that there was a wide difference in the behaviour of individual catalyst particles. They ascribed this to measured inhomogeneity in the MAO impregnation of the catalyst particles.

Conner et al. [86] were the first to use X-rays to look non-destructively inside the partially polymerised particles, observing the convection of inert silica fragments towards the particle edge. More recently, Jang et al. [87] used LSCFM to follow the fragmentation of silica supported metallocene catalysts. Polymerisation reactions were carried out in slurry at 70°C and 40 bar and individual catalyst particles which had undergone 5, 15 and 30 minutes of polymerisation were analysed. The images show the catalyst break up very clearly, occurring from the outside to the inside of the particle somewhat unevenly due to the heterogeneous nature of the support.

Tisse [88] carried out short duration slurry phase co-polymerisation reactions in a 2 litre stirred tank reactor with ethylene and 1-hexene using silica supported metallocene catalyst. The reaction was stopped before the fragmentation process was complete and SEM, X-ray tomography, X-ray holotomography and EDX were used to measure the distribution of silica and polymer in partially fragmented particles. Again, the particles break up from the outside in. However, differences in the initial particle structure lead to different fragmentation behaviours; particles which are quite uniform fragment towards their centre whereas more heterogeneous particles form silica sub-regions with fragmentation towards the centre of these. This makes sense because in the spray drying step of the manufacturing process for the catalyst support, small silica particles agglomerate. The silica sub-regions are possibly the original particles which agglomerated during spray drying. Boden et al. [89] used XMT to analyse fully polymerised polyproylene particles produced in their group's videomicroscopy reactor [67] with different hydrogen partial pressures. They produced 3D reconstructions and contoured porosity maps and the particle formed under more hydrogen rich conditions had less volume of densely packed polymer. This study is a nice demonstration of the power of XMT. However, a statistically significant sample of particles from each polymerisation would have to be analysed to be certain that the observed effect was due to the different process conditions used. Seda et al. [90] have also used X-ray tomography to reconstruct partially polymerised particles for modelling mass transport in gas phase ethylene polymerisation.

McDaniel [91] cites two other important features of the catalyst fragmentation observed through these methods. Firstly, that the size of the final catalyst fragments is reported to be 10 – 100 nm, which is of the same order as the reported size of the catalyst support primary

particles. Secondly, that a well designed catalyst produces polymer grains which replicate the shape of the original particles.

1.2.3.2 Measurement of Specific Surface

McDaniel [92] and Webb et al. [51] used nitrogen adsorption to measure the pore size distribution of partially polymerised silica supported CrO_x catalyst particles. McDaniel showed that larger pores fragment before smaller ones and this is discussed further in the next section. The polymerisations of Webb et al. were carried out under mild conditions. Measurements for non-friable catalyst support showed pore volume and diameters and also activity decreasing to zero as the particles became blocked with polymer. For friable catalyst the pore size reduced from the initial value then remained constant for polymer accumulation in the range 0.4 to 1.3 grams of polymer per gram of catalyst ($g.g^{-1}$). The authors also identified an unusual transient peak in the volume fraction of 0.7 nm micropores very early in the polymerisation. They linked this to the idea that, below 0.2 $g.g^{-1}$, the polymer forms a porous matrix which allows unimpeded access of the monomer to the catalyst surface.

1.2.3.3 Effect of Changing Support Properties

1.2.3.3.1 Pore Volume

McDaniel [2] discusses in detail the effect of silica catalyst support properties for CrO_x catalyst. He notes that pore volume is the most important property for catalyst activity, increasing from zero activity for pore volume of around 0.5 $mL.g^{-1}$ and levelling off by about 1.6 $mL.g^{-1}$. The explanation given for this is to do with the primary particles which form the catalyst support. The number of contacts between each primary particle is represented by a coordination number which decreases with pore volume; the fewer the number of contacts, the more friable the catalyst support and the more active the catalyst.

1.2.3.3.2 Friability

Hammawa & Wanke [15] used polymeric catalyst support particles to demonstrate the importance of support friability on polymerisation rate. They found all the supports in their study to show high initial activity. This was maintained throughout the whole duration of the polymerisation with more friable catalyst supports which also produced uniformly porous polymer particles. The less friable catalyst supports went on to have very low activity and produced polymer with embedded, unfragmented cores or hollow particles due to mass transfer resistance.

1.2.3.3.3 Pore Size Distribution

Pores must be large enough for the catalyst to be fixed to the surface of the support and also to allow diffusion of the monomer. The porosity within the catalyst particle can be classified by size into micropores (<2 nm), mesopores (2nm – 50nm) and macropores (>50nm) [44]. Webb et al. [51] use the same classification but draw the boundary between mesopores and macropores at 100nm. Industrial silicas have an average pore size diameter in the range 5 nm to >30 nm.

In work with Phillips type chromium catalyst, McDaniel [93] found that for catalysts prepared with silica supports of similar specific surface but varying pore size distribution, those with a greater proportion of pores of diameter <10nm were less active. Also for chromium catalyst, Weckhuysen et al. [94] report that there is a critical pore diameter below which almost no PE can be formed.

For metallocene catalyst, Kumkaew et al. [95] found an optimum pore size of around 6nm for gas phase ethylene polymerisation on mesoporous sieves and little activity for average pore diameter <2nm. They suggest the active form of the MAO structure is too large to enter the micropores. However, other explanations for the lack of activity in very small pores have also been postulated. Silveira et al. [96] measured activity increasing with pore diameters from 4nm to 12nm and suggest that micropores could be less active for metallocene catalysis as they retain more silanol groups during calcination. The greater surface concentration of silanol groups is thought to bind metallocene groups in such a way that they remain inactive for polymerisation. Alternatively, Tisse et al. [43] found no activity for catalyst of average pore diameter 3.7nm and suggest the polymer has insufficient hydraulic force to fracture these pores or there could be unfavourable interaction between the support and the active species.

Zechlin et al. [80] compared spray dried silica catalyst support with the associated internal cavities against a similar catalyst support prepared without the final spray drying step and with no cavities. Both catalysts produced the same reaction rate profile but the cavity free catalyst had a higher reaction rate. They explained this in part by catalyst leaching and also by the increased surface concentration of active species. However, as the cavity free particles were the ‘building blocks’ of the usual catalyst support, and were therefore significantly smaller, mass transfer limitations could also have contributed to the differences in reaction rate.

The effect of the catalyst pore size distribution appears to be similar for both CrO_x and metallocene catalyst, with an increased number of small pores resulting in a decrease in catalyst activity and a limiting pore size, below which no polymer is formed. However, the suggested explanations are not always relevant to both systems. For example, theories involving the MAO molecule can only be applicable to metallocene catalysts.

1.2.3.3.4 Primary Particle Size and Specific Surface

Silveira et al. [37] studied the effects of catalyst support size and structure on activity for ethylene slurry polymerisation. They characterised a wide range of commercial and treated silicas and found the most active of the silicas tested were those in commercial use. They demonstrated increasing activity with surface area and pore diameter and analysed the effect of the silica primary particle size. The highest activity was found for catalysts with primary particles of radius 8-9nm, which is a typical value for commercial catalysts, with activity increasing for decreasing primary particle diameter within this range. They also measured the interatomic distance between the Zr and C atoms in the metallocene molecule which varied for the different catalyst supports. On this subject, other workers have found increased catalyst activity from changing atomic distances by using spacer molecules to separate the metallocene from the silica surface [97].

Tisse et al. [43] compared different silicas and found that the general trend of increasing activity with catalyst specific surface did not continue to very high surface areas, even when total pore volume and average pore diameter were maintained. Where the catalyst distribution on the silica surface was measured it was found to be uniform. To increase specific surface and maintain total pore volume the silica structure must be formed from smaller primary particles. The reduced activity could, therefore, be due to either a decrease in support friability (increased coordination number) or a change in pore size distribution (more micropores).

1.2.3.3.5 Particle Size

Silveira et al. [37] report catalyst particles of ~50μm in diameter to be more active for polymerisation than particles of ~1μm because larger particles fragment more easily. Over the particle diameter range 10μm to 80μm Fink et al. [36] found increasing activity with decreasing particle diameter. Tisse et al. [34] fractionated a single grade of silica into narrow particle size distributions and showed that, within the size range of this grade, smaller particles are more active than larger ones for slurry polymerisation. This might be partially due to a better impregnation with the co-catalyst, MAO. However, when this problem was eliminated a significant particle size effect remained. Tioni [40] also found increasing

reaction rate with decreasing particle diameter for gas phase ethylene polymerisation with metallocene catalyst. Mass transfer limitation could not be ruled out as a possible explanation.

In summary, off-line studies have furnished a great deal of information about the early stages of heterogeneous polymerisation and modern computers can even be used to reconstruct a detailed 3D polymer distribution within the growing catalyst particles. There is a generally observed pattern for fragmentation from the outside of silica supported catalyst particles in towards the centre. The finer detail of the fragmentation seems to depend on the initial heterogeneity of the catalyst.

The various properties of the catalyst which can be measured, and hence their effects on the polymerisation, are interlinked. If pore sizes are too small, or if the catalyst is not sufficiently friable, activity is reduced or lost altogether. The fragmentation behaviour is highly dependent on the process conditions, the reaction rate and the properties of the silica support. Industrial silica catalyst supports have been optimised to reflect this.

Despite very effective silica catalyst supports having been developed, it is not completely clear why a particular catalyst support behaves in the way it does, nor how this affects the polymerisation rate or why the initial effects should continue to have repercussions into the later stages of particle growth. In order to create representative particle scale models, these factors need to be understood and this can only be done through measurement. Hence, the importance of the work carried out with stopped flow reactors such as that of Di Martino et al. [70] to study the very early stages of slurry phase polymerisation. It also highlights the aim in developing the fixed bed reactor for more precise study of the gas phase reaction.

1.3 Modelling

In heterogeneous gas-phase ethylene polymerisation, there are physical effects occurring at the molecular, particle and reactor length scales. Models have been created for the different effects but to represent the overall process they need to be used in combination. Most modelling efforts for heterogeneous olefin polymerisation are at the particle level.

1.3.1 Reaction Kinetics

The reaction kinetics observed for metallocene catalysts are not the same for heterogeneous polymerisation as measured in solution. Supporting the catalyst dramatically decreases the activity. There is no such difference between gas and slurry phase reactions. Bergstra & Weickert [98] used a reactive bed to carry out ethylene homo-polymerisation over $Ind_2ZrCl_2/MAO/SiO_2$ in the slurry phase and continued the reaction in the gas phase in the same reactor. They showed that the reaction order and propagation parameters were the same in both situations.

1.3.1.1 Rigorous Model

McAuley et al. [99] adapted a rigorous theoretical kinetic model to account for any number of active sites and comonomers in olefin polymerisation in a FBR. The model accounts for each different reaction separately. These include initiation, propagation, transfer, poisoning and spontaneous deactivation reactions for every type of active site. The propagation rates for polymer chains of different length are summed to give an overall rate and the method of moments is used to evaluate the molecular weight of the polymer formed. A rigorous model is particularly useful in solution polymerisations where it is a good assumption that all the active sites are under the same conditions, for example in the work of Soares [100]. This model has also been used to represent polymerisation in combination with industrial scale FBR models [101,102].

1.3.1.2 Simplified Models

The rigorous model requires a large number of parameters which are not known and have to be estimated. In order to represent experimental data as closely and reasonably as possible, simplified versions are often used. For example, Meier et al. [103] used a typical semi-empirical kinetic model based on their experimental data with polypropylene polymerisation. First order reactions were used to represent propagation and the activation and deactivation of catalyst active sites as follows:

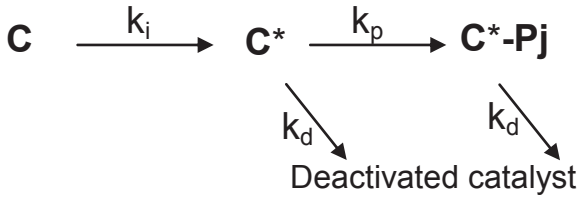

Where C is a potential active site, C* is an active site and C*-Pj is an active site with a growing polymer chain. Under isothermal conditions this leads to the reaction rate equation:

$$R_p = k_p C_m C_0 \frac{k_i}{k_d - k_i}\left(e^{-k_i t} - e^{-k_d t}\right)$$

With

R_p propagation rate

k_p effective propagation rate constant

C_m monomer concentration

C_0 initial lumped concentration of non activated sites

k_i initiation rate constant

k_d effective deactivation rate constant

t time

The same model was used by Xu et al. [104], Song & Luss [105] , Eriksson [106] and Mehdiabadi & Soares [107].

1.3.1.2.1 Activation Step

Some workers have observed an activation or induction period for olefin polymerisation which is dependent on monomer composition, reactor conditions and also on catalyst type. For example, CrO_x catalyst has a slow activation so that a pre-polymerisation is not necessary. Xu et al. [104] found activation times were longer for gas phase ethylene/propylene copolymerisation compared to ethylene homo-polymerisation under the same conditions. In this, and similar studies, polymerisation kinetics have been measured by mass flow methods under supposed isothermal conditions [103,104]. Pimplapure et al. [108] showed that during the first moments of the reaction this method is flawed. Because of the equipment response times, the reactor is not in steady state and, in fact, the catalyst seems to be fully active immediately on contact with the monomer.

An extremely rapid activation is also suggested by other authors: Tioni et al. [47] found the reaction rate for gas phase ethylene polymerisation with metallocene catalyst was 10 times

greater in the first 2 – 5 seconds than later in the reaction. Di Martino et al. [81] observed the reaction to start immediately at the maximum rate in their quenched flow reactor for slurry phase propylene polymerisation with ZN/$MgCl_2$ catalyst, as was also observed in other stopped-flow studies [73,74]. Also, no induction period was observed by Hamilton et al. [68] in their optical and infrared study of olefin polymerization using silica supported metallocene catalyst particles.

In some cases where an induction period has been observed, for example by Fink et al. [31], it can be ascribed to mass transfer effects and not intrinsic reaction rates. This draws attention to the point that different physical and chemical effects can produce similar observed behaviours and, so, to the interest of constructing models to try and identify which effects are controlling.

1.3.1.2.2 Propagation

Reaction parameter

The activity of a metallocene catalyst system depends on the molecular structure of the particular catalyst used; the ratio of co-catalyst to catalyst and the use of a scavenger. If the catalyst is supported, mass and heat transfers can also influence the apparent polymerisation rate. In the early stages of the reaction, these are dependent on rapidly changing physical properties. Propagation parameters are derived from the experimental data using a reaction model and parameter estimation techniques. A very wide range of values for the propagation constant can be found in the literature [55,104,109,110,111].

Activation Energy

In solution polymerisation, the apparent activation energy depends on the activation energies of both the propagation and deactivation reactions. The deactivation has a higher activation energy value and becomes dominant at high temperatures. In semi-batch reactors, the initial concentrations, prior to any deactivation, are known and so initial reaction rates are usually employed to estimate the activation energy. Busico et al. [74] measured an apparent activation energy of 50 $kJ.mol^{-1}$ for a homogeneous metallocene catalyst in a stopped flow reactor over the temperature range 20-60°C and Kaminsky et al. [112] cite 54 $kJ.mol^{-1}$ as being within the range of activation energies for metallocene catalysts. For heterogeneous polymerisation in semi-batch reactors, Roos et al. [110] found 39.2 $kJ.mol^{-1}$ for gas phase ethylene polymerisation (40-60°C) and Zechlin et al. [80] found 49 $kJ.mol^{-1}$ and 71 $kJ.mol^{-1}$ for slurry propylene polymerisation between 10°C and 50°C.

For heterogeneous polymerisation, mass transfer can also affect the apparent activation energy and, in the work of Zechlin et al., the lower value was measured during an initial stage of polymerisation which was diffusion limited due to an accumulation of polymer which encapsulated the catalyst particles. The increased value was measured later in the polymerisation, after the fragmentation stage and at higher catalyst activity with reaction rate controlling.

Bergstra & Weickert [98] measured the activation energy to be 75 $kJ.mol^{-1}$ for both gas and slurry phase experiments between 50°C & 90°C, with a slow deactivating metallocene catalyst. Dynamic reaction models have been used to derive activation energy values for the propagation reaction from 33 to 71 $kJ.mol^{-1}$ by parameter estimation methods. In conclusion, there is no clear consensus on the value of the activation energy for olefin polymerisation using heterogeneous metallocene catalysts with proposed values ranging from 33 to 75 $kJ.mol^{-1}$.

Table 1-4 summarises the reported activation energy data for olefin polymerisation with metallocene catalysts.

Catalyst	Ea_p $kJ.mol^{-1}$	Temp (°C)	Method	Phase (Polymer)	Max rate $kg.mol_{Zr}^{-1}.h^{-1}$	Ref
rac-Me2Si(2-methyl-4-phenyl-1-indenyl)2ZrCl2	50	20 - 60	Stopped-flow	Solution (PE)	3.1E6	74
rac-Me2 Si [Ind2] ZrCl2	39.2	40 – 60	Semi-batch t(0)	Gas (PE)	40000	110
Me2Si[R1Ind]2ZrCl2	49* 71	10 – 50 30 – 50	Semi-batch t(0)	Slurry (PP)	400 1100	80
[Ind2] ZrCl2	74.9	50 - 90	Semi-batch	Gas & Slurry (PE)	2.3E5	98
Unbridged zirconocene	56.5	62 - 80	Semi-batch (Perturbation)	Gas (PE)	-	104
(n-BuCp)2 ZrCl2	33 25,56**	60 - 85	Semi-batch Dynamic model	Gas (PE)	16000	111
Cp2 ZrCl2	74.9	50 - 70	Semi-batch Dynamic model	Slurry (PE)	40000	109
*Diffusion limited **Two site model						

Table 1-4: Reported activation energies for the propagation reaction with metallocene catalysts

Reaction Order

In terms of the order of the reaction, Mehdiabadi & Soares [107] show the propagation reaction is first order with respect to catalyst and monomer concentration in solution at 120°C

and 120 psi gauge. Rau et al. [9] show the same at the much higher pressure of 1500 bar. Tisse et al. [113] find the same for slurry polymerisations. Other experimental work has shown that at low monomer concentrations (~5 bar) the polymerisation deviates from first order behaviour [98] and it has been postulated that this may be because there is a reversible complex formation reaction between the available active sites and the monomer.

1.3.1.2.3 Deactivation

Deactivation of metallocene catalysts occurs by two different routes; spontaneous decay of the active site and poisoning, Kaminsky et al. [112] state that most metallocene catalysts are not very stable above 50°C and that stability at more than 100°C is unusual for zirconocenes, the most typical metallocene catalysts. The sites are very sensitive to poisoning and nearly all studies use a scavenger such as triisobutylalumina (TiBA) to reduce this. Even for very short duration reactions in the LCPP reactor, Tioni [40] found that using triethylaluminium (TEA) impregnated silica as the inert solid meant catalyst activity was maintained for longer.

Information pertaining to deactivation over two completely separate temperature ranges is available in the literature. Solution polymerisations of ethylene provide data for temperatures above 120°C. CSTR kinetic studies using metallocene catalysts between 140°C and 200°C show overall reaction rate decreasing rapidly with increasing temperature. Charpentier et al. [55] correlated this with an apparent activation energy of -93 kJ.mol^{-1}. Rau et al. [9] found almost exactly the same result at higher pressures and calculated an apparent activation energy of -73 kJ.mol^{-1}.

In the range 40°C to 80°C, most semi-batch reactor kinetic studies of gas and slurry phase polymerisation show reaction rate increasing with temperature [103,110,113] and decaying over time. However, not all authors are in agreement. For example, Ahmadi et al. [109] find catalyst activity to be decreasing with temperature over the range 50°C- 70°C.

The deactivation is usually modelled as a first order reaction dependent only on the number of active sites as described by equations 1-1, 1-2 and 1-3 for isothermal deactivation [55 103,104]. Mehdiabadi and Soares [107] confirmed this model for deactivation of the metallocene catalyst system rac-EtInd$_2$ZrCl$_2$ /MAO in solution polymerisation at 120°C and 120psig.

$$R_p = k_{p0} e^{-\frac{Ea_p}{RT}} C_m C^* \qquad \text{1-1}$$

$$\frac{dC^*}{dt} = -k_d C^* \quad \text{1-2}$$

$$R_p = k_p C_m C^* e^{-k_d t} \quad \text{1-3}$$

Alternatively, Roos et al. [110] represented the deactivation rate to be first order dependent on the reaction rate and hence, dependent on the kinetic parameters and on the concentrations of monomer and active sites as described in the following equation:

$$\frac{dC^*}{dt} = -k_d' R_p \quad \text{1-4}$$

The activation energy for deactivation is higher than that for propagation and can be found by parameter estimation. Values reported in the literature for k_d and Ea_d are as follows:

k_d at T (h^{-1})	T (°C)	Ea_d ($kJ.mol^{-1}$)	Scavenger	ref
4	120	-	AliBu3	107
0.1	80	-	TiBA	98
24.5	80	108	None reported	109
4.8	80	67	TEA	104
7.6	140	-	TMA	55

Table 1-5: Published reaction parameters for the deactivation of metallocene catalyst

1.3.1.3 Conclusion

The rigorous kinetic model needed to precisely represent olefin polymerisation becomes overly complex for heterogeneous catalysts in a real situation and simplified models are often used instead. First order propagation and deactivation reactions can be employed to represent the whole system quite closely. Catalyst activation is so rapid that it can be safely neglected and propagation and deactivation constants depend strongly on the catalyst system used. The activation energy for the deactivation reaction is higher than for propagation and care must be taken with activation energy data because observed values are lower if there are diffusion limitations within the catalyst.

1.3.2 Particle Scale Modelling

The aim of particle scale modelling is to describe the growing particles as accurately as possible in order to be able to predict the final properties of the polymer. Ideally, final polymer composition, molecular weight distribution, crystallinity, morphology and bulk density could be forecast from a knowledge of the initial catalyst and the process conditions. In order to develop such models, each of the physical processes occurring within the particle must be defined and quantified. This includes physical property values and characteristic length scales for diffusion. Figure 1-6 illustrates the main phenomena that need to be accounted for.

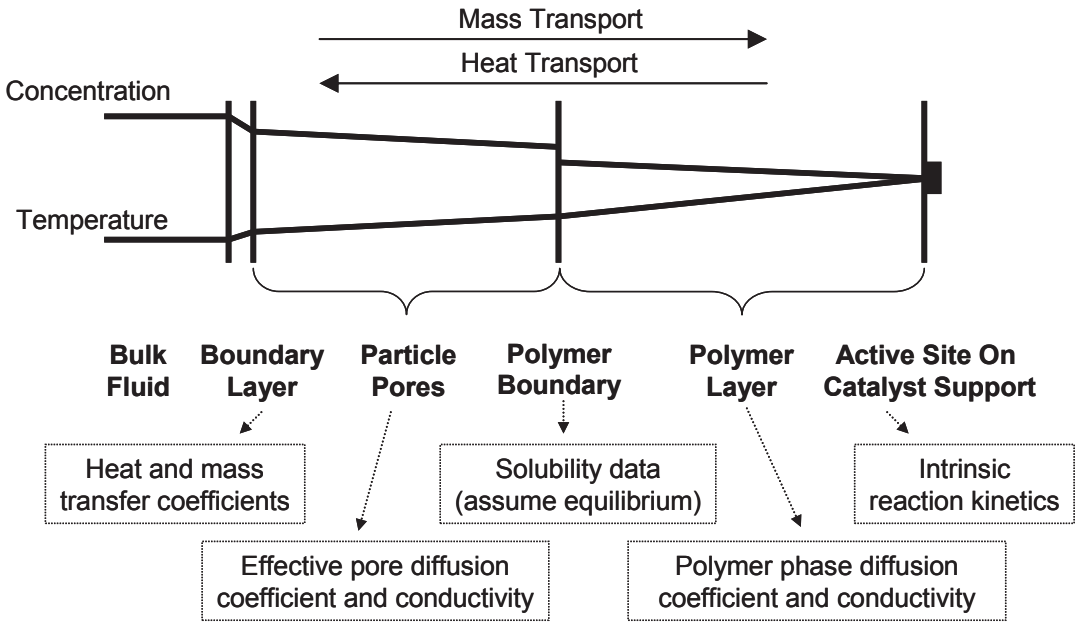

Figure 1-6: Main phenomena accounted for in particle scale models for olefin polymerisation

Determination of the particle growth rate and temperature and concentration gradients within the particle voids and accumulating polymer are crucial. They, in turn, depend on local properties of the polymer and reaction gas, for example the crystallinity and composition, and also on the fine structure of the particle. All these properties and conditions can be changing quickly at the start of the reaction. Because of the complexity of particle scale modelling and the variety of systems to be described there is no consensus on a single model which can describe all cases. The main models which have been developed are reviewed in this section. However, many other models have been proposed to take into account different physical parameters, polymerisation systems, time scales and types of catalyst support [3].

1.3.2.1 The Micrograin and Particle Flow Models

The two most well known particle scale models found in the literature are the Multigrain Model (MGM) and the Polymer Flow Model (PFM).

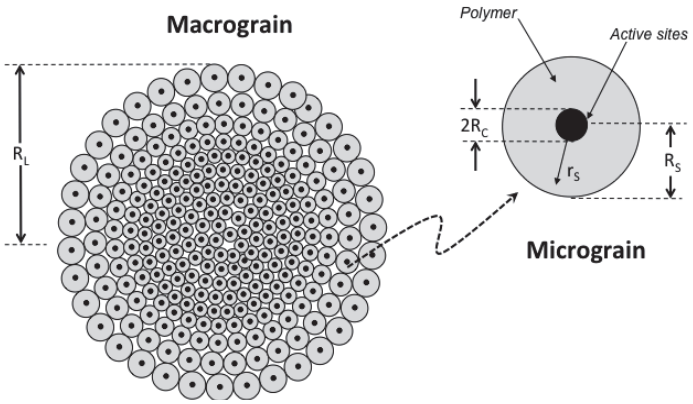

Figure 1-7: Schematic of the macrograin model

The MGM description of the polymer/catalyst particles comes from the knowledge that the internal structure of the catalyst support is formed of many small primary particles. In this model, fragmentation is often assumed instantaneous and complete and the catalyst is represented as a spherical macroparticle formed from smaller spherical microparticles. At the centre of each microparticle is a catalyst core with active sites where the polymerisation occurs. Polymer formation at the active sites adds a growing polymer layer to the microparticles, increasing their radius. Microparticles at any given macroparticle radius are all the same size and to reach the active sites the monomer must diffuse through the pores of the macroparticle then dissolve in and be transported through the polymer layer to the microparticle core. Likewise, heat generated at the active sites must be transported out through the polymer layer and then the pores of the macroparticle. Dynamic mass and heat balances are set up to describe these processes [3].

Floyd et al. [114] used the MGM to analyse the intraparticle heat and mass transfer resistances expected for olefin polymerisations in both gas and slurry phase. They calculated that at the macroparticle scale, heat and mass transfer limitations can be significant early in gas phase polymerisation for very active catalyst and mass transfer limitations could be expected for slurry polymerisation systems. At the microparticle scale, they calculated that heat transfer limitations are always negligible but mass transfer limitations can be significant in gas phase polymerisation.

The PFM is a simplified version of the MGM where the temperature and concentration gradients in the microparticles are neglected and the macroparticle is considered as a pseudo-homogeneous medium [3]. Sliepcevitch et al. [115] found the PFM to be more realistic for particles at the end of the polymerisation process. This was based on gas

chromatography, which showed the diffusion length scale of newly formed polymer particles to be closer to the macroparticle diameter than that of theoretical microparticles. Martin and McKenna [116] carried out similar experiments and found the diffusion length scale to be the macroparticle diameter for compact, ex-reactor, polymer beads. However, other polymer particles had a more open structure and a shorter diffusion length scale. The authors proposed a transition where early polymerisation behaviour could be well represented by the MGM and later the PFM was more realistic. An example of use of the PFM is the work of Yiagopoulos et al. [117] who use it to show that pre-polymerisation of catalyst particles can increase reaction rates whilst, at the same time, decreasing particle temperature excursions.

One example of an alternative particle scale model is that of Kittilsen & Svendsen [118] which takes into account three diffusion lengths within the growing particle. They do this by using a compound effectiveness factor determined from an effectiveness factor at each length scale. Another is the Dusty Gas Model (DGM), employed by Kosek et al. [119], which includes convective mass transfer in calculation of the intraparticle concentration gradient.

The relative merits of these models have been discussed elsewhere [3,12], but in general the consensus appears to be that while the MGM/PFM approach has its limitations, linked essentially to an inability to account for the impact of changes in particle morphology, it can be used to predict the evolution of the temperature and composition inside the growing particles if the parameters representing the reaction kinetics or monomer diffusivities are allowed to be adjustable. The general conclusions of the models are that:

- Heat and mass transfer resistances will be most important for larger virgin catalyst particles than for smaller ones, and obviously for higher intrinsic reaction rates.
- Heat and mass transfer resistances diminish as the particles grow because more surface area for exchange with the bulk phase becomes available.
- Mass transfer resistance is generally much less important for gas phase reactions than slurry phase reactions.
- Heat transfer resistance is lower for liquid bulk phases than for gas phase systems.
- In gas phase systems, the external temperature gradient (surface – bulk) can be much higher than the internal gradients.

McKenna et al. [120] used computational fluid dynamics (CFD) to investigate the effect of particle-particle interactions on the external heat transfer coefficient. For particles of the same size they calculated an overall reduction in heat transfer from the solid to the gas

phase for closely packed systems. This was due to particles touching one another and sheltering each other from the gas stream. However, for contact between particles of different sizes as might occur in a typical FBR, they found small grains of hot catalyst could be significantly cooled by conduction to larger particles. Dehnavi et al. [121] also used CFD to evaluate heat transfer coefficients in gas phase ethylene polymerisation and the effects of fluid velocity, particle size, shape and particle-particle interactions. As McKenna et al. [120], they find that an upstream particle causes a sheltering effect on subsequent particles, dramatically changing its heat transfer coefficient.

Kosek et al. [119] employed a dynamic model to study external heat and mass transfer and compared the results against those from existing steady state models. They found the dynamic model predicted lower peak temperatures than the steady state model because of particle growth.

1.3.2.2 Morphology Models

Chiovetta and Laurence [122] described the fragmentation process using a mathematical model which was further developed by Ferrero and Chiovetta [123]. Initially, the catalyst is represented as a discretized, porous sphere which gradually turns into the macrograin model. The transformation is accomplished through an algorithm which changes each shell of initial catalyst particle into micrograins, layer by layer, from the outside in. This occurs at a critical threshold of polymer accumulation in the shell, so that each newly fragmented micrograin starts with the same thickness polymer layer. So, the model divides the growing particle into an interior unfragmented core and a fragmented exterior section of spheres of increasing diameter. Active sites are distributed throughout the particle on the internal surface of the catalyst. To reach them, monomer must diffuse through the pores of the fragmented section and then, either through the polymer, or the pores of the unfragmented section. Diffusion rates are set to be different in each medium; fastest in the pores of the fragmented section, then the unfragmented core and slowest in the polymer. The work with this model showed the importance of the catalyst physical structure to the fragmentation rate and, in turn, in avoiding overheating.

In their 1996 review Hamielec and Soares [5] reported that Bonini et al. [124] had used a model similar to Ferraro and Chiovetta's which was able to give good predictions of polymer mass and molecular weight but not molecular weight distribution.

Estenoz and Chiovetta [125,126] created an alternative model where the fragmentation was described as a series of instantaneous steps, each increasing the active surface area of the

catalyst. In this model, the whole of the initial catalyst particle fragments into sub-particles which themselves fragment in turn and then the process repeats until the sub-particles become indivisible. Hitherto inaccessible active surface becomes available with each fragmentation step. In a later piece of work [127], the same authors propose another model similar to that of Ferrero and Chiovetta. The difference between the two models is in the initial structure of the catalyst particle which is more open. The predicted concentration gradients follow the same pattern as in the earlier work.

Grof et al. [128,129] constructed a dynamic model of the morphology evolution of the catalyst during the fragmentation stage. The initial particle is represented in a similar way to the MGM as a sphere formed from smaller spheres, but in this case no fragmentation has occurred and the microspheres are joined. Polymer formation causes the microparticles to grow and the forces of stress and strain leading to rupture of the links between microparticles are calculated. Non-uniformities, such as concentration gradients and irregularities in the initial catalyst structure lead to microparticles growing at various rates so different shaped structures are formed. For example, this model predicts the formation of hollow particles if mass transport limitations are significant, as is found experimentally. As opposed to the MGM or PFM, which attempt to represent an average particle behaviour to then be applied to a population of particles, this model demonstrates very clearly how some changes may occur during the fragmentation stage by focussing on individual particles. It is, therefore, not really a model which could be incorporated or combined into other models but a stand alone representation. It does highlight the complexity of fragmentation but is computationally intensive and requires values for the physical properties of the nascent polymer which may be in a state of rapid flux.

So, significant modelling work has been done to find ways of representing concentration and temperature gradients within polymer particles at different stages of growth including the initial fragmentation stage. The local conditions are needed for prediction of the polymer properties. It is particularly difficult to verify models for the fragmentation period experimentally. Heat transfer out of the catalyst particle can also be limiting and lead to temperature excursions. Few models take account of particle scale effects in combination with both reaction kinetics and the physical effects occurring on the reactor scale. Another problem is the heterogeneity in a batch of typical silica catalyst support which it is difficult to take account of in a single particle model.

Although a particle scale model has not so far been integrated into the reactor model described in this thesis it is important to have given it consideration. It gives a better

understanding of whether the assumptions made regarding reaction kinetics are reasonable and also further demonstrates the need for sensitive, well controlled methods and equipment to precisely measure the early behaviour of olefin polymerisation at industrial conditions.

1.3.3 Reactor Scale Modelling and Monitoring

1.3.3.1 Polymerisation Reactors

Reactor scale models are needed for design, control and improvement of industrial polymerisation plants and to gain a better understanding of olefin polymerisation. They can be used, for example, to account for temperature and concentration gradients within a reactor, to calculate a population balance over growing catalyst particles or to study the effects of multiple active sites. These models serve to show the complexity and interdependence of the effects occurring in a typical polymerisation reactor. A complete representation might include all the various phenomena occurring simultaneously and at different length scales. For example, a FBR model could combine a kinetic model, a particle scale model and reactor scale effects such as aggregation [130] or particle segregation [131]. Depending on the situation, assumptions are made regarding which effects can be neglected to provide a useful and workable model. Reactor models have been used to show that the final properties of the polymer are dependent on the initial catalyst morphology, reaction rate and reactor conditions [132, 133]. This is a wide ranging subject in itself and a detailed review is beyond the scope of this thesis. For more information and example models see Soares & McKenna [3] and also McAuley et al. [134] Kiashemshaki [101] and Shamiri [102]. Here, we will be focusing on fixed bed reactors as this is the type used in the experiments to be modelled.

1.3.3.2 Fixed Bed Reactor Modelling and Design

Fixed bed reactors are very common, so much so that Kapetijn & Moulijn [135] describe them as ‘the workhorse laboratory reactor for gas-solid reaction systems’. In the laboratory, capacities range from about ten milligrams to one gram of catalyst and flowrates of ten millilitres to one litre per minute at standard temperature and pressure. Diameters up to about 20 mm are usual. Laboratory fixed bed reactors are often used for testing new catalysts and analysis of kinetic parameters. Fixed bed reactors are also found in many industrial situations [136]. A few typical examples of industrial reactions which are carried out in catalytic fixed bed reactors are methane cracking, synthesis of acrolein, phosgene, phthalic-anhydride, ortho-xylene and catalytic combustion. These have high reaction rates and tend to be externally mass transfer limited or, in the case of catalytic combustion, externally heat and mass transfer limited. Ethylene polymerisation does not fall into this

category because the monomer remains within the catalyst particle creating a situation at the particle boundary layer which facilitates mass transfer and hinders heat transfer.

There is no precedent for modelling ethylene polymerisation in a fixed bed. As mentioned previously, FBRs are the only reactor type able to meet the commercial requirements for gas phase PE production. In the laboratory, a more diverse range of reactors has been used for the study of olefin polymerisation but no fixed bed model exists.

Fixed bed reactor modelling methods are well known. Standard texts treat the subject and give examples of model constructions [137, 138]. Tried, tested and comprehensively reviewed criteria and correlations are available for the determination of model type and for the estimation of necessary parameters [139]. These include heat and mass transfer coefficients and effective conductivity and diffusivity in the reactor bed.

The reactor to be modelled in this work is that used in the work of Tioni [40]. It was designed as a differential reactor with low conversion of the feed. The bed consists of two chemically and geometrically different solids (silica supported metallocene catalyst and salt particles in the form of NaCl agglomerates) with polymer accumulation. Also, the reactor is used for experiments of extremely short duration and the polymerisation is rapid and highly exothermic. A brief review of modelling methods and recent developments with particular regard to these specific points is given.

1.3.3.2.1 Model Type

Selection of model type depends on the relative sizes of the terms in the heat and mass balances over the reactor bed. Each term represents a particular heat or mass transfer phenomenon and those which can be neglected are removed, simplifying the model. Table 1-6 lists the heat and mass transfer rates which must be considered and the criteria against which they are evaluated. The criteria have been designed as guidelines for steady state or pseudo-steady state processes. Each compares the rates of two phenomena and is used to identify whether reaction rate is caused to vary beyond a defined allowable limit. For instance, Mears criterion compares the rates of heat generation in and evacuation from a packed bed and allows a maximum of 5% variation in the reaction rate. Karim et al. [140] provide a good illustration of its use in a study of steam reforming of methanol in a packed bed. The first moments of ethylene polymerisation are a time of rapid change in reaction rate and conditions. The steady state assumption made in the development of the criteria for choice of model type results in certain factors not being included. For example, in the development of Mears criterion bed heat capacity is neglected. In a dynamic situation, these

factors can be significant. For example, Kosek et al. [119] found that their dynamic particle scale model for gas phase olefin polymerisation calculated lower temperature peaks than were estimated by steady state methods.

Effect	Criterion	Competing Phenomena	Limit
Axial Dispersion	Peclet number, Pe_a	advection vs diffusion	$Pe_a < 20$ Or rule of thumb: Bed length/particle diameter >> 50
Internal mass transfer	Thiele modulus, φ	intrinsic reaction rate vs diffusion through catalyst pores	$\varphi < 0.3$ ~3% reduction in reaction rate
Internal heat transfer	Prater number	heat generation in the particle vs heat transfer through particle	~10% change in reaction rate
External mass transfer	F_{ex}	intrinsic reaction rate vs diffusion through boundary layer	$F_{ex} < 0.05$ 5% difference in reactant concentration
External heat transfer	δ_{ex}	heat generation in the particle vs heat transfer across boundary layer	$\delta_{ex} < 0.1$ ~10% change in reaction rate
Radial heat transfer	Mears criterion [141]	heat generation in the bed vs heat evacuation from the bed	5% variation in reaction rate

Table 1-6: List of main phenomena to be considered for inclusion in a fixed bed model

Mariani et al. [142] recently proposed a new criterion for heat transfer limitation over the whole bed volume. A simplified method is suggested for the first analysis of the thermal behaviour of laboratory scale packed bed reactors. The axial position of maximum bed temperature and its value are estimated from an equation which relates the heat generation rate to the bed length. The equation includes an adjustable parameter and is used in conjunction with the heat balance and the heat transfer properties of the system. From knowledge of the activation energy, and using the same approximation as Mears, it can then be estimated whether the temperature range across the whole volume of the packed bed causes more or less than an acceptable 5% variation in reaction rate.

As discussed in the single particle modelling section, accumulation of polymer at catalyst active sites means that the characteristics of the catalyst particle are not fixed. In polymerisation therefore, the Thiele modulus, which is usually used to determine whether a reaction rate is limited by internal diffusion, can only give precise information about the initial condition, prior to any polymer build up. Calculation of the Thiele modulus for conditions during the polymerisation would depend the instantaneous values for the effective diffusivity,

particle size, reaction rate and monomer surface concentration which would have to be estimated.

1.3.3.2.2 Heat Transfer Correlations for Packed Beds

For fixed bed reactor models where the reaction is highly exo- or endothermic significant radial temperature gradients are likely to exist and it is important to describe them as accurately as possible. The reviews of Van Antwerpen et al. (2010) [143] and Dixon (2012) [144] both emphasise the huge quantity of research which has gone into understanding radial heat transfer within packed beds. Van Antwerpen et al. provide an extensive and detailed analysis of correlations to date including graphs which compare the various models with one another and with measured data. Dixon argues that the accepted method of using an effective radial conductivity, λ_e, and a wall heat transfer coefficient, h_w, cannot account precisely for heat transfer near the wall and demonstrates that average radial temperature is insufficient for a good knowledge of the radial temperature profile in the bed. Where average radial temperature has been used to derive correlations [145, 146], they should not be extrapolated to different geometries or used with other sets of correlations. Attention is also drawn to the problem of measuring packed bed temperature profiles without affecting the bed. The use of an axial thermocouple or thermowell in a packed bed reactor disturbs the bed structure and can also be subject to stem effects [147]. These are due to heat conduction in the thermocouple wire and sheath or the metal thermowell. Axial temperature gradients in the bed tend to exacerbate this problem [148].

The Zehner Schlunder correlation is frequently used to estimate λ_e [149]. Van Antwerpen et al. [143] and Dixon [144] both recommend use of the later, amended 1978 Zehner, Bauer and Schlunder (ZBS) version of this correlation to estimate λ_e and for h_w, Dixon recommends the relationship of Yagi & Kunii [150]. However, Schweich [139] advises against combining correlations derived by different research groups as this can lead to inconsistency. The heat transfer parameters in packed beds are known to be very dependent on particle shape. For example, similar experiments with spheres and cylinders produce different measured values of h_w [149, 151].

Computational fluid dynamics (CFD) is currently being tested for calculation of temperature profiles [152] and used for investigation of heat transfer in packed beds [153,154]. Work to refine and confirm the accepted models also continues. For example, Beaver and Sircar [155] recently produced a model which reconfirms the earlier studies of Wakao et al. [156]. They showed that at very low Reynolds numbers (Re < 1) the usual assumptions for heat and mass transfer in packed beds are not true because intraparticle temperature and

concentration gradients can no longer be assumed symmetrical. Care must therefore be taken with correlations for the particle heat and mass transfer coefficients in this flow region.

1.3.3.2.3 Packed Bed Dilution

Bed dilution with an inert solid is a well known method for minimising reactor scale temperature gradients in packed beds by reducing the reaction rate per unit bed volume. The study of Taniewski et al. [157] concerning the oxidative coupling of methane to C_2 hydrocarbons in two different laboratory scale packed bed reactors is an example of bed dilution being used for this purpose. Bed dilution reduces conversion and this has been an area of investigation since the 1960s. Van den Bleek [158] introduced a criterion for maximum bed dilution and Mears [141] included the effect of bed dilution in his criteria for heat transport limitations. Some of the interest in this area comes from its use in laboratory scale trickle bed reactors where fines are mixed with the catalyst. This is useful because it increases the number of contact points in the reactor bed and thus helps with wetting. It also changes the hydrodynamics of the bed to being mostly determined by the packing of the smaller particles [159] with the added benefit of reducing external diffusion limitations for the catalyst [160]. Possible negative effects are associated with poor mixing, channelling and local bypassing of catalyst, in particular for unequal particle size distributions and different shaped particles in the same bed [161,162].

Moulijn et al. [163] carried out experiments representing packed beds similar to those envisioned in Van den Bleek's original model. As expected, they found that dilution is associated with bypassing, especially for non-homogeneously packed beds, and even for well mixed beds dilution always reduces the conversion to some extent. Based on the experimental data they extended the Van den Bleek criterion to include conversion. Mederos et al. [164] point out that these criteria were developed for systems with catalyst and inert solid of the same diameter and care must be taken when this is not the case. Kapteijn & Moulijn [135] write that diluting a catalyst bed can be used as a test for significant temperature gradients. If bed dilution results in a greater reduction in conversion than expected, then significant temperature gradients exist.

1.3.3.2.4 Design of Fixed Bed Reactors

Part of the remit of this project is to improve the design of the current reactor. Here some general points regarding the design of fixed bed reactors are briefly considered. The first requirement for constructing any piece of equipment is a design objective; it is important to understand clearly what information we want to get from the reactor. If the aim is to measure kinetic data, then isothermal operation, ideal flow and no transport limitations are all required

[161]. It also seems logical to suggest these conditions would be preferable for observation of catalyst morphology and polymer properties. Tioni [40] lists the design requirements for a reactor to study the early stages of gas phase olefin polymerization to be:

- Contact between reagants and catalyst must be immediate
- Reaction end must be effective and immediate
- Reaction time must be precisely controlled
- No excessive temperature or concentration gradients should form inside the reactor
- Reaction conditions (pressure, temperature, gas composition, gas velocity) should remain constant during the reaction
- Particles should be recovered without morphology alteration
- Enough polymer must be produced to perform the necessary analysis

Mears [141] and Perego & Peratello [161] both discuss design methods for isothermal fixed bed reactors. Interparticle temperature gradients can be reduced by dilution of catalyst, but also dilution of reactants and reduction of reactor diameter. Intraparticle gradients and axial dispersion can be reduced by decreasing particle size. If reactor diameter is reduced it is important for it to remain at least 10 times the particle diameter to avoid wall effects [161, 172]. Tioni [40] has already applied much of this theory to the existing reactor; temperature gradients have been reduced by operating the reactor with diluted catalyst and monomer and by reducing the particle size of the inert solid. There has been a trade off in this work between avoiding reactor overheating and providing enough polymer for analysis whilst maintaining temperatures and pressures close to industrial values.

In considering reactor designs for isothermal operation different shapes can be used and Cao et al. [165] developed a rectangular microchannel reactor to study the kinetics of catalytic methanol steam reforming. This reaction is very rapid and highly endothermic and so presents similar heat transfer problems to the initial stages of olefin polymerisation. Their design used a thin, slab shaped catalyst bed with heat transfer oil circulating at a high rate for rapid heat transfer.

An alternative packed bed reactor design objective is for adiabatic operation. This would be the ideal reactor type for use with calorimetry methods because, with no heat losses, all the heat of reaction would leave in the exit gas stream and hence be measurable. In industry, adiabatic packed beds represent the oldest fixed-bed reactor configuration [166] due to their simplicity. In the laboratory they can be found for use in catalyst testing. For example, de

Klerk [167] presents a design for an adiabatic laboratory packed bed reactor to be used for testing catalysts with high heat release. The design criterion for adiabatic operation is that heat loss from the bed or fluid to the equipment be negligible. Radial heat losses can be minimised by insulating the reactor wall and axial heat losses are minimised by control of the reactor hydrodynamics. Tavazzi et al. [168] use an alternative adiabatic packed bed reactor, designed for use at very high temperatures, to test catalyst and operating conditions for partial oxidative methane reforming. Adiabatic operation was found to be approached more closely at higher flowrates. This would be expected from the analysis of de Klerk [167] but was explained by an increase in reaction rate relative to heat losses from the reactor.

A similar design is that of a short contact time reactor (SCTR) which is the opposite case to the LCPP stopped-flow reactor and also the closest type of fixed bed found in the literature. In a SCTR, the gas has very brief contact with the catalyst whereas in our reactor it is the catalyst which must only have brief contact with the monomer. An example of an SCTR is reported by Ramaswamy et al. [169] for a study on methane reforming. In these reactors the gas stream is only in contact with the reactor bed for a few milliseconds.

An alternative, more recently developed, reactor type which is proposed for mechanistic and kinetic studies of fast reactions with supported catalyst is the temporal analysis of products reactor (TAP) [170, 171, 172]. Pressures of the order 20-200 Pa and tiny pulses of size 10^{13} to 10^{17} molecules of reactant and duration 250μs are used to create a situation where the only means of mass transport through the bed is Knudsen flow. This allows mass transport to be completely defined so reaction kinetics can be measured.

A wide range of olefin polymerisation reactor models therefore exist, adapted to particular situations and designed to study specific areas of interest. Fixed bed modelling is a mature science which continues to develop through use of more powerful computing methods but also through accumulation of new ideas and experimental data. However, most correlations are based on beds of spherical or cylindrical particles. Dilution of a fixed bed with solid inert can reduce conversion and care must be taken to ensure adequate mixing. Isothermal reactor conditions are usually required for evaluation of reaction kinetics. However, adiabatic packed beds are also reported for the study of highly exothermic reactions.

1.4 Conclusion

The subject of this thesis is the dynamic modelling of a fixed bed reactor to study the first instants of gas phase ethylene polymerisation. As such, a literature review focussing on the first instants of heterogeneous ethylene polymerisation with coordination catalysts has been provided. The literature review is quite wide ranging as it covers most aspects which could influence the first moments of this complex process. Following an introductory section, the chemical and physical phenomena which occur at this time have been discussed, along with the methods used to investigate them and the state of current research. Phenomena on three different length scales (molecular, particle and reactor) are important in this work. These are polymerisation reaction kinetics, the dynamics of the growing catalyst/polymer particles and heat and mass transfer in the fixed bed reactor. Modelling methods at all these levels have also been reviewed.

To recap, PE has been shown to be an important product with a large global market. PE properties depend on molecular chain length and branch structure so the term actually defines a range of materials. The main manufacturing routes are high pressure processes and use of CrO_x, ZN and metallocene catalysts. Despite advances in catalysis, each route produces specific types of PE with particular properties and thus retains its place in the market. The structure and properties of the amorphous silica catalyst support and the chemistry of metallocene catalyst in solution are well known. However, when olefin polymerisation catalysts are supported the process becomes more complex, both chemically and physically and so, the behaviour of the supported catalyst is less well understood.

The first moments of the polymerisation are a time of transition and rapid change. The high polymerisation rate and exothermicity combined with the evolution of the catalyst structure and polymer physical properties make this period particularly difficult to observe and study. The structural and surface properties of the catalyst support are both important to the process but sources of added complexity. The reaction conditions and polymer properties are also important, in flux and interdependent with the properties of the catalyst support. The small size of the fresh catalyst particles creates an initial risk of overheating which abates as the polymerisation progresses and the particles grow. The entire success of the polymerisation is dependant on this initial stage as there is a ‘sweet spot’ in the polymerisation rate. If the rate is too high or low the polymerisation will fail. This period also has a lasting impact on the polymerisation rate and final properties although the reason why is not clear.

Various reactor types are used for olefin polymerisation but gas phase PE formation is so rapid and highly exothermic that the only suitable reactor for industrial scale production is the FBR. Usual operating conditions are 70 to 110°C and 20 to 40 bar with the reactor containing a wide particle size distribution. The process is temperature controlled to avoid fouling which is principally caused by melting polymer or fines. FBRs do not scale down easily for laboratory scale study and do not lend themselves to detailed observation of the effects of reaction start-up, duration, flowrates and heat transfer on the growing particles so alternatives are used in laboratory research.

Many studies have analysed partially polymerised particles, usually obtained under mild conditions. These methods have provided much useful information, particularly with regard to the fine structure of the developing catalyst/polymer particle and the dynamic of the catalyst fragmentation step. For example, the knowledge that ZN/$MgCl_2$ break up is rapid and uniform whereas silica supported catalysts tend to fragment more slowly and from the outside of the particle towards the centre. Nevertheless, these methods provide only a snapshot of the polymerisation and also, as particle behaviour is known to vary with temperature and reaction rate, it is preferable to study the system under realistic conditions.

Designing a laboratory scale reactor to observe the first instants of gas phase heterogeneous olefin polymerisation under realistic conditions presents a challenge. The catalyst is oxygen sensitive and can therefore only be handled in a glove box, the timescale of interest is extremely short and the polymerisation reaction is very sensitive to operating conditions. Video-microscopy has been used to successfully observe real-time gas phase particle growth and surface temperatures, but requires stagnant gas conditions so cannot be used with realistic gas-particle relative velocities. Stopped flow reactors have also been adapted to study the first moments of both solution and slurry phase olefin polymerisation with good results. McKenna's group successfully implemented a high pressure stopped flow reactor to investigate the very early reaction rate and morphological development of the particles in slurry phase olefin polymerisation close to industrial conditions. They are the first to design and develop a fixed bed reactor to gain information about the very early stages of the gas phase system.

This literature review has considered modelling at the three relevant length scales, firstly the chemical kinetics which represent the molecular level, then modelling of the catalyst particles and finally fixed bed reactor modelling. It is difficult to draw precise information from the literature for the chemical kinetics of ethylene polymerisation using supported metallocene catalyst. Data is reported for similar, but not identical catalyst systems and reporting

methods are different. Rigorous kinetic models for olefin polymerisation are quite complex with several parameters required. Simplified kinetic models with lumped reaction constants are often used and, as the initial purpose of the reactor model is a better description of the conditions in the fixed bed, a simplified model is adequate in our particular case.

Significant efforts have been made to create particle scale models for the early stages of polymerisation and these demonstrate the importance of the morphology of the growing particles. The most favoured are the MGM and the PFM. However, the heterogeneity of the raw catalyst, the changes in the physical structure of growing polymer particles and the difficulty in observing the early stages of the polymerisation make these difficult to verify, particularly at industrial conditions. This is a potential future use of the fixed bed reactor and model. Modelling of packed bed reactors is a mature science with well known, accepted methods. However, the correlations which have been developed to estimate the heat transfer parameters are mainly derived from beds of spherical particles under steady state conditions. This is different to our case and so care must be taken in their application.

This literature survey has been broad to gain understanding of all the processes which occur in the reactor and to ascertain which might be controlling. However, the first aim of this work is to model the fixed bed reactor which has been developed to observe the first instants of olefin polymerisation in the gas phase by McKenna's group. It is not possible to include all the detail of the reactor and polymerisation at once and so the aim is to build up, starting with a simplified representation of the polymerisation and focussing on the reactor. This will allow a good estimate of the operating conditions to be made before advancing with further study and model developments.

A classical modelling approach will be used for the fixed bed reactor based on the heat and mass balances and the criteria and correlations described above. Care will be taken to represent the heat transfer through the mixed reactor bed of growing catalyst/polymer particles and NaCl agglomerates as closely as possible. This initial reactor model will then be used to consider the possibility of using the existing set-up as a calorimeter to gain information about the polymerisation kinetics and also to evaluate potential improvements to the reactor, the set-up and the operating methods. Finally, alternative polymerisation kinetics will be tested within the reactor model. The purpose of this thesis is, therefore, to use modelling techniques to gain a better understanding of conditions in the reactor and then, through knowledge of the reactor conditions, to improve the reactor design as necessary and gain a better understanding of the catalyst behaviour.

1.5 Nomenclature

C_m	Monomer concentration	$mol.m^{-3}$
C^*	Active site concentration	$mol.m^{-3}$
E_{ap}	Activation energy for propagation	$J.mol^{-1}$
k_d & k_d'	Deactivation rate constant	s^{-1} & (-)
k_{p0}	Pre-exponential reaction rate constant for propagation	$mol^{-1}.s^{-1}.m^3$
k_p	Reaction rate constant for propagation	$mol^{-1}.s^{-1}.m^3$
R	Ideal Gas Constant	$J.mol^{-1}.K^{-1}$
R_p	Propagation rate	$mol.s^{-1}.m^{-3}$
T	Temperature	K
t	Time	s

[1] http://www.britannica.com/EBchecked/topic/468698/major-industrial-polymers/76435/Polyethylene-PE

(8 May 2013)

[2] McDaniel M.P., Review of the Phillips Chromium Catalyst for Ethylene Polymerization in Handbook of Heterogeneous Catalysis, 2nd Ed. 2008, Wiley-VCH Verlag GmbH & Co. KGaA, Weinheim

[3] Soares J.B.P. & McKenna T.F.L., Polyolefin Reaction Engineering (2012) Wiley-VCH Verlag & Co., Weinheim, Germany

[4] http://www.nobelprize.org/nobel_prizes/chemistry/laureates/1963/

(26 September 2011)

[5] Hamielec A. & Soares J., Polymerisation Reaction Engineering – Metallocene Catalysts, Prog. Polym. Sci. 21 (1996) 651-706

[6] Soga K. & Shiono T., Ziegler-Natta Catalysts for Olefin Polymerisations, Prog. Polym. Sci. 22 (1997) 1503-1546

[7] Kaminsky W, The Discovery of Metallocene Catalysts and their Current State of the Art, J. Polym. Sci.: A 42 (2004) 3911–3921

[8] Alt H. & Koppl A. Effect of the Nature of Metallocene Complexes of Group IV Metals on Their Performance in Catalytic Ethylene and Propylene Polymerization, Chem. Rev. 100 (2000) 1205-1221

[9] Rau A., Schmitz S. & Luft G., Kinetic Investigations of the Metallocene – Catalyzed Polymerization of Ethylene at High Pressure, Chem. Eng. Technol. 25 (2002) 5

[10] Kaminsky W., Olefin Polymerization Catalyzed by Metallocenes, Adv. Catal. 46 (2001) 89-159

[11] Kaminsky W. & Laban A., Metallocene Catalysis, Appl. Catal. A: Gen. 222 (2001) 47–61

[12] McKenna T. & Soares J., Single Particle Modelling for Olefin Polymerization on Supported Catalysts: A Review and Proposals for Future Developments, Chem. Eng. Sci. 56 (2001) 3931–3949

[13] Choi Y. & Soares J., Supported Single-Site Catalysts for Slurry and Gas-Phase Olefin Polymerisation, Can. J. Chem. Eng. 9999 (2011) 1-26

[14] Harrison D., Coulter I.M., Wang S., Nistala S., Kuntz B. A., Pigeon M., Tian J. & Collins S., Olefin Polymerization Using Supported Metallocene Catalysts: Development of High Activity Catalysts For Use in Slurry and Gas Phase Ethylene Polymerizations, J. Mol. Cata. A: Chem. 128 (1998) 65-77

[15] Hammawa H. & Wanke S., Influence of Support Friability and Concentration of α-Olefins on Gas-Phase Ethylene Polymerization over Polymer-Supported Metallocene/Methylaluminoxane Catalysts, J. App. Polym. Sci. 104 (2007) 514-527

[16] Van Grieken R, Carrero A., Suarez I. & Paredes B., Ethylene Polymerization Over Supported MAO/$(nBuCp)_2ZrCl_2$ Catalysts: Influence of Support Properties, Eur. Polym. J. 43 (2007) 1267-1277

[17] Vakili M., Arabi H., Mobarakeh H.S. & Ghafelebashi M., Studying The Effects of SiO2 Specifications and Properties of (SiO_2/$MgCl_2$/TEOS/$TiCl_4$/$AlEt_3$) Catalyst System on Kinetic Behaviour and Hydrogen Responsibility of Ethylene Slurry Polymerization, J. App. Polym. Sci. 118 (2010) 2216-2224

[18] Rahiala H., Beurroies I., Eklund T., Hakala K., Gougeon R., Trens P. & Rosenholm J.B., Preparation and Characterization of MCM-41 Supported Metallocene Catalysts for Olefin Polymerization, J. Catal. 188 (1999) 14-23

[19] Garcia-Orozco I., Velilla T., Gallad G.B., Dos Santos J. H. Z., Williams R.J.J. & Quijada R., Metallocene Supported on a Polyhedral Oligomeric Silsesquioxane-Modified Silica: Structural Characterization and Catalytic Activity for Ethylene Polymerization, J. Polym. Sci.: A 48 (2010) 5938-5944

[20] Chang A., Liu X., Nelson P.J., Munzig G.R., Gegan T.A., & Kissin Y.V., Ziegler-Natta Catalysts for Propylene Polymerization : Morphology and Crystal Structure of a Fourth-Generation Catalyst, J. Catal. 239 (2006) 347-353

[21] Taniike T., Thang V.Q., Nguyen T.B., Yuichi H., Uozumi T & Terano M., Initial Particle Morphology Development in Ziegler-Natta Propylene Polymerization Tracked with Stopped-Flow Technique, Macromol. Chem. Phys. 212 (2011) 723-729

[22] Zhuravlev L.T., Concentration of Hydroxyl Groups on the Surface of Amorphous Silicas, Langmuir, 3 (1987) 316-318

[23] Unger K.K., Porous Silica, Journal of Chromatography Libraries, 16 (1979)

[24] Bergna H.E., Colloid Chemistry of Silica – an Overview, ACS 1994 ISBN13:9780841221031

[25] Severn J.R. & Chadwick J.C. Tailor-Made Polymers, Copyright 2008 Wiley-VCH Verlag GmbH & Co. KGaA, Weinheim

[26] http://www.grace.com/engineeredmaterials/materialsciences/precipitatedsilica/default.aspx (19th October 2012)

[27] Falconer K., Fractal Geometry, Mathematical Foundations and Applications, 2nd Ed., Wiley (2003)

[28] Schaefer D.W. & Keefer K.D., Fractal Geometry of Silica Condensation Polymers, Phys. Rev. Lett. 53,14 (1984) 1383-1386

[29] Aubert C. & Cannel D.S., Restructuring of Colloidal Silica Aggregates, Phys. Rev. Lett. 56,7 (1986) 738-741

[30] Tang P., Colflesh D.E. & Chu B., Temperature Effect on Fractal Stucture of Silica Aggregates, J. Colloid Interface Sci. 126,1 (1988) 304-313

[31] Fink G., Tesche B., Korber F. & Knoke S., The Particle-Forming Process of SiO2-Supported Metallocene Catalysts, Macromol. Symp. 173 (2001) 77-87

[32] Knoke S,. Korber F., Fink G. & Tesche B., Early Stages of Propylene Bulk Phase Polymerization with Supported Metallocene Catalysts, Macromol. Chem. Phys. 204 (2003) 607–617

[33] Steinmetz B., Tesche B., Przylbyla C., Zechlin J. & Fink G., Polypropylene growth on Silica-Supported Metallocene Catalysts: A Microscopic Study to Explain Kinetic Behavior Especially in Early Polymerization Stages, Acta Polymer 48 (1997) 392-399

[34] Tisse V., Briquel R.M. & McKenna T.F.L., Influence of Silica Support Size on the Polymerisation of Ethylene Using a Supported Metallocene Catalyst, Macromol. Symp. 285 (2009) 45-51

[35] Niegisch W.D., Crisafulli S.T., Nagel T.S. & Wagner B.E., Characterization Techniques for the Study of Silica Fragmentation in the Early Stages of Ethylene Polymerization, Macromol. 25 (1992) 3910-3916

[36] Fink G., Steinmetz B., Zechlin J., Przylbyla C. & Tesche B., Propene Polymerization with Silica-Supported Metallocene/MAO Catalysts, Chem. Rev. 100 (2000) 1377-1390

[37] Silveira F., Brambilla R., Pesca da Silveira N., do Carmo Martins Alves M., Stedile F.C., Pergher S.B.C. & Zimnoch dos Santos J.H., Effect of Textural Characteristics of Supported Metallocenes on Ethylene Polymerization, J. Mater. Sci. 45 (2010) 1760-1768

[38] Welborn H.C., Exxon, U.S. Patent No. 4,808,561 (1989)

[39] Takahashi T., Mitsubishi Petrochemical, U.S. Patent No. 5,026,797 (1991)

[40] Tioni E., Optimisation of a Tool to Study the Start-up of the Gas Phase Olefin Polymerisation, Ph.D. Thesis UCBL1 338-2011

[41] Zurek E. & Ziegler T., Theoretical Studies of the Structure and Function of MAO (Methylaluminoxane), Prog. Polym. Sci. 29 (2004) 107-148

[42] Severn J.R., Chadwick J.C., Duchateau R. & Friederichs N., Bound But Not Gagged – Immobilizing Single-Site r-Olefin Polymerization Catalysts, Chem. Rev. 105 (2005) 4073-4147

[43] Tisse V., Prades F., Briquel R., Boisson C. & McKenna T.F.L., Role of Silica Properties in the Polymerisation of Ethylene Using Supported Metallocene Catalysts, Macromol. Chem. Phys. 211 (2010) 91-102

[44] Silveira F., Pires G.P., Petry C.F., Pozebon D., Stedile F.C., dos Santos J.H.Z. & Rigacci A., Effect of the Silica Texture on Grafting Metallocene Catalysts, J. Mol. Cata. A: Chem. 265 (2007) 167-176

[45] Olalla B., Broyer J.P. & McKenna T.F.L., Heat Transfer and Nascent Polymerisation of Olefins on Supported Catalysts. Macromol. Symp. 271 (2008) 1-7

[46] Tioni E., Broyer J.P., Spitz R., Monteil V. & McKenna T.F.L., Heat Transfer in Gas Phase Olefin Polymerisation, Macromol. Symp. 285 (2009) 58-63

[47] Tioni E., Spitz R., Broyer J.P., Monteil V. & McKenna T.F.L., Packed-Bed Reactor for Short Time Gas Phase Olefin Polymerisation: Heat Transfer Study and Reactor Optimisation, AIChE J. 58,1 (2012) 256-267

[48] Grosso W. & Chiovetta M., Modeling a Fluidised-Bed Reactor for the Catalytic Polymerisation of Ethylene: Particle Distribution Effects, Latin Am. App. Res. 35 (2005) 67-76

[49] McKenna T.F.L., Di Martino A., Weickert G. & Soares J.B.P. Particle Growth During the Polymerisation of Olefins on Supported Catalysts 1- Nascent Polymer Structures, Macromol. React. Eng. 4 (2010) 40-64

[50] Di Martino A., Weickert G. & McKenna T.F.L., Contributions to the Experimental Investigation of the Nascent Polymerisation of Ethylene on Supported Catalysts 1: A Quenched Flow Appartaus for the Study of Particle Morphology and Nascent Polymer Properties, Macromol. React. Eng. 1 (2007) 165-184

[51] Webb S.W., Weist E.L., Chiovetta M.G. & Connor W.C., Morphological Differences in the Gas Phase Polymerization of Ethylene by Silica Supported Chromium Oxide Catalysts, Can. J. Chem. Eng. 69 (1991) 665-681

[52] McKenna T.F.L., Tioni E. Raneiri M.M., Alizadeh A., Boisson C. & Monteil V., Catalytic Olefin Polymerisation at Short Times: Studies Using Specially Adapted Reactors, Can. J. Chem. Eng. 9999 (2012) 1-26

[53] Machado F., Lima E.L., Pinto J.C. & McKenna T.F.L., Evaluation of the Initial Stages of Gas-Phase Ethylene Polymerizations with a SiO2-Supported Ziegler-Natta Catalyst, Macromol. React. Eng. 3 (2009) 47-57

[54] Cosewith C., Transient Response of Continuous-Flow Stirred-Tank Polymerization Reactors, AIChE J. 34,2 (1988) 272–282

[55] Charpentier P., Zhu S., Hamielec A.E. & Brook M.A., Continuous Solution Polymerisation of Ethylene Using Metallocene Catalyst System, Zircocene Dichloride/Methylaluminoxane/ Trimethylaluminum, Ind. Eng. Chem. Res. 36 (1997) 5074-5082

[56] Wang W., Yan D., Zhu S. & Hamielec A.E., Kinetics of Long Chain Branching in Continuous Solution Polymerization of Ethylene Using Constrained Geometry Metallocene, Macromol. 31 (1998) 8677-8683

[57] Zhang M., Karjala T.W. & Kolthammer B.W.S., Delayed Dynamics of Polymer Properties in Continuous Stirred Tank Polymerization Reactors, Ind. Eng. Chem. Res. 46 (2007) 5922-5935

[58] Mannan T.M., Hammawa H., Lynch D.T. & Wanke S.E., A Laboratory Reactor for Gas-Phase Olefin Polymerization, Can. J. Chem. Eng. 82 (2004) 371-381

[59] Bergstra M.F.& Weickert G., Semi-Batch Reactor for Kinetic Measurements of Catalyzed Olefin Co-Polymerizations in Gas and Slurry Phase, Chem. Eng. Sci. 61 (2006) 4909 – 4918

[60] Meier G.B., Weickert G. & van Swaaij W.P.M., Comparison of Gas- and Liquid-Phase Polymerization of Propylene with Heterogeneous Metallocene Catalyst, J. App. Polym. Sci. 81 (2001) 1193–1206

[61] Silva F.M., Lima E.L., Pinto J.C. & McKenna T.F.L., Synthesis of Propylene/1-Butene Copolymers with Ziegler-Natta Catalyst in Gas-Phase Copolymerizations, 1: Kinetics and Macromolecular Properties, Macromol. Chem. Phys. 206 (2005) 2333-2341

[62] Busico V. Metal-Catalysed Olefin Polymerisation into the New Millennium: A Perspective Outlook Dalton Trans. (2009) 8794–8802

[63] De Bellefon C., Tanchoux N., Caravieilhes S., Grenouillet P. & Hessel V., Microreactors for Dynamic, High Throughput Screening of Fluid/Lliquid Molecular Catalysis, Ange. Chem. 19 (2000) 3584-3587

[64] Neilsen C.A., Chrisman R.W., LaPointe R.E. & Miller T.E., Novel Tubing Microreactor for Monitoring Chemical Reactions, Anal. Chem. 74 (2002) 3112-3117

[65] Meier G.B., Fluidized Bed Reactor for Catalytic Olefin Polymerisation, Kinetics and Fluidization, Ph.D. Thesis (2000) ISBN 90-36514894

[66] Van Putten I.C., Propylene Polymerization in a Circulating Slugging Fluidized Bed Reactor, Ph.D. Thesis (2004) University of Twente

[67] Pater J.T.M., Weickert G. & van Swaaij W.P.M., Optical and Infrared Imaging of Growing Polyolefin Particles, AIChE J. 49,2 (2003) 450-464

[68] Hamilton P., Hill D.R. & Luss D., Optical and Infrared Study of Individual Reacting Metallocene Catalyst Particles, AIChE J. 54,4 (2008) 1054-1063

[69] Gomez-Hens A. & Perez-Bendito D., The Stopped Flow Technique in Analytical Chemistry, Anal. Chim. Acta. 242 (1991) 147

[70] Di Martino A., Weickert G. & McKenna T.F.L., Design and Implementation of a Novel Quench Flow Reactor for the Study of Nascent Olefin Polymerisation, Macromol. React. Eng. 1 (2007) 284-294

[71] Schnell & Fink G. Elementarprozesse der Ziegler-Natta-Katalyse. I. Oligomerenkinetik im Strömungsrohr, Ange. Makromol. Chem. 39,1 (1974) 131–147

[72] Fink G. & Zoller, Elementarprozesse löslicher Ziegler-katalysatoren. Polymerisationskinetische analyse und Mathematische Modellierung im System Cp2TiPropylCl/AlEtCl2/Ethylen, Makromol. Chem. 182,11 (1981) 3265–3278

[73] Shiono T., Ohgizawa M.& Soga K., Reaction of the Ti-Polyethylene Bond with Carbon Monoxide Over the bis(Cyclopentadienyl)titanium Dichloride-Methylaluminoxane Catalyst System, Polymer 35 (1994) 187

[74] Busico V., Cipullo R. & Esposito V., Stopped-Flow Polymerizations of Ethene and Propene in the Presence of the Catalyst System *rac*-Me2Si(2-methyl-4-phenyl-1- indenyl)2ZrCl2/methylaluminoxane, Macromol. Rapid Commun. 20 (1999) 116–121

[75] Janiak C., Versteeg U., Lange K., Weimann R. & Hahn E., The Influence of Electronic and Steric Effects and the Importance of Polymerization Conditions in the Ethylene Polymerization With Zirconocene/ MAO Catalysts, J. Organometallic Chem. 501 (1995) 219-234

[76] Song F., Cannon R.D. & Bochmann M., Zirconocene-Catalyzed Propene Polymerization: A Quenched-Flow Kinetic Study, J. Am. Chem. Soc. 125 (2003) 7641-7653

[77] Keii T., Terano M., Kimura K. & Ishii K., A Kinetic Argument For a Quasi-Living Polymerisation of Propene With a $MgCl_2$-Supported Catalyst, Macromol. Chem. Phys. Rapid. Commun. 8 (1987) 583-587

[78] Liu B., Matsuoka H. & Terano M. Stopped-Flow Techniques in Ziegler Catalysis, Macromol. Rapid Commun. 22 (2001) 1-24

[79] Soga,K., Ohgizawa M., Shiono T. & Lee D., Possibility of Mass-Transfer Resistance in Ethylene Polymerization with MgCl2- Supported Catalysts, Macromol. 24 (1991) 1699-1700

[80] Zechlin J., Steinmetz B., Tesche B. & Fink G., Development of a Refined Poly(propylene) Growth Model for Silica Supported Metallocene Catalyst Systems, Macromol. Chem. Phys. 201 (2000) 515–524

[81] Di Martino A ., Broyer J.P., Schweich D., De Bellefon C., Weickert G. & McKenna T.F.L., Contributions to the Experimental Investigation of the Nascent Polymerisation of Ethylene on Supported Catalysts 2a: Influence of Reaction Conditions, Macromol. React. Eng. 1 (2007) 229-242

[82] Taniike T., Nguyen T.B., Takahashi S., Thang V.Q., Ikeya M. & Terano M., Kinetic Elucidation of Comonomer-Induced Chemical and Physical Activation in Ziegler-Natta Heterogeneous Propylene Polymerization, J. Polym. Sci.: A 49 (2011) 4005-4012

[83] Silva F., Lima E.L., Pinto J.C. & McKenna T.F.L., Investigation of Catalyst Fragmentation in Gas-Phase Olefin Polymerisation: A Novel Short Stop Reactor, Macromol. Rapid Commun. 26 (2005) 1846-1853

[84] Tisse V., Sheibat-Othman N. & McKenna T.F.L., A Lab-Scale Reaction Calorimeter for Olefin Polymerization, Can. J. Chem. Eng. 88 (2010) 783-792

[85] Ruddick V.J. & Badyal J.P.S., AFM Study of the Breakup of Catalyst Particles during Ethylene Polymerization, J. Phys. Chem. B 101 (1997) 1791-1793

[86] Conner W. C., Webb S.W., Spanne P. & Jones K.W., Use of X-ray Microscopy and Synchrotron Microtomography to Characterise Polyethylene Polymerization Particles, Macromol. 23 (1990) 4742-4747

[87] Jang Y-J., Naundorf C., Klapper M. & Müllen K., Study of the Fragmentation Process of Different Supports for Metallocenes by Laser Scanning Confocal Fluorescence Microscopy (LSCFM), Macromol. Chem. Phys. 206 (2005) 2027-2037

[88] Tisse V., Kinetics and Morphology of Metallocene Catalysts used in Ethylene Polymerisation, Ph.D. Thesis UCBL1 50-2006

[89] Boden S., Bieberle M., Weickert G. & Hampel U., Three-Dimensional Analysis of Macroporosity Distributions in Polyolefin Particles Using X-Ray Microtomography, Powder Technol. 188 (2008) 81-88

[90] Seda L., Zubov A., Bobak M., Kosek J. & Kantzas A., Transport and Reaction Characteristics of Reconstructed Polyolefin Particles, Macromol. React. Eng. 2 (2008) 495-512

[91] McDaniel M.P., A Review of the Phillips Supported Chromium Catalyst and its Commercial Use for Ethylene Polymerization, Adv. Catal. 53 (2010) 123-606

[92] McDaniel M.P, Fracturing Silica-Based Catalysts During Ethylene Polymerization, J. Polym. Sci.: A 19 (1981) 1967-1976

[93] McDaniel M.P., Supported Chromium Catalysts for Ethylene Polymerization, Adv. Catal. 33 (1985) 47-98

[94] Weckhuysen B.M. & Schoonheydt R.A., Olefin Polymerization Over Supported Chromium Catalysts, Catal. Today 51 (1999) 215-221

[95] Kumkaew P., Wu L., Praserthdam P. & Wanke S.E., Rates and Product Properties of Polyethylene Produced by Co-polymerization of 1-Hexene and Ethylene in the Gas Phase With (n-BuCp)2ZrCl2 on Supports With Different Pore Sizes, Polymer 44 (2003) 4791-4803

[96] Silveira F., do Carmo Martins Alves M., Stedile F.C., Pergher S.B., Rigacci A., Zimnoch J.H. & dos Santos J.H.Z., Effect of the Silica Texture on the Structure of Supported Metallocene Catalysts, J. Mol. Cata. A: Chem. 298 (2009) 40-50

[97] Lee D. & Yoon K., Polymerization of Ethylene by Using Zirconocene Catalyst Anchored on Silica with Trisiloxane and Pentamethylene Spacers, Macromol. Rapid Commun. 18 (1997) 427-431

[98] Bergstra M.F. & Weickert G., Ethylene Polymerization Kinetics with a Heterogeneous Metallocene Catalyst – Comparison of Gas and Slurry Phases, Macromol. Mater. Eng 290 (2005) 610-620

[99] McAuley K.B., MacGregor J.F., Hamielec A.E., A Kinetic Model for Industrial Gas-Phase Ethylene Copolymerization, AIChE J. 36,6 (1990) 837-850

[100] Soares J.B.P., Mathematical Modelling of the Microstructure of Polyolefins Made by Coordination Polymerization: A Review, Chem. Eng. Sci. 56 (2001) 4131-4153

[101] Kiashemshaki A., Moustoufi H. & Sotudeh-Gharebagh R., Two-Phase Modelling of a Gas Phase Polyethylene Fluidized Bed Reactor, Chem. Eng. Sci. 61 (2006) 2997-4006

[102] Shamiri A., Hussain M.A., Mjalli F.S. & Mostoufi N, Kinetic Modeling of Propylene Homopolymerization in a Gas-Phase Fluidized-Bed Reactor, Chem. Eng. J. 161 (2010) 240-249

[103] Meier G.B., Weickert G. & Van Swaaij P.M., Gas-Phase Polymerization of Propylene: Reaction Kinetics and Molecular Weight Distribution, J. Polym. Sci: A 39 (2001) 500-513

[104] Xu Z., Chakravarti S., Harmon Ray W., Kinetic Study of Olefin Polymerization with a Supported Metalocene Catalyst. 1. Ethylene/Propylene Copolymerization in Gas Phase, J. App. Polym. Sci. 80 (2001) 81-114

[105] Song H. & Luss D., Impact of Initiation and Deactivation on Melting during Gas-Phase Olefin Polymerization, Ind. Eng. Chem. Res. 43 (2004) 4789-4795

[106] Eriksson E., Investigation of Heat Transfer and Kinetic Mechanisms in Olefin Polymerisation, Ph.D. Thesis UCBL1 41-2005

[107] Mehdiabadi S. & Soares J.B.P., Influence of Metallocene Type on the Order of Ethylene Polymerisation and Catalyst Deactivation Rate in a Solution Reactor, Macromol. Symp. 285 (2009) 101-114

[108] Pimplapure M., Zheng X., Loos J. Weickert G., Low-Rate Propylene Slurry Polymerisation: Morphology and Kinetics, Macromol. Rapid Commun. 26 (2005) 1155-1158

[109] Ahmadi M., Nekoomanesh M., Jamjah R., Zohuri G. & Arabi H., Modeling of Slurry Polymerization of Ethylene Using a Soluble Cp2ZrCl2/MAO Catalytic System, Macromol.Theory Simul. 16 (2007) 2557-2565

[110] Roos P., Meier G.B., Samson J.J.C., Weickert G. & Westerterp K.R., Gas Phase Polymerization of Ethylene With a Silica Supported Metallocene Catalyst: Influence of Temperature on Deactivation, Macromol. Rapid Commun. 18 (1997) 319-324

[111] Kou B., McAuley K.B., Hsu C.C., Bacon D.W. & Zhen Yao K., Mathematical Model and Parameter Estimation for Gas-Phase Ethylene Homopolymerization with Supported Metallocene Catalyst, Ind. Eng. Chem. Res., 44 (2005) 2428-2442

[112] Kaminsky W., Muller F. & Sperber O., Comparison of Olefin Polymerization Processes with Metallocene Catalysts, Macromol. Mater. Eng. 290 (2005) 347-352

[113] Tisse V.F., Boisson C., Prades F. & McKenna T.F.L., A Systematic Study of the Kinetics of Polymerisation of Ethylene Using Supported Metallocene Catalysts, Chem. Eng. J. 157 (2010) 194-203

[114] Floyd S., Choi K.Y., Taylor T.W. & Ray W.H., Polymerization of Olefins Through Heterogeneous Catalysis III. Polymer Particle Modelling with an Analysis of Intraparticle Heat and Mass Transfer Effects, J. App. Polym. Sci. 32 (1986) 2935-2960

[115] Sliepcevich A., Storti G. & Morbidelli M., Measurement of Diffusivity and Solubility of Olefins in Polypropylene by Gas Chromatography, J. App. Polym. Sci. 78 (2000) 464–473

[116] Martin C. & McKenna T., Particle Morphology and Transport Phenomena in Olefin Polymerisation, Chem. Eng. J. 87 (2002) 89-99

[117] Yiagopoulos A., Yiannoulakis H., Dimos V. & Kiparissides C., Heat and Mass Transfer Phenomena During the Early Growth of a Catalyst in Gas-Phase Olefin Polymerization : the Effect of Prepolymerization Temperature and Time, Chem. Eng. Sci. 56 (2001) 3979-3995

[118] Kittilsen P. & Svendsen H.F., Three-Level Mass-Transfer Model for the Heterogeneous Polymerization of Olefins, J. App. Polym. Sci. 91 (2004) 2158-2167

[119] Kosek J., Grof Z., Novak A., Stepanek F. & Marek M., Dynamics of Particle Growth and Overheating in Gas-Phase Polymerization Reactors, Chem. Eng. Sci. 56 (2001) 3951-3977

[120] McKenna T., Spitz R.& Cokljat D., Heat Transfer From Catalysts with Computational Fluid Dynamics, AIChE J. 45,11 (1999) 2392-2410

[121] Dehnavi M.A., Shahhosseini S., Hashemabadi S.H. & Ghafelebashi S.M., CFD Based Evaluation of Polymer Particles Heat Transfer Coefficient in Gas Phase Polymerization Reactors, Int. Commun. Heat. Mass. 35 (2008) 1375-1379

[122] Chiovetta M.G. & Laurence R.L., Polymer Reaction Engineering: Influence of Reaction Engineering on Polymer Properties, Reichert K.H. & Geiseler W. Eds (1983) Hanser Publishers, Munich

[123] Ferrero M. & Chiovetta,M., Catalyst Fragmentation During Polypropylene Polymerization: Part 1. The Effects of Grain Size and Structure, Polym. Eng. & Sci. 27,19 (1987) 1436-1447

[124] Bonini F., Fraaije V. & Fink G., J. Propylene Polymerization Through Supported Metallocene/ MAO Catalysts: Kinetic Analysis and Modelling, J. Polym. Sci.: A 33 (1995) 2393-2402

[125] Estenoz D. & Chiovetta M., A Structural Model for the Catalytic Polymerization of Ethylene Using Chromium Catalysts. Part I: Description and Solution, Polym. Eng. & Sci. 36,17 (1996) 2208-2228

[126] Estenoz D. & Chiovetta M., A Structural Model for the Catalytic Polymerization of Ethylene Using Chromium Catalysts. Part II: Thermal Effects, Polym. Eng. & Sci. 36,17 (1996) 2229-2240

[127] Estenoz D. & Chiovetta M., Olefin Polymerization Using Supported Metallocene Catalysts: Process Representation Scheme and Mathematical Model, J. App. Polym. Sci. 81 (2001) 285-311

[128] Grof Z., Kosek J. & Marek M., Modeling of Morphogenesis of Growing Polyolefin Particles, AIChE J. 51,7 (2005) 2048-2067

[129] Grof Z., Kosek J. & Marek M., Principles of the Morphogenesis of Polyolefin Particles, Ind. Eng. Chem. Res. 44 (2005) 2389-2404

[130] Alexopoulos A.H., Roussos A. & Kiparissides C.A., Part V : Dynamic Evolution of the Multivariate Particle Size Distribution Undergoing Combined Particle Growth and Aggregation, Chem. Eng. Sci. 64 (2009) 3260-3269

[131] Dompazis G., Kanellopoulos V., Touloupides V & Kiparissides C., Development of a Multi-scale, Multi-phase, Multi-zone Dynamic Model for the Prediction of Particle Segregation in Catalytic Olefin Polymerization FBRs, Chem. Eng. Sci. 63 (2008) 4735-4753

[132] Ha K.-S. Yoo, K.-Y. & Rhee H.-K., Modeling and Analysis of a Slurry Reactor System for Heterogeneous Olefin Polymerization: The Effects of Hydrogen Concentration and Initial Catalyst Size, J. App. Polym. Sci. 79 (2001) 2480-2493

[133] Dompazis G., Kanellopoulos V. & Kiparissides C., A Multi-scale Modeling Approach for the Prediction of Molecular and Morphological Properties in Multi-site Catalyst, Olefin Polymerization Reactors, Macromol. Mater. Eng. 290 (2005) 525-536

[134] McAuley K.B., Talbot J.P. & Harris T.J., A Comparison of Two-Phase and Well Mixed Models for Fluidized Bed Polyethylene Reactors, Chem. Eng. Sci. 49 (1994) 2035-2045

[135] Kapteijn F. & Moulijn J.A., Laboratory Catalytic Reactors: Aspects of Catalyst Testing, in Ertl G., Knozinger H., Schuth F. & Weitkamp J., Handbook of Heterogeneous Catalysis Volume 4, 2nd Edition (2008) Wiley-VCH Verlag

[136] Eigenberger G., Catalytic Fixed Bed Reactors, in Ertl G., Knozinger H., Schuth F. & Weitkamp J., Handbook of Heterogeneous Catalysis Volume 4, 2nd Edition (2008) Wiley-VCH Verlag

[137] Richardson J.F. & Peacock D.G., Coulson & Richardson's Chemical Engineering Volume 3, 3rd Edition (1994) Elsevier Science Ltd UK.

[138] Perry R.H. & Green D.W., Perry's Chemical Engineers' Handbook 7th Ed. (1999) McGraw-Hill Handbooks

[139] Schweich D., Génie de la Réaction Chimique, Technique & Documentation, Paris 2001

[140] Karim A., Bravo J. & Datye A., Nonisothermality in Packed Bed Reactors for Steam Reforming of Methanol, App. Cat. A: Gen. 282 (2005) 101-109

[141] Mears D.E., Diagnostic Criteria for Heat Transport Limitations in Fixed Bed Reactors, J. Catal. 20 (1971) 127-131

[142] Mariani N.J., Keegan S.D. Martinez O.M., & Barreto G.F., Thermal Behaviour of Laboratory Scale Catalytic Packed Beds, Chem. Eng. J. 198-199 (2012) 397-411

[143] Van Antwerpen W., du Toit C.G. & Rousseat P.G., A Review of Correlations to Model the Packing Structure and Effective Thermal Conductivity in Packed Beds of Mono-Sized Spherical Particles, Nucl. Eng. Des. 240 (2010) 1803-1818

[144] Dixon A.G., Fixed Bed Catalytic Reactor Modelling – The Radial Heat Transfer Problem, Can. J. Chem. Eng. 90 (2012) 507-527

[145] Yagi S. & Wakao N., Heat and Mass Transfer from Wall to Fluid in Packed Beds, AIChE J. 5 (1959) 79-85

[146] Kunii D., Suzuki M. & Ono N., Heat Transfer from Wall Surface to Packed Beds at High Reynold's Number, J. Chem. Eng. Jpn. 1 (1968) 21-26

[147] Thoméo J.C., Rouiller C.O. & Freire J.T, Experimental Analysis of Heat Transfer in Packed Beds with Air Flow, Ind. Eng. Chem. Res. 43 (2004) 4140-4148

[148] Puszynski, J. & Hlavacek, V., Experimental Study of Traveling Waves in Nonadiabatic Fixed Bed Reactors for the Oxidation of Carbon Monoxide, Chem. Eng. Sci. 35,8 (1980) 1769-1774

[149] Zehner P. & Schlunder E.U., Warmeleitfahigkeit von Schuttungen bei Massigen Temperaturen, Chem. Ing. Tech. 42 (1970) 933-941

[150] Yagi S. & Kunii D., Studies on Heat Transfer Near Wall Surface in Packed Beds, AIChE J. 6 (1960) 97-104

[151] Winterberg M. & Tsotsas E., Correlations for Effective Heat Transport Coefficients in Beds Packed With Cylindrical Particles, Chem. Eng. Sci. 55 (2000) 5937-5943

[152] Pianko-Oprych P., Modelling of Heat Transfer in a Packed Bed Column, Pol. J. Chem. Technol. 13,4 (2011) 34-41

[153] Zhou Z.Y., Yu A.B & Zulli P., A New Computational Method for Studying Heat Transfer in Fluid Bed Reactors, Powder Tech. 197 (2010) 102-110

[154] Augier F., Idoux F. & Delenne J.Y., Numerical Simulations of Transfer and Transport Properties Inside Fixed Beds of Spherical Particles, Chem. Eng. Sci. 65 (2010) 1055-1064

[155] Beaver M.G. & Sircar S., Short Communication: Comments on the Role of Gas-Phase Axial Thermal Dispersion and Solid-Phase Thermal Conduction for Heat Transfer in a Packed Bed of Solid Particles, Ind. Eng. Chem. Res. 51 (2012) 5826-5829

[156] Wakao N., Kaguei S. & Funazkri T., Effect of Fluid Dispersion Coefficients on Particle to Fluid Heat Transfer Coefficients in Packed Beds, Chem. Eng. Sci. 34 (1979) 325-336

[157] Taniewski M., Lachowicz A., Skutil K. & Czechowicz D., The Effect of Dilution of the Catalyst Bed on its Heat Transfer Characteristics in Oxidative Coupling of Methane, Chem. Eng. Sci. 51 (1996) 4271-4278

[158] Van den Bleek C.M., Van den Wiele K. & Van den Berg P.J., The Effect of Dilution on the Degree of Conversion in Fixed Bed Catalytic Reactors, Chem. Eng. Sci. 24 (1969) 681-694

[159] Al-Dahhan M.H., Wu Y. & Dudukovii,M.P., Reproducible Technique for Packing Laboratory-Scale Trickle-Bed Reactors with a Mixture of Catalyst and Fines, Ind. Eng. Chem. Res 34 (1995) 741-747

[160] Al-Dahhan M.H. & Dudukovii,M.P., Catalyst Wetting Bed Dilution for Improving Catalyst in Laboratory Trickle-Bed Reactors, AIChE J. 42, 9 (1996) 2594-2606

[161] Perego C. & Peratello S., Experimental Methods in Catalytic Kinetics, Catal. Today 52 (1999) 133-145

[162] Berger R.J., Pérez-Ramirez J., Kapeteijn F. & Moulijn J.A., Catalyst Performance Testing; Radial and Axial Dispersion Related to Dilution in Fixed-Bed Laboratory Reactors, Appl. Catal. A: Gen. 227 (2002) 321–333

[163] Moulijn J.A., Pérez-Ramirez J., Berger R.J., Hamminga G., Mul G. & Kapeteijn F., High-Throughput Experimentation in Catalyst Testing and in Kinetic Studies for Heterogeneous Catalysis, Catal. Today 81 (2003) 457–471

[164] Mederos F.S., Ancheyta J. & Chen J., Review on Criteria to Ensure Ideal Behaviours in Trickle-Bed Reactors, Appl. Catal. A: Gen. 355 (2009) 1-19

[165] Cao C., Xia G., Holladay J., Jones E. & Wang Y., Kinetic Studies of Methanol Steam Reforming Over Pd/ZnO Catalyst Using a Microchannel Reactor, Appl. Catal. A: Gen. 262 (2004) 19-29

[166] Eigenberger G., Fixed-Bed Reactors in Ullmann's Encyclopedia of Industrial Chemistry. Vol B4, 1992 VCH Publishers Inc.

[167] De Klerk A., Adiabatic Laboratory Reactor Design and Verification, Ind. Eng. Chem. Res. 44 (2005) 9440-9445

[168] Tavazzi I., Maesti M., Beretta A., Groppo G., Tronconi E. & Forzatti P., Steady-State and Transient Analysis of a CH4-Catalytic Partial Oxidation Reformer, AIChE J. 52,9 (2006) 3234-3245

[169] Ramaswamy R.C., Ramachandran P.A. & Dudukovic M.P., Modeling Catalytic Partial Oxidation of Methane to Syngas in Short-Contact-Time Packed-Bed Reactors, Ind. Eng. Chem. Res. 46 (2007) 8638-8651

[170] Gleaves J.T., Yablonkskii G.S., Phanawadee P. & Schuurman Y., TAP-2: An Interrogative Kinetics Approach, App. Cat. A: 160 (1997) 55-88

[171] Yablonsky G.S, Olea M. & Marin G.B., Temporal Analysis of Products: Basic Principles, Applcations and Theory, J. Cata. 216 (2003) 120-134

[172] Schuurman Y., Aspects of Kinetic Modelling of Fixed Bed Reactors, Catalysis Today 138 (2008) 15-20

Chapter 2

Reactor Model Development

2 Reactor Model Development

The first part of this chapter fully describes the reactor system as it exists, and its purpose. The system and operating method are reviewed in detail and the impact of each aspect considered is evaluated with respect to inclusion in the reactor model. The second section describes the analysis required for the creation of the reactor model followed by its mathematical construction and programming in MATLAB.

2.1 Reactor and System

2.1.1 Purpose

Before creating the model it is useful to understand the background and purpose of the fixed bed polymerisation reactor and the reasons for modelling it.

2.1.1.1 Experimental Set-up

This reactor set-up has been developed as a gas phase alternative to the slurry phase stopped-flow reactor designed by Di Martino et al. [1]. In this light, the main objective for this experimental set-up is to observe the initial moments of the gas phase polymerisation on supported catalysts. Areas of interest are the evolution of particle morphology, physical properties of the polymer and the reaction kinetics during the first few moments of the reaction (0.1-100 seconds). The reactor has already been used to compare the activities of different catalysts and also the effects of varying other parameters which affect catalyst behaviour, such as particle size and co-catalyst concentration [2].

In order to enhance the function of the reactor, another objective of the current thesis is to use the reactor as a calorimeter to gain precise measurements of the initial polymerisation rate, much as was done by Tisse et al. for longer time frames [3].

2.1.1.2 Reactor Model

The purpose of the reactor model is to gain a clear understanding of the temperature and concentration profiles within the reactor during the reaction period and, in particular, the very early moments of the polymerisation when the reaction rate is changing rapidly. The aim is to then use this information in two main ways. Firstly, for prediction, for example, from the measured temperatures the model should be able to calculate how much polymer has been produced in the reactor. Secondly, to analyse whether the reactor is suitable to meet its objectives and what improvements, if any, should be made. Consideration should be given not only to the reactor itself but also to the whole experimental set-up. This version of the model should be suitable for further development, so that a more detailed representation of the polymerisation can be incorporated later. The final aim of the reactor model is to use any

knowledge gained about the polymerisation rate to get a better understanding of the catalyst behaviour.

2.1.2 Description

2.1.2.1 Reactor and Set-up

The system to be modelled consists of a laboratory scale, stainless steel, fixed bed reactor designed to contain a mixture of catalyst and inert solid. It was originally developed by Silva et al. [4], and then further improved by Olalla et al. [5] and Tioni et al. [6].

Images of the reactor are shown in Figure 2-1 and a diagram of how the reactor is assembled is given in Figure 2-2. It is constructed in three sections: an inner cartridge, A, which contains the reactor bed, an outer chamber, B, and a lid, C. The bed volume is 1cm long by 2cm diameter and is enclosed at each end by a porous stainless steel frit of thickness 3mm, and an average pore diameter of 15 microns. The frits are visible in images A and C of Figure 2-1. A black sealing ring to prevent the escape of high pressure reaction gases can also be seen in image C and there is an identical one behind the inner cartridge which holds the reactor bed. The reactor is equipped with two 1mm T-type thermocouples, one at the inlet chamber and one at the exit chamber.

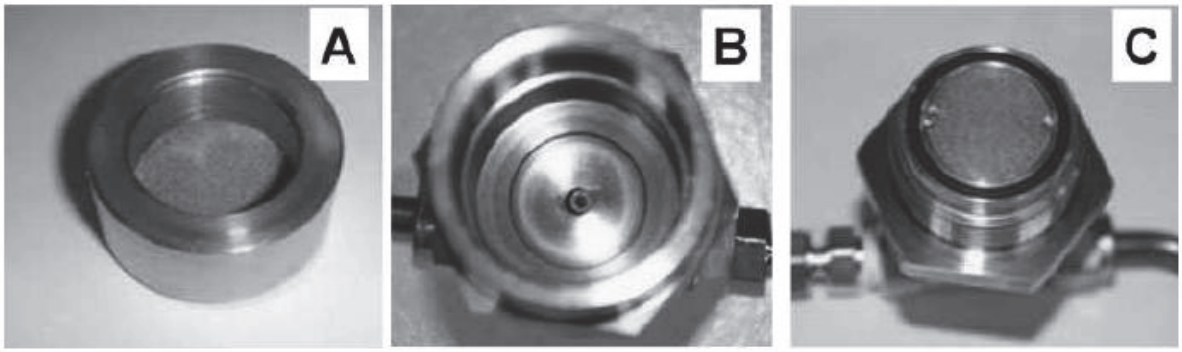

Figure 2-1: View of the three separate parts of the packed bed reactor (A) inner cartridge (B) outer chamber (C) lid

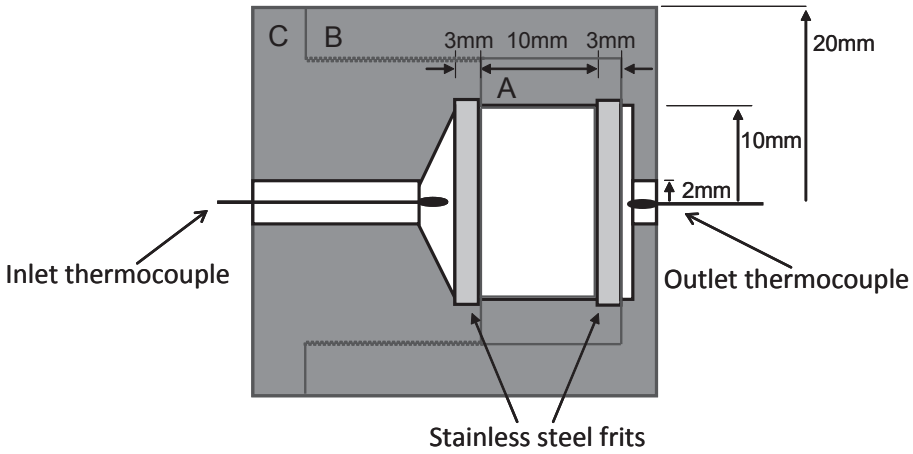

Figure 2-2: Diagram of the assembled packed bed reactor

The flow diagram in Figure 2-3 describes the experimental set-up. The reactor is plunged into a hot water bath controlled at 353±1 K that fixes the external temperature. The reaction gas is supplied from a ballast tank fitted with a pressure indicator. The supply line passes through a pressure regulator which is used to set the downstream reactor pressure followed by a set of coils in the hot water bath and finally a miniature solenoid valve. The valve and piping outside the hot water bath are electrically traced. Argon is supplied to the system downstream of the pressure regulator and CO_2 is supplied via another miniature solenoid valve.

The reactor outlet line is fitted with a manual flow controller and a ball float flowmeter, calibrated under reaction conditions [2]. There is an alternative route directly to vent fitted with a third miniature solenoid valve. The solenoid valves are all controlled directly by computer. They are set to open and close for a preset time period which fixes the reaction duration. The minimum time between subsequent operations of the automatic valves is 0.1s.

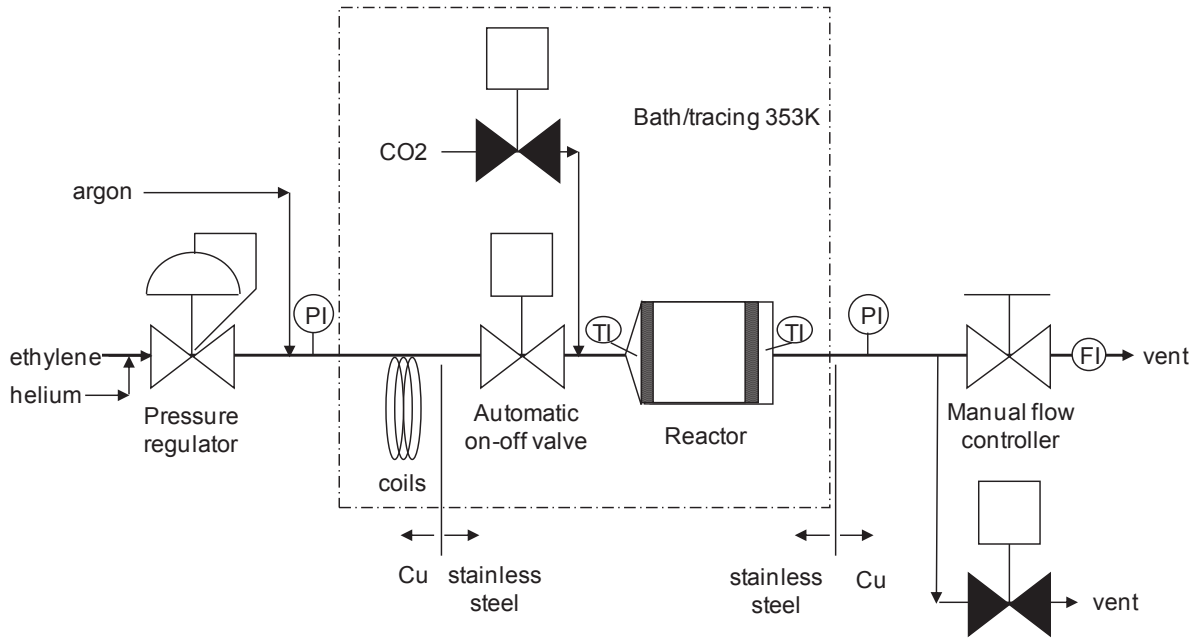

Figure 2-3 Flow diagram of the reactor and experimental set-up

2.1.2.2 Materials

For a standard experiment the reaction gas composition is 67mol% ethylene and 33mol% helium. It is possible to operate with other gas compositions and this is controlled by filling the upstream ballast in the desired proportions.

The reactor bed composition is a mixture of catalyst and inert solid with the catalyst comprising 3 – 5 wt% of the bed. The catalyst is a silica supported metallocene, of average particle diameter 58 μm, prepared using the method described by Tioni [2].

The inert solid can be silica in the form of the raw catalyst support or NaCl prepared according to the methods described by Tioni [2]. Two types of NaCl are used: cubes of 250μm – 500 μm and smaller NaCl particles of diameter 45 – 63 μm, with an open structure of agglomerated 5 – 10 μm cubes.

2.1.2.3 Operating Method

The reactor bed is filled and the reactor assembled under argon in the glove box. The initial masses of catalyst and inert solid are recorded. The reactor system is prepared by setting the hot water bath and electrical tracing temperatures, filling the ballast tank and sweeping with argon at atmospheric pressure to remove impurities.

When the reactor is put in position it is swept with argon whilst the temperatures measured in the reactor inlet and outlet chambers stabilise. Once the temperatures are steady, the gas pressure is set to 9 bar gauge at the upstream pressure controller and the computer is set to control the automatic opening and closing of the miniature solenoid valves. The gas flows through the reactor and the flowrate is measured manually using the flowmeter on the reactor outlet line. At the end of the reaction period the automatic valves switch to allow rapid degassing and also CO_2 flow through the reactor. This quenches the polymerisation reaction by catalyst poisoning and provides cooling to the reactor bed. Temperature data is collected automatically from the thermocouples and saved to computer.

The reactor is returned to the glove box for weighing and to recover the polymer produced for analysis. The mass of polymer produced is found from the difference in the initial and final masses of the reactor inner cartridge.

2.1.2.4 Experimental Results

A list of experiments is given in Appendix 1. For each experiment, measured inlet and outlet temperatures are recorded on the computer by the data acquisition program. Also recorded are:

- reaction duration (from 0.1s to 30s)
- mass of catalyst (45 – 120 mg)
- mass of inert (<1 g)
- polymer yield (<1.4 $g.g^{-1}$)
- reactor exit gas flowrate (90 – 310 $mL.s^{-1}$)

The data ranges for the experiments initially presented for modelling are shown in brackets. The maximum average reaction rate observed was for the experiment of shortest duration (0.1s) with a yield of 0.068 g_{PE}. $g^{-1}_{catalyst}$ giving an average polymerisation rate of about 2500g_{PE}. $g^{-1}_{catalyst}.h^{-1}$.

The measured temperatures for a typical experiment of duration 4s are shown in Figure 2-4. It can be seen that a significant proportion of the total heat of reaction is removed during the cooling by CO_2.

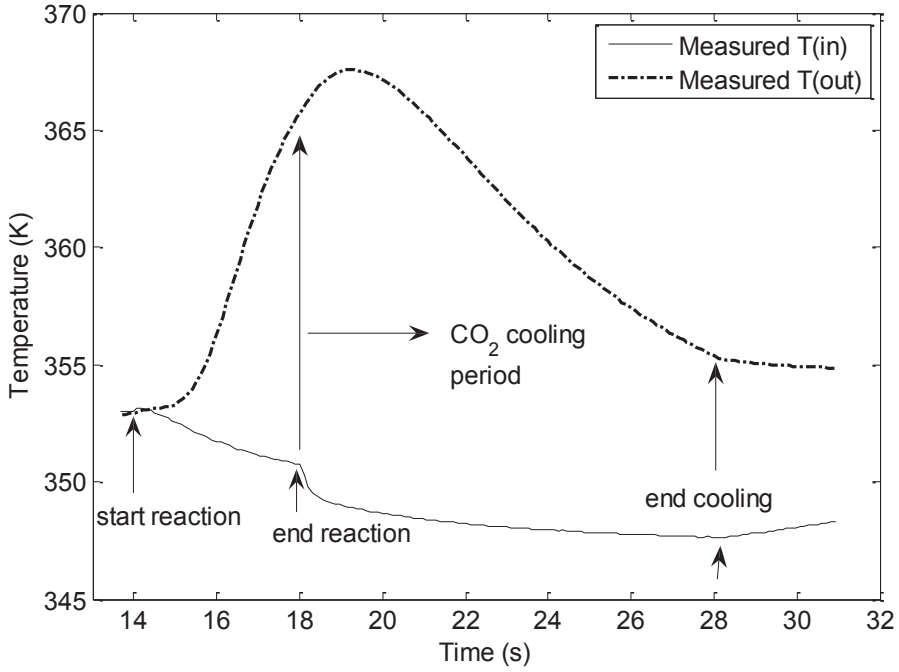

Figure 2-4: Temperature measurements for typical reaction of duration 4s

2.1.3 Review of the Experimental System and Operating Methods

A first consideration of the experimental temperature profiles led to some early points and questions about the reactor system:

- It is clear from Figure 2-4 that the heat generated during the polymerisation is evacuated from the reactor during both the reaction and cooling stages of the experiment and so these will both need to be studied. In the existing set-up the flowrate of CO_2 used for the cooling stage is not measured.

- A peak in the measured inlet temperature can be identified at the start of each experiment as shown in Figure 2-5. It was not known whether this was related to the very strong heat of reaction or an artefact of the system.

- At the start of each experiment the measured reactor outlet temperature always seems to behave in the same way as shown in Figure 2-6. This is unexpected because there is variation in the mass of catalyst and in the observed average reaction rates.

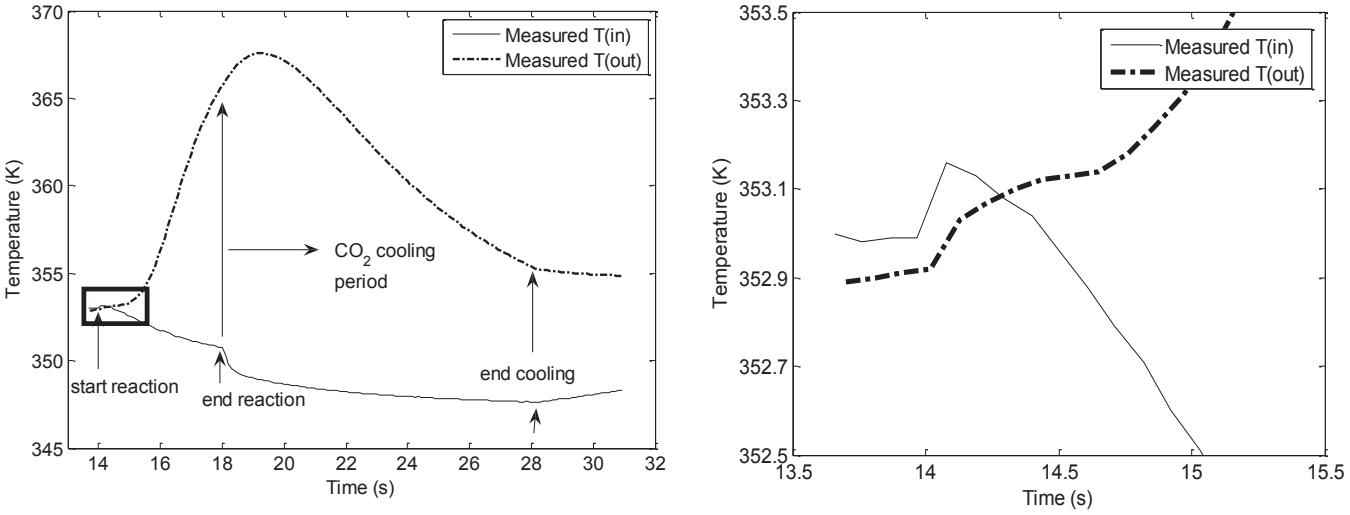

Figure 2-5: Zoom on measured reactor inlet temperature at the start of typical experiments (NaCl seedbed, 90 mL.s^{-1} reaction gas)

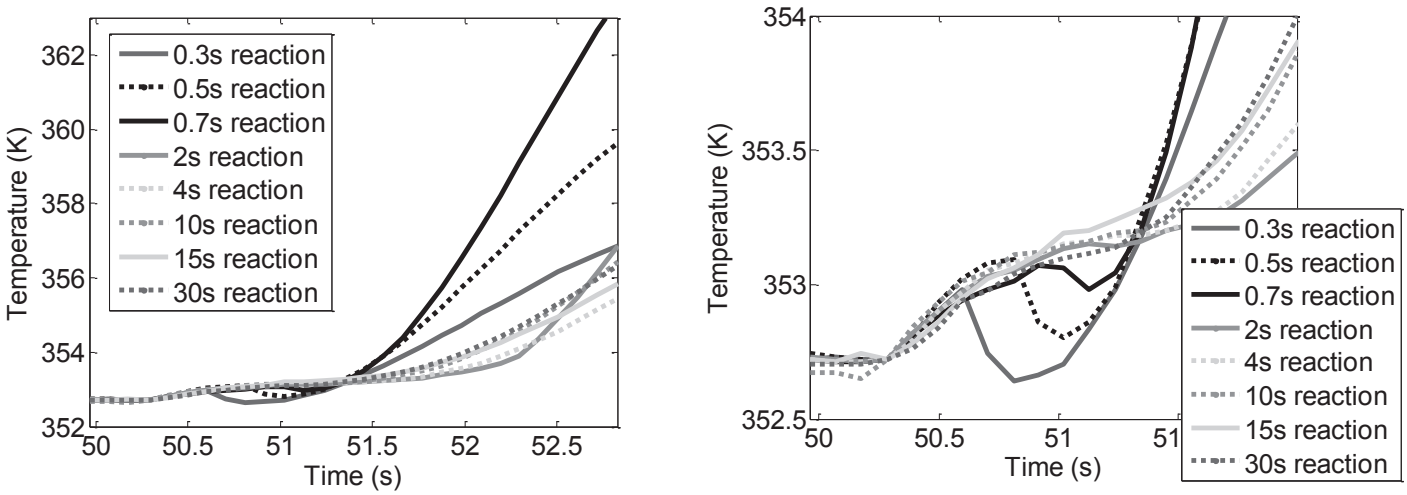

Figure 2-6: Zoom on measured reactor outlet temperature at the start of typical experiments (NaCl seedbed, 90 mL.s^{-1} reaction gas)

Before constructing a model of the reactor, the whole system along with its method of operation and typical experimental results was reviewed. Some experiments were carried out with no catalyst (listed in Appendix 1) to understand the behaviour of the system. As

would be expected, there is some overlap with the work of Tioni [2] who was working with the same system.

To review the reactor system, we need to know the physical properties of the materials used. Physical data and estimation methods for gas viscosity, thermal conductivity, and specific heat capacity are given in Appendix 2.

2.1.3.1 Stainless Steel Frits

The purpose of the stainless steel frits at each end of the reactor bed is to contain the bed without causing significant pressure drop and, also, to evenly distribute the gas flow at the reactor inlet. A frit was weighed and carefully measured to determine its porosity and thickness. The porosity was found to be 0.398 and the thickness was 3.03 mm. It is important to note that the thermocouples are outside these frits with respect to the reactor bed.

2.1.3.2 System Pressure Drops

The pressure drops across the reactor bed and in the tubing were evaluated. The flowrates of 90 and 300 mL.s^{-1} (STP) during the reaction period are towards the high end compared to the usual values of 0.17 mL.s^{-1} to 17 mL.s^{-1} for laboratory scale fixed beds cited by Kapetijn & Moulijn [7]. Note that the pressure drop over the system can be estimated from the pressure gauge readings on the lines upstream and downstream from the reactor. For reaction gas flowing at 90 mL.s^{-1} (flowmeter conditions) the measured pressure drop is about 0.25 bar; at the higher flowrate and with the CO_2 it is much higher (>1 bar) and quite variable.

2.1.3.2.1 Reactor Bed

The Ergun equation (2-1) is used to estimate pressure drop across a packed bed.

$$-\frac{dP}{dz} = \frac{150(1-\varepsilon)^2}{\varepsilon^3}\frac{\mu}{d_p^2}u_v + \frac{1.75(1-\varepsilon)\rho u_v^2}{\varepsilon^3 d_p}$$

2-1

Using the reaction conditions given in Appendix 1 and the physical data listed in Appendix 2, the pressure drop was calculated for the two flowrates used and both types of seedbed. The Ergun equation was developed for a fixed bed of spherical particles which applies well to the silica seedbed but the NaCl particles are agglomerates of small cubes with an open structure, so the result for this seedbed is more approximate. The maximum pressure drop is found for the seedbed of fine NaCl at 9 bar gauge pressure with 310 mL.s^{-1} gas flow as measured at the flowmeter. This seedbed has an extremely high porosity, around 0.8, because of the

unusual shape of the particles. The calculated value is 0.1 bar. At the lower flowrate of 90 mL.s^{-1}, the value is 0.03 bar. This is negligible when compared against the total reactor pressure.

2.1.3.2.2 Heating Coils

The line sizes and lengths used in the reactor system are detailed in Appendix 2. The main pressure drop will be over the heating coils as they are the longest length of pipe and have the smallest diameter. The approximate pressure drop over a section of pipe can be checked using the equation for isothermal flow of ideal gas in a horizontal pipe with the kinetic energy term neglected [8]:

$$\frac{\Delta P}{v_m} + 4\frac{R'}{\rho u^2}\frac{l}{d}\left(\frac{G}{A}\right)^2 = 0 \qquad \textbf{2-2}$$

Applying this equation to a flow of 310 mL.s^{-1} (STP) of reaction gas through the coils gives an estimated pressure drop of 0.26 bar. This value for the maximum flow case seems quite high. For a reaction gas flow of 90 mL.s^{-1} (STP) the calculated pressure drop for the same section of pipe is only 0.02 bar

2.1.3.2.3 Stainless Steel Frits

The two 15 µm stainless steel frits of thickness 3 mm which hold the reactor bed in place were evaluated for pressure drop. The pressure drop for flow through a fritted metal filter is determined by its permeability. Equation 2-3 is the Darcy equation for flow through a porous medium where α_0 is the permeability coefficient.

$$P\frac{\Delta P}{P_m} = \frac{l_f \mu Q}{A\alpha_0} \qquad \textbf{2-3}$$

Hydraulic data is available in the literature for 10 µm and 20 µm fritted stainless steel filters [9]. From the literature data and the Darcy equation, the permeability of 15 µm stainless steel frit is estimated to be 1.86E-13 m^2. From this, the maximum pressure drop across the stainless steel frits during the reaction period is calculated to be 0.38 bar for the higher flowrate of 310 mL.s^{-1} as measured at the flowmeter.

2.1.3.2.4 CO_2 Pressure and Flowrate

To analyse the system behaviour during the cooling stage of operation, the CO_2 pressure and flowrate are needed. The CO_2 gauge pressure is set at the bottle to either 6 bar or 9 bar. With the bottle pressure set to 6 bar gauge, the reactor inlet and outlet gauge pressure readings are about 1.85 bar and 0.3 bar respectively during the cooling period. This is a total pressure drop of 1.55 bar for the whole reactor and fittings. The reactor pressure is estimated as the midpoint of these two values.

The CO_2 flowrate could not be measured using the existing flowmeter. Tioni made an estimate using a soap bubble flowmeter and found it to be slightly > 200 $mL.s^{-1}$ with the bottle pressure set to 6 bar gauge. Estimating the flowrate at 298K and atmospheric pressure by calculation from the reactor pressure drop gives CO_2 flowrates of 220 $mL.s^{-1}$ and 330 $mL.s^{-1}$ with respective bottle pressures of 6 and 9 bar gauge. The measured and calculated values are in good agreement and will be used in the model. These values are estimates because polymer can build up on the outlet frit affecting measured reaction gas flowrates and this factor is not taken into account.

A check of the pressure drop over the reactor bed during cooling with CO_2 gives a maximum of 0.43 bar. This is at the higher flowrate of 330 $mL.s^{-1}$, assuming 2.1 bar absolute reactor pressure and with the fine NaCl seedbed.

2.1.3.2.5 Conclusion

At the lower reaction gas flowrate pressure drops are negligible but at the maximum flowrate the system is very close to capacity and the pressure drop starts to become significant. Most of the pressure drop in the experimental set-up is across the coils in the hot water bath and the two stainless steel frits which hold the fixed bed in place. During the cooling period pressure drops are also quite high.

2.1.3.3 Temperature Measurement

The first observation that can be made from the measured outlet temperature profiles is that a significant proportion of the total heat of reaction is removed during cooling by CO_2 so this period must be included in the modelling work. As mentioned earlier, another observation is that the measured outlet temperature seems to always respond initially in the same way for different experimental conditions.

2.1.3.3.1 Accuracy of Thermocouples

In this experimental set-up, thermocouple accuracy is important as temperatures are expected to be changing rapidly. 1 mm sheathed T-type (copper/constantan) thermocouples are used and these have a response time of 150 ms. This is defined as the time to reach 63.2% of the instantaneous step change in temperature on being plunged from air at 293 K into boiling water. Where measured temperatures are changing rapidly, the thermocouple time constant can be used to calculate back to the real system temperatures [10]. Moffat [11] states that T-type thermocouples are very susceptible to conduction error because of the high conductivity of the copper wire used to make them and that they should not be run along a temperature gradient. Because of this, two verifications of the thermocouples were made. In the first, a finer thermocouple was tested. No difference in measured temperatures was found between the thermocouples but the finer one was less mechanically robust. In a second test, the thermocouple was subjected to a steep temperature gradient in the laboratory and the measurement error was found to be negligible.

2.1.3.3.2 Compression Effects

As mentioned previously, a peak in the measured inlet temperature is observed at the start of each experiment. To determine whether this was related to the strong heat of reaction or an artefact of the system, experiments with no catalyst were carried out. Figure 2-7 compares the measured inlet temperature for an experiment with no catalyst (solid line) against experiments with catalyst (dashed lines). It is clear that the initial peak occurs in the case with no catalyst, so cannot be linked to the reaction.

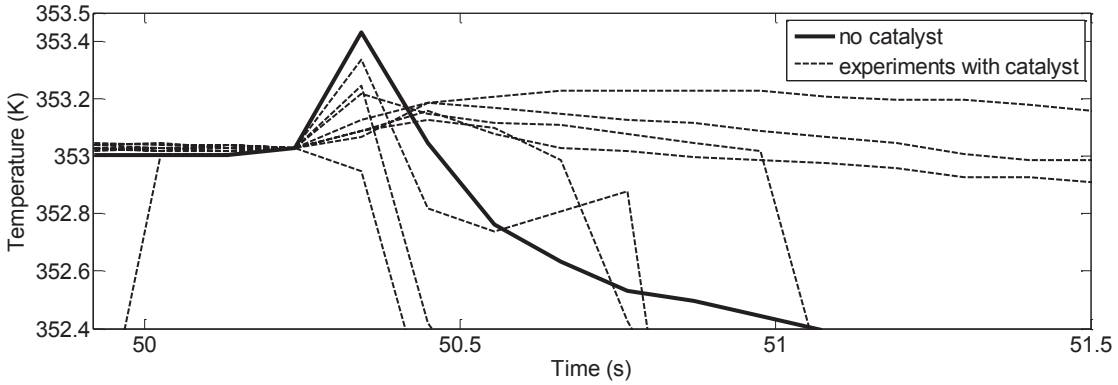

Figure 2-7: Comparison of inlet temperatures in the first moments of the reaction period for several experiments of short duration with fine NaCl seedbed. Solid line represents experiment with no catalyst.

A possible explanation for this small temperature peak is in the system operating method. The reactor is swept with argon prior to the experiment but not pressurised. At the instant the solenoid valve opens to allow the flow of reaction gas, there is a sudden pressurisation of

the argon remaining in the system from about atmospheric pressure to 9 bar gauge pressure. The temperature peak observed seems to be due to the heat of compression.

To evaluate whether this is the case, and if it is significant, the system must be considered in more detail. The thermocouple is positioned in the reactor inlet chamber. The volume of gas between the automatic valve and the thermocouple is 6 mL. The system is open and gas passes from the inlet chamber through the stainless steel frit and into the reactor. Equation 2-4 can be used to calculate the temperature rise of a gas under isentropic compression. In our case the compression is not isentropic, the system is open and heat is transferred to the surroundings. However, this equation can be used with the specific heat of the gas to estimate whether this extra energy entering the reactor is significant and if the observed temperature rise is close to what would be expected for the compression of this small volume of gas.

$$\frac{T_2}{T_1} = \left(\frac{P_2}{P_1} \right)^{\frac{\gamma-1}{\gamma}}$$

2-4

The energy produced by the isentropic compression of 6 mL of argon from atmospheric pressure to 9 bar gauge pressure is about 1.5 J. From the reactor diagram, it seems likely that most of this heat would be transferred to the stainless steel frit at the reactor inlet. 1.5 J would be enough to raise the frit by 0.66 K. This is slightly more than the measured temperature peak, but considering the position and response time of the thermocouple and the high gas flowrate, it seems reasonable to conclude that the observed temperature effect is due to compression.

A quick comparison with the heat generated in a polymerisation experiment will serve to determine whether this effect is significant. The heat of reaction for ethylene polymerisation is 3830 $J.g^{-1}$ and the smallest measured quantity of polymer formed is 4.5 mg. The minimum heat release by the polymerisation in an experiment with catalyst will then generate 17 J, significantly more than the heat of compression, which can therefore be assumed negligible.

One other effect of the sudden compression of the system is a slight compaction of the reactor bed. The reduction in bed volume was measured to be 1 mm, or about 10% of the total.

2.1.3.3.3 Position of the Inlet Thermocouple

Before the experiment, the reactor inlet temperature is steady at 353K. During the experiment, it reduces slightly towards a new steady value. This is because heat now has to be transferred to a flowing gas, as for a standard heat exchanger. Because the position of the thermocouple in the reactor inlet chamber cannot be inspected visually it is not certain whether the measured temperature is that of the inlet frit or the gas in the inlet chamber. This point will be considered during the model validation in Chapter 3 section 3.1.3.

2.1.3.3.4 Adsorption of Ethylene on Silica

To gain a better understanding of the influence of the reactor itself on the measured outlet temperatures, experiments without catalyst were carried out and with two alternative seedbeds, NaCl and silica, with particles of similar size. Figure 2-8 shows the response of the measured reactor temperatures to the initial flow of reaction gas and Figure 2-9 compares them on the same graph. It is clear that behaviour of the reactor is different for each seedbed. It was thought that this could be due to the adsorption of ethylene onto the surface of the silica. This is as a result of the large difference in specific surface between the two seedbeds; the surface of the silica is 290 $m^2.g^{-1}$ [12] compared to an estimated 0.074 $m^2.g^{-1}$ for the NaCl.

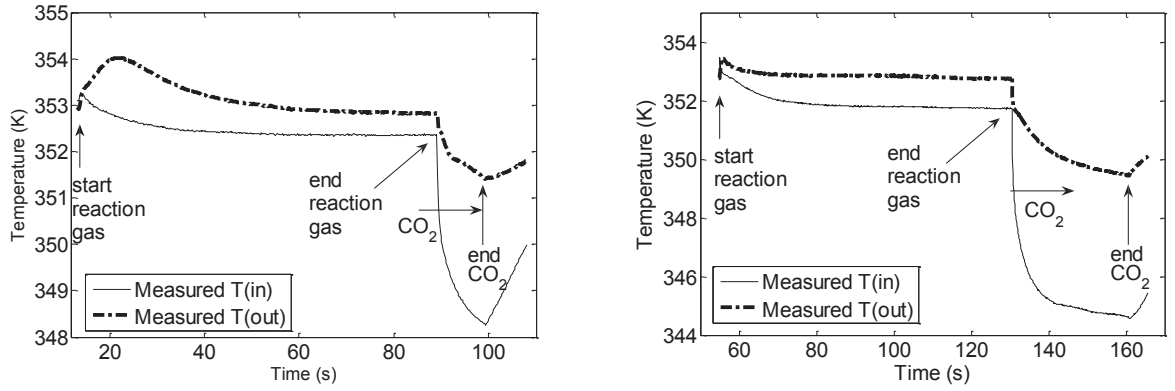

Figure 2-8: Measured inlet and outlet temperatures for 90 $mL.s^{-1}$ ethylene/helium with no catalyst at 353K (a) EXP_2 silica seedbed (b) EXP_17 fine NaCl seedbed

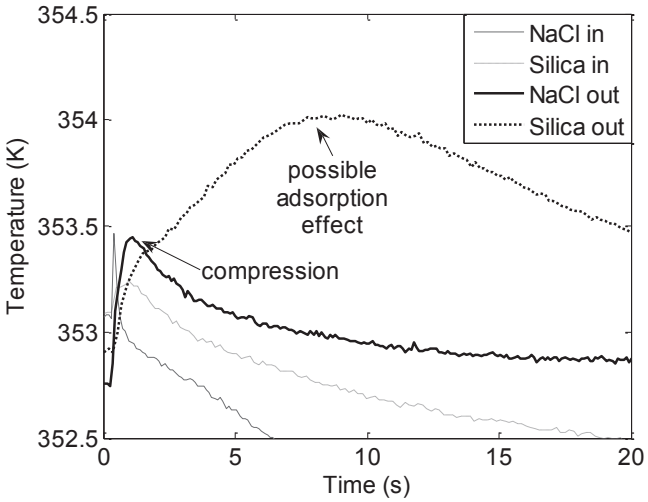

Figure 2-9: Measured inlet and outlet temperatures for experiments with alternative seedbeds and no catalyst

No data was found in the literature for the adsorption of ethylene on amorphous silica. However, data is available for the adsorption of ethylene on silica gel [13, 14]. If the simplifying assumption of similar surface chemistry for silica gel and precipitated silica is made, the quantity of ethylene adsorbed on the amorphous silica surface and the heat of adsorption can be estimated. From this, the expected effect of ethylene adsorption on reactor outlet temperatures can be evaluated.

Olivier & Jadot [14] measured the quantity of ethylene adsorbed on a silica gel of surface 720 $m^2.g^{-1}$ as 2.43 $mmol.g^{-1}$ at 293 K and 6.67 bar absolute. Simply multiplying by the ratio of the two specific surfaces, 290 $m^2.g^{-1}$ to 720 $m^2.g^{-1}$, gives an estimate of 0.98 $mmol.g^{-1}$ ethylene adsorbed by our amorphous silica under the same conditions.

Olivier & Jadot's data is measured at three different temperatures. This means the Clausius-Clapeyron equation (2-5) can be used to estimate the heat of adsorption for a fixed quantity of ethylene adsorbed. The calculated value is 23.8 $kJ.mol^{-1}$ at 0.98 $mmol.g^{-1}$ which equates to 23.3 $J.g^{-1}$ of silica and is of the same order as the value of 35.1 $kJ.mol^{-1}$ for ethylene on hexagonal mesoporous silica published by Newalker et al. [15].

$$\ln P = \frac{\Delta H_{ads}}{R}\frac{1}{T} + C \qquad \text{2-5}$$

Experiment EXP_9 was carried out at 293 K with a silica seedbed of 0.5 g, 6.67 bar absolute ethylene and no catalyst. Figure 2-10 shows the measured temperatures at the reactor inlet and outlet. From the heat of adsorption calculated above, the energy released for this experiment should be about 12 J. Assuming the reactor to be adiabatic, integration of the

difference between the measured inlet and outlet temperatures by Simpson's rule allows a rough estimate of the heat released as 8.4 J. This value is of the same order as would be expected for the adsorption of ethylene on silica. The difference in the two values could come from the fact that our silica was not dried prior to this experiment and from the assumption of adiabacity. It therefore seems reasonable to assume that adsorption of ethylene on the silica surface is the cause of the difference between the measured outlet temperatures for the silica bed and the NaCl bed.

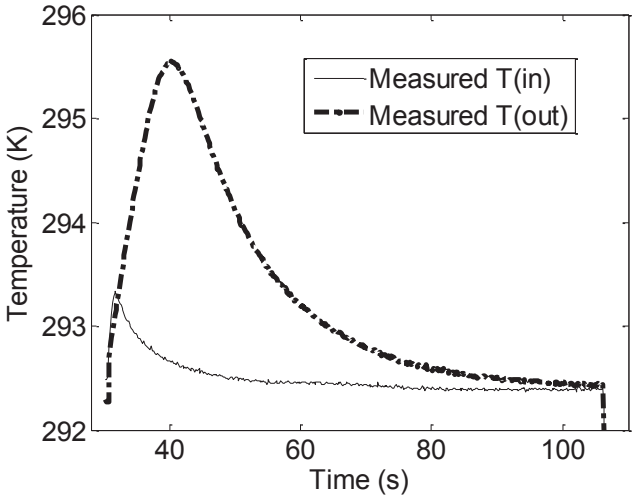

Figure 2-10: Measured inlet and outlet temperatures for EXP_9 with silica seedbed, 6.67 bar absolute of ethylene and no catalyst at 293 K

Another experiment, EXP_2, was carried out at the usual operating temperature of 353 K with a silica bed, 6.67 bar absolute of ethylene and no catalyst. Again, assuming the reactor to be adiabatic, and integrating the difference between the measured inlet and outlet temperatures, the quantity of heat released is calculated at 5.3 J. This is significant when compared with the minimum heat of polymerisation of 17 J. Another difficulty with this seedbed was the problem of separating polymer/catalyst from the raw silica after the reaction [2] and the use of the raw silica seedbed was not continued. Following this exercise it was decided to use only NaCl as the inert solid in the reactor bed in order to avoid unnecessary complication.

As the raw form of the catalyst support undergoes significant temperature increase on the sudden contact with ethylene, there may also be a similar effect with actual catalyst, despite the changes in surface chemistry.

2.1.3.3.5 Gas Expansion

Figure 2-11 shows the measured inlet and outlet temperatures for an experiment carried out at room temperature with a NaCl seedbed, no catalyst and no bath. It can be observed that

the outlet temperature remains below the inlet temperature during the argon sweep and the passage of the reaction gas and the CO_2. The gas expands with the pressure drop over the reactor causing some cooling. As this experiment was carried out with no water bath it does not represent the system exactly. However, it is important to note that the reactor pressure drop has an influence on measured outlet temperatures and that the greater the gas flowrate the greater this effect will be.

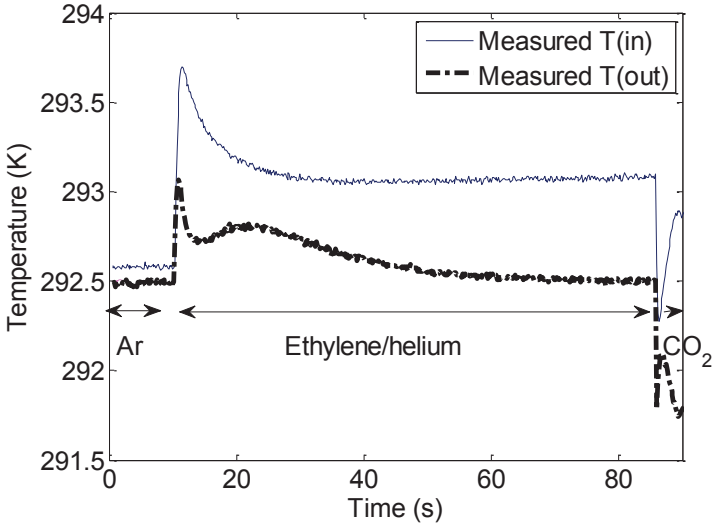

Figure 2-11: Measured inlet and outlet temperatures for EXP_14. NaCl seedbed, No catalyst, 90 mL.s^{-1} ethylene/helium, room temperature, no bath

2.1.3.3.6 Conclusion

To sum up the observations regarding temperature measurement of the reactor: firstly, the thermocouples used are sufficient for the requirements of this experimental set-up. The small peak in measured inlet temperature which marks the start of each experiment is due to sudden compression of gas in the system and is negligible compared to the heat of reaction. Adsorption of ethylene on silica causes a significant temperature effect if a silica seedbed is used, so it is better to use NaCl, and reactor pressure drop has a measurable effect on outlet temperature.

2.1.3.4 Reaction Rate Profile

Figure 2-12 shows a typical reaction rate profile which has been calculated from the measured mass of polymer formed for experiments of different duration. As observed by Tioni [2], there is a rapid decrease in the reaction rate during the first few seconds of the polymerisation. The reason for the decreasing reaction rate is not completely known. However, this profile is typical for ethylene polymerisation using this reactor and Tioni's [2] reaction conditions. Metallocene active sites are sensitive to poisoning and no scavenger is used in this reactor which suggests that the deactivation is due principally to chemical effects.

There is also an unexplained oscillation in the reaction rate during the first second of the experiment. No corresponding oscillation is found in the measured outlet temperature. However, it should be underlined that the rate curve in Figure 2-12 is assembled from 6 separate experiments. Very little polymer is produced in experiments of duration <1s so weighing errors are possible. Also, the apparent fluctuation in reaction rate is very rapid and it is possible that the measured outlet temperature is not sensitive to this.

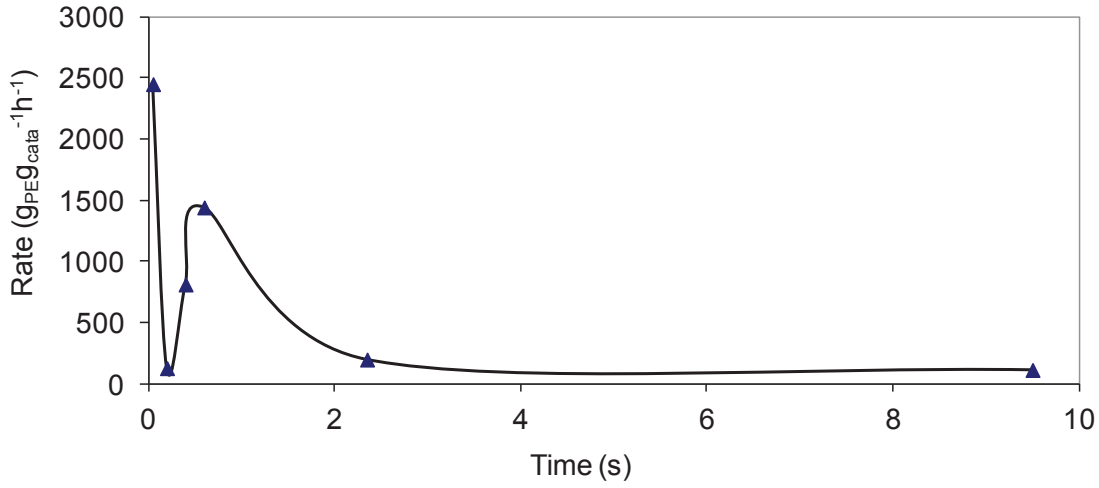

Figure 2-12: Instantaneous reaction rate calculated from the measured mass of polymer formed with the fine NaCl seedbed and at the maximum gas flowrate

2.1.3.5 Packed Bed Dilution

As discussed in the literature survey, dilution of the catalyst in a packed bed using an inert solid is useful for reducing thermal gradients. Points to consider are the effect on the hydrodynamics of the packed bed including an eventual effect of poor mixing, channelling and bypassing on the reaction kinetics and also the effect on the particle heat transfer coefficient of an increased number of contact points with the surrounding solid. Particle shape and growth effects will be discussed later in this chapter, section 2.2.1.1.

2.1.3.5.1 NaCl Particle Size

Tioni [2] experimented with two types of NaCl seedbed; the first consisted of crystals in the size range 250 – 500 µm, the second was crystals of size 5-10 µm agglomerated into particles of 45 – 63 µm. Experiments carried out at 353K and with a measured gas flowrate of 30 $mL.s^{-1}$ at the flowmeter showed the smaller NaCl crystals to be more effective in moderating the reactor temperature and reducing temperature excursions.

As discussed later, in section 2.2.2, axial dispersion is negligible in this reactor under all the operating conditions studied. The effect of the smaller NaCl crystals on reactor temperature

can be explained by the difference in the heat transfer rates for the two seedbeds. Table 2-1 compares the heat transfer rate out of the catalyst particles against the heat transfer rate to the alternative NaCl seedbeds. The values are calculated for the whole reactor volume and the experimental conditions. The heat transfer coefficients are determined using the correlations described later in this chapter, section 2.2.1. Although the larger NaCl crystals have more mass, and hence more total heat capacity, they have much less surface area and a lower heat transfer coefficient. The total heat transfer rate to the large NaCl crystals is about the same as the heat transfer rate from the catalyst particles whereas for the small NaCl particles the heat transfer rate is much greater so they can be far more responsive in absorbing rapid heat production.

	Catalyst Particles	Large NaCl	Small NaCl
Diameter (μm)	58 (d_{50})	250 – 500	45 – 63
Shape	spheres	cubes	agglomeration of 5-10 μm cubes
Typical mass used (g)	0.04	3.3	1
Particle density ($g.cm^{-3}$)	0.795	2.17	2.17 (sub particles)
Total volume of particles (cm^3)	0.05	1.52	0.46
Bed porosity (cm^3)	-	1.57	2.63
Total solid surface (cm^2)	52	180-365	2800-5500
Heat transfer coefficient ($W.m^{-1}.K^{-1}$)	3000	540-880	12000-22000
Heat transfer rate per degree of temperature difference ($W.K^{-1}$)	15.6 (evacuation rate)	10-32 (uptake rate)	3000-12000 (uptake rate)

Table 2-1: Comparison of heat transfer rates from catalyst and to large and fine NaCl crystals

2.1.3.5.2 Bed Uniformity and Stability

To get an idea of the make up of the bed with fine NaCl as the inert solid, consider that the catalyst typically represents 3 – 5 wt% of the total bed weight and also that a typical charge of catalyst is about 40 mg with approximately 1 g of small NaCl particles. This means that the total numbers of catalyst and NaCl particles are about 10^5 and 3×10^7 respectively, which is a ratio of about 1:300.

The method of mixing the catalyst and inert together is simply to shake them in a round bottomed flask so there is probably some heterogeneity within the bed. The less well mixed the bed, the less effective the inert solid will be at moderating temperature as clumps of catalyst particles could lead to hot spots.

The gas flowrate through the reactor is very high so an experiment was carried out to check whether the catalyst particles could be blown through the bed towards the outlet frit. Reaction gas was passed through a mixed reactor bed of silica and NaCl then the bed was divided into upstream and downstream sections. The material from each section was weighed then washed and dried and the remaining silica weighed again. The upstream and downstream sections were found to contain 6 wt% and 5.5 wt% silica respectively. It was therefore concluded that the reactor bed is quite stable.

2.1.3.5.3 Effect on Reaction Kinetics

As discussed in the literature review, section 1.3.3.2.3, dilution with an inert solid reduces the conversion in a catalyst bed. Equation 2-6 is the criteria of Moulijn et al. [16] to evaluate the impact of bed dilution on conversion.

$$\Delta = \left(\frac{b_d}{1 - b_d} \right) \left(\frac{d_p}{l_b} \right) \left(\frac{x_{idil}}{2} \right) n$$

2-6

Where Δ is a measure of the reduction in conversion given by:

$$\Delta = \left(\frac{x_{und} - x_{idil}}{x_{und}} \right)$$

2-7

Applying equation 2-6 to the packed bed shows that when the fine salt particles are used as the inert solid, the effect of reactor bed dilution on conversion is negligible (<1%). However, for the larger salt particles it would have to be taken into consideration.

2.1.4 Conclusion

A thorough review of the system and its operation has been carried out. Pressure drops are becoming significant at the higher reaction gas flowrate with the greatest pressure drops calculated for the stainless steel frits and the coils in the hot water bath. The observed thermal effects for the measured inlet temperature are due to the compression of the system and this can be neglected. However, the effect of adsorption of ethylene on raw silica must be included if experiments with a silica seedbed are modelled.

The reaction rate is initially high and decreases extremely rapidly. Small NaCl particles are more effective at stabilising bed temperatures. The effects of dilution on the polymerisation should be negligible but there is a risk of poor mixing of catalyst and inert solid.

2.2 Model Construction

The measured temperatures in this system are at the reactor inlet and outlet chambers, outside of the stainless steel frits with respect to the packed bed, and so, the frits must be included in the reactor model. Likewise, the temperature of the hot water bath is known, but not the temperature of the 10mm thick reactor wall and so this must also be modelled.

The following assumptions are made in the initial model construction:

- constant total pressure.
- constant bath temperature at 353 K.
- constant flowrate at reactor exit.

Later, in Chapter 4, the assumptions will be reviewed in conjunction with the new information provided by the model validation. In particular, we will see that the pressurisation time of the reactor system should be taken into account.

2.2.1 Heat Transfer Correlations

Heat transfer parameters are required for determination of the required type model and construction of the reactor model. The correlations used to evaluate the heat transfer parameters are widely accepted and are listed in Table 2-2 with values calculated for typical reactor conditions.

2.2.1.1 Particle Heat Transfer Coefficient

In general, correlations for particle heat transfer coefficients are derived from experiments using packed beds of spherical particles where heat transfer occurs through convection and point contact. For the model, a particle heat transfer coefficient is only required for the catalyst particles which are quite spherical in shape. No heat transfer coefficient is needed for the NaCl particles as they are not taken into account separately.

The particle heat transfer coefficient value given in Table 2-2, per the Kunii & Levenspiel correlation, was compared to the values predicted by the correlations of Martin [33] (3860 $W.m^{-2}.K^{-1}$) and of Wakao et al. [33] (4160 $W.m^{-2}.K^{-1}$) which are of the same order and within the range of those found in the literature [17]. The Reynolds numbers for the catalyst particles are in the range 1 – 4 depending on the gas flow rate.

Parameter	Correlation	Calculated Value [a]
Heat transfer coefficients:		
catalyst particle	Kunii & Levenspiel [18]	4870 $W.m^{-2}.K^{-1}$
reactor internal wall	Specchia et al. [19]	3815 $W.m^{-2}.K^{-1}$
reactor external wall [32]		3000 $W.m^{-2}.K^{-1}$
Effective bed conductivity:		
radial	Kunii & Smith [20]	0.09 $W.m^{-2}.K^{-1}$
axial	Yagi et al. [21]	0.04 W $W.m^{-2}.K^{-1}$
Effective conductivity:		
stainless steel frit	Maxwell [22]	5.25 $W.m^{-2}.K^{-1}$

[a] 353 K, inlet gas composition & full flow/pressure

Table 2-2: Parameter values used in the model.

Tioni's images of partially polymerised catalyst particles [2] show that as they grow they expand into NaCl particles which form the surrounding seedbed. It can therefore be expected that as the polymerisation progresses, particle growth will lead to increased contact with surrounding particles, and therefore more heat transfer by conduction and the catalyst particle temperature will approach the bulk temperature more closely. So, the correlation used will provide a good estimate of the particle heat transfer coefficient for experiments of very short duration. For longer experiments (>5s) the difference between catalyst and bulk temperature may be overestimated and the estimate of catalyst temperature will be conservative.

2.2.1.2 Effective Conductivity and Internal Wall Heat Transfer Coefficient

As the inert solid represents at least 95% of the total bed weight, the effect of the catalyst/polymer particles on effective bed conductivity is neglected. The seedbed particle size is small, 58 μm for silica and 45 – 63 μm for fine NaCl and wall effects extend for about 5 particle diameters into the bed. So a maximum of about 0.3 mm in this case, and they are accounted for only by remaining consistent between correlations. The correlations of Specchia et al. [19] were chosen for determination of the internal wall heat transfer coefficient to be consistent with those of Kunii & Smith [20] for effective bed conductivity.

The effective radial conductivity value given in Table 2-2, was checked against the value given by from the Zehner Schlunder correlations [23] which gave a very similar result. Both

correlations were developed for a packed bed containing spheres. The Zehner Schlunder correlations do include a shape factor for cylinders but not unusual particle shapes such as the fine NaCl seedbed which consists of open agglomerated cube structures.

2.2.2 Model Type

This section evaluates the type of model that is required to represent the reactor bed. A comparison of the particle size (<0.1 mm) against the bed length (10 mm) shows the ratio of bed length to particle size is >100, well above the limit of 50 so axial dispersion can be neglected and plug flow assumed [24]. Further to this, a Peclet number of 17 was determined using the correlation of Wen & Fan for the worst case of minimum flowrate, 30 $mL.s^{-1}$, and coarse NaCl particles [25] and the criterion developed by Mears for axial dispersion in packed beds shows it to be negligible in this reactor [26]. The other important phenomena are considered below.

2.2.2.1 Radial Heat Transfer

Equation 2-8 is Mears criterion [27] which is used to evaluate whether the radial temperature profile across the reactor bed must be taken into account. As discussed in the literature review, Mears criterion is designed for steady state and the model to be constructed is dynamic. However, the criterion considers the worst case and is the most straightforward way to make a first estimate of the required model type. The heat of reaction and activation energy for ethylene polymerisation are about 10^5 $J.mol^{-1}$ and 4 $x10^5$ $J.mol^{-1}$ respectively [28,29]. The effective radial conductivity of the reactor bed, estimated using the Kunii and Smith correlations (see Table 2-2, section 2.2.1), is 0.09 $W.m^{-1}.K^{-1}$. The combination of very high initial reaction rate and heat of reaction lead to a value of Mears criterion for this system of about 1800 which is far in excess of the limit of 0.4. Nearly all the resistance to heat transfer is in the packed bed. So much so, that the value for the overall heat transfer coefficient has little importance. A two dimensional model is therefore essential.

$$(1-\varepsilon)r_v|\Delta H|\frac{\frac{E_a}{R}d_{reac}^2}{4l_{sfer}T_w^2}\left(1+\frac{8l_{sfer}}{Ud_T}\right)>0.4 \qquad \text{2-8}$$

For axial heat transfer, Mears [30] states that for beds with length-to-pellet diameter ratios sufficiently great that plug flow occurs, axial conduction can be neglected and this is the case for our reactor.

2.2.2.2 Inter-particle Heat and Mass Transfer

The reactor bed contains not only reaction gas and solid catalyst but also solid inert and accumulating polymer. A reactor can be modelled as a single pseudo-homogeneous phase

if the temperatures and concentrations at the particle surface are sufficiently close to the bulk fluid values to make negligible difference in the reaction rate. The effects of both mass and heat transfer were evaluated to determine whether this is the case.

For mass transfer in polymerisation with supported catalysts, there is the potential situation described by Floyd et al. [31] who state that for homo-polymerisation with only pure monomer present in the gas phase, a diffusive mechanism for boundary layer mass transfer does not apply. However, here the ethylene is diluted with helium, so a boundary layer does exist. The ratio of maximum reaction rate to mass transfer rate across the catalyst boundary layer, F_{ex}, calculated from equations 2-9, 2-10 and 2-11 is used to determine the effect of external mass transfer limitations. The Sherwood number, Sh, is close to its minimum value of 2 due to the very small catalyst particle diameter and at the reaction conditions the molecular diffusivity of helium in ethylene is 7.3 x10^{-6} $m^2.s^{-1}$ [32]. A correction can be made for the difference in the number of moles of gas entering and leaving the particle. In this case, the correction is not needed as it would only increase k_D. Based on the maximum observed reaction rate, the calculation result is F_{ex} < 0.002. Mass transfer across the boundary layer is therefore not limiting.

$$F_{ex} = \frac{\bar{r}_{cat} d_{cat}}{6 k_D C_{ex}}$$

2-9

$$Sh = 2 + 1.8 \mathrm{Re}_v^{\,0.5} \, Sc^{0.33}$$

2-10

$$k_D \approx k_{D0} = \frac{Sh D_m}{d_{cat}}$$

2-11

For heat transfer across the catalyst boundary layer, a similar ratio can be determined using equation 2-14 [33]. The difference in temperature between the catalyst surface and the bulk gas is estimated to be at least 7 K from equation 2-15, again at the maximum observed reaction rate and with h_{cat} estimated by Kunii and Levenspiel's method (equations 2-12 & 2-13). The value of δ_{ex} is greater than 0.1 indicating that for these conditions the catalyst surface temperature is raised above the average temperature enough to cause a significant

increase in reaction rate. The catalyst particles and the gas phase must therefore be accounted for separately.

$$Nu = 2 + 1.8\,\mathrm{Re}_v^{\,0.5}\,\mathrm{Pr}^{0.33} \qquad \textbf{2-12}$$

$$h_{cat} = \frac{Nu.l_f}{d_{cat}} \qquad \textbf{2-13}$$

$$\delta_{ex} = \frac{E_a}{RT_g}\left|\frac{T_c - T_g}{T_c}\right| \qquad \textbf{2-14}$$

$$T_c - T_g = \frac{\bar{r}_{cat} d_{cat} \Delta H}{6h_{cat}} \qquad \textbf{2-15}$$

As discussed in this chapter section 2.1.3.5.1, the heat transfer rate from the gas to the fine NaCl seedbed is very high. Also, for a raw silica seedbed the surface of the inert solid is about 20 times greater than that of the catalyst. So, in both cases temperature gradients at the gas/inert solid boundary can be neglected and a pseudo-homogeneous model can be used to describe these two phases.

2.2.2.3 Intraparticle Mass Transfer

Internal mass transfer limitations, particle growth and catalyst deactivation are amongst the possible particle scale effects occurring during the reaction period studied here. Since the aim is to provide a model that can give a good estimate of the conditions throughout the reactor bed, rather than predict the behaviour of the catalyst particles, the effects of pore diffusion in both the catalyst support and polymer layer are not considered separately in this part of the work.

To get a rough idea of whether intraparticle concentration gradients exist, the Weiss modulus, φ'_e, given in equation 2-16, can be calculated for the raw catalyst at the maximum observed reaction rate. For φ'_e <<< 1, the reactant concentrations at the surface and centre of the catalyst particle can be assumed the same. For φ'_e > 1 there is a significant concentration

gradient within the catalyst particle and the observed reaction kinetics are affected by diffusion.

$$\varphi'_e = \frac{\bar{r}_{cat} L^2}{D_e C_{ex}}$$

2-16

The catalyst support is Grace 948 amorphous silica. The porosity of the catalyst support is determined as 0.79 and tortuosity is estimated as 3 [33,34]. Based on these values, Knudsen diffusion is controlling within the pores of catalyst particle and the diffusion coefficient, D_e, is 1.26 x10^{-7} $m^2.s^{-1}$. This gives a Weiss module for the maximum observed reaction rate of 0.4 which indicates the intermediate region where there are some diffusion effects. However, as soon as the polymerisation starts several changes take place simultaneously:

- The reaction rate decreases. If this is due to chemical effects it moves the observed reaction rate towards its intrinsic value.
- Catalyst pores reduce in size as polymer takes up volume inside the catalyst. This increases the diffusion resistance in the pores moving the observed reaction rate towards a diffusion limited regime.
- A polymer layer forms around the active sites creating another potential diffusion resistance.

Because it is not certain which of these effects has the greatest impact on the polymerisation rate no real conclusion can be drawn.

2.2.2.4 Conclusion

Radial heat transfer must be included in this model but axial heat transfer can be neglected. At the catalyst boundary, the effects of mass transfer resistance can be neglected but temperature gradients must be taken into account. The gas and inert solid can be assumed to be pseudo-homogeneous. Intraparticle temperature and concentration gradients are possible but they are not to be included in the model at this stage.

2.2.3 Adsorption

With a view to modelling the experiments already carried out using a silica seedbed the adsorption data in the literature was put into mathematical form. Olivier & Jadot's data [14] is determined at three different temperatures for a silica gel of specific surface 720 $m^2.g^{-1}$. The quantities adsorbed can be represented using the Toth equation [35] (2-17):

$$q = q_s^{\infty} e^{\frac{A_{ads}}{RT}} \frac{(bp)^m}{1+(bp)^m}$$

2-17

The three constants q^{∞}_s, b and m were found by non-linear regression of the published data at each fixed temperature using the MATLAB function lsqnonlin. An Arrhenius plot was then used to find the constant A_{ads}. The equation fits the published data for the particular silica gel well (Figure 2-13).

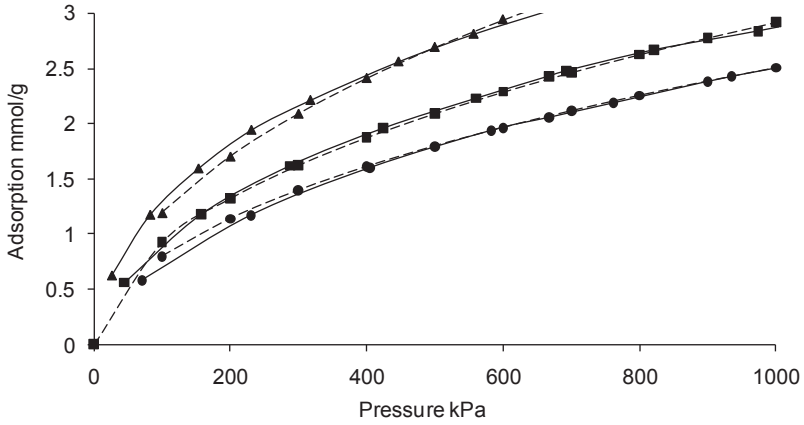

Figure 2-13: Calculated quantities of ethylene adsorbed on silica gel (dashed lines) vs measured data (solid lines) at 278K (▲), 298K (■) and 303K (●)

To represent the adsorption of ethylene for our case, the constant q^{∞}_s was reduced by the ratio of the specific surface of our amorphous silica to the silica gel i.e. 290 $m^2.g^{-1}$ to 720 $m^2.g^{-1}$ to give the final formula:

$$q = 0.0858.e^{\frac{1363}{T}} \frac{(0.003p)^{0.54}}{1+(0.003p)^{0.54}}$$

2-18

with q in mmol.g^{-1}, T in K and p in bar.

2.2.4 Mass and Heat Balances

In this section, the mass and heat balances for the reactor are developed. The terms relating to the adsorption of ethylene on silica are included, but are only necessary for the case where a silica seedbed is used. The reactor is split into finite elements along both length and radius and the balances are for a single element. The heat and mass balances for the frits are identical to those for the reactor bed but with the reaction rate set to zero. Similarly, within the reactor wall there is only heat transfer by conduction.

2.2.4.1 Reaction Period

2.2.4.1.1 Material Balances

Under the assumptions of constant reactor pressure and exit gas flowrate, the reaction gas flowrate decreases along the length of the reactor as ethylene is consumed (equation 2-19).

$$\frac{dF_T}{S_r dz} = -\bar{r}_v$$

2-19

The mole balance for ethylene in the gas phase is as follows, with the adsorption term only required if the solid inert is silica:

Flow + Radial diffusion in = Flow + Radial diffusion out + Reaction + (Adsorption) + Accumulation

$$F_{C2}\big|_z + \pi d_{reac} dz D_R \varepsilon \left.\frac{\partial C_{C2}}{\partial r}\right|_r = F_{C2}\big|_{z+dz} + 2\pi r dz D_R \varepsilon \left.\frac{\partial C_{C2}}{\partial r}\right|_{r+dr} + \bar{r}_v S_r dz + \left(J S_r dz\right) + \varepsilon S_r dz \frac{dC_{C2}}{dt}$$

2-20

substituting:

$$F_{C2} = y_{C2} F_T$$

2-21

$$C_{C2} = \frac{y_{C2} P}{RT}$$

2-22

and,

$$J = \rho\left(\frac{\partial q}{\partial y}\frac{\partial y}{\partial t} + \frac{\partial q}{\partial T}\frac{\partial T}{\partial t}\right)$$

2-23

The equation to be resolved becomes:

$$\frac{\partial y_{C2}}{\partial t} = \frac{-1}{\left(\alpha + \frac{P\varepsilon}{RT_g}\right)}\left(\bar{r}_v(1+y_{C2}) - F_T\frac{\partial y_{C2}}{S_r\partial z} - \frac{D_r\varepsilon P}{rRT_g}\frac{\partial}{\partial r}\left(r\frac{\partial y_{C2}}{\partial r} + \frac{y_{C2}}{T_g}\frac{\partial T_g}{\partial r}\right) + \left(\beta + \frac{y_{C2}\varepsilon P}{RT_g^2}\right)\frac{\partial T_g}{\partial t}\right)$$

2-24

with the adsorption parameters, α and β, (only to be used for a silica seedbed):

$$\alpha = \frac{\rho(1+y_{C2})q_s^{\infty}e^{\frac{A_{ads}}{RT}}mb(by_{C2})^{m-1}}{\left(1+(by_{C2})^m\right)^2}$$

2-25

$$\beta = \rho(1+y_{C2})q_s^{\infty}e^{\frac{A_{ads}}{RT}}\left(\frac{-A_{ads}}{RT^2}\right)\frac{(by_{C2})^m}{\left(1+(by_{C2})^m\right)}$$

2-26

The inlet ethylene mole fraction and the outlet flowrate are fixed, there is no ethylene in the reactor wall section and no reaction in the stainless steel frits:

$$F_T = F_{T0}\big|_{z=lreac}$$

2-27

$$y_{C2} = y_{C20}\big|_{z=0}\ \forall r \quad \text{and} \quad y_{C2} = 0\big|_{dreac/4<r<dreac/2}\ \forall z$$

2-28, 2-29

$$\frac{\partial y_{C2}}{\partial z} = 0\big|_{\substack{0<z<lf1 \\ (lr-lf2)<z<lreac}}$$

2-30

Radial diffusion is assumed to be symmetrical about the reactor centre-line and zero at the reactor wall:

$$\frac{\partial y_{C2}}{\partial r} = 0\Big|_{r=0} \quad \text{and} \quad \frac{\partial y_{C2}}{\partial r} = 0\Big|_{r=dreac/4}$$

2-31, 2-32

The balance for the mass of accumulating polymer is:

$$\frac{dM_R}{dt} = Mwt_{C2}\bar{r}_v$$

2-33

The radial diffusivity is required for the gas phase ethylene mole balance and is found to be 2.56 x 10^{-6} $m^2.s^{-1}$ from the correlation of Wen & Fan [33]:

$$\frac{1}{Pe_r} = \frac{D_R}{ud_p} = \frac{0.4}{(\mathrm{Re}\,Sc)^{0.8}} + \frac{0.09}{1+\frac{10}{\mathrm{Re}\,Sc}}$$

2-34

2.2.4.1.2 Energy Balances

Figure 2-14 shows the different heat flows in an element of the fixed bed. The letters correspond to the terms written in the heat balances.

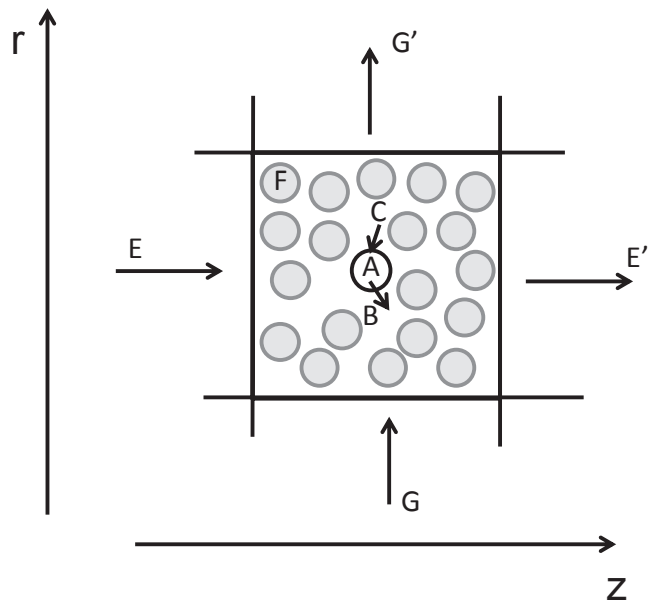

Figure 2-14: Heat flows in an element of the reactor bed

The heat balance for the combined catalyst and polymer (T_c) is:

$$S_R dz \bar{r}_v \Delta H = S_R dz S_{cat} h_{cat} \left(T_g - T_c\right) + S_R dz Mwt_{C2} \bar{r}_v c_{pC2} \left(T_g - T_c\right) + S_R dz \sum \left(\rho c_p\right)_c \frac{dT_C}{dt} \quad \textbf{2-35}$$

heat of reaction (A) = heat transfer across boundary layer (B) + cooling by reaction gas entering particle (C) + Accumulation (D)

Rearranging, the equation to be resolved becomes,

$$\frac{dT_C}{dt} = \frac{1}{\sum \left(\rho c_p\right)_c} \left(Mwt_{C2} \bar{r}_v \left(\frac{\Delta H}{Mwt_{C2}} + c_{pC2} \left(T_g - T_c\right) \right) + S_{cat} h_{cat} \left(T_g - T_c\right) \right) \quad \textbf{2-36}$$

The heat balance for the combined gas and inert solid (T_g) is as follows, once again adsorption terms are only required if the solid inert is silica:

$$u_v S_R \rho_{rg} h\big|_z + \left(\frac{\partial q}{\partial t} \Delta H_{ads} S_R dz \right) + l_{sfer} \left(\frac{\partial T_g}{\partial r} \right) 2\pi r dz \Big|_r + h_{cat} S_{cat} S_R dz \left(T_c - T_g\right)$$

heat in gas entering segment (E) + heat of adsorption (F) + radial conduction (G) + heat transfer from catalyst (B)

$$= u_v S_R \rho_{rg} h\big|_{z+dz} + l_{sfer} \left(\frac{\partial T_g}{\partial r} \right) 2\pi r dz \Big|_{r+dr} - S_R dz Mwt_{C2} \bar{r}_v c_{pC2} \left(T_g - T_c\right) + S_R dz \sum \left(\rho c_p\right)_g \frac{dT_g}{dt} \quad \textbf{2-37}$$

heat in gas leaving segment (E') + radial conduction (G') + cooling by reaction gas entering particle (C) + Accumulation (H)

substitute:

$$\frac{dh}{dz} = c_p \frac{dT}{dz}$$

2-38

$$\frac{\partial q}{dt} = \alpha \frac{\partial y}{\partial t} + \beta \frac{\partial T}{\partial t}$$

2-39

And finally the equation to be resolved is,

$$\frac{\partial T_g}{\partial t} = \frac{1}{\sum\left(\left(\rho c_p\right)_g - \left(\beta \Delta H_{ads}\right)\right)} \left(\begin{array}{l} \left(\alpha \Delta H_{ads} \frac{\partial y}{\partial t}\right) - \left(S_{cat} h_{cat} - Mwt_{C2} \bar{r}_v c_{pC2}\right)\left(T_g - T_c\right) \\ + F_T Mwt_{rg} c_{prg} \frac{\partial T_g}{S_r \partial z} + \frac{l_{sfer}}{r} \frac{\partial}{\partial r}\left(\frac{r \partial T_g}{\partial r}\right) \end{array} \right)$$

2-40

To calculate the heat transfer rate within the stainless steel reactor wall l_{sfer} is replaced by the conductivity of stainless steel:

$$l_{sfer} = l_{s\ inox} \Big|_{dreac/4<r<dreac/2} \forall z$$

2-41

Symmetry about the reactor centre-line is assumed:

$$\frac{\partial T_g}{\partial r} = 0 \Big|_{r=0} \forall z$$

2-42

At the reactor internal and external walls the boundary conditions are:

$$l_{sfer}\left(\frac{\partial T_g}{\partial r}\right) = h_{\text{int}}^{sf}\left(T_g - T_w\right) \Big|_{dreac/4<r<dreac/2} \forall z$$

2-43

$$l_{s\_inox}\left(\frac{\partial T_g}{\partial r}\right) = h_{bath}\left(T_w - T_b\right) \Big|_{dreac/4<r<dreac/2} \forall z$$

2-44

2.2.4.2 Cooling Period

During the cooling period there is no reaction, the reactor bed can therefore be modelled as pseudo-homogeneous with only one temperature value for each reactor element. The heat balance to be resolved is identical with the heat balance for the gas/inert phase during the reaction period.

2.2.5 Reaction Rate

As reported in the literature survey the observed polymerisation rate is the combined result of initiation, propagation and deactivation reactions. We assume that the initiation rate is fast enough to be neglected and the propagation rate is well represented by a single lumped formula for a first order reaction:

$$\bar{r}_v = k_{p0} e^{-\frac{Ea_p}{RT}} C_{C2} C*$$

2-45

For our reactor, the reaction rate is decreasing rapidly but it is unknown whether this is due to physical or chemical effects. A simple kinetic model based on the observed data is therefore used to represent this.

The ethylene concentration at the active sites, C_{C2}, is needed. Because the experiments are of such short duration it is assumed that the layer of amorphous polymer forming around each active site is still very thin. So, the ethylene concentration at the active sites is taken to be the dissolved quantity in equilibrium with the gas phase. Note that in section 2.2.2.3 of this chapter, intraparticle mass transfer was discussed and it was concluded that concentration gradients within the pores of the catalyst particle are possible. Diffusion rates through the polymer layer are a separate consideration. The ethylene diffusion coefficient in PE is lower than the effective diffusivity in the catalyst pores. However, the concentration gradients through the polymer layer are assumed to be negligible on the basis that the diffusion length is very small.

2.2.5.1 Kinetic Model

From the experimental data the reaction rate is known to be decreasing rapidly and this must be represented in the model. In the first instance the method chosen to reduce the reaction rate was to link the pre-exponential factor for propagation to the accumulation of polymer. A linear function was avoided because it is important that the calculated reaction rate does not fall below zero.

The formula used for the pre-exponential factor is as follows:

$$k_{p0}C^* = a - b(M_R)^c$$

2-46

Where a, b & c are constants.

Figure 2-15 compares values for the pre-exponential factor calculated from the experimental data and from equation 2-46 against the apparent polymer density in the reactor bed and against time.

In the model the value of $k_{p0}C^*$ is adjusted via the constant b to get the best fit between measured and calculated output temperatures.

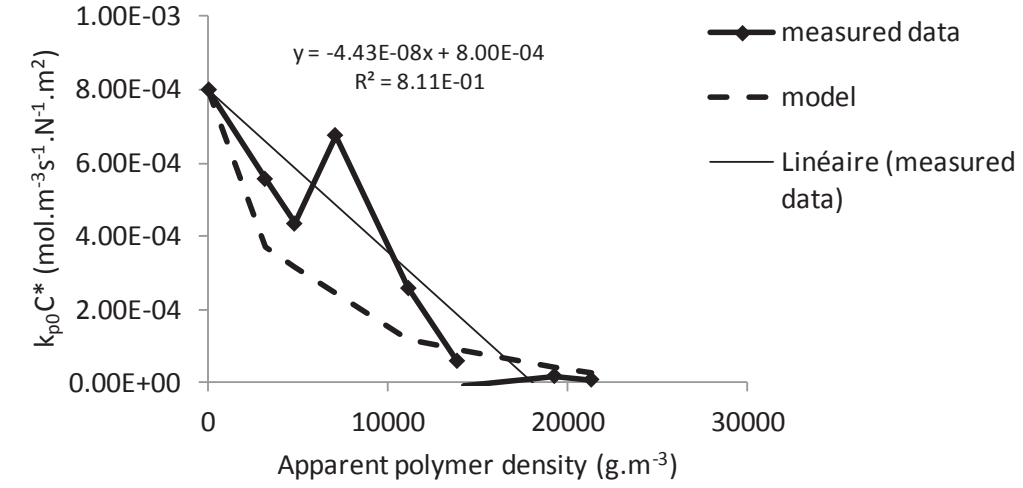

(a)

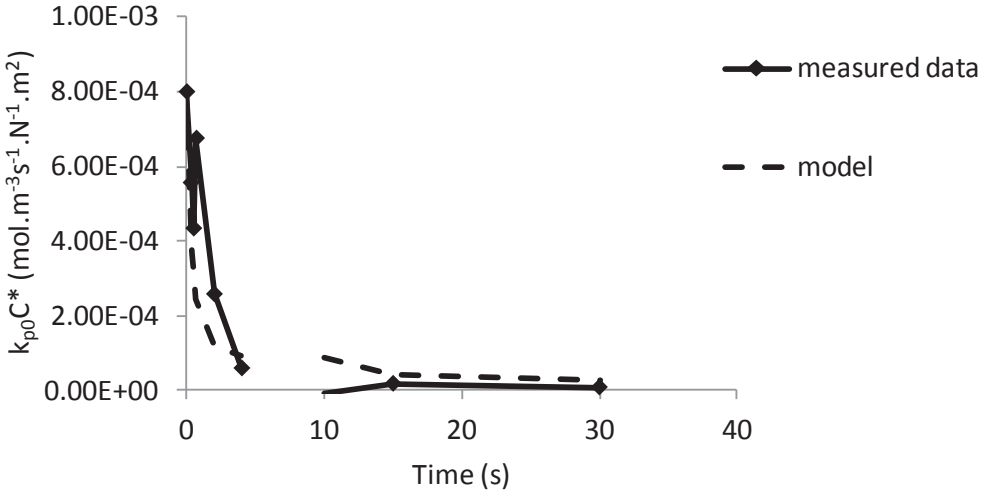

(b)

Figure 2-15: Comparison of $k_{p0}C^*$ calculated from measured data and kinetic model (a) against apparent polymer density (b) against time

2.2.5.2 Ethylene Solubility in PE

Experimental data for the solubility of ethylene in PE is reported by several sources in the literature [36,37,38,39,40]. Values for ethylene solubility in the amorphous phase of the polymer are shown in Table 2-3. The total temperature range covered by the data is 278 K to 363 K and the values can be seen to decrease with increasing temperature and increasing crystallinity.

Solubility ($mol.L_{amPE}^{-1}.atm^{-1}$)	Solubility ($g.g_{amPE}^{-1}.MPa^{-1}$)	Temp (K)	PE density ($g.cm^{-3}$)	Vol frac amorphous	Reference
	0.0103	301	0.954	0.298	[36]
	0.0087	321			
	0.007	341			
	0.0053	361			
0.0373	0.0111	298	0.9327	0.49	Li & Long in [37]
0.0461	0.0139	278	0.918	0.55	
0.0392	0.0118	293			Kulkarni &
0.0324	0.0098	308			Stern in [37]
	0.01	333	0.92	0.52	
	0.009	363			[38]
0.0278	0.0090	323	0.854	0.262	
0.0249	0.0081	333	(amorph.)		[39]
0.0204	0.0066	353			
1 (approx.) $cc\,g^{-1}_{amPE}\,bar^{-1}$	0.0114	343	0.957		[40]

Table 2-3: Experimental data for the solubility of ethylene in PE

At pressures below 100atm the solubility of ethylene in PE can be represented using Henry's Law with the Henry constant decreasing with increasing temperature [41]. Three different correlations have been used to relate the Henry constant to temperature:

a simple Flory Huggins model [38]

$$\varphi_p = 1 - \frac{p}{p_i^{\,0} \exp(1+\chi)}$$

2-47

the Van't Hoff relation [42]

$$H = H_0 \exp\left(\frac{-\Delta H_s}{RT}\right)$$

2-48

and an empirical formula [43] where the constant b includes the critical temperature of the gas.

$$\ln(H) = a + \frac{b}{T^2}$$

2-49

Hutchinson and Ray [37] reviewed data from several authors and recommended the third correlation.

The Sanchez-Lacombe equation of state is also often used for modelling the solubility of gases in polymers, particularly at high pressures and for mixtures of gases. However, for our conditions the Henry constant provides a good estimation.

To calculate the concentration of ethylene at the active sites the model requires a value for the Henry constant which describes the solubility of ethylene gas in PE. The value used must represent the solubility as closely as possible and so the correlation recommended by Hutchinson and Ray [37] is used together with the data from Moore and Wanke [44] for HDPE formed using metallocene catalyst.

The constants to be used in the equation are found by regression, resulting in:

$$\ln(H) = -20.5 + \frac{194000}{T^2}$$

with temperature, T, in K and Henry's constant, H, in $g_{C2}.g^{-1}_{(amorphous\ polymer)}.N^{-1}.m^2$.

Figure 2-16 shows a graph comparing calculated values of ethylene solubility with the published experimental values. Although the published data appears to decrease linearly with temperature, it is preferable to avoid a linear relationship as this could cause a negative solubility to be calculated by the model during temperature excursions.

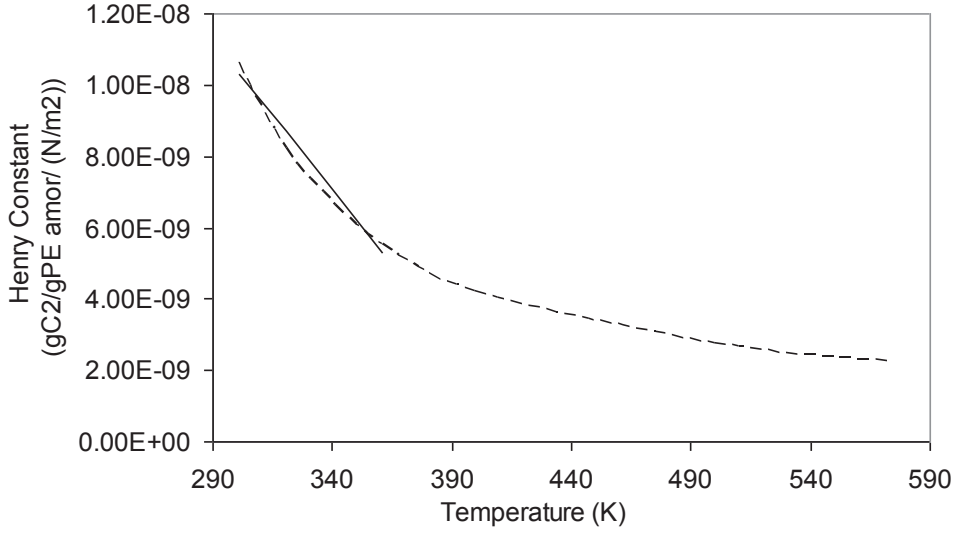

Figure 2-16: Graph comparing calculated values of ethylene solubility with published experimental values, solid line represents published values, dashed line represents calculated values

A source of inaccuracy could be that, even with metallocene catalyst, polymer with low crystallinity is formed for very short duration experiments. For example, polymer produced in experiments of 100 ms, 300 ms and 500 ms had 10%, 37% and 63% crystallinity respectively. After the first 500 ms the value was steady. During the initial unsteady phase one might expect ethylene to be more soluble in the polymer surrounding the active sites than later in the experiment. A typical value for ethylene solubility in LLDPE is about 40% greater than for HDPE at the same temperature [36].

2.2.6 Conclusions

The model must include the reactor bed, the stainless steel frits and the reactor wall. Constant pressure, exit gas flowrate and hot water bath temperature are assumed. The type of model required was determined to be two dimensional and heterogeneous, with two phases taken into account; the catalyst/polymer particles and the gas/solid inert. Plug flow is assumed and although there may be intraparticle effects these are neglected for the time being.

The heat transfer correlations to be used in the model have been reviewed and chosen. Adsorption data for ethylene on silica was put into mathematical form that could be used

within the model. Finally, mass and heat balances for the model were developed and also an equation to represent the fluctuation in reaction rate.

2.3 Programming the model

2.3.1 Structure

Figure 2-17 shows the structure of the reactor model. The reactor is modelled in MATLAB using a suite of function files. The files are organised so that one file handles the data inputs, calls the reactor model and creates the output graphics. The reactor model calls other function files as necessary to carry out the different calculation steps. This allows good organisation of the calculations and also for the model to be used later for optimisation or parameter estimation.

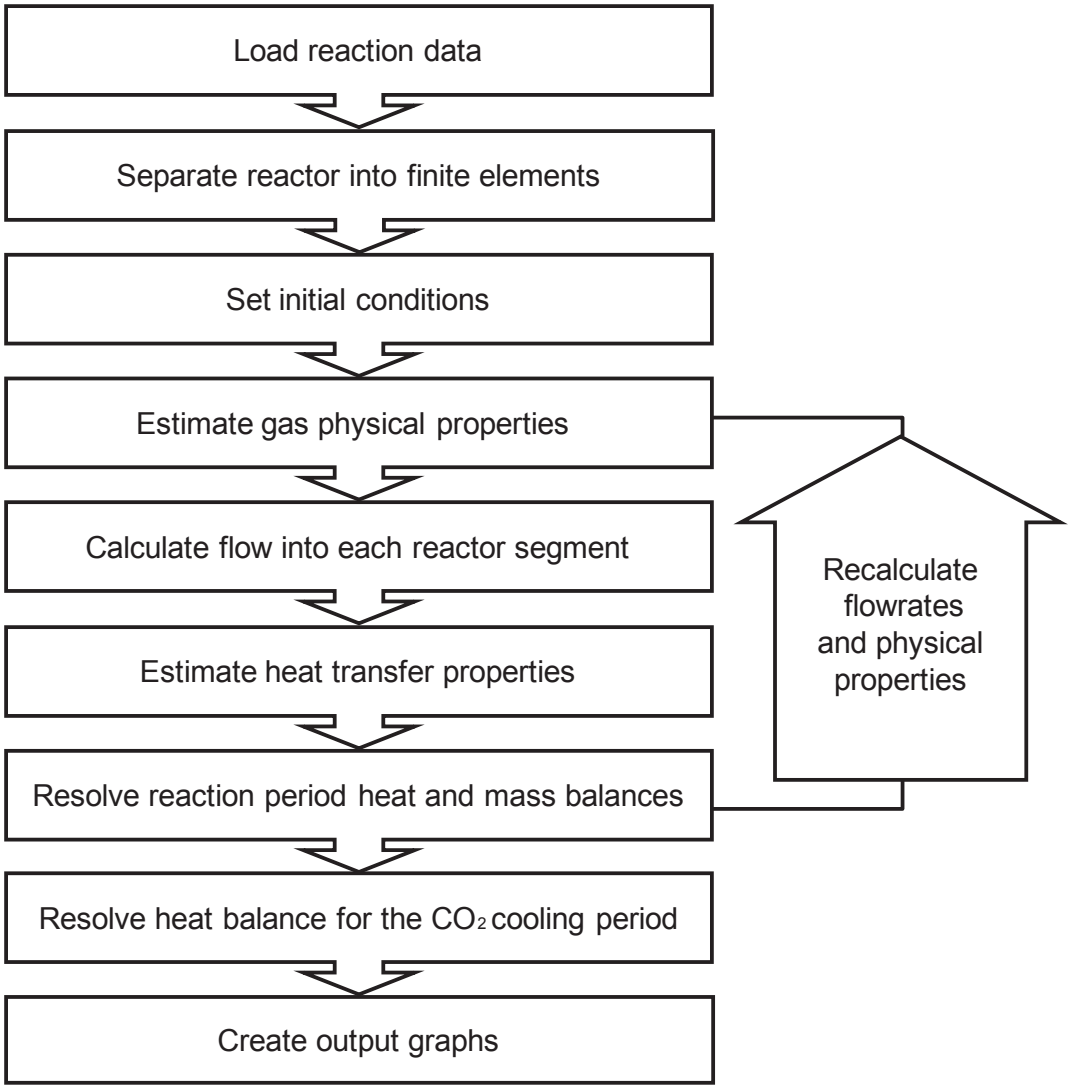

Figure 2-17: Reactor Model Flow Diagram

2.3.2 Resolution of Differential Equations

The differential equations are resolved by the MATLAB function ode45, which uses a 4^{th} and 5^{th} order explicit Runge-Kutta method. In the initial stages of the reaction things are changing rapidly and then the system becomes more stable. In order to save computing

time without losing too much accuracy the physical properties, heat transfer parameters and reaction gas flowrate into the reactor are recalculated every 20ms for the first second then every 1s for the rest of the duration of the experiment.

2.3.3 Number of Elements

The model is constructed of finite elements. For each element there are five differential equations to be solved simultaneously and so, increasing the number of elements increases the computing time. On the other hand, if the number of elements is insufficient there will be error due to numerical dispersion. Initially the model is constructed to create 1mm segments axially and radially, this is reviewed in Chapter 3 section 3.1.8.

2.4 Conclusion

The reactor set-up and operation have been reviewed and assessed. Polymerisation rates in this system are initially high and decrease rapidly. Analysis of pressure drops shows the whole system is close to capacity when operated at the maximum flowrate. An initial temperature peak at the reactor inlet has been identified as due to compression of the reaction gas. In this reactor, catalyst is diluted with silica or NaCl to create a seedbed. If silica is used there is a significant thermal effect due to the heat of adsorption of ethylene on the silica surface. The seedbed of small NaCl particles (45 – 63 μm) is best as adsorption is avoided and high surface area and heat transfer coefficient allows these particles to be very efficient at damping temperature variations in the fixed bed. Also, the effect of the dilution on the polymerisation kinetics is found to be negligible for this particular seedbed. Although the volume of the reactor bed is slightly reduced by the initial compression and high flowrates used in the experiments its structure remains stable.

A model has been created for the fixed bed reactor assuming constant pressure, bath temperature and reaction gas flowrates. Radial temperature gradients are significant as are those at the catalyst particle boundary so a bi-dimensional, heterogeneous model is required. Temperature and concentration gradients inside the catalyst particle are also suspected but not accounted for at this stage. The model includes the effects of adsorption where a silica seedbed is used. The reaction rate is represented by a single equation, including a lumped reaction parameter which is decreased as polymer accumulates. Standard heat transfer correlations for fixed beds have been used.

The model has been programmed in MATLAB with the reactor represented as a series of finite elements. The heat and mass balances are resolved by the MATLAB function ode45. The model validation will be presented in the next chapter.

2.5 Nomenclature

A_{ads}	Constant for the Toth equation	$J.mol^{-1}$
A	Cross sectional area	m^2
b	Constant for the Toth equation	-
b_d	bed dilution factor (volume inert/total volume solids)	-
C	Constant	-
C_{C2}	Ethylene concentration	$mol.m^{-3}$
C_{ex}	Bulk monomer concentration	$mol.m^{-3}$
C^*	Active site concentration	$mol.m^{-3}$
c_p	Specific heat capacity	$kJ.kg^{-1}.K^{-1}$
c_{pC2}	Specific heat capacity ethylene	$kJ.kg^{-1}.K^{-1}$
D_m	Molecular Diffusivity	$m^2.s^{-1}$
D_e	Effective Diffusivity	$m^2.s^{-1}$
D_R	Radial Diffusivity	$m^2.s^{-1}$
d	Pipe diameter	m
d_{reac}	Reactor diameter	m
d_{cat}	Catalyst particle diameter	m
d_p	Particle diameter	m
E_a	Activation energy	$J.mol^{-1}$
E_{ap}	Activation energy for propagation	$J.mol^{-1}$
F_{C2}	Molar flow ethylene	$mol.s^{-1}$
F_T	Total molar flow	$mol.s^{-1}$
F_{ex}	Ratio of reaction rate to diffusion rate in boundary layer	-
G	Mass flowrate	$kg.s^{-1}$
h	Specific enthalpy	$kJ.kg^{-1}$
h_{cat}	Catalyst heat transfer coefficient	$W.m^{-2}.K^{-1}$
H	Henry Constant	$g_{C2H4}.g_{am\ polym}^{-1}.N^{-1}.m^2$
H_0	Henry Constant at reference temperature	$g_{C2H4}.g_{am\ polym}^{-1}.N^{-1}.m^2$
ΔH	Heat of reaction	$J.mol^{-1}$
ΔH_{ads}	Heat of adsorption	$J.mol^{-1}$
ΔH_s	Heat of dissolution	$J.mol^{-1}$

J	Adsorption rate	$mol.s^{-1}.m^{-3}$
k_D	Mass transfer coefficient	$m.s^{-1}$
k_{D0}	Uncorrected mass transfer coefficient	$m.s^{-1}$
k_{p0}	Pre-exponential reaction rate constant for propagation	$mol^{-1}.s^{-1}.m^3$
l	Pipe length	m
l_b	Bed length	m
l_f	Frit thickness	m
l_{reac}	Reactor length	m
l_{sfer}	Effective bed conductivity	$W.m^{-1}.K^{-1}$
L	Characteristic length	m
M_R	Mass of PE per unit volume of reactor	$g.m^{-3}$
Mwt_{C2}	Molecular weight ethylene	$g.mol^{-1}$
m	Constant for the Toth equation	-
n	Reaction order	-
P	Total pressure	$N.m^{-2}$
P_m	Mean pressure	$N.m^{-2}$
p	Partial pressure	$N.m^{-2}$
p_i^0	Vapour pressure	$N.m^{-2}$
$\mathrm{Pe_r}$	Radial Peclet number	-
q	Quantity adsorbed	$mol.kg^{-1}$
q^{∞}_s	Constant for the Toth equation	$mol.kg^{-1}$
Q	Volumetric flowrate	$m^3.s^{-1}$
R	Ideal gas constant	$J.mol^{-1}.K^{-1}$
R'	Shear stress	$N.m^{-2}$
Re	Reynold's number based on interstitial velocity	
Re_v	Reynold's number based on superficial velocity	
r	Radial distance	m
$\bar{r}_{cat}$	Apparent reaction rate per unit volume of catalyst	$mol.s^{-1}.m^{-3}_{cata}$
$\bar{r}_v$	Apparent reaction rate per unit bed volume	$mol.s^{-1}.m^{-3}$
r_p	propagation rate	$mol.s^{-1}.m^{-3}$
S_{cat}	Catalyst surface area	m^2
S_R	Cross sectional area of segment	m^2
Sc	Schmidt number	-

Sh	Sherwood number	-
T	Temperature	K
T_w	Wall Temperature	K
t	Time	s
U	Overall Heat Transfer Coefficient	$W.m^{-2}.K^{-1}$
u	Interstitial velocity	$m.s^{-1}$
u_v	Superficial velocity	$m.s^{-1}$
v_m	Specific volume of gas mixture	$m^3.kg^{-1}$
x_{idil}	Conversion in diluted bed	-
x_{und}	Conversion in undiluted bed	-
y_{C2}	Mole fraction ethylene	-
z	Axial distance	m
α_0	Viscous permeability coeff.	m^2
Δ	Fraction of conversion lost due to bed dilution	-
δ_{ex}	Measure of effect of heat transfer resistance on reaction rate	-
ε	Porosity of reactor bed	-
μ	Viscosity	$Ns.m^{-2}$
ρ	Density	$kg.m^{-3}$
φ'_e	Module de Weiss	-
φ_p	Volume fraction of solvent	-
χ	Flory-Huggins interaction parameter	-
γ	Ratio of specific heats	-

Suffixes

c	Catalyst & polymer
g	Gas & inert solid
rg	Reaction gas

[1] Di Martino A., Weickert G. & McKenna T.F.L., Design and Implementation of a Novel Quench Flow Reactor for the Study of Nascent Olefin Polymerisation, Macromol. React. Eng. 1 (2007) 284-294

[2] Tioni E., Optimisation of a tool to study the start-up of the gas phase olefin polymerisation, Ph.D. Thesis UCBL1 338-2011

[3] Tisse V., Sheibat-Othman N. & McKenna T.F.L., A Lab-Scale Reaction Calorimeter for Olefin Polymerization, Can. J. Chem. Eng. 88 (2010) 783-792

[4] Silva F., Lima E.L., Pinto J.C. & McKenna T.F.L., Investigation of Catalyst Fragmentation in Gas-Phase Olefin Polymerisation: A Novel Short Stop Reactor, Macromol. Rapid Commun. 26 (2005) 1846-1853

[5] Olalla B., Broyer J.P. & McKenna T.F.L., Heat Transfer and Nascent Polymerisation of Olefins on Supported Catalysts. Macromol. Symp. 271 (2008) 1-7

[6] Tioni E., Spitz R., Broyer J.P., Monteil V. & McKenna T.F.L., Packed-Bed Reactor for Short Time Gas Phase Olefin Polymerisation: Heat Transfer Study and Reactor Optimisation, AIChE J. 58,1 (2012) 256-267

[7] Kapteijn F. & Moulijn J.A., Laboratory Catalytic Reactors: Aspects of Catalyst Testing, in Ertl G., Knozinger H., Schuth F. & Weitkamp J., Handbook of Heterogeneous Catalysis Volume 4, 2nd Edition (2008) Wiley-VCH Verlag

[8] Backhurst J.R., Harker J.H., Coulson J.M. & Richardson J.F., Coulson & Richardson's Chemical Engineering, 6th edn (1999) Elsevier

[9] http://www.chandeisenmann.com/tech_info/pore_size.asp
(4 December 2009)

[10] Asay B.W., Son S.F., Dickson P.M., Smilowitz L.B. & Henson B.F., An Investigation of the Dynamic Response of Thermocouples in Inert and Reacting Condensed Phase Energetic Materials, Propell. Explos. Pyrot. 30 (2005) 199-208

[11] Moffat, R.J., Notes on Using Thermocouples, Electronics Cooling Magazine, Jan 1997.

[12] Tisse V., Kinetics and Morphology of Metallocene Catalysts used in Ethylene Polymerisation, Ph.D. Thesis UCBL1 50-2006

[13] Lewis W.K., Gilliland E.R., Chertow B. & Cadogan W.P., Adsorption Equilibria Hydrocarbon Gas Mixtures, Ind. Eng. Chem. 42 (1950) 1319-1326

[14] Olivier M.G. & Jadot R., Adsorption of Light Hydrocarbons and CO2 on Silica Gel, J. Chem. Eng. Data 42 (1997) 230-233

[15] Newalkar,B.L. et al. [Adsorption of light hydrocarbons on HMS type mesoporous silica Microporous and Mesoporous Materials 65 (2003) 267-276

[16] Moulijn J.A., Pérez-Ramirez J., Berger R.J., Hamminga G., Mul G. & Kapeteijn F., High-Throughput Experimentation in Catalyst Testing and in Kinetic Studies for Heterogeneous Catalysis, Catal. Today 81 (2003) 457–471

[17] Dehnavi M.A., Shahhosseini S., Hashemabadi S.H. & Ghafelebashi S.M., CFD Based Evaluation of Polymer Particles Heat Transfer Coefficient in Gas Phase Polymerization Reactors, Int. Commun. Heat. Mass. 35 (2008) 1375-1379

[18] Kunii D. & Levenspeil O., Fluidisation Engineering, Wiley (1969)

[19] Specchia V., Baldi G. & Sicardi S., Heat Transfer in Packed Bed Reactors with One Phase Flow, Chem. Eng. Commun. 4 (1980) 361-380

[20]Kunii D. & Smith J.M., Heat Transfer Characteristics of Porous Rocks, AIChE J. 6 (1960) 71-78

[21] Yagi S., Kunii D. & Wakao N., Studies on Axial Effective Thermal Conductivities in Packed Beds, AIChE J. 6 (1960) 543-546

[22] Maxwell J.C., Electricity and Magnetism, Clarendon Press, Oxford UK (1873)

[23] Zehner P. & Schlunder E.U., Warmeleitfahigkeit von Schuttungen bei Massigen Temperaturen, Chem. Ing. Tech. 42 (1970) 933-941

[24] Perego C. & Peratello S., Experimental Methods in Catalytic Kinetics, Catal. Today 52 (1999) 133-145

[25] Wen C.Y. & Fan L.T., Models for Flow Systems and Chemical Reactors, Marcel Dekker Inc. (1975)

[26] Mears D.E., The Role of Axial Dispersion in Trickle Flow Reactors, Chem. Eng. Sci. 26 (1971) 1361-1366

[27] Mears D., Tests for Transport Limitations in Experimental Catalytic Reactors, Ind. Eng. Chem. Proc. Des. Develop., 10 (1971) 541-547

[28] Eriksson E. & McKenna T.F.L, Heat-Transfer Phenomena in Gas-Phase Olefin Polymerisation Using Computational Fluid Dynamics, Ind.Eng.Chem.Res 43 (2004) 7251-7260

[29] Roos P., Meier G.B., Samson J.J.C., Weickert G. & Westerterp K.L., Gas Phase Polymerisation of Ethylene with a Silica-Supported Metallocene Catalyst: Influence of Temperature on Deactivation, Macromol. Rapid Commun. 18 (1997) 319-324

[30] Mears D.E., Diagnostic Criteria for Heat Transport Limitations in Fixed Bed Reactors, J. Catal. 20 (1971) 127-131

[31] Floyd S., Choi K.Y., Taylor T.W. & Ray W.H., Polymerisation of Olefins Through Heterogeneous Catalysis IV. Modeling of Heat and Mass Transfer Resistance in the Polymer Particle Boundary Layer, J.App.Polym.Sci, 31 (1986) 2231-2265

[32] Perry R.H. & Green D.W. Perry's Chemical Engineers' Handbook, seventh ed., McGraw Hill, New York, 1997.

[33] Schweich D., Génie de la réaction chimique, Technique & Documentation, Paris, 2001.

[34] Scott,D.C. An Assessment of Reasonable Tortuosity Values, Pharmaceutical Research, Vol.18, No.12 Dec 2001

[35] Do .D.D., Adsorption analysis equilibria and kinetics, Imperial College Press, 1998.

[36] Moore S.J. & Wanke S.E., Solubility of Ethylene, 1-Butene and 1-Hexene in Polyethylenes, Chem. Eng. Sci. 56 (2001) 4121-4129

[37] Hutchinson R.A. & Ray W.H., Polymerisation of Olefins Through Heterogeneous Catalysis VIII Monomer Sorption Effects, J. App. Polym. Sci. 41 (1990) 51-81

[38] McKenna T.F., Solubility and Crystallinity Data for Ethylene/Polyethylene Systems, Eur. Polym. J. 34,9 (1998) 1255-1260

[39] Kiparissides C., Dimos V., Boultouka T., Anastasiadis A. & Chasiotis A., Experimental and Theoretical Investigation of Solubility and Diffusion of Ethylene in Semicrystalline PE at Elevated Pressures and Temperatures, J. App. Polym. Sci. 87 (2003) 953-966

[40] Yao W., Hu X. & Yang Y., Modelling Solubility of Gases in Semicrystalline Polyethylene, J. App. Polym. Sci. 103 (2007) 1737-1744

[41] Lui D.D. & Prausnitz J.M., Calculation of Phase Equilibria for Mixtures of Ethylene and Low-Density Polyethylene at High Pressure, Ind. Eng. Chem. Proc. Des. Dev. 19 (1980) 205-211

[42] Michaels A.S. & Bixler H.J., Solubility of Gases in Polyethylene, J. Polym. Sci. 50,154 (1961) 393-412

[43] Maloney D.P. & Prausnitz J.M. Solubility of Ethylene in Liquid Low-Density Polyethylene at Industrial Separation Pressures, Ind. Eng. Chem. Proc. Des. Dev. 15,1 (1976) 216-220

[44] Moore S.J. & Wanke S.E., Solubility of ethylene, 1-butene and 1-hexene in polyethylenes, Chem. Eng. Sci. 56 (2001) 4121-4129

Chapter 3

Reactor Model Validation, Estimation and Simulations

3 Reactor Model Validation, Estimation and Simulations

3.1 Validation

A number of methods were used to check and validate the model as far as possible. This section describes the work that was carried out with this purpose. In some cases, points were raised which indicated the limitations of both the reactor system and the model and showed where improvements could be made.

3.1.1 Experiments without Catalyst

The experiments using a raw silica seedbed provide a useful validation for the model because adsorption is so rapid that it can be assumed instantaneous. This allows the heat and mass balances to be checked separately from the reaction. Figure 3-1 compares the model output with measured outlet temperatures for the passage of reaction gas over a raw silica seedbed with no catalyst. It shows that they provide a reasonable fit with the measured data. To model this particular experiment, the required step change in bed temperature is 4.5K, which is less than predicted by equation 2-18 derived earlier. As mentioned previously, this is possibly because the silica used had not been dried.

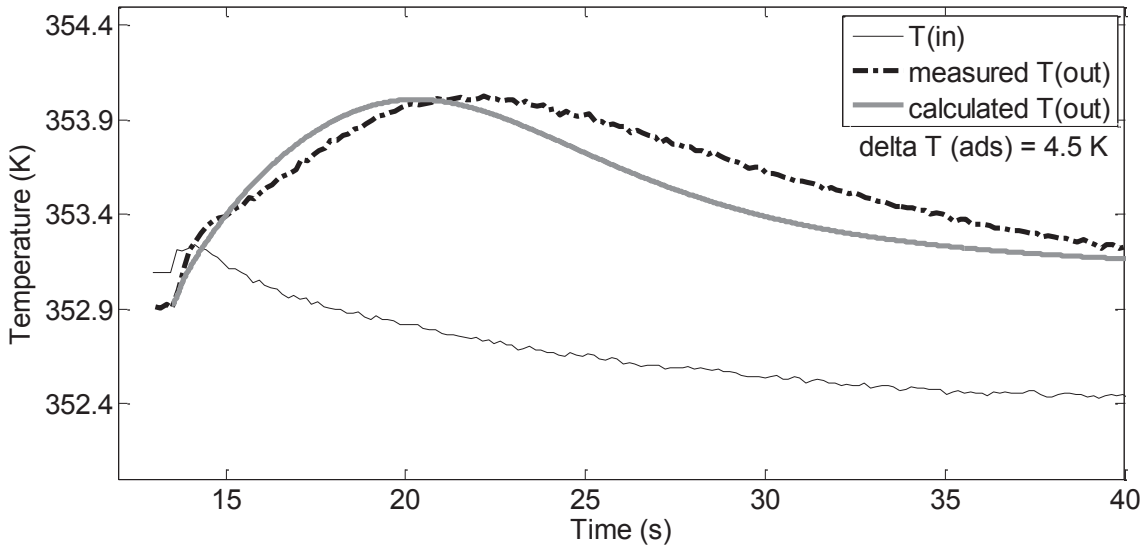

Figure 3-1: Comparing model output with measured outlet temperatures for silica seedbed at 353 K with no catalyst, EXP_9, 90 mL.s^{-1} reaction gas

Figure 3-2 shows the result of modelling experiment, EXP_17, at 353 K with the fine NaCl seedbed and no catalyst. The calculated temperatures fit well with the measured values. There are two visible discrepancies between the calculated and measured data. The first is the thermal effect of the initial bed compression, which was discussed in Chapter 2 section 2.1.3.3.4 and determined to be negligible compared to the heat of reaction and not included in the model. The second is due to the gas expansion at the instant the reactor pressure is

released. This was sometimes observed but not consistently and is not included in the model.

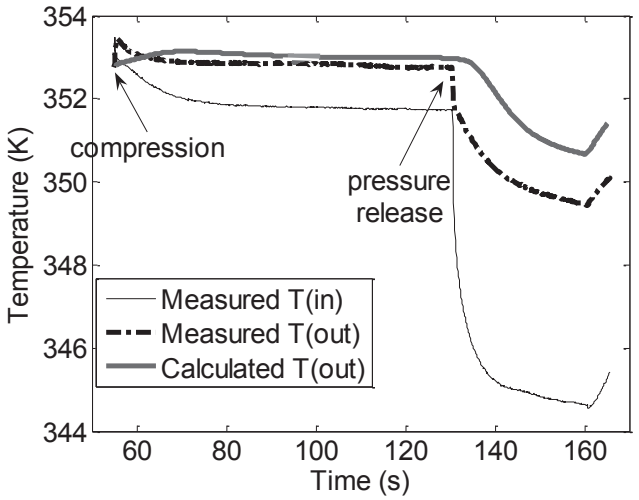

Figure 3-2: Comparing model output with measured outlet temperatures for NaCl seedbed at 353 K with no catalyst, EXP_17, 90 mL.s^{-1} reaction gas

3.1.2 Experiments with Catalyst

The figures in this section all relate to the same typical experiment of 4 seconds duration with 47 mg of catalyst, ET_PE_SFG_200. Figure 3-3 shows that the simulated reactor outlet temperature profile gives a good fit with measured values, particularly for maximum temperature and cooling rate. The fit for the heating rate is less good because it is dependent on the simple, lumped reaction constant. The model works by using the MATLAB function, lsqnonlin, to vary the lumped reaction constant until a minimum in the difference between measured and calculated output temperatures is reached. The corresponding mass of polymer is then calculated. In this example, the calculated mass of polymer formed is 20.9 mg for a measured value of 21 mg.

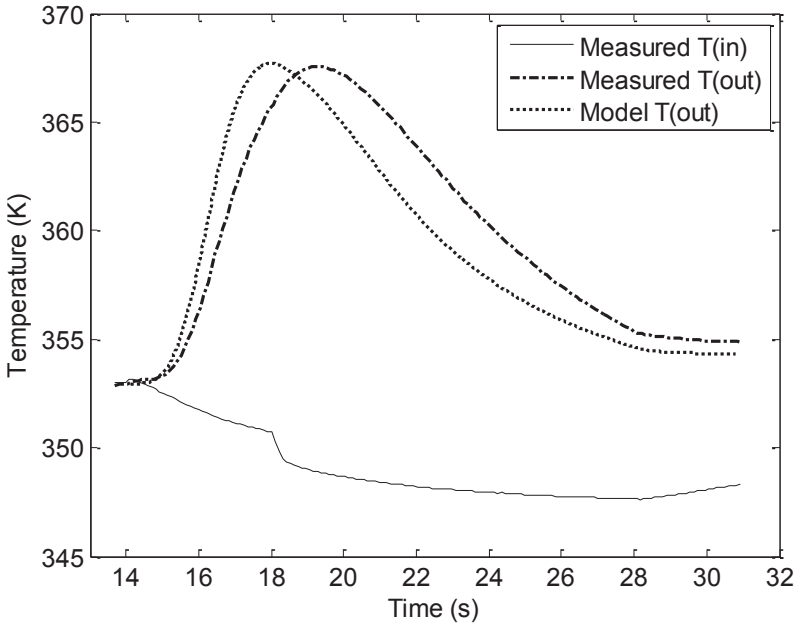

Figure 3-3: Comparison of calculated output temperatures against measured values for an experiment of 4s duration (T = 353 K, P = 6.67 bars of C_2H_4, nominal gas/particle velocity = 11 cm.s^{-1}).

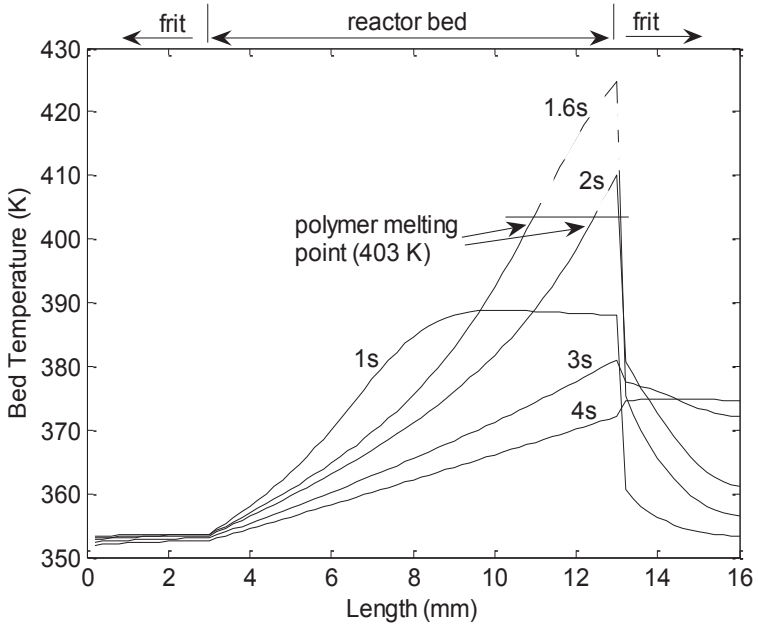

Figure 3-4: Calculated temperatures of gas and inert solid along reactor length at centre at different reaction times

Calculated reactor bed temperatures are shown in Figure 3-4. The model predicts a steep gradient along the reactor length with a maximum after 1.6 seconds of reaction. Under the given experimental conditions the polymerisation rate decreases quickly, and this then leads to a rapid reduction in the bed temperature. It can be seen that, towards the end of the bed, the melting point of PE is exceeded and this is discussed later, in section 3.1.5.1 of this chapter. After 4 seconds, the temperature has recovered to well below the polymer melting point.

The prediction of axial temperature gradients by the model is also supported by analysis of the polymer formed in the reactor. For the experiments ET_PE_SFG_430 and ET_PE_SFG_431 which were carried out under maximum flow (~300 $mL.s^{-1}$), 6 bar ethylene, 3 bar helium and at 353K, Tioni found the PDI to be increasing along the reactor length. The PDI gives a measure of the reaction temperature because transfer reactions have a higher activation energy than propagation, so they occur relatively more often at higher temperature. Increased transfer causes a greater spread of polymer chain lengths and hence a larger PDI. For catalyst charges of 27.7 mg and 50 mg respectively the PDI increased from 3.1 to 4.3 and from 8.9 to 10.2. This implies an axial temperature gradient in the reactor bed and also a higher bed temperature for the experiment with more catalyst.

It is also important to note that the exit frit temperature, and therefore the measured reactor outlet temperatures are much more stable than the calculated bed temperature because of the relatively high heat capacity of the stainless steel frit and at very short time scales, the frit absorbs most of the energy produced in the bed. The effect of this is to mask very rapid fluctuations occurring within the bed. Care must therefore be taken as reactor bed temperatures could be quite different to those measured at the reactor outlet.

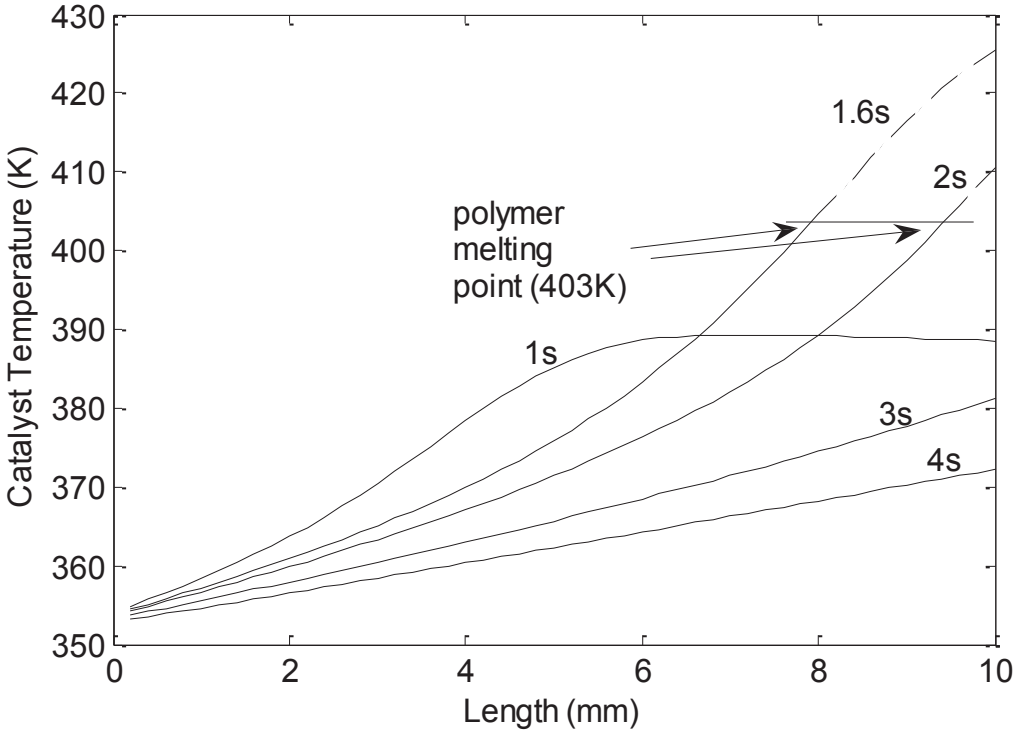

Figure 3-5 Calculated temperatures of catalyst/polymer along reactor length at centre at different reaction times

Figure 3-5 shows the calculated temperatures for the catalyst/polymer which are very similar to those found for the gas/inert and Figure 3-6 shows the radial temperature profile for the

catalyst/polymer particles at the hot section, towards the end of the bed, with a fairly flat profile across the centre of the bed and a cool section close to the reactor wall.

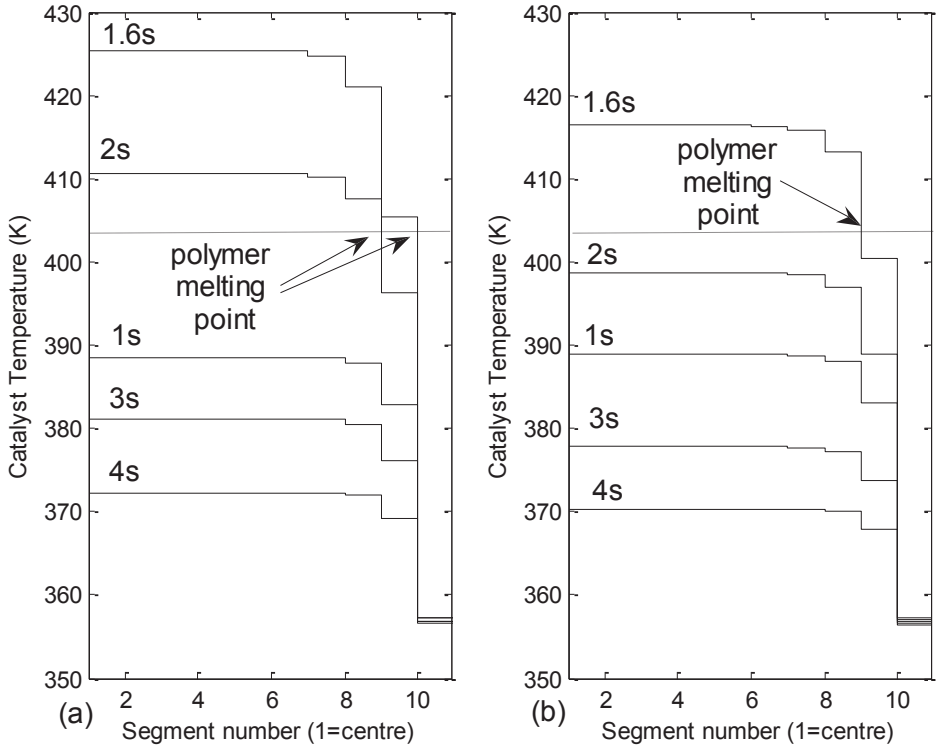

Figure 3-6: catalyst/polymer temperature radial profiles at (a) end of reactor bed and (b) 1mm from end of bed at different reaction times

3.1.3 Position of Inlet Thermocouple

As mentioned in Chapter 2 section 2.1.3.3.3, the position of the thermocouple in the reactor inlet chamber is not visible. The thermocouple could be pushed up against the frit or, further back, in the space of the chamber. The measured temperature would be either that of the stainless steel frit or of the gas entering the reactor. To try and deduce which is the case, the model was run with the inlet gas temperature fixed at the lowest measured gas temperature for both reaction and cooling periods.

Figure 3-7 compares the calculated temperature of the inlet frit with the measured inlet gas temperature for this run. The calculated response is similar to the measured values so it is possible that the measured temperature is the inlet frit rather than the gas. However, the reactor inlet chamber has thick stainless steel walls which could also cause this thermal response so it is not possible to be certain. However, Figure 3-8 shows the effect on calculated outlet temperatures is negligibly small, so the measured inlet temperature is maintained in the model as the gas inlet temperature.

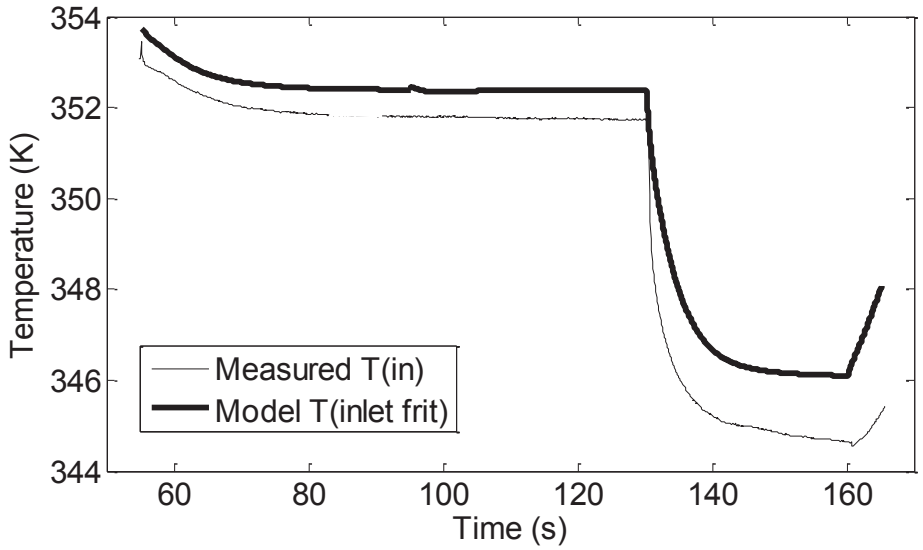

Figure 3-7: Compare measured temperatures (EXP_17) with calculated inlet frit temperatures for model run with fixed inlet gas temperature

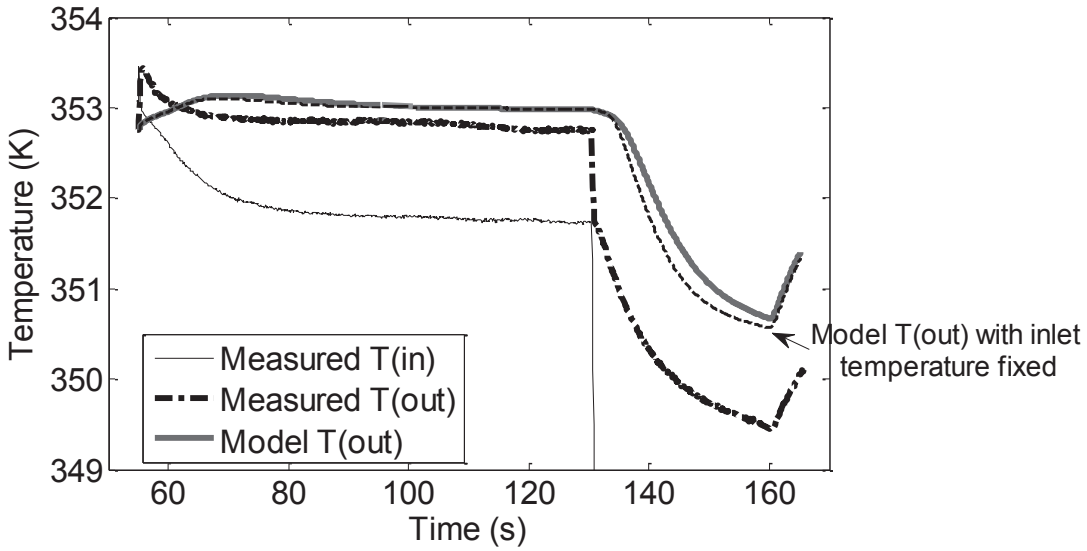

Figure 3-8: Comparison of the calculated outlet temperatures for EXP_17 with the gas inlet temperature taken as the measured value and fixed at the minimum measured value

3.1.4 Position of Exit Thermocouple

From the design of the reactor, and the position of the thermocouple in the exit chamber, there was some debate regarding whether the measured temperature was the average of the gas leaving the reactor or the centre point value. In fact, these are the limiting conditions and it is probable that the actual temperature which is measured falls somewhere between the two cases. To try and find a solution, both scenarios were modelled for the 4s polymerisation, ET_PE_SFG_200. The results are shown in Figure 3-9. The measured mass of polymer for this experiment was 21 mg. If the average reactor gas outlet temperature is fitted to the measured data, the model calculates a mass of polymer formed of

20.9 mg but only 15.2 mg if the centre point temperature is used. It seems that the average temperature of the gas leaving the reactor gives a much better representation and this is used in the model.

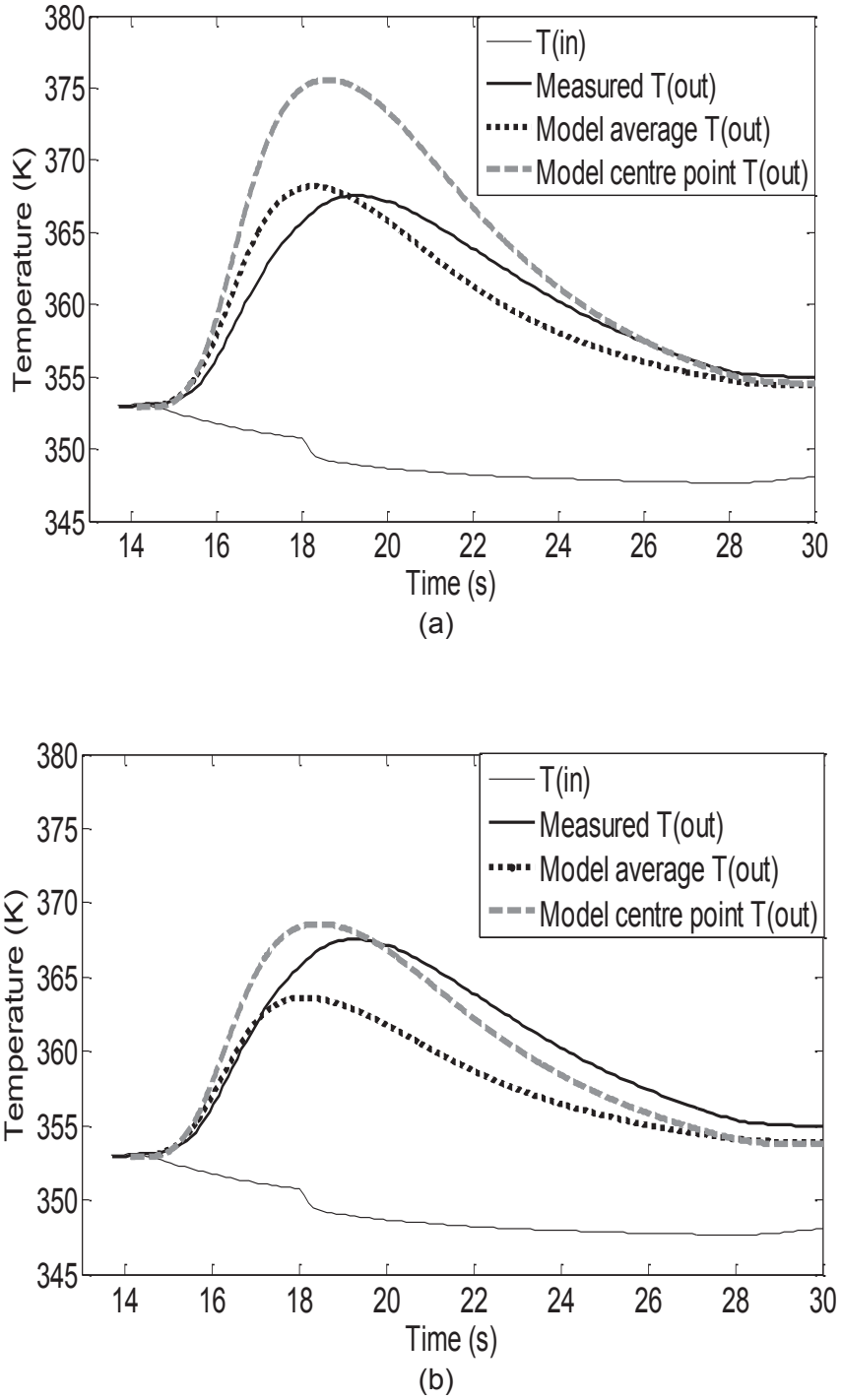

Figure 3-9: Compare model outputs for optimising with (a) the average calculated gas outlet temperature (b) the gas outlet temperature calculated at the centre point (experiment of 4s duration, T = 353 K, P = 6.67 bar C_2H_4, nominal gas/particle velocity = 11 cm.s^{-1})

3.1.5 Internal Thermocouple

As the model predicts temperature fluctuations in the reactor bed which can be quite different from the measured temperatures at the reactor outlet, the reactor was modified so that a thermocouple could be inserted through the reactor exit frit for direct measurement of the bed temperature. The thermocouple protruded by 2 mm into the reactor bed. Figure 3-10 shows the result which confirms that there can be a significant difference between the temperatures measured at the reactor exit and in the reactor bed. The temperatures calculated by the model are also shown for comparison with the measured data. Although the thermocouple in the reactor bed was able to illustrate a difference between reactor bed and outlet temperature, its use was quite problematic and is discussed later in Chapter 4, section 4.1.

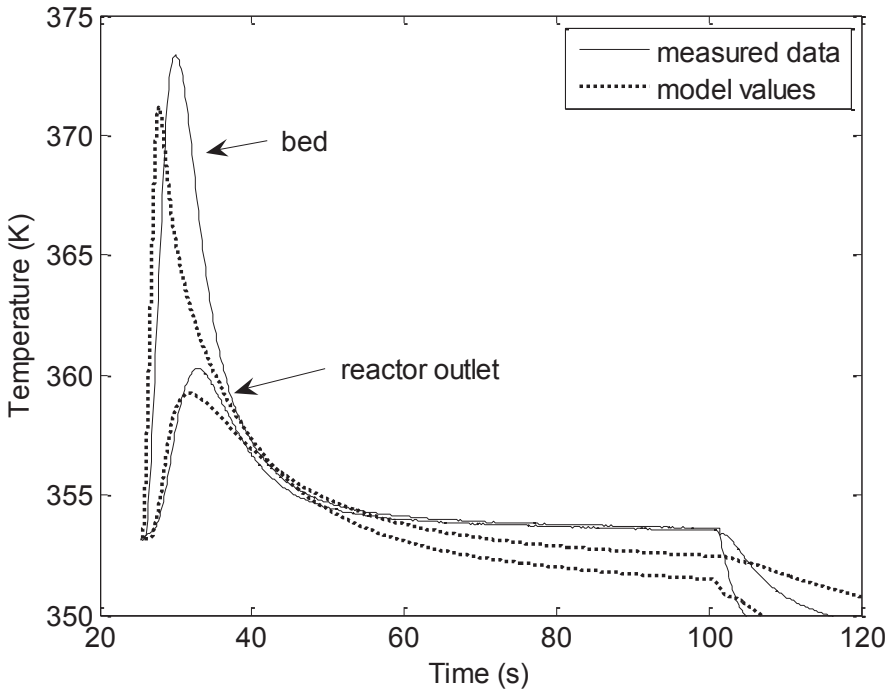

Figure 3-10: Comparison between model and measured reactor bed and outlet temperatures for the same experiment (ET_SFG_462)

In this experiment, the thermocouple in the bed measures a much faster temperature fluctuation than those at the reactor inlet and outlet. The measured temperature values were therefore corrected using the thermocouple time constant. It can be seen from Figure 3-11 that this suggests only a slight difference (~1K) between the measured and corrected values, even during the initial rapid temperature rise.

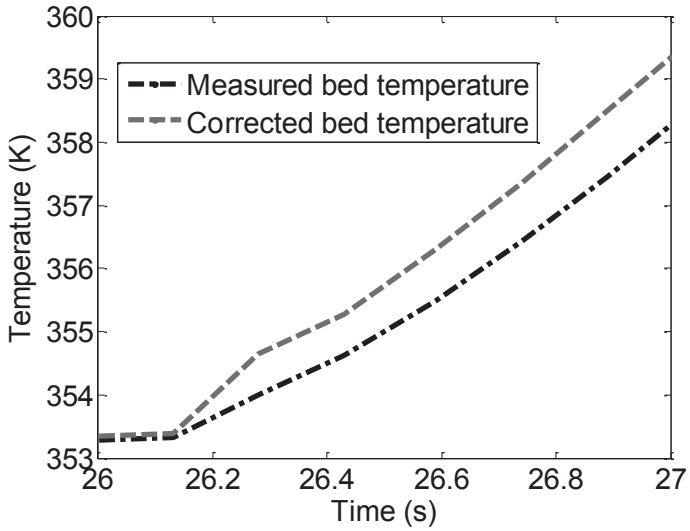

Figure 3-11: Measured and corrected bed temperatures for initial 1s of experiment ET_462

The measured bed temperature from the experiment only allows a rough check of the heat balance over the exit frit. This is because the temperature measured is for a single point on the reactor centreline, and 2mm from the exit of the reactor bed. It therefore includes no information about the radial temperature gradient. However, the check was carried out by inserting the measured bed temperature into the model as the bed exit temperature. Whilst, as expected, this predicts a reactor outlet temperature which is slightly too high, it also shows that the calculated and measured temperature profiles are very similar (Figure 3-12).

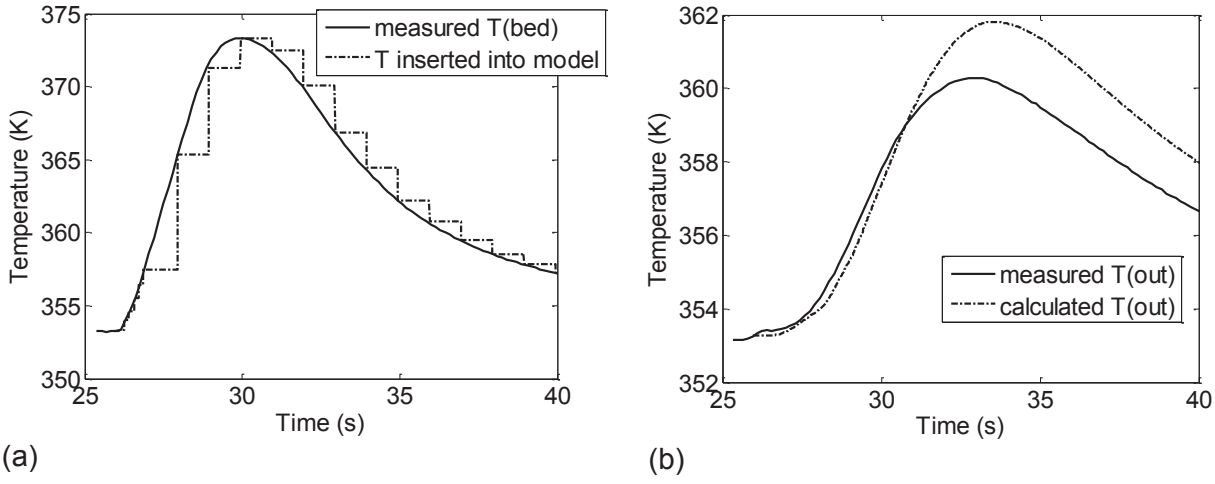

Figure 3-12: Graphs (a) showing the temperature inserted into the model as the bed exit value (b) comparing the measured and calculated outlet temperatures

3.1.5.1 Polymer Melting Point

Returning to the typical experiment described in section 3.1.2, simulated reactor bed temperatures include a brief excursion which exceeds the melting point of polyethylene. Melting is undesirable because the initial polymer structure is lost. If reactor temperatures become very high there will also be rapid catalyst deactivation and possibly even the loss of some short polymer chains as gas. It was not possible to verify whether melting had

occurred by visual inspection since the yields on this time scale are very low. For this particular experiment the yield is 0.38 $g_{PE}.g_{cata}^{-1}$. The reactor zone concerned is at the centre and end of the reactor bed (13% of the total volume), the area near the reactor wall remains below the melting point. While it might be possible that the pores of the particle become blocked with the melted material, causing the reaction in the particles to shut down (at least locally) [1] we see no evidence of that here. The powder recovered at the end of the bed was essentially free-flowing and visual inspection of the bed revealed no lumps that would indicate that the particles had melted and stuck to the salt or each other. However, it can be pointed out that the excursion is brief, lasting between 0s and 1.2s so polymer would re-crystallise as the reactor temperature recovers and allow fragmentation to continue. In addition, at this stage of the polymerisation the pore volume is actually greater than the amount of polymer produced, so it is unlikely that pore blockage could occur to a significant degree.

Catalyst temperatures are not thought to be able to dramatically exceed the melting point of PE and to investigate whether this is this case for these early polymerisation conditions the model was amended to represent this scenario. The calculation was changed so that if the catalyst temperature is at or above 413 K, 10 K above the PE melting point, the reaction rate term in the model is set to zero. The results are shown in Figure 3-13. The model has calculated 22.1 mg of polymer formed for 21 mg measured. Changing the model in this way only makes a slight difference to the calculated reactor outlet temperatures and predicted yield. This suggests that the short temperature excursion is too small and rapid to be of great consequence in terms of yield.

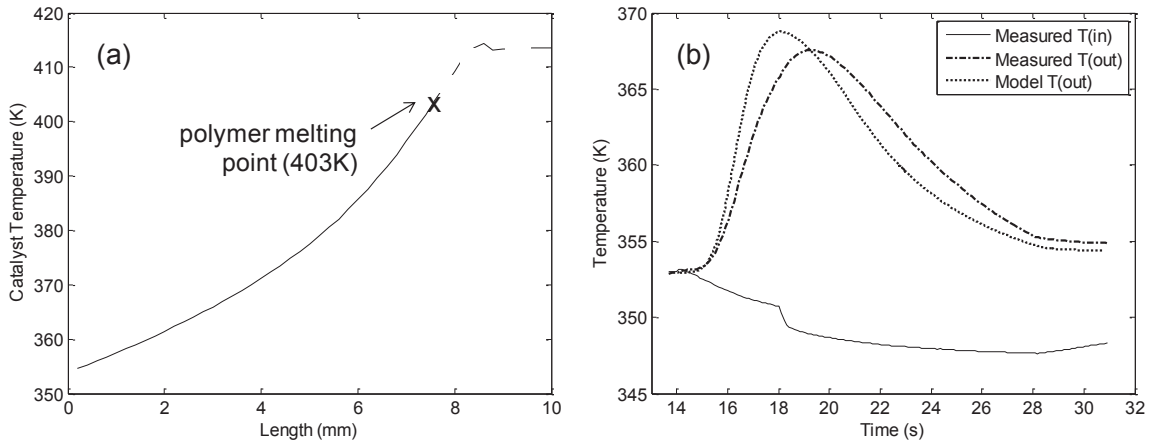

Figure 3-13: (a) Maximum calculated catalyst temperatures along reactor length at centre (b) Comparison of calculated outlet temperatures against measured values for the same experiment of 4s duration with reaction rate = 0 at and above 413K.

Results above the PE melting point are not valid temperature points because changes in physical properties are not taken into account. For example, diffusion mechanisms in molten polymer and amorphous polymer are not the same and there can be a step change in diffusion rates on polymer melting [2]. To make a correct calculation, the properties of molten polymer would be needed in the model and, also, the heat of fusion of the polymer would have to be taken into account.

The heat of fusion of PE depends on the crystallinity and is approximately 146 $J.g^{-1}$. It might be expected that melting would influence the temperature in the reactor bed. A quick comparison can be made with the heat capacity of the reactor bed. The specific heat capacity of NaCl is 0.89 $J.g^{-1}.K^{-1}$, the weight fraction of catalyst in the bed is 3% and the polymer yield at the time of maximum temperature is around 0.5 $g_{PE}.g_{cata}^{-1}$. So, melting of all the polymer in the reactor bed would absorb about the same amount of heat as raising the bed temperature by 2.5 K. We can conclude that two thermal effects have about the same order of magnitude and that polymer melting should produce a slight temperature effect in the reactor bed. However, the effect of a small volume of local melting would not be discernable in the measured outlet gas temperature because the outlet gas is coming from the whole cross section of the bed including the cool region at the reactor wall. Also, the effect of the exit frit is to damp temperature fluctuations in the bed.

3.1.6 Polymer Distribution

As reported by Tioni [3], the distribution of polymer formed in the reactor was evaluated by sampling 6 different reactor zones after a polymerisation reaction lasting 30s (Experiment ET_PE_SFG_383). Thermo gravimetric analysis (TGA) was then used to analyse their composition. The results are given in Table 3-1 and Figure 3-14 and the model predictions are shown in Figure 3-15.

Reactor	Centre	Edge
Inlet	6.74	6.44
Centre	7.26	6.81
Outlet	8.08	7.52

Table 3-1: Measured mass fraction polyethylene in different reactor zones (wt%) for ET_PE_SFG_383

The model shows the same trends as found in the measured data; the local mass fraction of polymer increases along the length of the reactor and is higher at the reactor centre than at the wall. The discrepancies between the absolute values of polymer in the bed and the mass fraction predicted by the model can be explained by the approximate nature of the experimental method (the bed was fractionated by hand on a small volume).

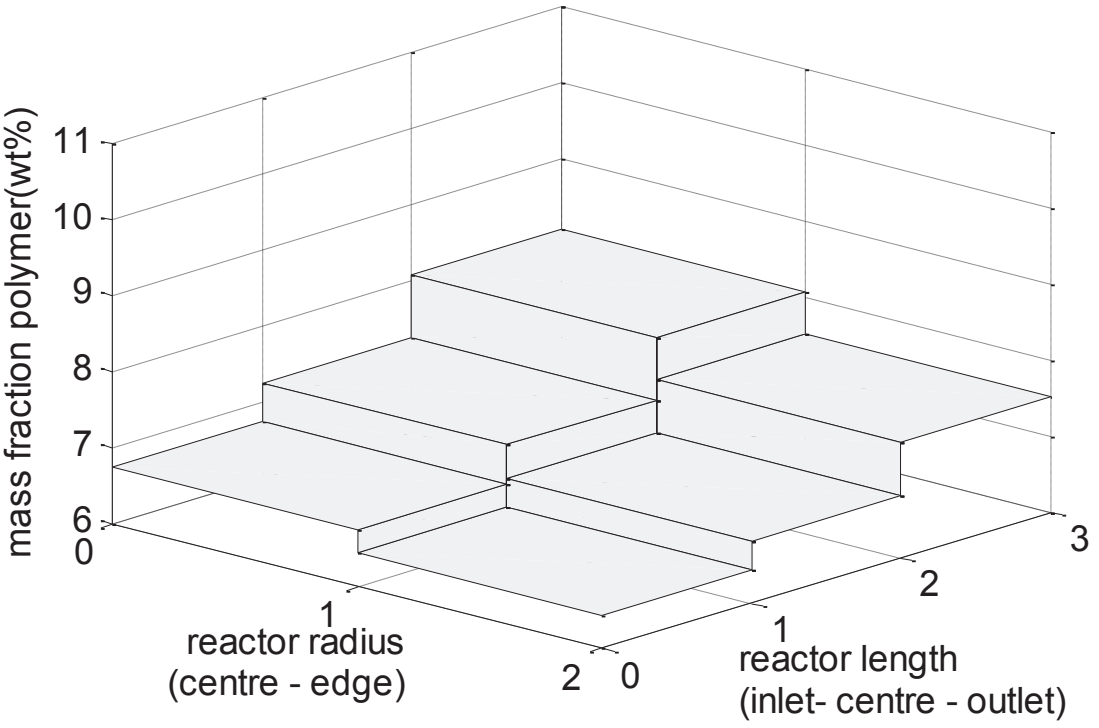

Figure 3-14: Measured mass fraction of polyethylene across different reactor zones (wt%) for ET_PE_SFG_383

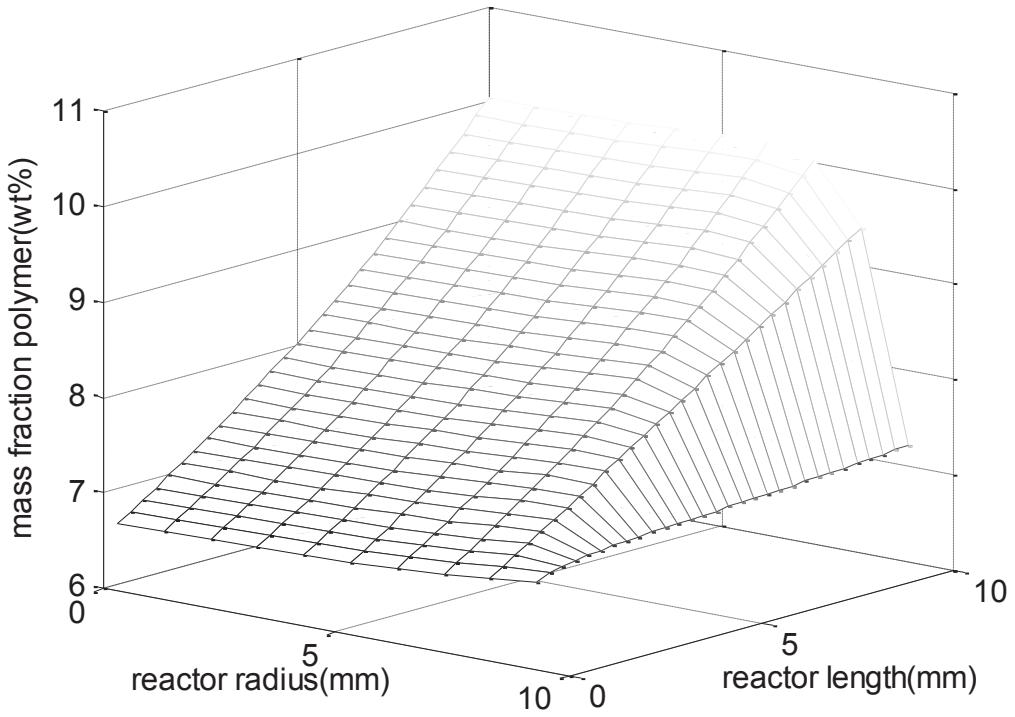

Figure 3-15: Calculated mass fraction of polyethylene across different reactor zones (wt%) for ET_PE_SFG_383

A factor in the optimisation of the reactor was that sufficient polymer be produced for analysis. For longer duration reactions, this was possible with less catalyst. In this experiment, the mass of catalyst was 39.4 mg and the maximum calculated temperature in the reactor was 393 K, well below the polymer melting point. Figure 3-16 compares the calculated and measured outlet temperatures. We can see that whilst the simple lumped reaction constant produces a temperature profile with the right trends it gives a less accurate prediction for longer duration experiments. The model predicts 88 mg of polymer for 69 mg measured with a yield of 1.76 $g_{PE}.g_{catalyst}^{-1}$. Figure 3-17 shows the calculated accumulation and distribution of polymer in the reactor bed at different times during the polymerisation. We can see that the accumulation rate is quite steady.

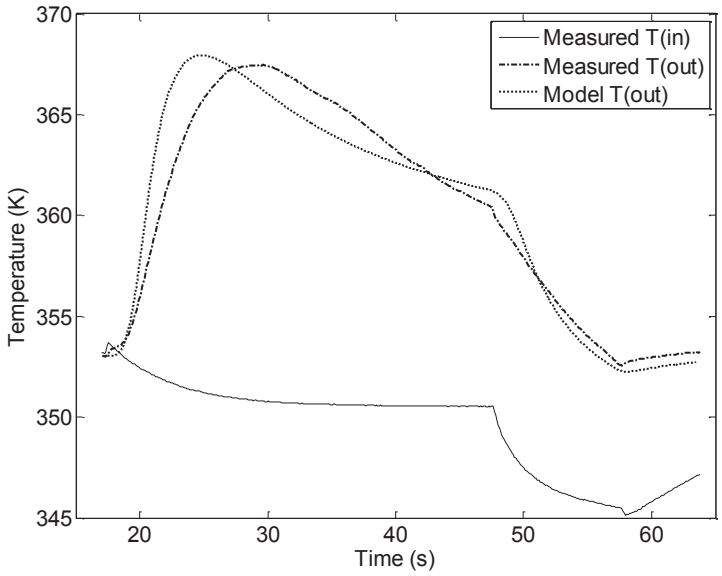

Figure 3-16: Comparison of measured and calculated reactor outlet temperatures for the 30s duration polymer distribution experiment, ET_PE_SFG_383

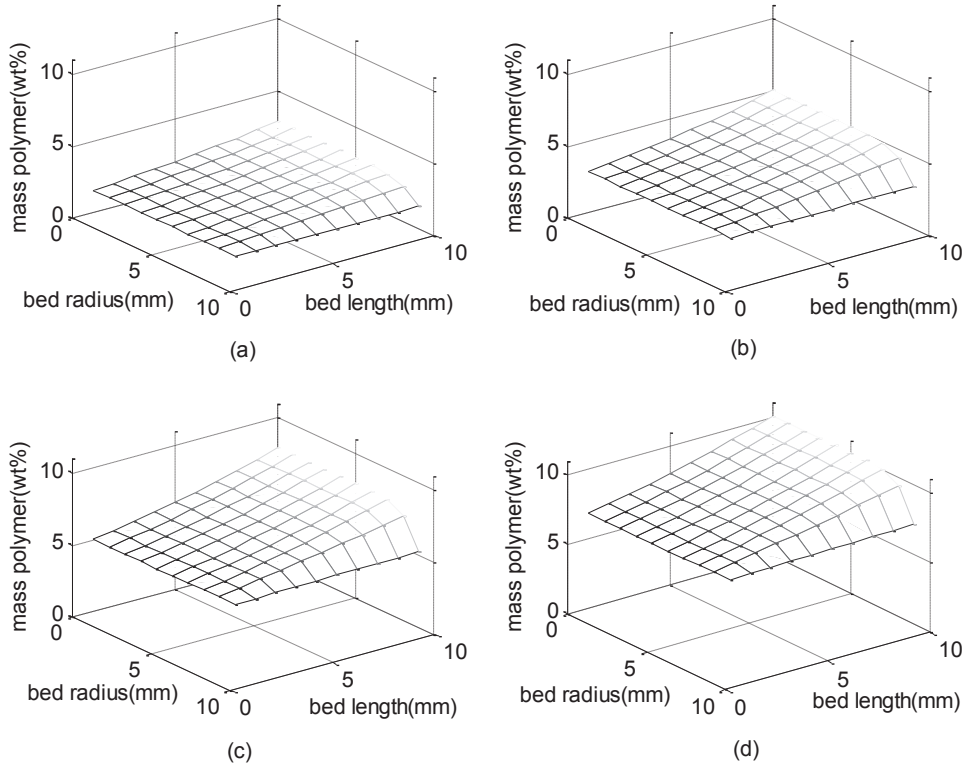

Figure 3-17: Graph showing the calculated distribution of polymer in the reactor bed at (a) 5s (b) 10s (c) 20s and (d) 30s for ET_PE_SFG_383

3.1.7 CO_2 Flowrate

A good estimate of the CO_2 flowrate is particularly important for very short duration experiments where most of the heat of reaction is evacuated with the CO_2. As this flow is not measured and there is variation in the measured reaction gas flowrate, possibly due to the exit frit becoming slightly blocked with polymer, some error is clearly unavoidable.

Figure 3-18 shows the sensitivity of the model to a ±20% change in the CO_2 flowrate. It can be seen by comparing the gradients of the calculated temperature curves during the cooling period that the value in the model is reasonable.

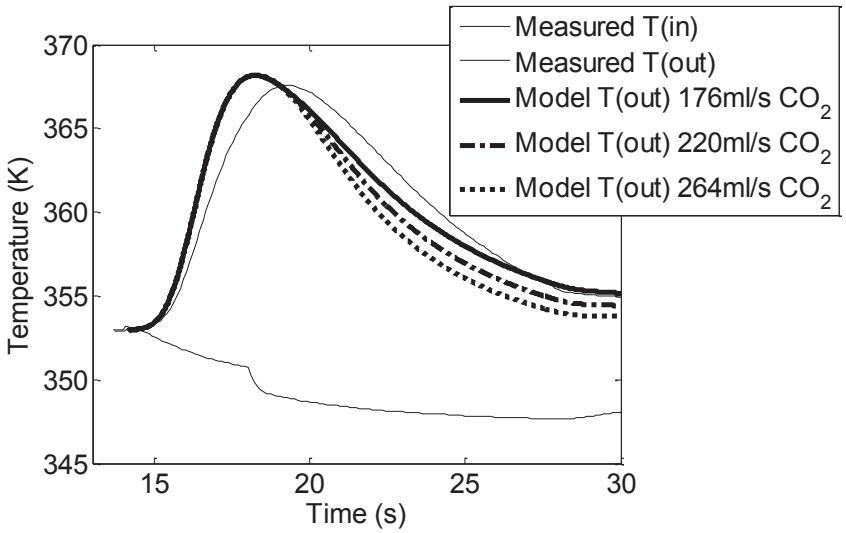

Figure 3-18: Effect of using different CO_2 flowrates (±20%) on the calculated outlet temperatures

3.1.8 Numerical Dispersion

Figure 3-19 shows the maximum temperatures calculated along the reactor centreline for the same model inputs and with increasing numbers of axial elements. There is some numerical dispersion because the gradients of the temperature curves are increasing with the number of elements. However, computing time also increases with number of elements. The model with ten one millimetre elements is sufficient to show general profiles and to compare the effects of changing parameters. Where more precision is required the number can be increased, for example, 50 0.2 mm axial elements could be used.

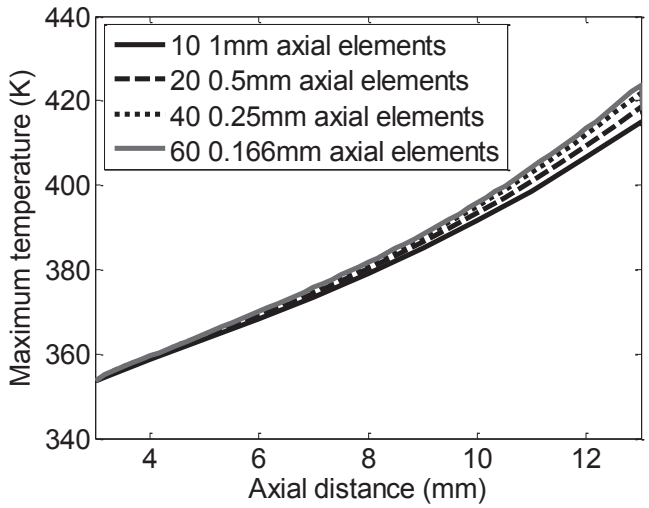

Figure 3-19: Maximum temperatures calculated by the model along the reactor centre with different numbers of axial finite elements

3.1.9 Conclusion

The model provides a good fit with experimental data for experiments with and without catalyst. From the measured reactor outlet temperature, the gas seems to be well mixed at the thermocouple and this is assumed in the model. The calculated value for the CO_2

flowrate seems reasonable when applied to the model. The model predicts the formation of axial temperature gradients in the reactor and this is supported by analytical data. Predictions of temperatures above the polymer melting point cannot be considered accurate data points. However, the possibility of temperature excursions beyond the melting point is not ruled out.

The exit frit temperature is more stable than that of the bed and can mask rapid temperature variation within the reactor. This is confirmed by experiments with a thermocouple inserted into the reactor bed and a check of the heat balance over the exit frit using the measured bed temperature.

Calculated and measured values for the distribution of polymer formed in the reactor bed are in agreement. However, for longer experiments the simple kinetics used in the model represent the polymerisation less well than for very short duration experiments.

In summary, the heat and mass balances in the reactor model are validated. The simple lumped kinetics provide a good fit for short duration individual experiments but are less accurate for longer experiments. Also, no general formula for the kinetics which can be used to model all the experiments has been found so far and the model is limited to representing experiments individually.

3.2 Calorimetry

As stated in section 2.1.1, one objective of this experimental set-up and model is to use the reactor as a calorimeter to gain precise measurements of the initial polymerisation rate. Calorimetry is commonly used for monitoring polymerisation reactors [4]. Lahti et al. [5] tested a laboratory scale calorimeter for slurry, suspension, bulk and solution polymerisations and found accurate reaction monitoring to be possible. In their 2011 review, Frauendorfer et al. [6] include reaction calorimetry as one of the main methods used for on-line monitoring of industrial scale polymerisation reactors.

In the use of calorimetry for polymerisation reaction monitoring, estimation methods are used to calculate reaction rates from measured temperatures [7]. Different approaches can be used and, recently, Soares et al. [8] demonstrated use of the Monte Carlo method and Rincon et al. [9] tested an unscented Kalman filter for calorimetric estimation of conversion in batch emulsion polymerisation reactors. Both were able to find good agreement with measured data obtained by sampling and composition analysis and both point out that the main difficulty in using estimation techniques to monitor polymerisation reactions is that parameters and physical properties are in flux. In particular, there is a decrease in the heat transfer coefficient at the reactor wall due to fouling and increasing viscosity of the reaction medium.

For laboratory scale slurry polymerisation, calorimetric techniques have been used successfully to monitor early reaction rates. Examples are the work of Korber et al. [10] and Tisse et al. [11] who both studied olefin polymerisation with silica supported metallocene catalysts. Korber et al. [10] showed that a commercially available isothermal reaction calorimeter was able to give more precise reaction rate data than measurement of monomer consumption rate by mass flowmeter. Tisse et al. [11] constructed a nonlinear state observer which allowed on-line reaction rates to be monitored directly and found this to be complimentary with mass flow measurement which was more accurate at low polymerisation rates.

Soares et al. [8] give reaction calorimetry the wide definition of ‘the monitoring of heat balances in a reacting system to allow inference of the rates of exothermic (or endothermic) reactions and some additional correlated variables, such as compositions’. If calorimetric estimation could be applied to gas phase polymerisation in the laboratory fixed bed reactor, accurate reaction rate data for the first few seconds of the reaction period might be obtained.

This could be particularly useful in elucidating which of the rapidly changing physical and chemical properties are controlling the reaction rate dynamic.

3.2.1 The Fixed Bed Reactor as a Calorimeter

Kammona et al. [4] state that only the isothermal reaction calorimeter is suitable for monitoring polymerisation reactions. In such an arrangement, the reactor and jacket temperatures are measured continuously and the temperature of the polymerisation medium is maintained constant by rapid control of the reactor jacket temperature. A heat balance over the reactor then allows the rate of heat generation in the vessel to be calculated. The main design principles for construction of this type of calorimeter are good mixing of the reactor contents, good heat transfer at the reactor wall and minimal/known heat losses. The laboratory scale fixed bed polymerisation reactor under study does not match these criteria. The main heat transfer route out of the reactor is the outlet gas stream and the reactor bed temperature fluctuates during the first moments of the polymerisation. However, these factors are accounted for in the heat balances which have been constructed and validated. The heat balances can be considered as the first step in using the reactor as a calorimeter. The second step is to create a state estimator which will calculate the polymerisation rate from the measured temperature data.

3.2.2 Construction of the High Gain Observer

An observer is used to find values for unmeasured states from a model of a system and its measured data. Calculated and measured data are compared at each time step to calculate a corrective term that is used in the next step to adjust the dependent parameter. In this particular case the polymerisation rate will be estimated from the measured reactor inlet and outlet temperatures.

3.2.2.1 Model Simplifications

In state space form, an observer is written as:

$$\dot{\hat{X}} = A\hat{X} + \phi + correction\_term \qquad \textbf{3-1}$$

Where

$$\dot{X} = AX + \phi \qquad \textbf{3-2}$$

is the model and $\hat{X}$ is the estimated values of X. Only the heat balances from the fixed bed reactor model are required as it is these which relate the reaction rate to the outlet temperature. They are given by equations 2-36 and 2-40, developed previously:

$$\frac{dT_c}{dt} = \frac{1}{\sum(\rho c_p)_c}\left(Mwt_{C2}\bar{r}_v\left(\frac{\Delta H}{Mwt_{C2}} + c_{pC2}\left(T_g - T_c\right)\right) + S_{cat}h_{cat}\left(T_g - T_c\right)\right)$$

2-36

$$\frac{\partial T_g}{\partial t} = \frac{1}{\sum\left((\rho c_p)_g - (\beta \Delta H_{ads})\right)}\left(\begin{array}{l} \left(\alpha \Delta H_{ads}\frac{\partial y_{C2}}{\partial t}\right) - \left(S_{cat}h_{cat} - Mwt_{C2}\bar{r}_v c_{pC2}\right)\left(T_g - T_c\right) \\ + F_T Mwt_{rg}c_{prg}\frac{\partial T_g}{S_r \partial z} + \frac{l_{sfer}}{r}\frac{\partial}{\partial r}\left(\frac{r\partial T_g}{\partial r}\right) \end{array}\right)$$

2-40

With the reactor internal wall boundary condition:

$$l_{sfer}\left(\frac{\partial T_g}{\partial r}\right) = h_{\text{int}}^{sf}\left(T_g - T_w\right)\Big|_{dreac/4<r<dreac/2} \forall z$$

3-3

For the initial observer development these equations can be simplified. The adsorption terms in equation 2-40 are not necessary as a silica seedbed is not considered. The term $c_{pC2}\left(T_g - T_c\right)$ in equations 2-36 and 2-40 represents catalyst particle cooling by incoming ethylene which is small compared to the heat of reaction and is neglected. Thermal gradients are known to exist in the reactor bed and in the reactor model; these are accounted for by using finite elements in both the radial and axial directions. The first observer construction will include finite elements in the axial direction with a view to including radial temperature gradients later. For this case, a different wall heat transfer coefficient is used, including the resistance to heat transfer in the reactor bed and at the wall, as determined from equation 3-4 [12].

$$\frac{1}{\bar{h}_{\text{int}}} = \frac{d_t}{8l_{sfer}} + \frac{1}{h_{\text{int}}^{sf}}$$

3-4

The model includes both the reaction and cooling periods of the polymerisation experiments. This is because, for short duration experiments, most of the heat of reaction is evacuated from the reactor during the cooling period, as discussed in Chapter 2, section 2.1.3. The observer estimates real-time values of the state vector relative to its input, so the cooling period cannot be used the estimate the polymerisation rate as the reaction is over. To overcome this, it is assumed that the heat transfer calculations for the reactor walls and frits

are correct so the reactor bed outlet temperature, upstream of the exit frit, is known and is the value used as the measured temperature.

Also, all the parameters in the heat balances except T_c, T_g and $\bar{r}_v$ are assumed constant. A longer duration experiment (15s) is considered for the initial observer development.

The heat balances for each finite element become:

$$\frac{dT_c}{dt} = \frac{1}{\sum(\rho c_p)_c}\left(\Delta H \bar{r}_v + S_{cat} h_{cat}\left(T_g - T_c\right)\right)$$

3-5

and

$$\frac{\partial T_g}{\partial t} = \frac{1}{\sum(\rho c_p)_g}\left(-S_{cat} h_{cat}\left(T_g - T_c\right) + F_T Mwt_{rg} c_{prg} \frac{\left(T_g - T_{g\,in}\right)}{S_r \partial z} - \bar{h}_{\text{int}} A_w \left(T_g - T_w\right)\right)$$

3-6

3.2.2.2 State-Space Form of Model

To create the high gain observer the model must be put into state-space form as per equation 3-2. The heat balances become:

$$\underbrace{\begin{bmatrix} \dot{T}_g \\ \dot{T}_c \\ \dot{\bar{r}}_v \end{bmatrix}}_{\dot{X}} = \underbrace{\begin{bmatrix} 0 & \dfrac{S_c h_{cat}}{\sum(\rho c_p)_g} & 0 \\ 0 & \dfrac{-S_c h_{cat}}{\sum(\rho c_p)_c} & \dfrac{\Delta H}{\sum(\rho c_p)_c} \\ 0 & 0 & 0 \end{bmatrix}}_{A} \cdot \underbrace{\begin{bmatrix} T_g \\ T_c \\ \bar{r}_v \end{bmatrix}}_{X}$$

$$+ \underbrace{\begin{bmatrix} \dfrac{1}{\sum(\rho c_p)_g}\left(-S_c h_{cat} T_g + F_T Mwt_{rg} c_{prg} \dfrac{\left(T_g - T_{g\,in}\right)}{S_r \partial z} + \bar{h}_{\text{int}} A_w \left(T_g - T_w\right)\right) \\ \dfrac{S_c h_{cat}}{\sum(\rho c_p)_c} T_g \\ \varepsilon \end{bmatrix}}_{\phi}$$

3-7

Where ε represents the unknown dynamic of $\bar{r}_v(t)$. A is written to depend only on measured or known variables. The rest is in ϕ. Equation 3-7 can be expanded to represent the same equations for n finite reactor elements:

$$\underbrace{\begin{bmatrix} \dot{T}_{gn} \\ \vdots \\ \dot{T}_{g2} \\ \dot{T}_{g1} \\ \dot{T}_{cn} \\ \vdots \\ \dot{T}_{c2} \\ \dot{T}_{c1} \\ \dot{\bar{r}}_{vn} \\ \vdots \\ \dot{\bar{r}}_{v2} \\ \dot{\bar{r}}_{v1} \end{bmatrix}}_{\dot{X}} = \underbrace{\begin{bmatrix} 0 & \cdots & \cdots & 0 & \frac{S_c h_{cat}}{\sum(\rho c_p)_g} & 0 & \cdots & 0 & 0 & \cdots & \cdots & 0 \\ \vdots & \vdots & \vdots & \vdots & 0 & \ddots & \ddots & \vdots & \vdots & \vdots & \vdots & \vdots \\ 0 & \cdots & \cdots & 0 & \vdots & \ddots & \ddots & 0 & 0 & \cdots & \cdots & 0 \\ 0 & \cdots & \cdots & 0 & 0 & \cdots & 0 & \frac{S_c h_{cat}}{\sum(\rho c_p)_g} & 0 & \cdots & \cdots & 0 \\ 0 & \cdots & \cdots & 0 & \frac{-S_c h_{cat}}{\sum(\rho c_p)_c} & 0 & \cdots & 0 & \frac{\Delta H}{\sum(\rho c_p)_c} & 0 & \cdots & 0 \\ \vdots & \vdots & \vdots & \vdots & 0 & \ddots & \ddots & \vdots & 0 & \ddots & \ddots & \vdots \\ 0 & \cdots & \cdots & 0 & \vdots & \ddots & \ddots & 0 & \vdots & \ddots & \ddots & 0 \\ 0 & \cdots & \cdots & 0 & 0 & \cdots & 0 & \frac{-S_c h_{cat}}{\sum(\rho c_p)_c} & 0 & \cdots & 0 & \frac{\Delta H}{\sum(\rho c_p)_c} \\ 0 & \cdots & \cdots & 0 & 0 & \cdots & \cdots & 0 & 0 & \cdots & \cdots & 0 \\ \vdots & \vdots & \vdots & \vdots & \vdots & \vdots & \vdots & \vdots & \vdots & \vdots & \vdots & \vdots \\ 0 & \cdots & \cdots & 0 & 0 & \cdots & \cdots & 0 & 0 & \cdots & \cdots & 0 \\ 0 & \cdots & \cdots & 0 & 0 & \cdots & \cdots & 0 & 0 & \cdots & \cdots & 0 \end{bmatrix}}_{A} \cdot \underbrace{\begin{bmatrix} T_{gn} \\ \vdots \\ T_{g2} \\ T_{g1} \\ T_{cn} \\ \vdots \\ T_{c2} \\ T_{c1} \\ \bar{r}_{vn} \\ \vdots \\ \bar{r}_{v2} \\ \bar{r}_{v1} \end{bmatrix}}_{X}$$

$$+ \underbrace{\begin{bmatrix} \frac{1}{\sum(\rho c_p)_g}\left(-S_c h_{cat} T_{gn} + F_T Mwt_{rg} c_{prg} \frac{\left(T_{gn} - T_{g\,n-1}\right)}{S_r \partial z} + \bar{h}_{\text{int}} A\left(T_{gn} - T_w\right)\right) \\ \vdots \\ \frac{1}{\sum(\rho c_p)_g}\left(-S_c h_{cat} T_{g2} + F_T Mwt_{rg} c_{prg} \frac{\left(T_{g2} - T_{g1}\right)}{S_r \partial z} + \bar{h}_{\text{int}} A\left(T_{g2} - T_w\right)\right) \\ \frac{1}{\sum(\rho c_p)_g}\left(-S_c h_{cat} T_{g1} + F_T Mwt_{rg} c_{prg} \frac{\left(T_{g1} - T_{g\,in}\right)}{S_r \partial z} + \bar{h}_{\text{int}} A\left(T_{g1} - T_w\right)\right) \\ \frac{S_c h_{cat}}{\sum(\rho c_p)_c} T_{gn} \\ \vdots \\ \frac{S_c h_{cat}}{\sum(\rho c_p)_c} T_{g2} \\ \frac{S_c h_{cat}}{\sum(\rho c_p)_c} T_{g2} \\ \varepsilon_n \\ \vdots \\ \varepsilon_2 \\ \varepsilon_1 \end{bmatrix}}_{\phi}$$

3-7 bis

In this arrangement, the state vector X is written with the measured bed exit gas/inert temperature in row 1. This is a necessary structure for observer construction because the states are estimated from the top of the matrix down.

3.2.2.3 Observability

To usefully apply a state observer to a system of equations, they must be observable. This requires that the state(s) to be estimated can be completely defined over the required time interval from knowledge of the inputs and measured outputs. The observability of a linear system can be checked by the Kalman criteria using A & C, where A is the matrix represented in equation 3-7 and C is the output matrix. For a system to be observable the matrix

$$\begin{bmatrix} C \\ CA \\ CA^2 \\ CA^3 \\ \vdots \end{bmatrix}$$

must have the same rank as the number of states. For example, if the fixed bed reactor were considered as a single uniform element it would have 3 states, T_c, T_g and $\bar{r}_v$, so

$$\begin{bmatrix} C \\ CA \\ CA^2 \end{bmatrix}$$

must be of rank 3 for the system to be observable. The observability test for our system using the Kalman criteria is given in Appendix 3 and shows that this system of equations is observable only for a single reactor element (equation 3-7) and not for multiple elements (equation 3-7 bis). The case for the single element will be developed below as a first step.

3.2.2.4 Change of Variables

To create an observer, the system of equations must be written with matrix A in canonical form. Equation 3-7 shows that this is not the case so a change of variables is carried out. The method is to replace X with Z where:

$$Z = \begin{bmatrix} z_1 \\ z_2 \\ z_3 \end{bmatrix} = \begin{bmatrix} y \\ L_f y \\ {L_f}^2 y \end{bmatrix} = \begin{bmatrix} y \\ \dfrac{dy}{dX} f \\ \dfrac{d\left(L_f y\right)}{dX} f \end{bmatrix} \qquad \text{3-8}$$

and

$$f = AX \quad [7].$$

The transformation is described in Appendix 3.

The replacement variable, Z, is:

$$Z = \begin{bmatrix} z_1 \\ z_2 \\ z_3 \end{bmatrix} = \begin{bmatrix} T_g \\ \dfrac{S_c h_{cat}}{\sum (\rho c_p)_g} . T_c \\ \dfrac{S_c h_{cat}}{\sum (\rho c_p)_g \sum (\rho c_p)_c} \left(- S_c h_{cat} . T_c + \Delta H . \bar{r}_v \right) \end{bmatrix}$$

3-9

3.2.2.5 Correction Term

The correction term for the observer is:

$$\left(\frac{dz}{dX} \right)^{-1} S_\theta^{-1} C^T \left(y - \hat{y} \right)$$

3-10

where $\left(\frac{dz}{dX} \right)^{-1} S_\theta^{-1} C^T$ is a single, constant, independent matrix, calculated before applying the observer, and where $\left(y - \hat{y} \right)$ is the difference between measured and estimated data, in this case $\left(T_g - \hat{T}_g \right)$. The calculations for $\left(\frac{dz}{dX} \right)^{-1}$ are given in Appendix 3. The result is:

$$\left(\frac{dz}{dX} \right)^{-1} = \begin{bmatrix} I & 0 & 0 \\ 0 & \dfrac{\sum (\rho c_p)_g}{S_c h_{cat}} I & 0 \\ 0 & \dfrac{\sum (\rho c_p)_g}{\Delta H} I & \dfrac{\sum (\rho c_p)_g \sum (\rho c_p)_c}{S_c h_{cat} \Delta H} I \end{bmatrix}$$

3-11

- Tuning Parameter

S_θ^{-1} is used to incorporate θ which is the observer tuning parameter. High θ values allow rapid convergence to the value of the estimated state(s), but increase the sensitivity to noise.

So, a compromise should be found. S_θ is of the same dimension as $\frac{dz}{dX}$ and is the explicit solution of the algebraic Lyapunov equation:

$$S_\theta(i,j) = \frac{(-1)^{i+j}}{\theta^{i+j-1}} \frac{(i+j-2)!}{(i-1)!(j-1)!}$$

3-12

- Matrix C

C represents the measured data. In this case, three states are to be estimated for each finite elements, (T_g, T_c and $\bar{r}_v$), so there are 3 states in total but only T_g is measured. The number of states to be estimated is 2 and C is written:

$$C = y.X^{-1} = \begin{bmatrix} 1 & 0 & 0 \end{bmatrix}$$

3-13

3.2.2.6 Observer Programming

The observer is programmed in MATLAB. Figure 3-20 shows a block diagram of the observer program. The values for the bed outlet temperature, used as the measured variable, are obtained from the validated model. This is necessary because, as discussed in section 3.1.2, the effect of the exit frit is to mask temperature fluctuations in the reactor bed from the true measured reactor outlet temperature. Possible methods to overcome this problem are discussed later in section 3.3.4.

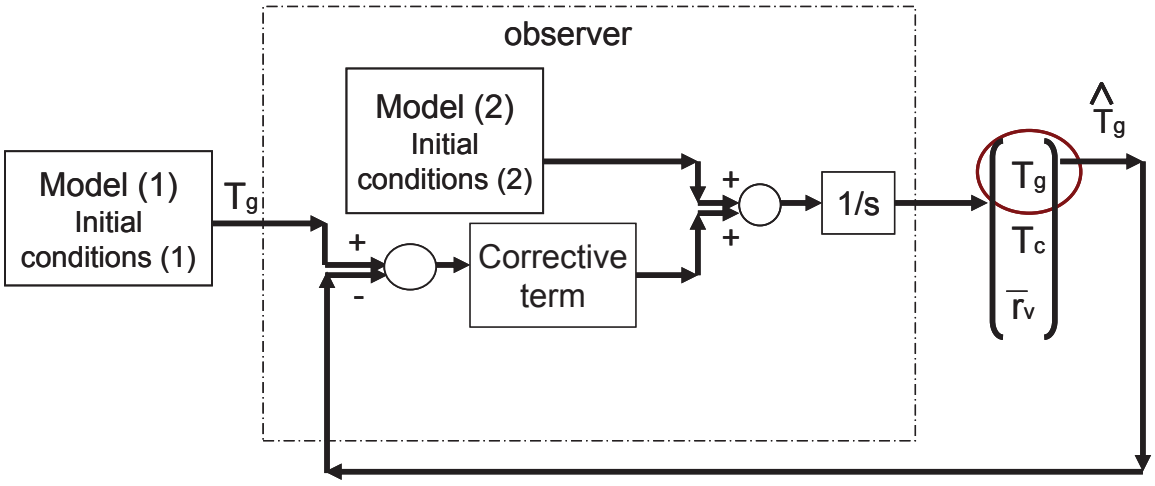

Figure 3-20: Block diagram of the observer

3.2.2.7 Data from Model

As mentioned above, the input data from the observer is calculated by the model. Figure 3-21 compares the model output to the measured data for this experiment. The model divides the reactor bed into both axial and radial finite elements but the observer divides it into axial elements only. To harmonise the model output data with the requirements of the observer, the average temperatures and reaction rates over the radial elements of each axial segment were calculated from the model outputs. Figure 3-22 shows the results for experiment ET_PE_SFG_124 of 15 seconds duration at the maximum flowrate. The input data for the observer is the gas/inert phase temperatures, T_g, calculated for the end segment (bold line). 10 axial segments of thickness 1mm were used in this run of the model.

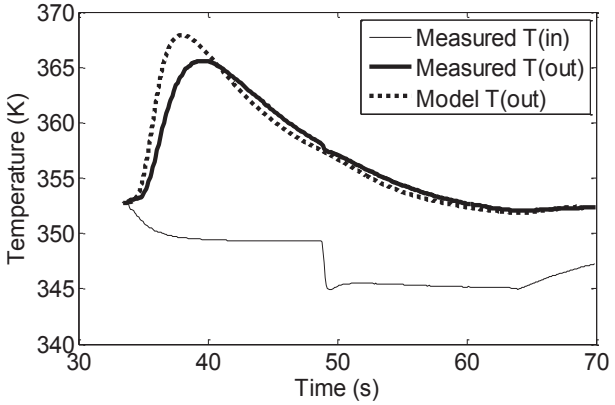

Figure 3-21: Comparison between model and measured reactor outlet temperatures for experiment ET_PE_SFG_124 of 15s duration at the higher flowrate

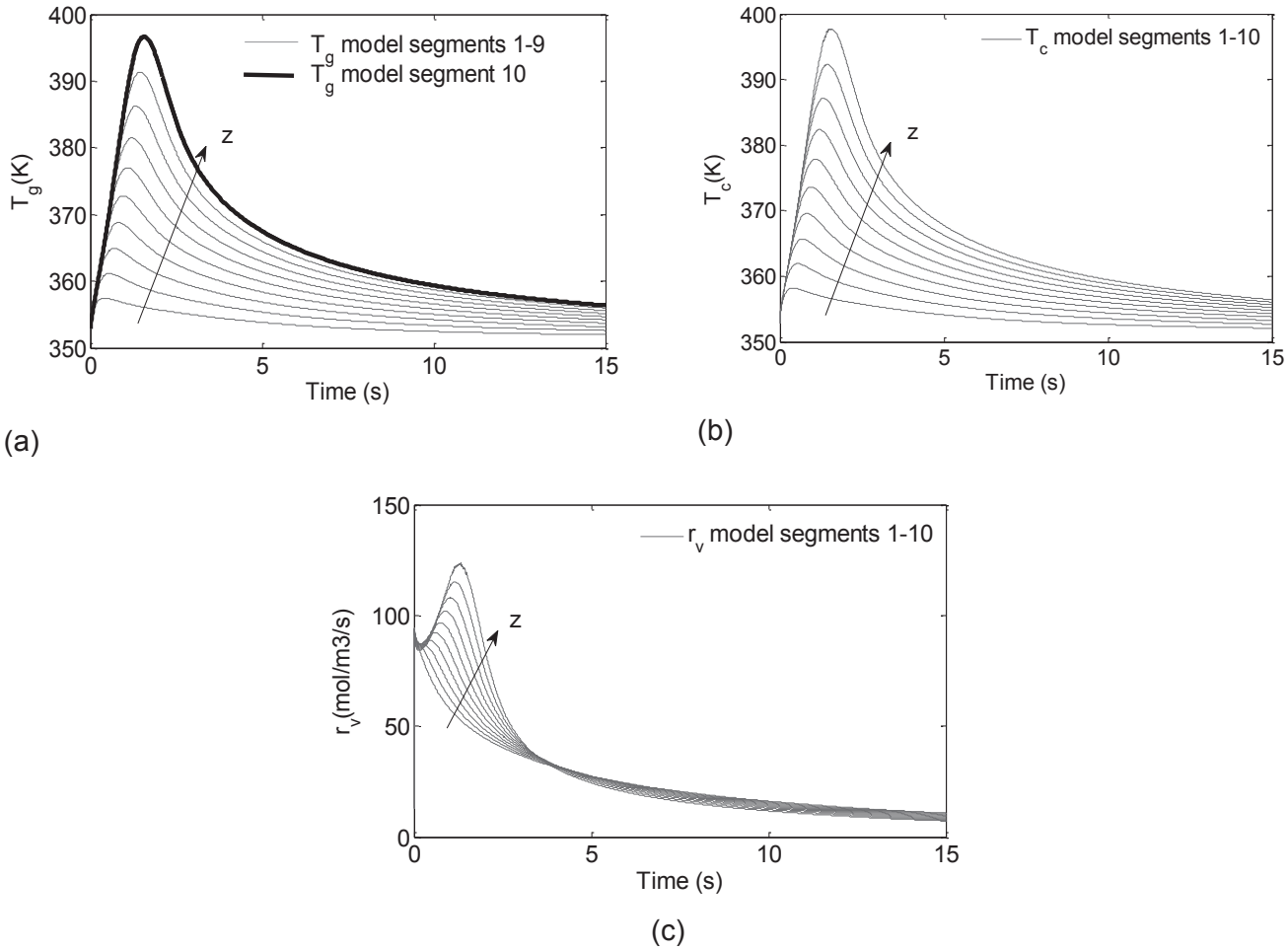

Figure 3-22: Calculated for experiment ET_PE_SFG_124 of 15s duration (a) gas/inert temperatures (b) catalyst temperatures (c) polymerisation rates

3.2.2.8 Results for Single Element Observer

First of all we consider a single element observer using heat balances for both T_c and T_g. An observer works to force the error between the estimated and measured data to zero. Figure 3-23 compares the estimated bed outlet temperature to the measured values with observer sensitivity set too low (θ = 1). The estimated temperatures lag behind the measured data.

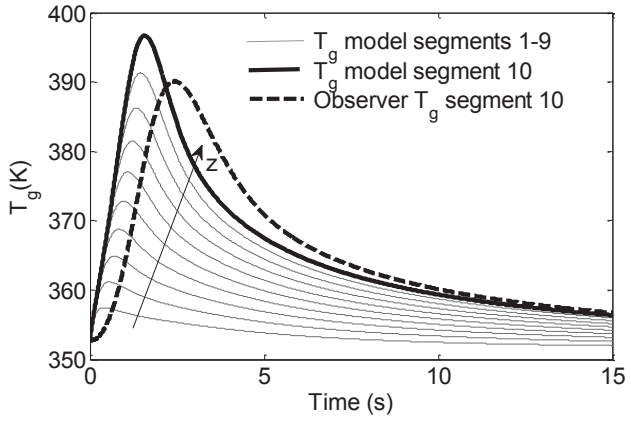

Figure 3-23: Observer results for gas/inert temperature in end segment with Θ=1 for experiment ET_PE_SFG_124

The result of increasing θ to 5 is that the observer returns the input data, as shown in Figure 3-24(a). Figure 3-24(b) shows that the estimated catalyst temperatures follow the same pattern as the temperatures of the gas and solid NaCl.

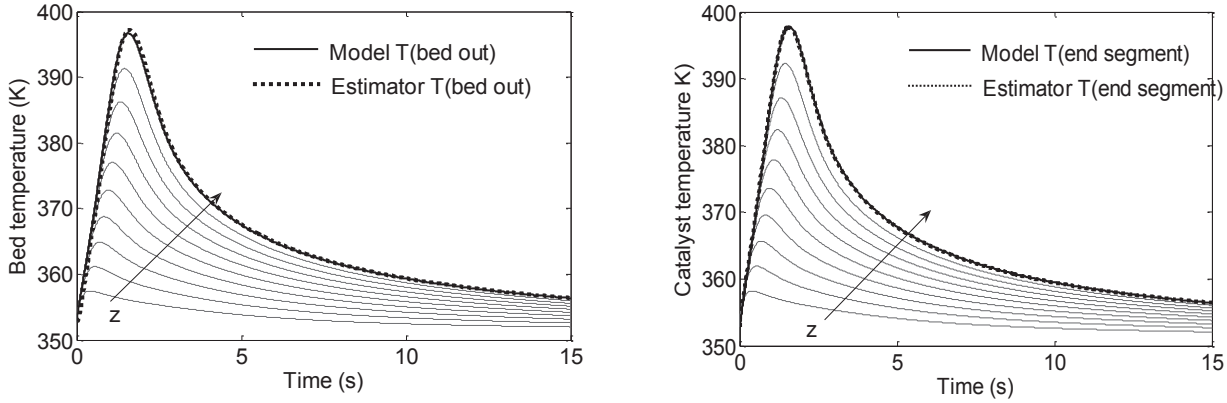

(a) (b)

Figure 3-24: Compare estimator and model values for experiment ET_PE_SFG_124 with Θ=5 for (a) bed temperature, T_g (b) catalyst temperature, T_c

Figure 3-25(a) shows that this observer calculates reaction rate values which are too high. The mass of polymer estimated by the observer is 87.6 mg for 33.3 mg measured for this experiment. This is because, with only a single uniform element set at the reactor bed outlet temperature, the estimated temperature is assumed that of the whole bed which is not true. There is a temperature gradient between the bed inlet and outlet. This is one reason why the estimated reaction rate is higher than the true value. Also, the calculated temperature difference between the reactor bed and wall is higher than the true average value experienced by the bed. The estimator calculates an increased heat flow at the reactor wall and is forced to create this heat using the polymerisation reaction. Figure 3-25 (b) shows the effect of setting the wall heat transfer coefficient to zero for the observer. The calculated mass of polymer is reduced to 26.7 mg, which is below the measured value.

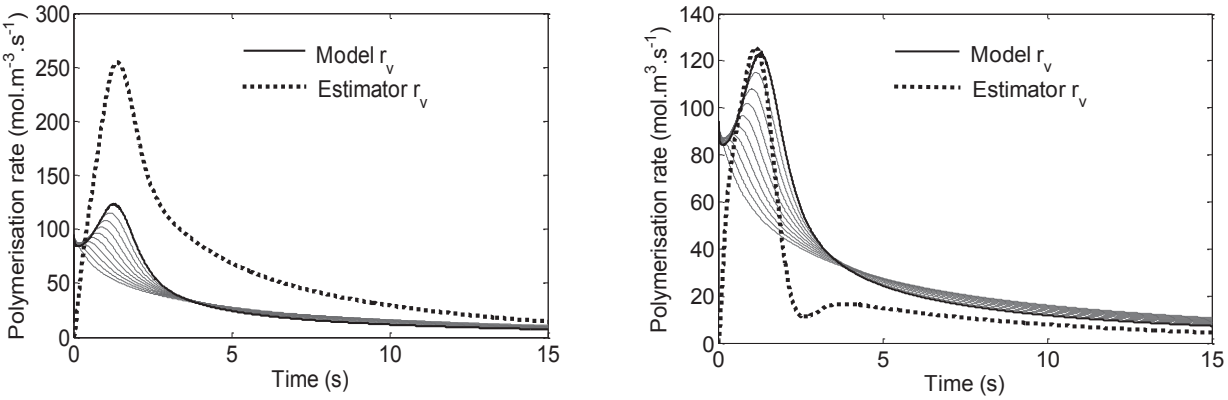

Figure 3-25: Compare estimator and model values for polymerisation rate for experiment ET_PE_SFG_124 with Θ=5 with wall heat transfer coefficient (a) calculated per equation 3-3 (b) set to zero

This shows the importance of taking into account the thermal gradients which form in the reactor bed.

3.2.2.9 Results for Multiple Element Observer

The effect of increasing the observer size to 10 axial reactor segments was tested. This step cannot produce useful results as the system is not observable, but helps to demonstrate the behaviour of the state observer. Figure 3-26 compares the estimated bed outlet temperature to the measured values with θ set to 0.3. This is the case where observer sensitivity is too low. The estimated temperatures lag behind the measured data.

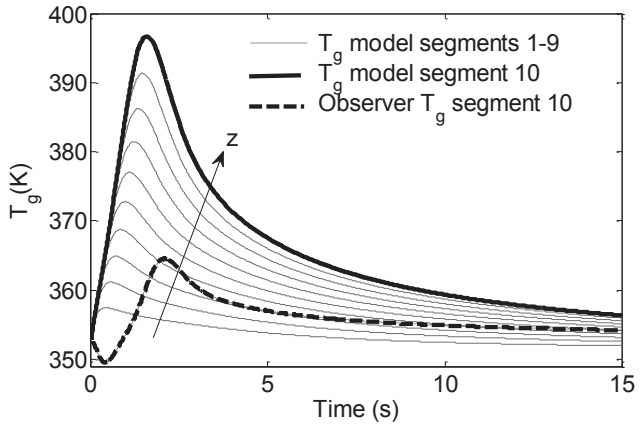

Figure 3-26: Observer results for gas/inert temperature in end segment with Θ=0.3 for experiment ET_PE_SFG_124

The effect of increasing θ is to increase the sensitivity of the observer and Figure 3-27 shows the result of increasing θ to 0.5. The observer finds the correct end segment value of T_g rapidly and continues to follow it closely. The predicted axial temperature profiles for the gas/inert and the catalyst in the reactor bed are identical, with a hot spot in segment 8. The observer is not sensitive enough to estimate $\bar{r}_v$.

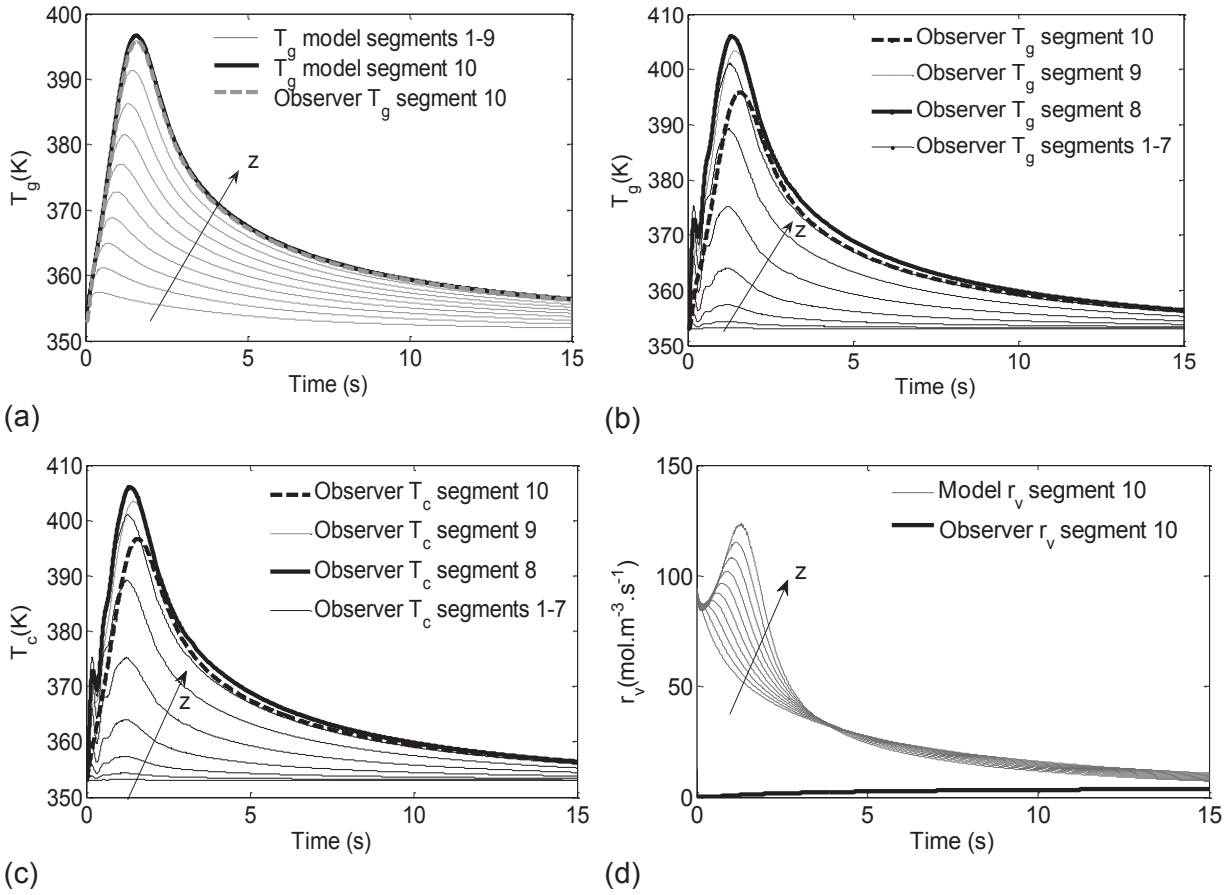

Figure 3-27: Observer results with Θ = 0.5 for experiment ET_PE_SFG_124 (a) T_g in end segment compared to bed temperatures calculated by the model (b) T_g (c) T_c (d) comparison between r_v calculated by model and observer

Figure 3-28 shows the results of further increasing θ to 0.64. The observer continues to find the measured data but the T_g estimates for the rest of the bed have become noisy. The observer is still not sensitive enough to predict the expected values for $\bar{r}_v$. This shows that this form of observer cannot be used for such a large system. It is too sensitive for states close to the measured data in X and not sensitive enough for states which are further away. Also, the estimated position of the hotspot has changed to segment 7. This confirms the system of equations is not observable, as θ should only affect sensitivity and not the values of estimated states.

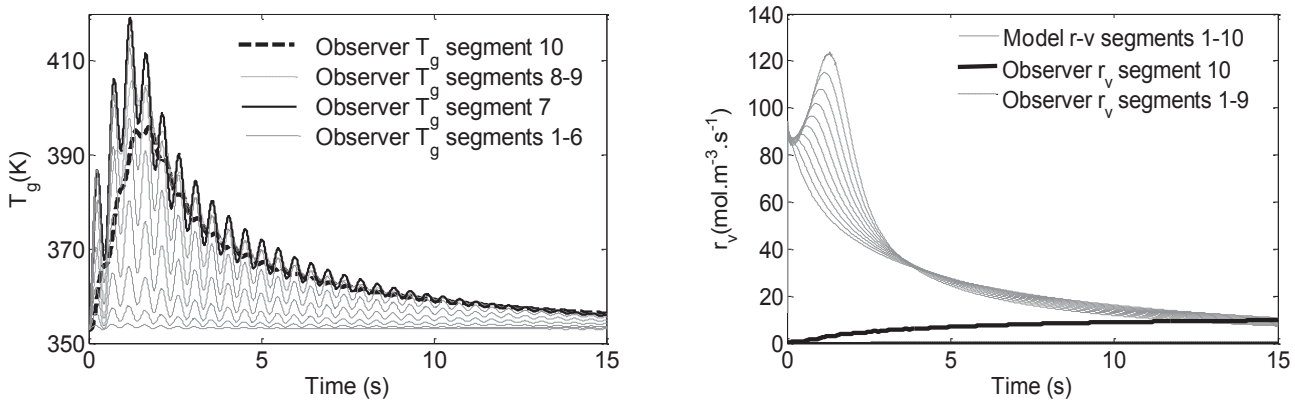

(a) (b)

Figure 3-28: Observer results with Θ=0.64 for experiment ET_PE_SFG_124 (a) T_g **(b)** r_v

3.2.3 Observer for $kC_{C2}C^*$

To create an observer which takes account of the axial thermal gradient in reactor bed using finite elements, an observable system of equations is required. In general, reaction rates vary with temperature according to their activation energy. As discussed in Chapters 1 & 2 sections 1.3.1.2.3 and 2.2.5 respectively, an accepted form of the reaction rate equation for ethylene polymerisation is given by equation 3-14.

$$r_p = k_{p0} e^{-\frac{Ea_p}{RT}} C_{C2} C^* \qquad \textbf{3-14}$$

If it is assumed that all the variation in polymerisation rate in the reactor bed at any one point in time is due to the activation energy of the propagation reaction, it is no longer necessary to estimate a reaction rate for each reactor element. Instead, an observer for a single variable, $k_{p0}C_{C2}C^*$, can be created. This implies the following assumptions:

- negligible mass transfer limitations
- the polymerisation kinetics represented by a single lumped reaction constant

Also, the observer for $\bar{r}_v$ estimates almost identical values for T_g and T_c. This is reasonable for experiments from this series, at the higher flowrate. T_g and T_c can therefore be combined to reduce the number of states to be estimated.

The heat balance becomes:

$$\frac{\partial T}{\partial t} = \frac{1}{\sum \rho c_p}\left(\Delta H k_{p0} e^{-\frac{Ea_p}{RT}} C_{C2} C^* + F_T Mwt_{rg} c_{prg} \frac{(T - T_{in})}{S_r \partial z} - \bar{h}_{\text{int}} A (T - T_w) \right) \qquad \textbf{3-15}$$

Figure 3-29 shows the results from an observer for $k_{p0}C_{C2}C^*$ for the fixed bed considered as a single uniform element. The observer returns the input values for T and estimates values for $k_{p0}C_{C2}C^*$. The predicted profile for $k_{p0}C_{C2}C^*$ is an increase to a maximum during the first second followed by a decay.

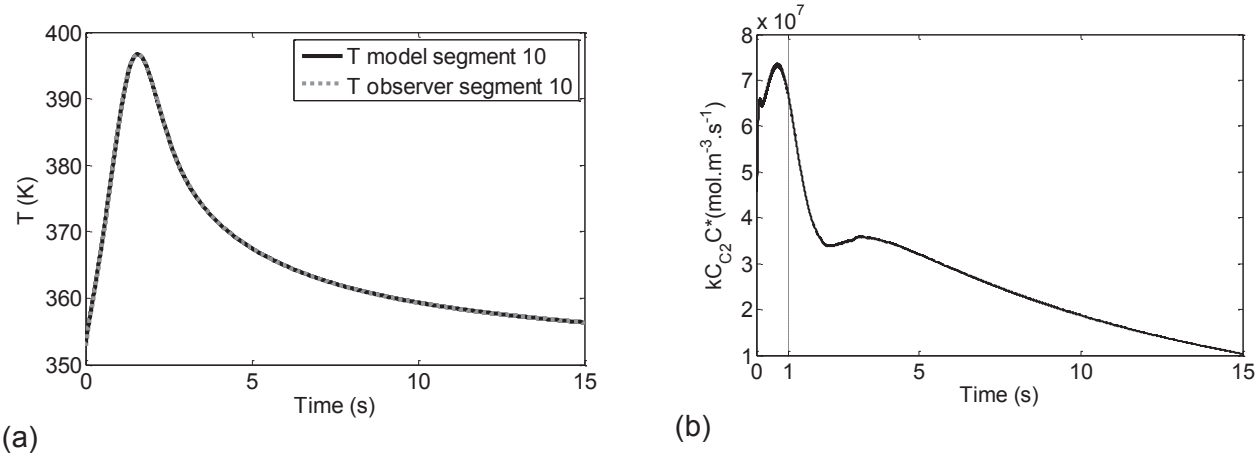

Figure 3-29: Results of observer for $k_{p0}C_{C2}C^*$, Θ=40 (a) Comparison of T to bed exit temperature calculated by the model (b) $k_{p0}C_{C2}C^*$

Figure 3-30 shows that using $k_{p0}C_{C2}C^*$ to recalculate the reaction rate gives very similar results to the observer for $\bar{r}_v$. This validates the use of a single, combined temperature, T, and the assumption of negligible mass transfer limitations for this particular case. The estimated mass of polymer is still too high with 88.8 mg predicted and 33.3 mg measured for this experiment.

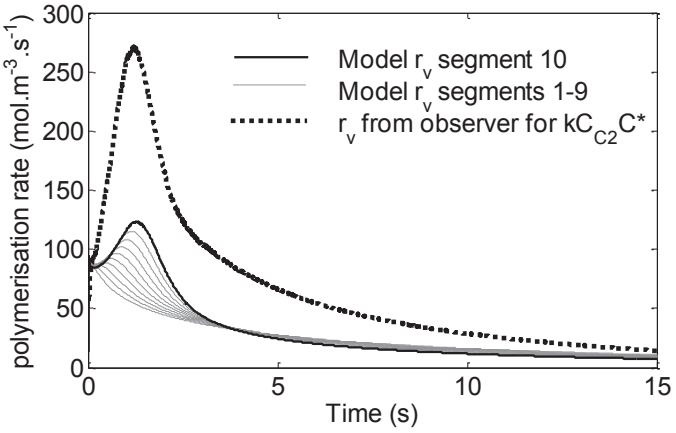

Figure 3-30: Comparison of polymerisation rate calculated using model and from observer for $k_{p0}C_{C2}C^*$

Having verified its performance against the observer for $\bar{r}_v$ considering a single reactor element, this observer for $k_{p0}C_{C2}C^*$ can be expanded to include more reactor elements. Figure 3-31 shows the result of applying this observer to the reactor bed divided into 10

discrete elements. The predicted temperatures are consistent with those of the model and the estimated profile for $k_{p0}C_{C2}C^*$ is now quite level during the first second followed by a smoother decay than with only one element.

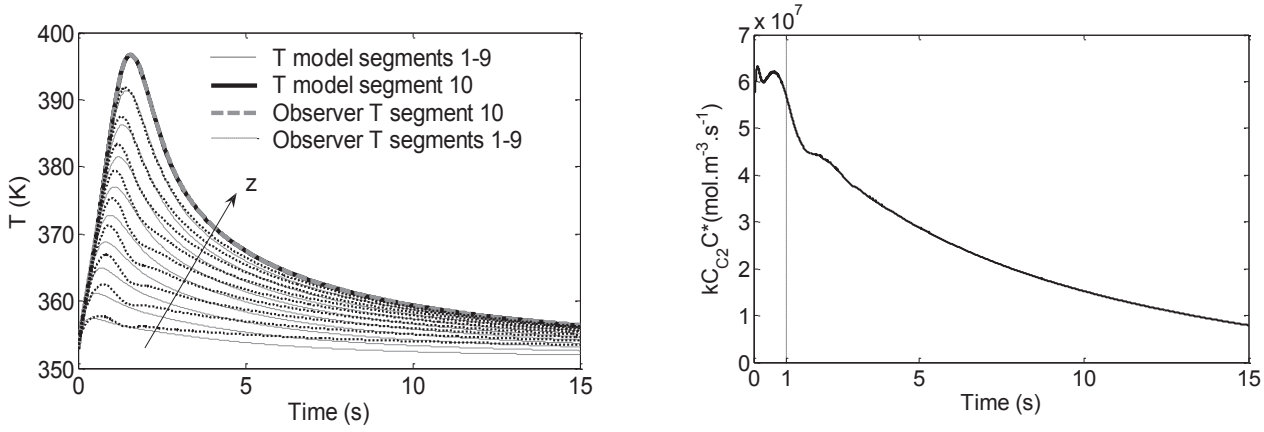

(a) (b)

Figure 3-31: Results of observer for $k_{p0}C_{C2}C^*$ with 10 axial reactor elements (a) Comparison of T to bed temperatures calculated by the model (b) $k_{p0}C_{C2}C^*$

Figure 3-32 shows the reaction rates found in each segment based on the estimation of $k_{p0}C_{C2}C^*$. These are still above those of the model and the calculated total mass of polymer for this case is 62.9 mg, which is closer to the measured value, but still too high.

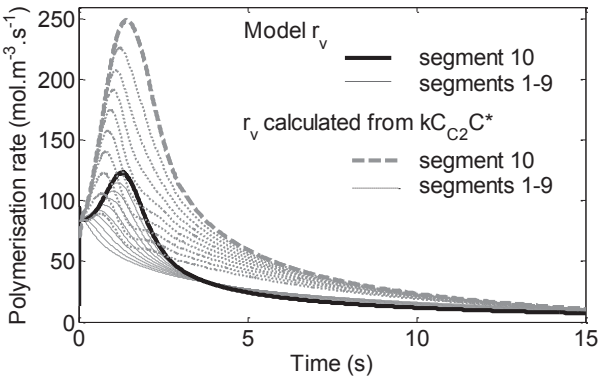

Figure 3-32: Comparison of polymerisation rate calculated using model and from observer for $k_{p0}C_{C2}C^*$ with 10 axial reactor elements

Figure 3-33 shows the effects of increasing the number of axial elements in the reactor bed, increasing the tuning parameter and changing the initial value of $k_{p0}C_{C2}C^*$. It can be seen that this observer is very robust and predicts almost identical results in each case.

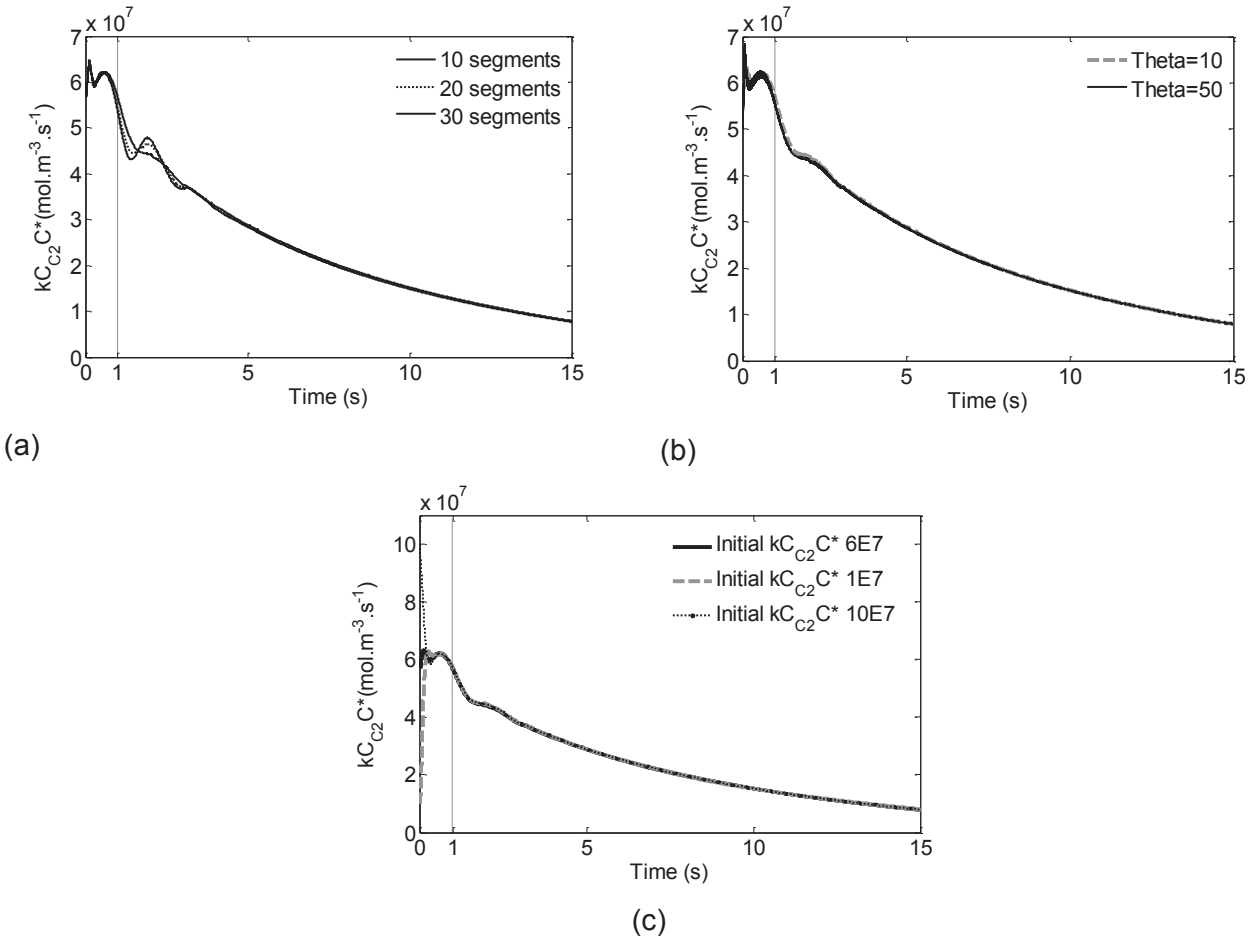

Figure 3-33: : Results of observer for $k_{p0}C_{C2}C^*$ with (a) increased axial reactor elements (b) the tuning parameter increased to 50 (c) alternative initial values for $k_{p0}C_{C2}C^*$

Figure 3-34 shows the observer predictions for $k_{p0}C_{C2}C^*$ during the first second with different initial values. It can be seen that even with the tuning parameter set to 50 the observer takes about the first 100 ms of the data to converge, so the predictions before this point must be discarded.

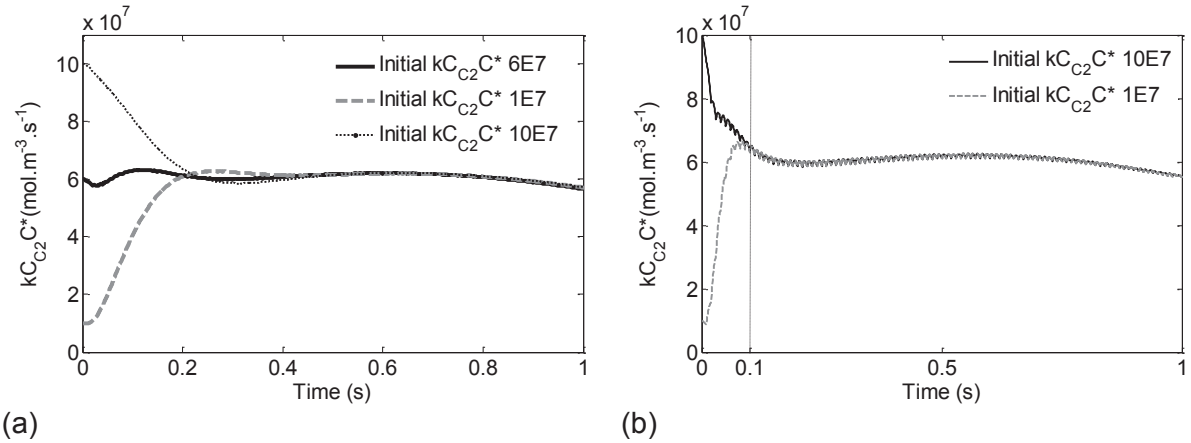

Figure 3-34: Results of observer for $k_{p0}C_{C2}C^*$ with alternative initial values (a) tuning parameter = 10 (b) tuning parameter = 50

Figure 3-35 shows the result of setting the wall heat transfer coefficient to zero. The predicted mass of polymer formed falls to 27.4 mg which is below the measured value of 33.3 mg. The predicted values of $k_{p0}C_{C2}C^*$ are lower and decay from the start of the experiment. The predicted reaction rates are close to the values from the model.

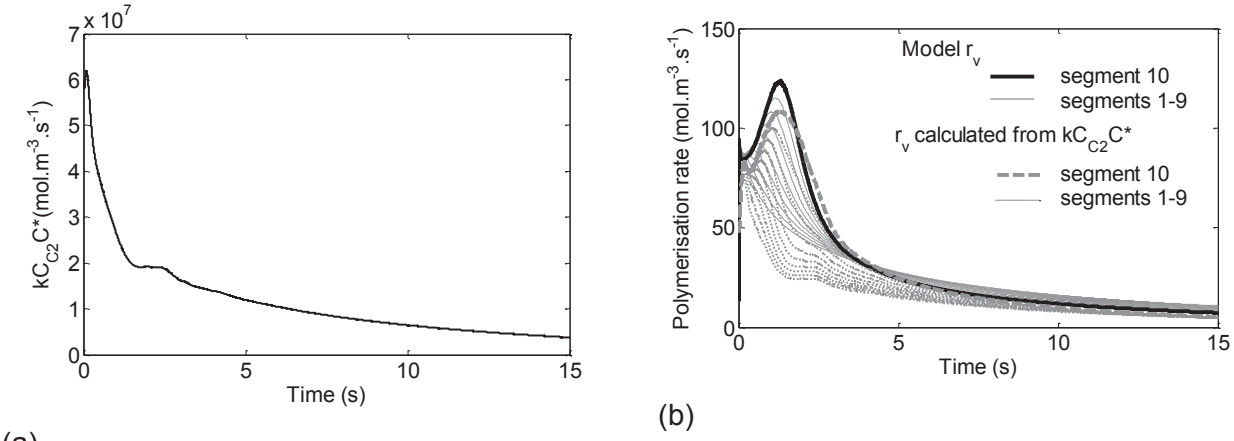

Figure 3-35: Results of observer for $k_{p0}C_{C2}C^*$ with 10 axial reactor elements and no heat transfer at the reactor wall (a) $k_{p0}C_{C2}C^*$ (b) comparison of polymerisation rate calculated using model and from observer

It seems that the observer is still over estimating the heat transfer rate at the reactor wall. A potential cause is the correlation for the wall heat transfer coefficient given in equation 3-4. In discussing this correlation, Froment [12] states that 'except for 'mild' conditions, the one-dimensional model may fail to predict the mean temperatures', also the correlation was derived for beds of porosity close to 0.4, formed of spherical particles and with Reynolds number >3, which is not our case. The logical next step in development of the observer would therefore be to eliminate this correlation by creating a two dimensional observer for the reactor bed which could account for the effective conductivity in the bed and the wall heat transfer coefficient separately.

Also, unlike the model, the observer does not include the reactor wall temperature. The observer uses a fixed wall temperature when, in reality, there is an increase in wall temperature during the experiment. This decreases the temperature difference between the reactor bed and wall and hence the heat transfer rate. However, the reactor wall temperature varies much less than that of the reactor bed and so this is unlikely to account for the whole difference between measured and predicted reaction rates.

To briefly recap, the results shown in Figure 3-35 are determined by running the model for an experiment of duration 15s to find a bed exit temperature profile. This bed exit temperature

profile is the input for the observer, run with the wall heat transfer coefficient set to zero, as if for an adiabatic reactor. At present, this gives the closest fit with the measured mass of polymer. The shape of the curve for $k_{p0}C_{C2}C^*$ predicted by the observer for this case is very similar to the curve developed previously to represent the pre-exponential constant, k_{p0}, in the model, as shown in Figure 2-15 (b). This is as might be anticipated but it is difficult to make a direct quantitative comparison because the terms are not identical. So, despite the observer having more simplifying assumptions than the model, it returns the expected kinetic profile.

3.2.4 Conclusion

Use of the fixed bed reactor as a calorimeter has been considered and initial work towards the development of a state observer for the polymerisation rate has been done. An observer for $k_{p0}C_{C2}C^*$ for the fixed bed divided into finite elements has been created. The conditions under which the experiment was carried out allowed simplification to a pseudo-homogeneous reactor bed, considering only a single value of T in each element. The predicted form of $k_{p0}C_{C2}C^*$ is consistent with expectations, decaying rapidly from very early in the experiment. However, the observer over estimates the heat transfer rate out of the reactor bed, possibly because it does not take account of the reactor wall and also because the correlation for the internal wall heat transfer coefficient was developed for milder conditions.

One drawback is that the input data for the observer was not the measured data but the bed outlet temperatures calculated by the model. If the reactor could be modified such that temperatures measured at the outlet were more sensitive to the bed temperatures, the true measured data could be used and this problem could be overcome. Also, if reactor bed temperatures were more uniform, development of the single segment observer could be continued, which would be a very simple way to gain direct access to the reaction rate. To this end, reactor improvements are considered in the next section, including simulations of alternative exit frit materials and different reaction gases and flowrates.

Later, in Chapter 4, alternative polymerisation kinetics are considered for the model and we will use them to reconsider the observer. It will be shown how sensitive it is to small changes in the bed exit temperature, which further confirms the need for measured reactor outlet temperatures close to the values found in the reactor bed and which could be used directly as the observer input.

3.3 Simulations

The model was used to simulate all the experiments listed in Appendix 1. The results discussed so far are typical for the reactor operating under optimised conditions. This section will cover the model outputs for experiments carried out at the lower reaction gas flowrate and also simulations to calculate the predicted effects of changing the reactor dimensions, flow capacity, exit frit and inert gas. The typical 4s experiment (ET_PE_SFG_200) which was used as an example for validation of the reactor model is also used as the basis for modelling throughout this section.

3.3.1 Reduced Flowrate Experiments

Experiments have also been carried out during the optimisation of this reactor at the lower reaction gas flowrate of 90 mL.s^{-1}, and hence with less cooling in the reactor. Figure 3-36 shows the results of modelling a reaction of duration 4s at the lower flowrate (nominal gas/particle velocity = 3 cm.s^{-1}). Calculated temperatures compare well with the measured data but, if no adjustments are made in the simulation to account for the melting of the polymer, the model calculates unrealistically high catalyst temperatures.

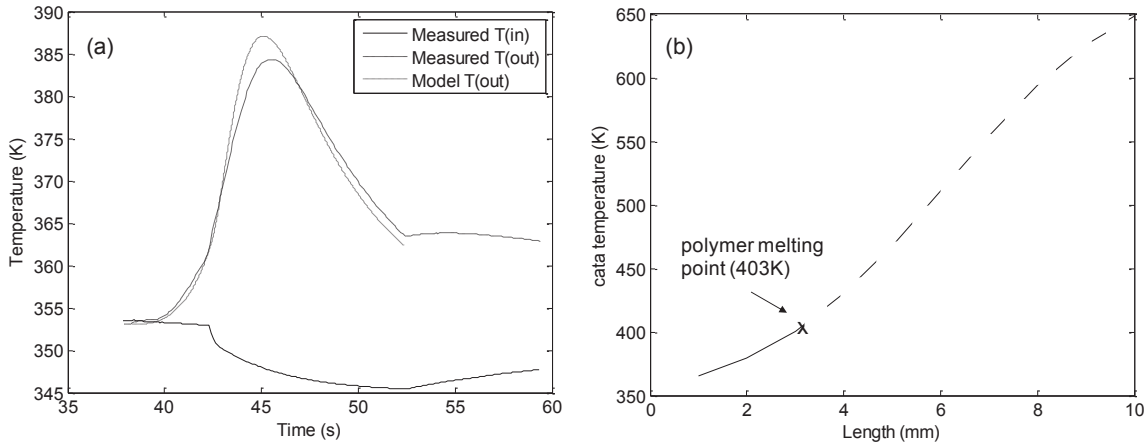

Figure 3-36: (a) Comparison of calculated outlet temperatures against measured values (b) Maximum catalyst temperatures along reactor length at centre

Also, at the lower flowrate of 90 mL.s^{-1}, the model calculates quite a strong fluctuation in the ethylene concentration. This is because, at the initial polymerisation rate, ethylene is consumed more quickly than it is supplied to the reactor. Figure 3-37 shows the variation in ethylene mole fraction in the reaction gas with a dip towards the end of the reactor.

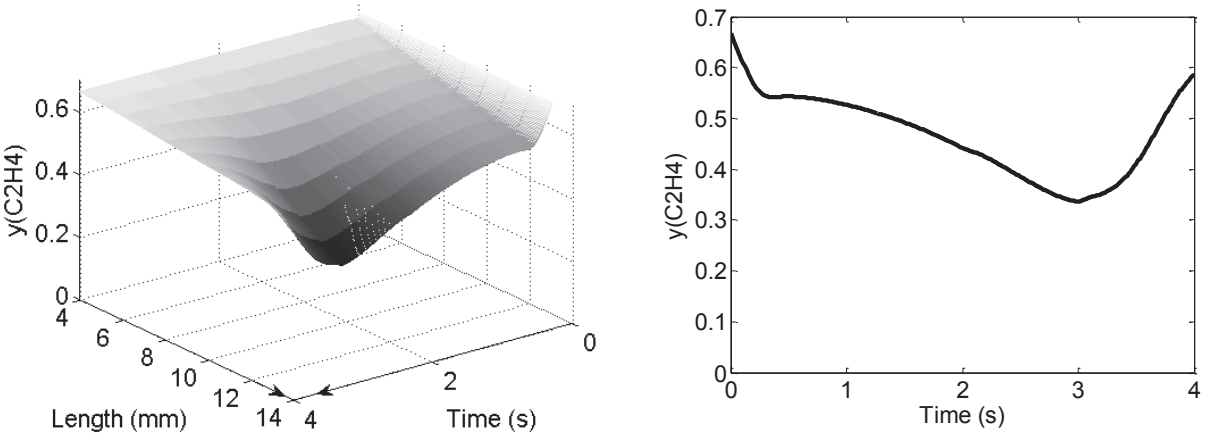

Figure 3-37: Variation in ethylene mole fraction for 4s polymerisation with flowrate of 90 mL.s^{-1} (a) along reactor centre line (b) at centre end element of reactor bed

Figure 3-38 shows the results of modelling the same experiment with the catalyst temperature limited to 413 K. It is not possible to fit the measured outlet temperature data or mass of polymer, which is 31.5 mg against 43.4 mg measured. Reactor temperatures must therefore exceed 413 K for this lower flowrate. In fact, the minimum bed temperature limitation which allows the model to fit with the measured data for this experiment is 473 K. Figure 3-39 shows the maximum calculated polymer temperatures and the comparison between the simulated and measured data for this case.

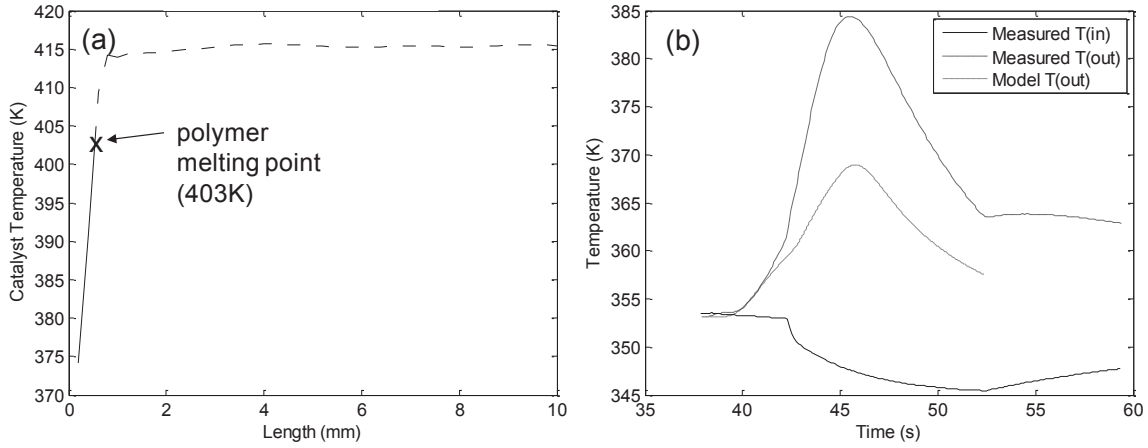

Figure 3-38: (a) Maximum calculated catalyst temperatures along reactor length at centre limited to 413 K (b)Comparison of calculated output temperatures against measured values for same experiment of 4s duration with low flowrate.

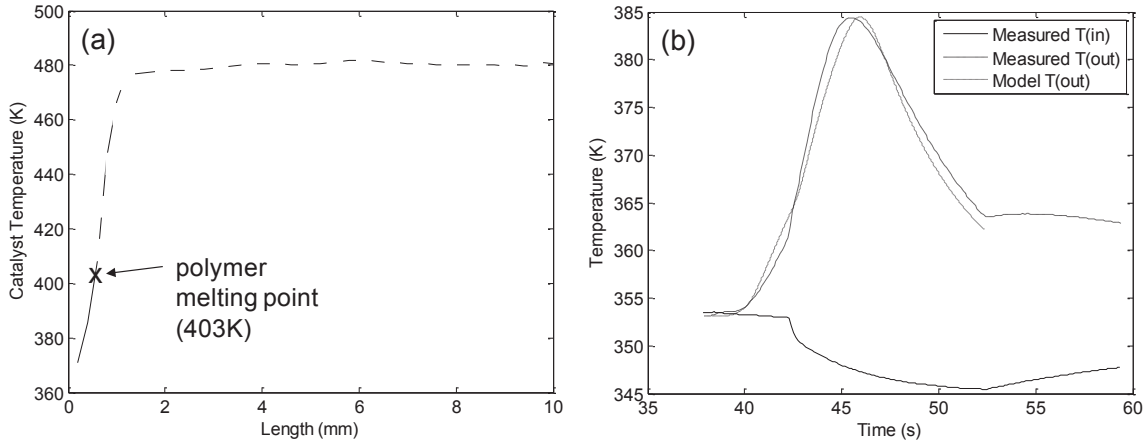

Figure 3-39: (a) Maximum calculated catalyst temperatures along reactor length at centre limited to 473K (b) Comparison of calculated output temperatures against measured values for same experiment of 4s duration with low flowrate.

The very high temperatures in the reactor for experiments at the lower flowrate were also corroborated experimentally by the polymer formed having a broad molecular weight distribution and PDI of around 8 [3]. Under the optimised reactor conditions PE is formed with a PDI of about 4. It seems that under certain reaction conditions very high temperatures can occur in this reactor and, over the short time period considered, deactivation and polymer melting are not sufficient to stop the reaction.

3.3.2 Alternative Reactor Geometries

To understand the impact of reactor geometry on catalyst and seedbed temperatures the reactor was modelled with different dimensions. The bed volume was kept the same and simulations were carried out with the length doubled to give a cigar shape and halved to give a disc shape. The aim was to find whether changing the shape could help provide more uniform temperatures within the reactor. Equation 2-40, the heat balance for a reactor bed element, shows the only significant ways for heat to be evacuated are by radial conduction or in the exit gas stream. In accordance with this, Mears [13] proposes reducing reactor diameter to reduce temperature gradients by providing more surface area for heat transfer out of the bed.

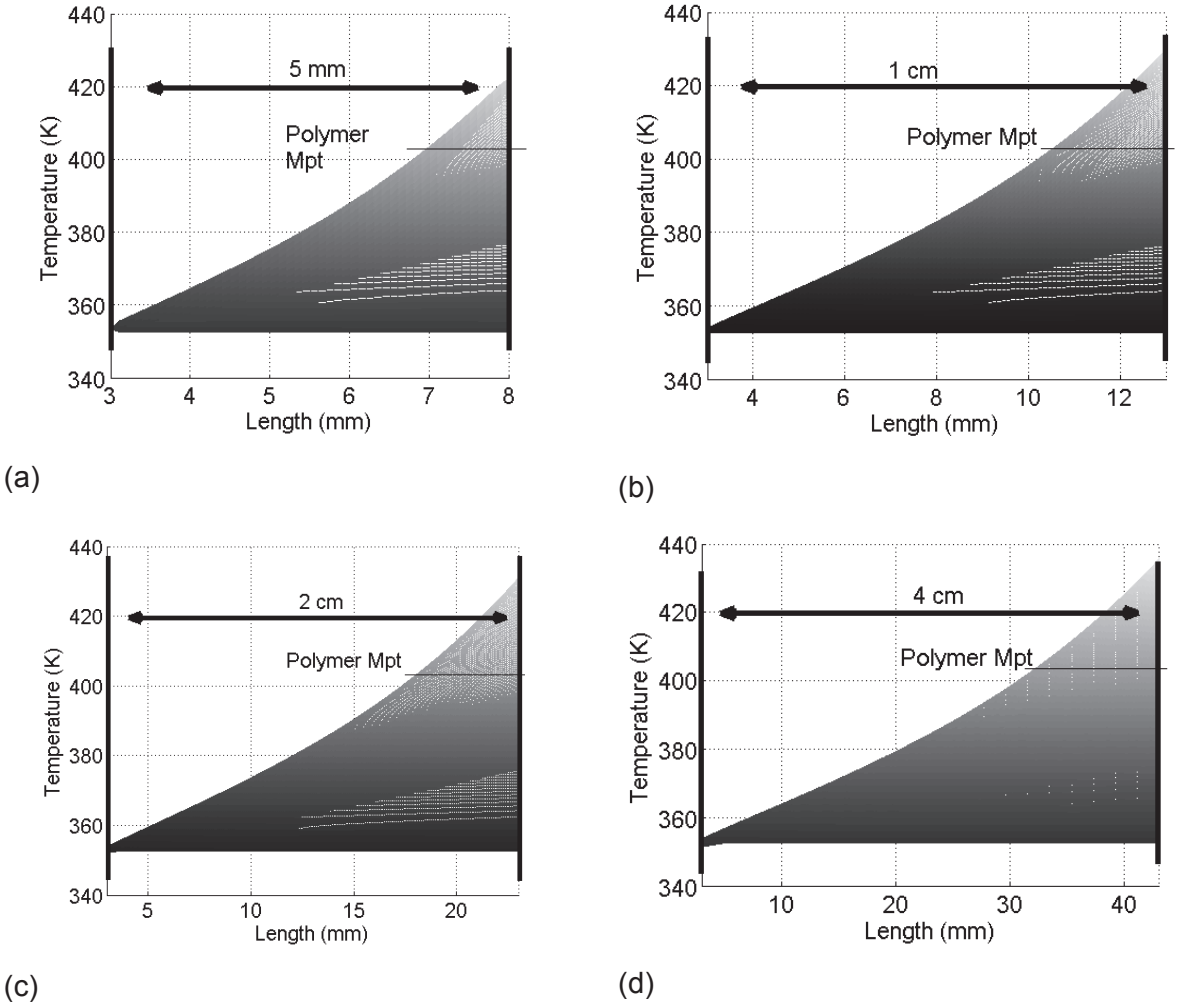

Figure 3-40: Maximum calculated catalyst temperatures against axial position for cylindrical packed beds of same volume and of length (a) 5 mm (b) 1 cm (c) 2 cm & (d) 4 cm

Experiment ET_PE_SFG_200 is taken as the basis for modelling alternative reactor geometries. The same total reaction gas flowrate is used in each case, so the smaller the reactor diameter, the greater the gas velocity. Figure 3-40 shows the maximum catalyst temperatures calculated against axial position for cylindrical packed beds of the same volume but different lengths. Changing the reactor dimensions has little effect on the maximum temperatures reached in the bed because they occur so rapidly and early in the polymerisation (<2s) that conduction out of the bed is negligible and the reactor can be considered adiabatic in these first few seconds.

3.3.3 Increasing Flowrate

The maximum relative gas-particle flowrate obtained in the packed bed reactor is 0.13 $m.s^{-1}$ and this is also the optimised condition. This is significantly below the values found in a typical industrial FBR (0.5-1 $m.s^{-1}$) [14]. To increase the flowrate through the reactor bed in the existing system the manual flow controller would need to be replaced. Other

modifications to the set-up would also be required to ensure that pressure drops remain acceptable and sufficient ballast capacity be maintained. As well as this, the effect on the reactor seedbed would have to be verified as it is extremely porous and the existing pressurisation and gas flow is enough to cause a 10% reduction in volume.

Reaction gas make-up and pressure	Reaction gas flowrate ($mL.s^{-1}$ stp)	Gas velocity ($m.s^{-1}$ reactor conditions)
Base case: 6 bar ethylene 3 bar helium	310	13
Increased helium pressure: 6 bar ethylene 6 bar helium	410	13.4
Increased gas flowrate: 6 bar ethylene 3 bar helium	620	26
6 bar ethylene 3 bar helium	930	39

Table 3-2: Simulations with increased reaction gas flowrate

The simulations carried out with increased gas flowrate are listed in Table 3-2 . Ethylene partial pressure was maintained at 6 bar to avoid impacting the reaction kinetics. Figure 3-41 shows the maximum bed temperatures calculated along the reactor centre line for the different cases. The model predicts that increasing the reaction gas flowrate by raised partial pressure of the diluent gas or total mass flow would be a suitable method to produce a more uniform reactor bed.

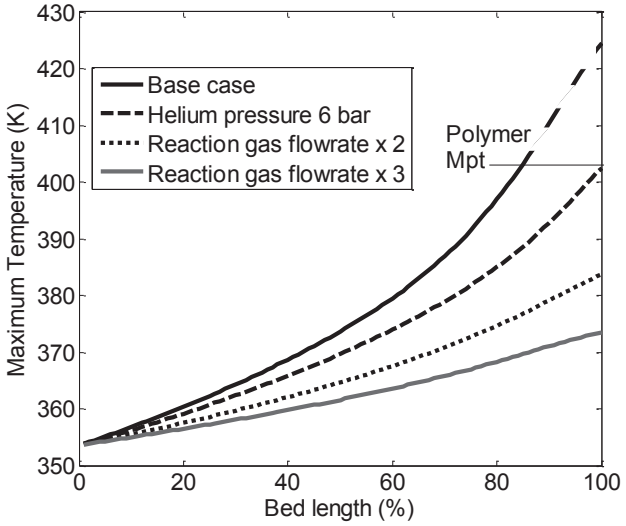

Figure 3-41: Maximum bed temperature calculated along reactor centre-line for different reaction gas flowrates

Increased reaction gas flowrate could be achieved with the same relative gas-particle velocity in the reactor bed as found in the existing set-up by changing the reactor geometry. For example, a disc shaped reactor bed of length 5 mm and diameter 14 mm, as used in the

model to produce Figure 3-40 (a), has twice the cross sectional area of the existing bed. Therefore, double the current volumetric gas flowrate would result in an unchanged gas velocity through the bed. This could be useful to avoid potential problems with increasing the gas velocity through the fragile fine NaCl reactor seedbed.

3.3.4 Exit Frit

The model has shown that the stainless steel frit at the reactor exit can hide rapid temperature variations occurring in the packed bed. This is due to the relatively high mass, heat capacity and conductivity of the frit. As discussed in the literature survey, Hamilton et al. [15] also found that the heat capacity of the reactor internals could have a significant effect on observed temperatures. They minimised the effect by replacing the metal support plate in their microreactor by nylon mesh. In our case, alternative frit materials were also considered as a means to improve the reactor response, as well as reducing the frit thickness. The model was used to simulate the different scenarios. The particle size of the fine NaCl seedbed is 45 – 63 µm and the existing 15 µm frit is sufficient to retain the bed, so any bed support considered must have a similar specification.

3.3.4.1 Existing Frit

The existing frit is 3 mm thick stainless steel of approximately 40% porosity. Figure 3-42 shows the calculated temperature profiles at the reactor centre for experiment ET_PE_SFG_200 and this experiment is used for comparison throughout this section. The model calculates that, of a total 82 J heat of reaction, 21 J are lost from the existing exit frit to the reactor wall during reaction and cooling.

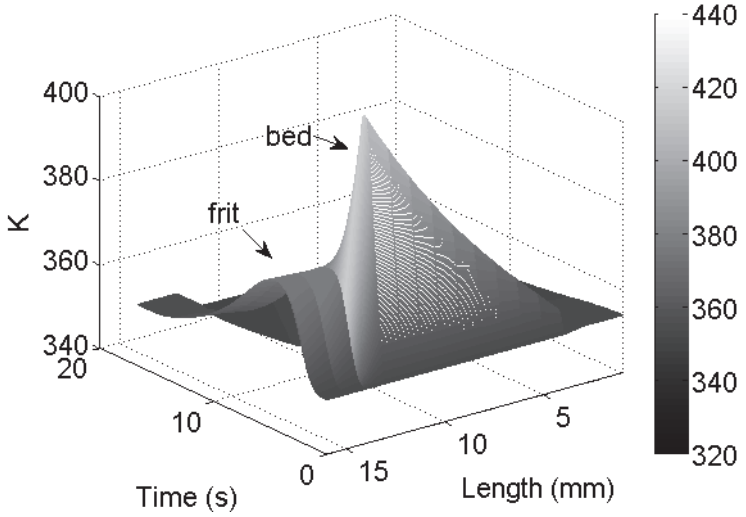

Figure 3-42: Response of reactor bed and existing frit

Figure 3-43 shows the calculated radial temperature profiles in the frit during this experiment and Figure 3-44 shows the difference between calculated bed and frit outlet temperatures

(averaged across the reactor radius). In both figures the impact of the exit frit on measured temperatures is clear.

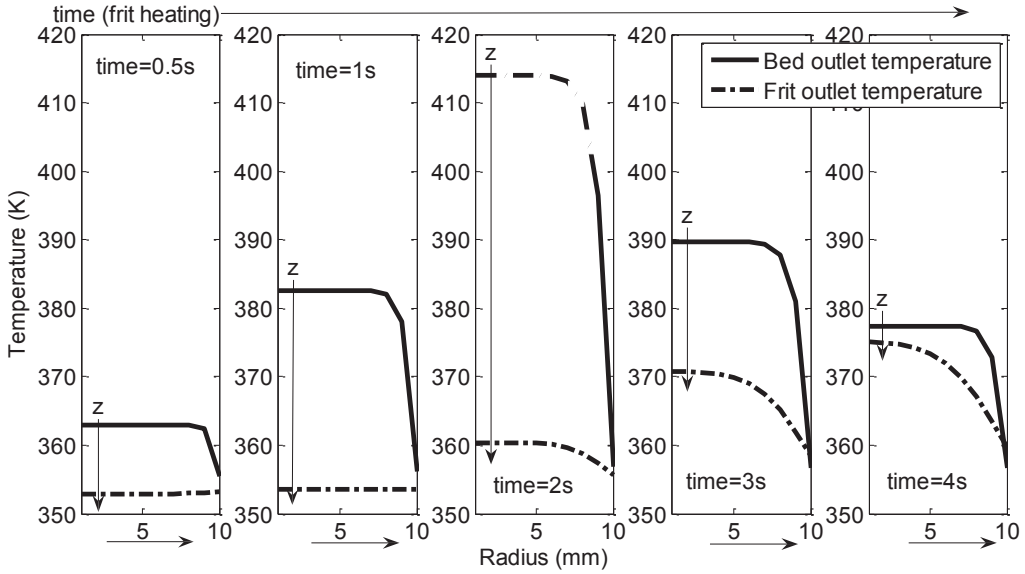

Figure 3-43: Radial profiles for existing 3mm stainless steel frit of 40% porosity

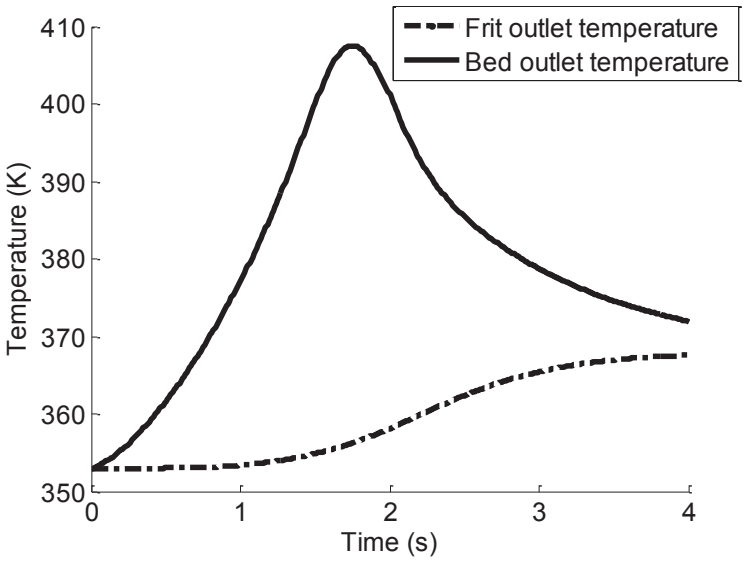

Figure 3-44: Response of existing 3mm stainless steel frit of 40% porosity to reactor bed outlet temperature. Bed and frit temperatures averaged across reactor radius.

3.3.4.2 Reduced Mass Exit Frit

To reduce the mass of the exit frit, the existing frit could be replaced by a fine mesh of thickness 0.2 – 0.3 mm. The porosity of the screen would be close to zero. Modelling a stainless steel frit of 0.3 mm and 1% porosity gives a reactor outlet response much closer to that of the reactor bed, as shown in Figure 3-45. The amount of heat lost to the reactor wall by conduction from the frit is calculated to be only 0.03 J for this scenario. Figure 3-46 and Figure 3-47 also both show that this bed support would be much more responsive to the reactor bed temperature.

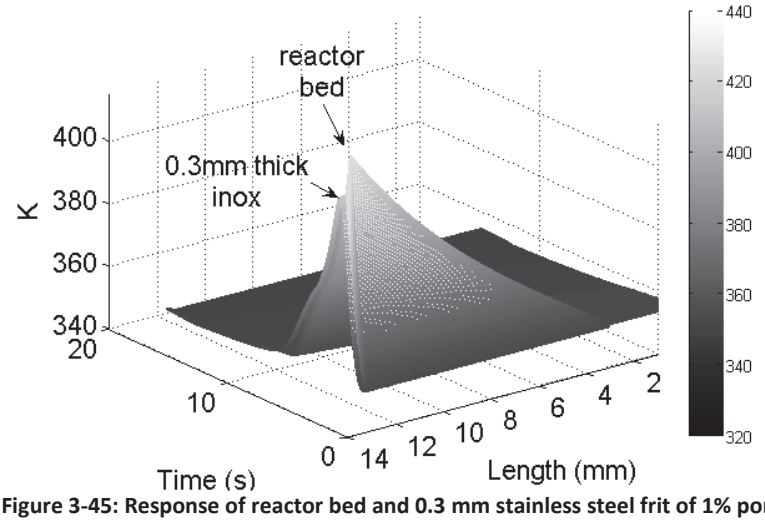

Figure 3-45: Response of reactor bed and 0.3 mm stainless steel frit of 1% porosity

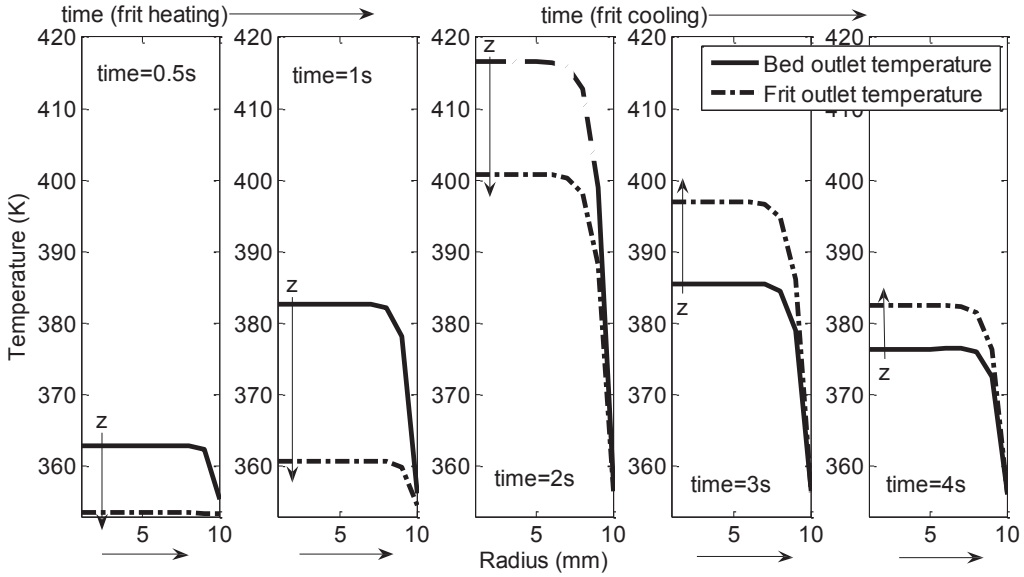

Figure 3-46: Radial profiles for 0.3 mm stainless steel frit of 1% porosity

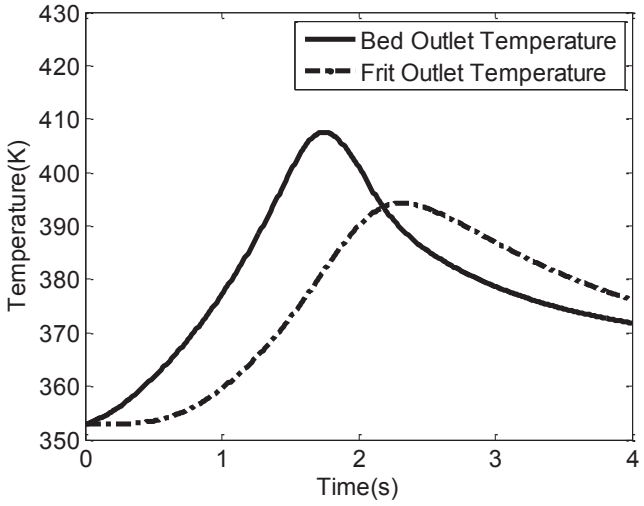

Figure 3-47: Response of 0.3 mm stainless steel frit of 1% porosity to reactor bed outlet temperature. Bed and frit temperatures averaged across reactor radius.

3.3.4.3 Alternative Frit Materials

Alternative materials which can be used to make sintered frit and are therefore of potential use for the reactor bed support are other metals, ceramics and Pyrex or quartz. The existing frit is spot welded to the reactor cartridge, so, for non-metals and ceramics, another method of fixing the frit in place would need to be found. The model was used to simulate the effect of changing to several alternatives. The physical properties used are listed in Table 3-3.

	Solid density ($g.cm^{-3}$)	Specific Heat Capacity ($J.g^{-1}.K^{-1}$)	Thermal conductivity ($W.m^{-1}.K^{-1}$)	Porosity (%)	Ref
Alumina	3.98	0.837	30		7
Porous mullite	3.11	0.78	0.8	47	16
Silicon carbide	3.2	1	90	35	17
Pyrex	2.23	0.84	1.005	42	7
Quartz(Fused silica)	2.2	0.67	1.4	40	18
Titanium	4.5	0.54	21.9		7
Hastelloy C-276	8.89	0.427	10.2		19
Inconel 625	8.44	0.446	11.4		20
Nickel 200	8.89	0.456	70.2		21
Monel 400	8.8	0.445	24		22

Table 3-3: Physical Properties of Alternative Frit Materials

Other available sintered metals which could be used are titanium, hastelloy C-276, inconel 625, nickel 200 and monel 400. Of these, only titanium offers a significant reduction in heat capacity for the same size and shape of frit because of its low weight, but the conductivity of

titanium is slightly higher than for stainless steel. Figure 3-48 shows the benefit of changing to a titanium frit is less than replacing the stainless steel frit with mesh.

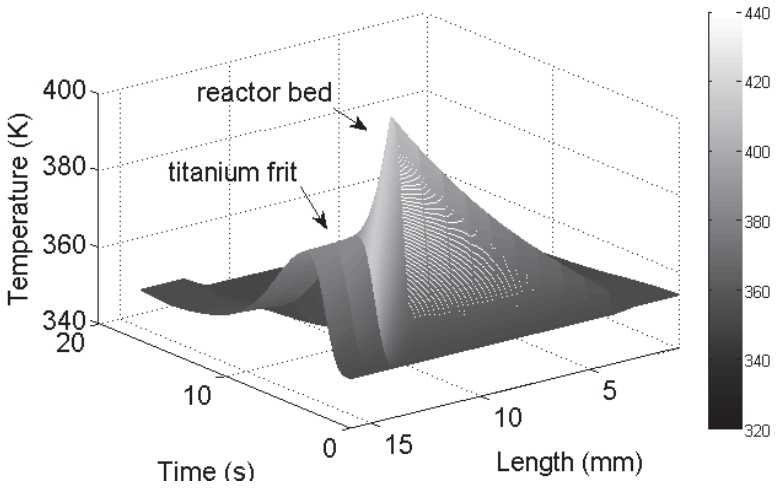

Figure 3-48: Response of reactor bed and 3mm titanium frit of 40% porosity

Three ceramic materials were considered: alumina, porous mullite and silicon carbide. From comparison of the physical properties in Table 3-3 it can be seen that, of these, porous mullite has the lowest heat capacity and conductivity. Figure 3-49 compares the reactor outlet temperatures predicted by the model for a 3 mm porous mullite frit against the stainless steel mesh and shows that the mesh gives a better response.

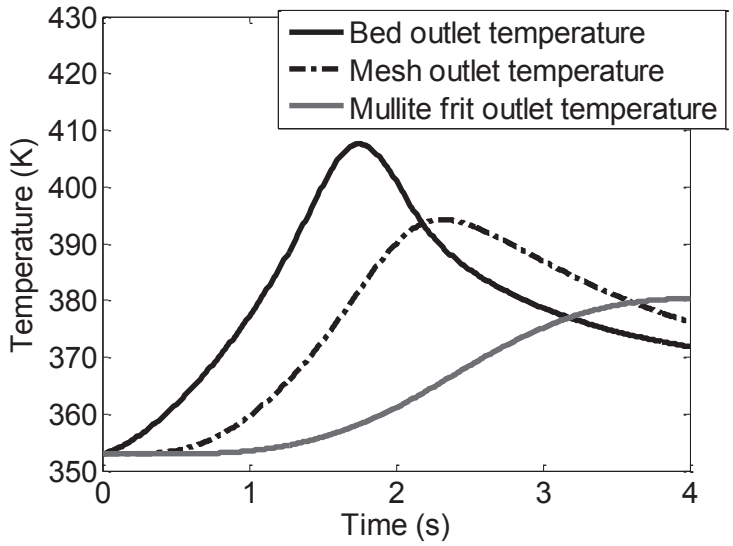

Figure 3-49: Compare response of 3 mm mullite frit and inox mesh to reactor bed outlet temperature. Bed and frit temperatures averaged across reactor radius.

Pyrex and quartz both have significantly lower heat capacity and thermal conductivity than stainless steel so use of an exit frit made from these materials would be expected to improve the reactor response. However, a potential problem is lack of resistance to the

sudden pressurisation of the reactor. Both were modelled and quartz frit was found to be the more responsive to bed temperature, with calculated heat loss to the reactor wall of 2.6 J. Figure 3-50 shows the temperatures calculated by the model along the reactor centreline with a quartz frit and Figure 3-51 compares the responses of a 3 mm quartz frit and a 0.3 mm stainless steel mesh bed support.

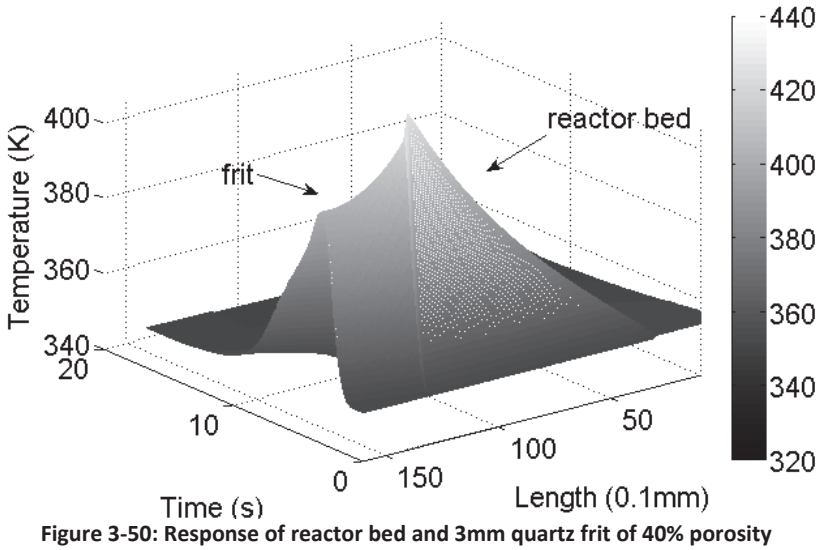

Figure 3-50: Response of reactor bed and 3mm quartz frit of 40% porosity

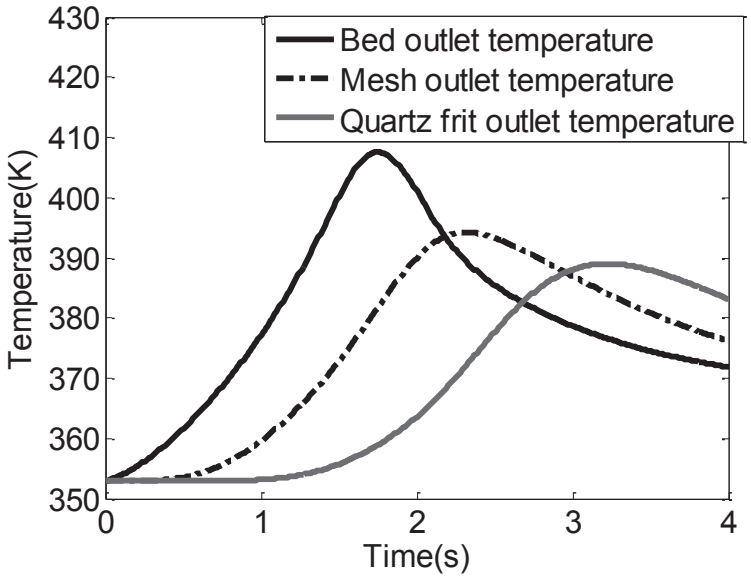

Figure 3-51: Response of 0.3 mm stainless steel mesh, 3mm quartz frit to reactor bed outlet temperature. Bed and frit temperatures averaged across reactor radius.

3.3.4.4 Conclusion

Of the arrangements and materials considered, a stainless steel mesh or quartz frit would improve the response of the reactor outlet temperature the most. Stainless steel mesh seems the better of these two options as there would be less heat lost to the reactor wall and fitting the support to the reactor cartridge would be more straightforward.

3.3.4.5 Experimental Test

A new reactor cartridge was made with the 3 mm stainless steel outlet frit replaced by 20 μm stainless steel mesh of theoretical thickness 0.12 mm and porosity 59%. The mesh was welded into place. The cartridge was first tested empty, to ensure it would resist the reactor pressurisation, and then with an inert NaCl reactor bed to verify that the mesh did not become blocked with fine particles. This did not seem to be a problem as pressure drops measured in the reactor set-up were the same as with the original cartridge. Finally, the thermal response was tested using adsorption of ethylene onto dried silica. The results are shown in Figure 3-52. It can be seen that, with the modified cartridge, the temperature measured by the outlet thermocouple increases much more rapidly and to a higher maximum. The response time of the system is therefore improved. The total energy transferred to the gas can be found by integration of the area under the curves. The area under the curve with the existing frit is greater. Correcting the measured data by accounting for the thermocouple time constant of 0.15 makes only a slight difference to the area under the outlet temperature curve for the cuve fitted with stainless steel mesh and so, although this is extremely promising, if the stainless steel mesh were to be adopted as a bed support, further tests would be required.

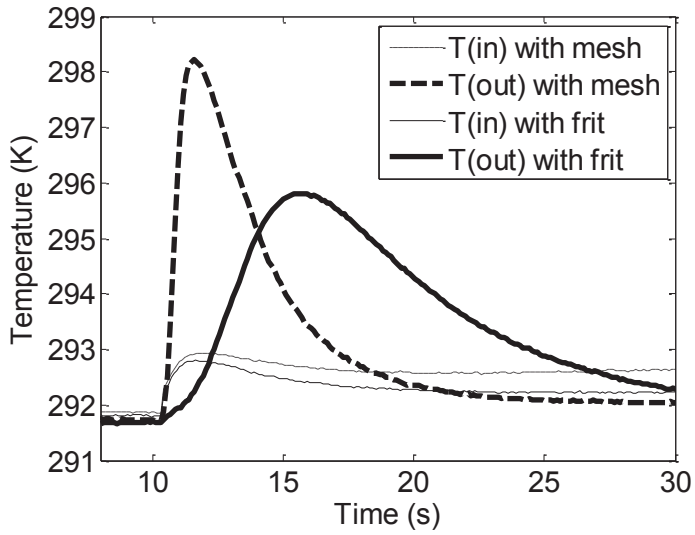

Figure 3-52: Comparison of reactor response for existing outlet frit vs stainless steel mesh

3.3.5 Alternative Inert Gases

The optimised reactor operating conditions [3] use helium to dilute the ethylene monomer and improve heat transfer from the catalyst particles. Helium use is not practical in industry and alternatives were modelled to see whether they might replace helium in the laboratory reactor.

Table 3-4 shows the molar specific heat capacities and thermal conductivities calculated in the model for pure gases and mixtures at the gas inlet conditions (353 K, 2:1 moles ethylene: inert gas). The ethylene/helium mixture has the highest conductivity and the ethylene/propane mixture has the highest specific heat capacity. Table 3-5 gives the particle heat transfer coefficients calculated in the model, also for the inlet conditions and for reaction gas flowrates of both 310 $mL.s^{-1}$ and 90 $mL.s^{-1}$. At the higher flowrate all the particle heat transfer coefficients are 35-40% greater than at the lower flowrate.

	Specific heat capacity at 353K ($J.mol^{-1}.K^{-1}$)	Thermal conductivity at 353K ($W.m^{-1}.K^{-1}$)
Pure gas:		
Ethylene	48.5	0.0294
Helium	20.8	0.1663
Nitrogen	29.2	0.0294
Propane	85.0	0.0260
Gas mixture (2:1 molar):		
Ethylene : Helium	39.2	0.0606
Ethylene : Nitrogen	42.0	0.0368
Ethylene : Propane	60.7	0.0370

Table 3-4: Specific heat capacity and thermal conductivity of gas mixtures calculated in the model

Flowrate $mL.s^{-1}$	310	90
Catalyst particle heat transfer coefficient, h_{cat}, $W.m^{-2}.K^{-1}$		
Gas mixture (2:1 molar)		
Ethylene : Helium	4870	3590
Ethylene : Nitrogen	3380	2410
Ethylene : Propane	3850	2660

Table 3-5: Catalyst particle heat transfer coefficients calculated in the model

Figure 3-53 shows the reactor bed outlet temperatures calculated by the model for the different gas mixtures. The model predicts use of nitrogen as the inert gas would have a similar effect to helium and that propane would be more effective in reducing reactor temperatures.

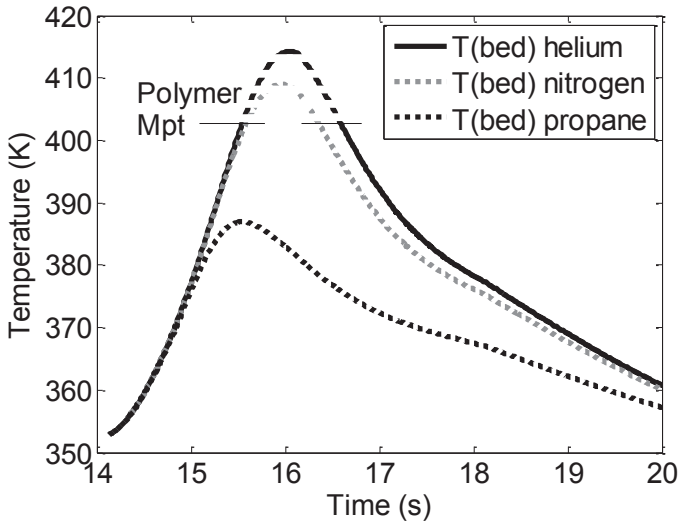

Figure 3-53: Comparison of calculated reactor bed outlet temperatures (centre point before exit frit) for helium, nitrogen and propane as the inert gas

Tioni [23] found that helium was more effective than nitrogen for avoiding thermal run away in this reactor. This apparent contradiction can be explained by the experimental conditions used to make the comparison, which were the lower flowrate of 90 $mL.s^{-1}$ and the coarse 250 - 500 µm NaCl seedbed. At the lower flowrate, the model finds that the rapid initial polymerisation rate reduces the ethylene concentration in the reactor bed, changing the physical properties of the reaction gas. Figure 3-54 shows the calculated reaction gas conductivity in the end segment of the reactor bed, where the variation is greatest, for a polymerisation reaction of 4s with reaction gas flowrate of 90 $mL.s^{-1}$. The effect on the gas conductivity is much greater for the ethylene/helium mixture than for the ethylene/nitrogen and this would not only have improved heat transfer out of the catalyst particles, but also increased the heat transfer rate to the less responsive large NaCl seedbed crystals. This would have allowed the seedbed to absorb more of the heat produced and helped regulate the bed temperature. Under the optimised conditions with the higher flowrate the reaction gas concentration fluctuates much less and the fine NaCl seedbed has much greater surface area so this effect would become negligible.

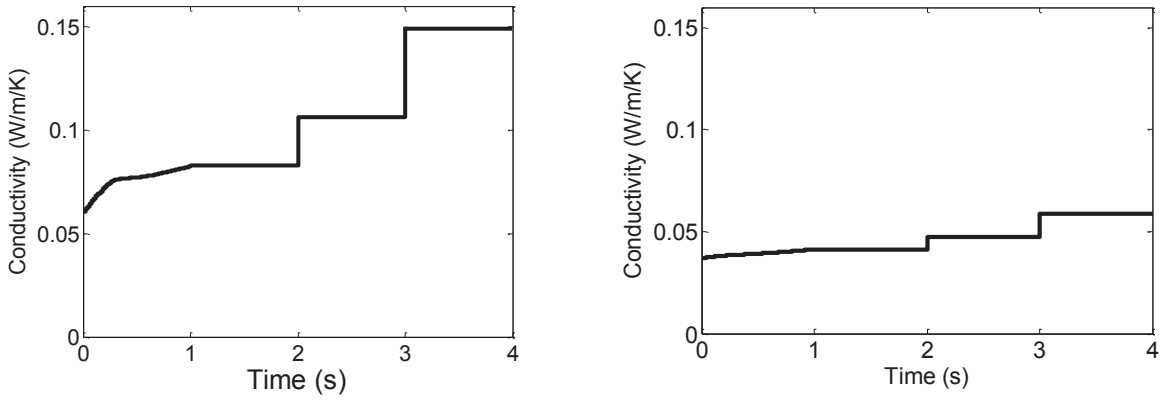

Figure 3-54: Calculated evolution of reaction gas conductivity in the reactor bed (end segment) for 4s polymerisation with flowrate 90 mL.s^{-1} with (a) ethylene/helium (b) ethylene/nitrogen

In conclusion, propane should be tested for use as ethylene diluent for the reactor as the model calculates it to be more effective than helium. The model predicts similar thermal behaviour for the reactor with helium or nitrogen as the inert gas under the optimised conditions. This can be explained by the increases in seedbed surface area and flowrate which make the need for increased reaction gas conductivity redundant.

3.3.6 Aluminium Reactor

The existing reactor cartridge weighs approximately 40 g, whereas the quantities of catalyst used and polymer formed are below 100 mg. The mass of catalyst and polymer are found by weighing the cartridge empty and before and after the polymerisation and taking the differences. The relatively high mass of the cartridge increases the risk of error and one way considered to reduce this is the use of aluminium as construction material.

Table 3-6 compares the physical properties of stainless steel and aluminium. From the difference in density, the weight of an aluminium cartridge of the same size and shape as the existing one would be 12.75 g. Aluminium has a much higher thermal diffusivity than stainless steel, so would be expected to transport heat through the reactor wall more quickly. Figure 3-55 shows the maximum reactor temperatures calculated across the reactor radius at the hot spot for a stainless steel and an aluminium reactor. The slight difference in reactor wall temperatures can be seen but also that the temperature profile across the reactor bed remains unchanged.

Figure 3-56 compares the outlet temperatures calculated for an aluminium reactor and a stainless steel reactor. As expected from the bed temperature profile, there is only a slight difference between the two. The coefficients of thermal expansion are very similar so using

an aluminium cartridge with a stainless steel reactor should not lead to problems on heating. However, the construction of the cartridge would have to be reviewed as the stainless steel outlet frit is welded into place. An alternative way to reduce the weight of the reactor cartridge would be to reduce the wall thickness. For example, a reduction to 4 mm would also result in a cartridge weight of 12.8 g.

	Thermal conductivity ($W.m^{-1}.K^{-1}$)	Density ($kg.m^{-3}$)	Specific heat capacity ($kJ.kg^{-1}.K^{-1}$)	Thermal diffusivity (10^{-6} $m^2.s^{-1}$)	Coefficient of thermal expansion ($m.m^{-1}.K^{-1}$)
Stainless steel	17	8000	0.51	4.16	16×10^{-6}
Aluminium	205	2550	0.925	86.9	22.2×10^{-6}

Table 3-6: Physical properties of stainless steel and aluminium

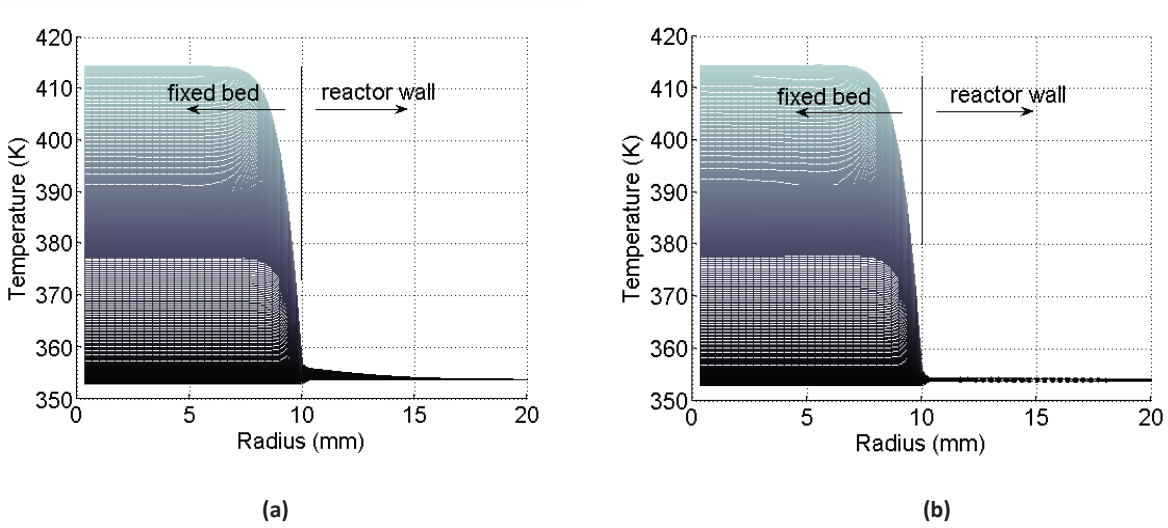

Figure 3-55: Calculated reactor bed and wall temperatures across section at hot spot (a) stainless steel reactor (b) aluminium reactor

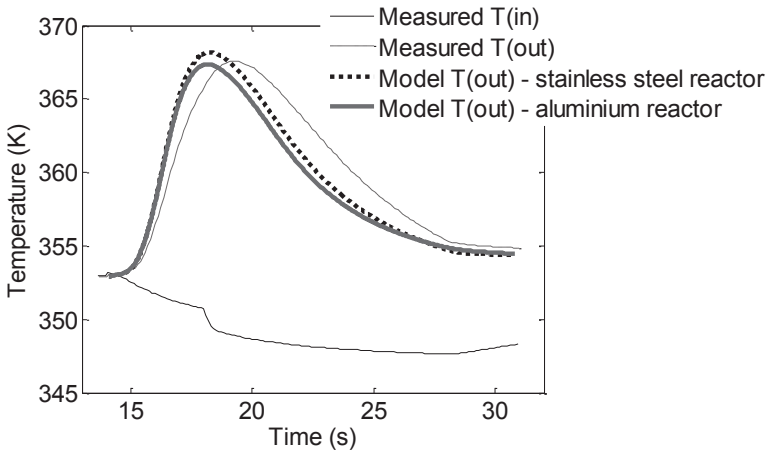

Figure 3-56: Compare calculated outlet temperatures for typical 4s reaction modelled for the existing stainless steel reactor and for an aluminium reactor

3.3.7 Conclusion

Simulations have been carried out using the validated reactor model. The model finds that the lower reaction gas flowrate of 90 $mL.s^{-1}$ is insufficient to maintain a steady ethylene concentration in the reactor. Very high temperatures and steep thermal gradients also occur in the reactor bed for this case.

Under the optimised operating conditions, the reactor bed is more uniform but some temperature gradients still exist. Simulating different reactor geometries shows that changing the reactor dimensions would have little effect to further reduce temperature gradients because they occur so rapidly and early in the polymerisation (<2s) that conduction out of the bed is negligible and the reactor can be considered adiabatic in these first few seconds. Increasing gas flowrates would be effective, as would replacement of helium with propane as reaction gas diluent. Also, the reactor outlet temperature measurement could be made more responsive to bed temperature by replacing the exit frit with stainless steel mesh.

The reactor cartridge weight could be reduced by using aluminium as material of construction. However, this could also be done by reducing the wall thickness which would facilitate fitting of a stainless steel bed support at the reactor outlet.

3.4 General Conclusions

The model was validated against experiments with and without catalyst for both silica and NaCl seedbeds. Further validation was done by positioning a thermocouple within the reactor bed and by comparison of the measured and calculated polymer distributions. The model is found to provide a good fit for individual, short duration experiments. Thermal gradients exist in the reactor bed and the position of the reactor outlet thermocouple, downstream of the outlet frit, can hide temperature fluctuations. Brief excursions beyond the melting point of polyethylene are calculated towards the exit of this reactor exit, even under optimal experimental conditions.

The use of the reactor as a calorimeter has been discussed and, to this end, an observer has been developed. An initial observer construction was able to estimate a polymerisation rate from a uniform reactor bed temperature. However, this system was not observable for the system of equations for the reactor bed divided into finite elements and needed to describe temperature gradients more accurately. This was overcome by including an activation energy to construct an observer which could estimate a reaction rate independently of temperature. This observer takes account of the axial temperature gradient in the reactor and is robust, but over estimates the mass of polyethylene formed. This seems to be because the effective radial conductivity in the bed and the wall heat transfer coefficient are not considered separately and the next step in development of the observer would be to create a 2D version. The main drawback with this observer is the current need to use temperature data from the model as input as opposed to the true measured data. This could be overcome by modifying the reactor to reduce the thermal effect of the exit frit.

Simulations of experiments carried out at the lower flowrate of 90 $mL.s^{-1}$ showed that fluctuations in ethylene concentration, high temperatures and steep thermal gradients occur for this case. Alternative reactor geometries were considered as a means to reduce the early temperature excursion but the rapidity of the initial reaction relative to the heat transfer rate through and from the bed means the reactor can be considered adiabatic during this period and so changing the reactor shape would not be effective for this. Increased reaction gas flowrate or use of propane as ethylene diluent were both shown to have more potential to stabilise reactor temperatures. The reactor bed is very porous and quite fragile and a shorter reactor bed of increased diameter would allow increased volumetric gas flowrates at the existing velocity which could avoid potential problems with bed instability. The effect of replacing the existing reactor exit frit by frits of alternative materials or a stainless steel mesh in order to improve the sensitivity of the reactor was considered. Fine stainless steel mesh

was calculated to be the most promising alternative and a reactor cartridge was modified and tested. The results were very positive and the next step would be to test this reactor cartridge using catalyst. It was not possible to carry out this experiment as a part of this thesis, as unfortunately this type of catalyst had been completely consumed by Estevan Tioni and I. To able to do these experiments correctly, a new batch of catalyst would have been required and there was not sufficient time to do this. Finally, an aluminium reactor was modelled as a potential method to reduce the reactor weight relative to that of the catalyst and polymer formed.

3.5 Nomenclature

A	State matrix	-
A_w	Wall area for heat transfer	-
C	Output matrix	-
C_{C2}	Ethylene concentration	$mol.m^{-3}$
C^*	Active site concentration	$mol.m^{-3}$
c_p	Specific heat capacity	$kJ.kg^{-1}.K^{-1}$
c_{pC2}	Specific heat capacity ethylene	$kJ.kg^{-1}.K^{-1}$
d_t	Reactor diameter	m
E_a	Activation energy	$J.mol^{-1}$
F_T	Total molar flow	$mol.s^{-1}$
h_{cat}	Catalyst heat transfer coefficient	$W.m^{-2}.K^{-1}$
h^{sf}_{int}	Wall heat transfer coefficient (2D model)	$W.m^{-2}.K^{-1}$
$\bar{h}_{\text{int}}$	Wall heat transfer coefficient (1D model)	$W.m^{-2}.K^{-1}$
ΔH	Heat of reaction	$J.mol^{-1}$
ΔH_{ads}	Heat of adsorption	$J.mol^{-1}$
K	Lumped reaction constant	
l_{sfer}	Effective bed conductivity	$W.m^{-1}.K^{-1}$
L_f	Lie derivative	
Mwt_{rg}	Molecular weight reaction gas	$g.mol^{-1}$
Mwt_{C2}	Molecular weight ethylene	$g.mol^{-1}$
R	Ideal gas constant	$J.mol^{-1}.K^{-1}$
r	Radial distance	m
$\bar{r}_v$	Apparent reaction rate per unit bed volume	$mol.s^{-1}.m^{-3}$
S_{cat}	Catalyst surface area	m^2
S_r	Cross sectional area of segment	m^2
S_Θ	Explicit solution to Lyapunov equation	-
T	Temperature	K
T_w	Wall Temperature	K
t	Time	s
X	State vector	-
y	Measured variable	-

y_{C2}	Mole fraction ethylene	-
Z	State vector after change of variables	
z	Axial distance	m
Θ	Tuning parameter	
ε	Dynamic to be found by observer	-
ρ	Density	$kg.m^{-3}$

Suffixes

c	Catalyst & polymer
g	Gas & inert solid
rg	Reaction gas

[1] McKenna T.F.L., Di Martino A., Weickert G. & Soares J.P.B., Particle Growth During the Polmerisation of Olefins on Supported Catalysts,1 – Nascent Polymer Structures, Macromol.React.Eng, 4, (2010) 40-64

[2] Lowell P.N. & McCrum N.G., Diffusion Mechanisms in Solid and Molten Polyethylene, J. Polym. Sci.: A-2 9,11 (1971) 1935-1954

[3] Tioni E., Optimization of a Tool to Study the Start-up of the Gas Phase Olefin Polymerization, Phd thesis, UCBL1

[4] Kammona O., Chatzi E.G. & Kiparissides C., Recent developments in Hardware Sensors For the On-line Monitoring of Polymerization Reactions, J. Macromol. Sci, C: Polym. Rev. 39,1 (1999) 57-134

[5] Lahti M., Avela A. & Seppala J., Polymerization Calorimeter. Part 2. Practical Use and Application in Polymerizations, Thermochim. Acta, 262 (1995) 33-43

[6] Frauendorfer E., Wolf A. & Hergeth W-D., Polymerization Online Monitoring, Chem. Eng. Technol. 33,11 (2010) 1767-1778

[7]Othman N., Advanced Stategies for Composition Control in Semi-Continuous Emulsion Polymerisation, PhD Thesis, University Claude Bernard Lyon 1, Lyon (2000)

[8] Soares M., Machado F., Guimaraes A., Amaral M.M. & Pinto J.C., Real-Time Monitoring and Parameter Estimation of the Emulsion Polymerisation of Carboxylated Styrene/Butadiene Latexes, Polym. Eng. Sci. 51 (2011) 1919-1932

[9] Rincon F.D., Esposito M., de Araujo P.H.H., Sayer C. & Le Roux G.A.C., Calorimetric Estimation Employing the Unscented Kalman Filter for a Batch Emulsion Polymerisation Reactor, Macromol. React. Eng. 7 (2013) 24-35

[10] Korber F., Hauschild K., Winter M. & Fink G., Reaction Calorimetric Investigation of the Propylene Slurry Phase Polymerization with a Silica-Supported Metallocene/MAO Catalyst, Macromol. Chem. Phys., 202 (2001) 3323-3328

[11] Tisse V., Sheibat-Othman N. & McKenna T.F.L., A Lab-Scale Reaction Calorimeter for Olefin Polymerization, Can. J. Chem. Eng. 88 (2010) 783-792

[12] Froment G.F., Fixed Bed Catalytic Reactors, Ind. Eng. Chem. 59 (1967) 18-27

[13] Mears D.E., Diagnostic Criteria for Heat Transport Limitations in Fixed Bed Reactors, J. Catal. 20 (1971) 127-131

[14] Soares J.B.P. & McKenna T.F.L., Polyolefin Reaction Engineering (2012) Wiley-VCH Verlag & Co., Weinheim, Germany

[15] Hamilton P., Hill D.R. & Luss D., Optical and Infrared Study of Individual Reacting Metallocene Catalyst Particles, AIChE J. 54,4 (2008) 1054-1063

[16] http://www.final-materials.com/materiaux/produits/ceramique-frittee-117.html (22/10/2012)

[17] http://www.final-materials.com/materiaux/produits/ceramique-frittee-15.html (22/10/2012)

[18] http://www.technicalglass.com/technical_properties.html (22/10/2012)

[19] http://www.hightempmetals.com/techdata/hitempHastC276data.php (22/10/2012)

[20] http://www.hightempmetals.com/techdata/hitempInconel625data.php (22/10/2012)

[21] http://a-1wire.com/nickel200.html (22/10/2012)

[22] http://www.specialmetals.com/documents/Monel%20alloy%20400.pdf (22/10/2012)

[23] Tioni E., Broyer J.P., Spitz R. Monteil V.& McKenna T.F.L., Heat Transfer in Gas Phase Olefin Polymerisation, Macromol. Symp. 285 (2009) 58-63

Chapter 4

Reactor Model:

Further Developments

4 Reactor Model: Further Developments

Because the version of the model described in Chapters 2 and 3 can only represent the reaction period for individual experiments, further work was done to try and better understand this period and improve the reactor model. This section describes this work which includes: experiments with the reactor modified to include an internal thermocouple, study of the reactor pressurisation rate and inclusion of catalyst deactivation as a separate reaction in the model.

4.1 Experiments with Internal Thermocouple

4.1.1 Reactor Configuration

Because of the difference between the calculated temperatures in the reactor bed and the measured temperature at the outlet, it was decided to fit the reactor with an internal thermocouple. Figure 4-1 shows the configurations which were tried. In configuration (a) a small hole was drilled through the stainless steel frit at the reactor inlet to pass a 1mm T-type thermocouple into the bed. Figure 4-2 (a) shows the results with this arrangement. The measured inlet and bed temperatures were very similar which suggested gas channelling along the thermocouple. To avoid this, the reactor was reversed to give configuration (b) so that the inlet became the outlet and vice versa. Figure 4-2 (b) shows this was an effective way to stop the channelling. However, in this second arrangement uneven flow distribution was suspected due to the sudden enlargement at the new reactor inlet with an uneven seedbed residue observed on the inside of the reactor lid. Finally, it was decided to construct a new reactor which would have a conical inlet chamber and also allow the thermocouple to be inserted via the outlet as configuration (c). This is the reactor used in experiment ET_SFG_462, described in Chapter 3 section 3.1.5 and Figure 3-10 where the difference in temperatures between the reactor bed and the reactor outlet could be observed.

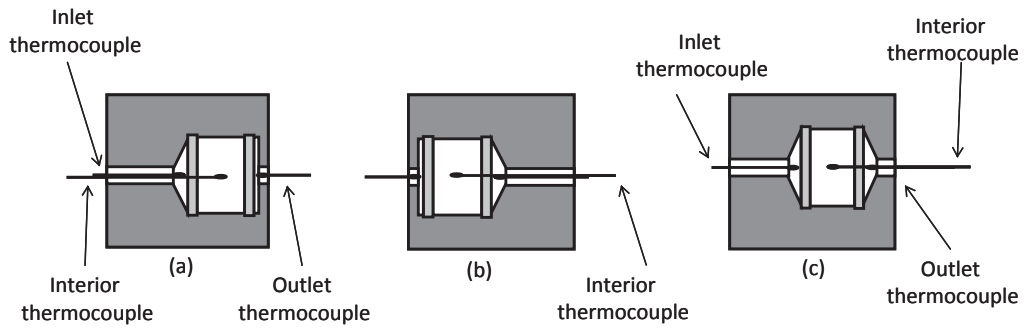

Figure 4-1: Different reactor configurations: (a) with interior thermocouple via inlet (b) identical reactor but reversed (c) symmetrical and with thermocouple via exit

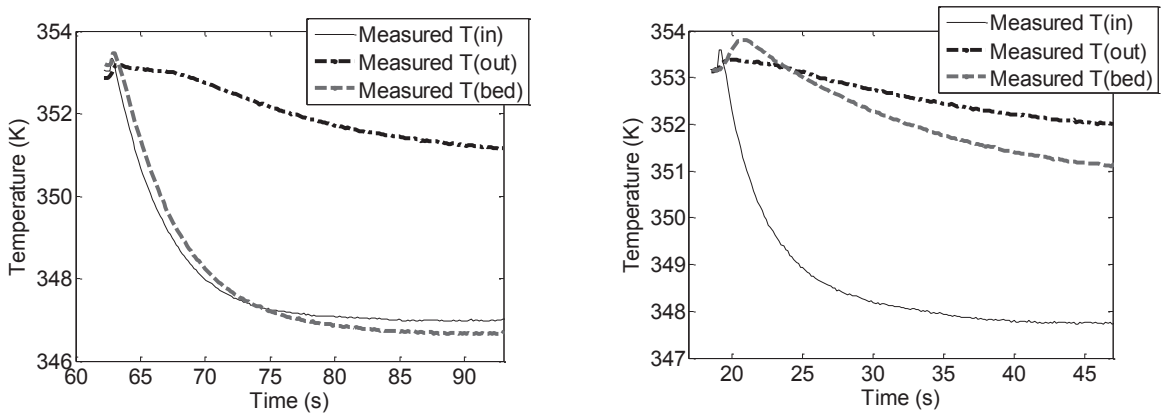

(a) (b)

Figure 4-2: Measured temperatures for experiments with no catalyst and fine NaCl seedbed in reactor configurations (a) EXP_30 interior thermocouple via inlet and (b)EXP_34 interior thermocouple via outlet

4.1.2 Reactor Testing

For testing of the new reactor per Figure 4-1 (c) the thermocouple was sealed into place with glue with the tip protruding 2 mm into the reactor bed. This reactor configuration was achieved by reversing the original reactor. So, in this arrangement the reaction gas flow pushes the seedbed against the reactor cover and not into the cartridge. This means a small amount of mass is lost and the method of measuring the mass of polymer formed by the difference in cartridge weight before and after polymerisation is compromised.

Nevertheless, the reactor response with and without catalyst was tested in the hope of gaining bed temperature data. Figure 4-3 shows the temperatures recorded at the reactor inlet, bed and outlet for an experiment with a fine NaCl seedbed, no catalyst and a measured flowrate of 340 $mL.s^{-1}$ (at flowmeter conditions). The inlet and outlet temperatures follow the same pattern as reported for the original reactor and the measured bed temperature is between the two.

Figure 4-4 shows measured reactor outlet and bed temperatures for some experiments using catalyst in this reactor. There is a lot of variability and inconsistency in these results. Possible explanations are that there is a problem with the reactor or inhomogeneity in the mixing of the catalyst and seedbed which is done by hand.

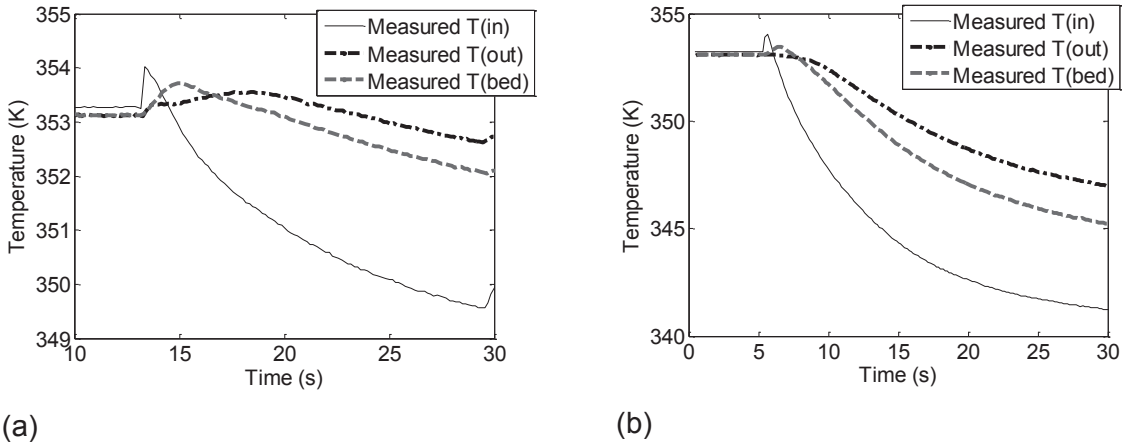

Figure 4-3: Measured inlet and outlet temperatures for EXP_48, fine NaCl seedbed with no catalyst at 353K (a) 340 mL.s-1 ethylene/helium (b) CO2 with set pressure 9 bar gauge

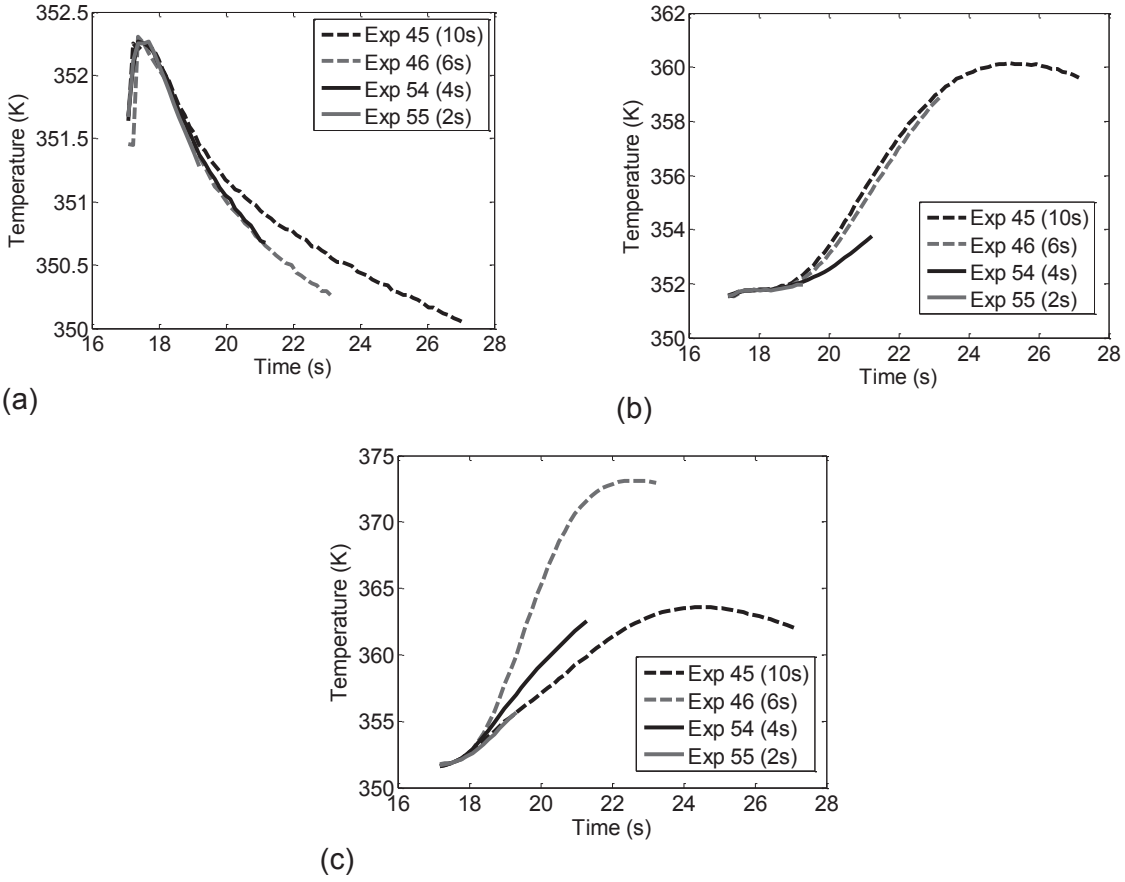

Figure 4-4: Measured values for typical experiments with catalyst in the modified reactor (a) inlet temperatures (b) outlet temperatures (c) bed temperatures

4.1.3 Reduced Catalyst Activity

The introduction of the thermocouple into the reactor bed also led to a significant loss of yield. The reduction in activity using the modified reactor can be demonstrated by considering four similar experiments of 10s duration. Experiments 44 and 67 were carried out in the original reactor. Experiments 45 and 66 were carried out in the modified reactor with the internal thermocouple. The results are shown in Table 4-1 and Figure 4-5. Temperatures and yields in the new reactor are significantly lower than for similar experiments carried out in the original reactor.

Exp. No.	Mass catalyst (mg)	Mass inert (g)	Gas flowrate ($mL.s^{-1}$ stp)	Yield ($g.g^{-1}$)
44	49.4	1.133	297	1.18
45	45.1	1.185	288	0.52
66	41.9	1.303	344	0.57
67	38.8	1.299	344	0.87

Table 4-1: Experimental data for four similar reactions in the original and modified reactors

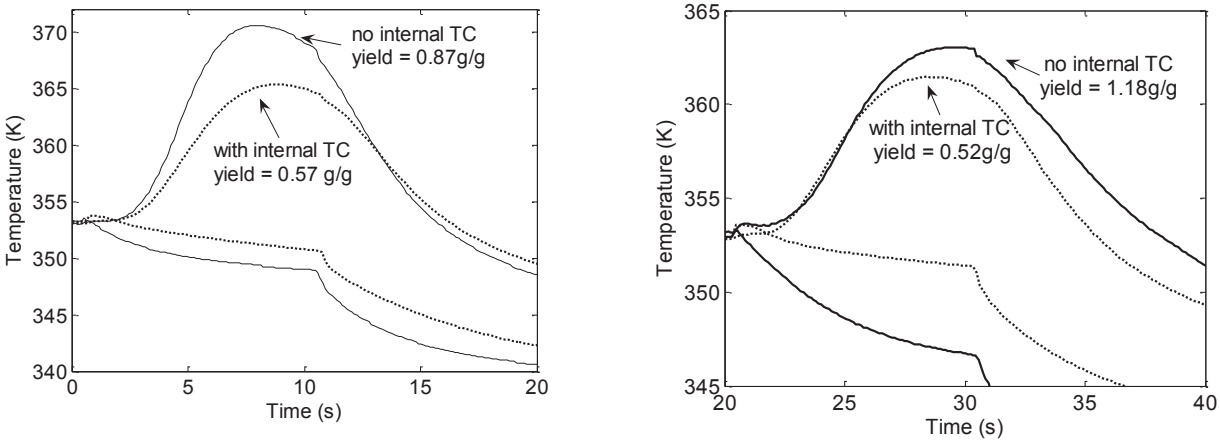

(a)

Figure 4-5: Comparison of measured inlet and outlet temperatures for similar experiments in the reactor with no thermocouple and the reactor with thermocouple: (a) Exp 67 & Exp 66 (b) Exp 44 & Exp 45.

To check that the difference is not due to variation in reaction gas flowrate, mass of catalyst or mass of inert, similar experiments were modelled using the same reaction kinetic parameters. However, the measured values for the reactor with the internal thermocouple are still low (Figure 4-6).

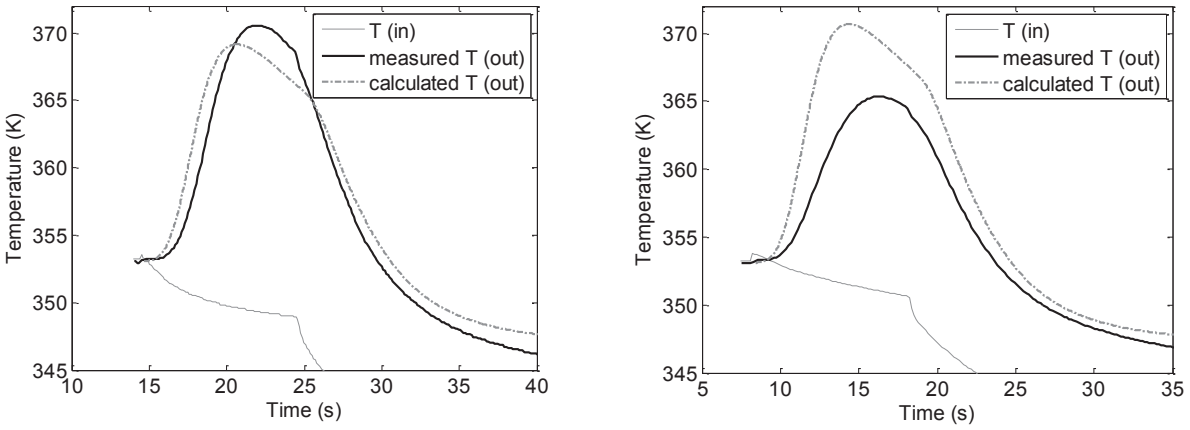

Figure 4-6: Calculated reactor output temperatures compared to measured values for (a)Exp 67 with optimised kinetics (b) Exp 66 using the optimised kinetics for Exp 67

The position of the thermocouple is at the hottest, most active section of the bed where it replaces a small bed volume. The space taken up by the thermocouple is 2mm x 1mm at the end and centre of the reactor bed. Setting the reaction rate to zero for this volume in the model is not sufficient to account for the effect of the thermocouple. In fact, the mass of polymer calculated for Experiment 67 in these segments is only 0.1 mg out of a total 40.5 mg. However, the thermocouple provides extra heat capacity and affects the temperature of the surrounding reactor seedbed, and thus the reaction rate.

Another possible cause of the reduced activity is channelling at the edges of the inlet frit. This may have been possible because in fitting the thermocouple to the reactor the flow direction was reversed. The inlet frit became the one fitted to the reactor cartridge which was tightly in place but not sealed. If channelling occurred, bed temperatures and reaction rate would have been affected.

Finally, it was concluded that, whilst able to show that reactor outlet and bed temperatures differ significantly, direct measurement could not be used to investigate bed temperatures without impacting reactor conditions.

4.2 Reactor Pressurisation

4.2.1 Measurement of the Pressurisation Rate

To evaluate the response of the system pressure on opening the automatic valve, the pressure downstream of the reactor outlet was measured. The reactor and bed were in place but no catalyst was used. An oscilloscope was used to record the data off the pressure meter for a few seconds, including the system pressurisation. The original data was noisy and the experiment was repeated three times. The curve shown in Figure 4-7 has been smoothed by calculating a rolling average over 16 data points and also by averaging over all three experiments. The reactor can be seen to reach full pressure after about 1s.

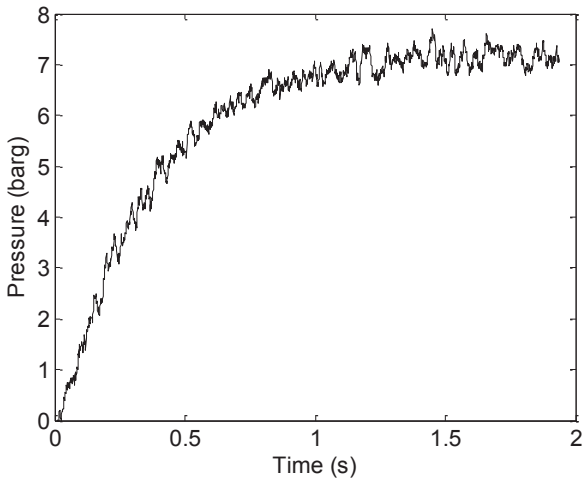

Figure 4-7: Pressurisation of the reactor system as measured at the reactor outlet

4.2.1.1 First Order System

The pressurisation follows the response of a first order system to a step change. This can be represented by the equation:

$$P = AK_p(1 - e^{-\frac{t}{\tau}})$$

4-1

The gain and time constant were calculated to be 0.8 and 0.3625 respectively, by non-linear regression using MATLAB. The results are shown in Figure 4-8. Note that this calculates the pressure near the outlet of the reactor and not in the reactor bed. Because the pressurisation is of similar duration to some of the experiments it cannot be neglected and must be included in the reactor model.

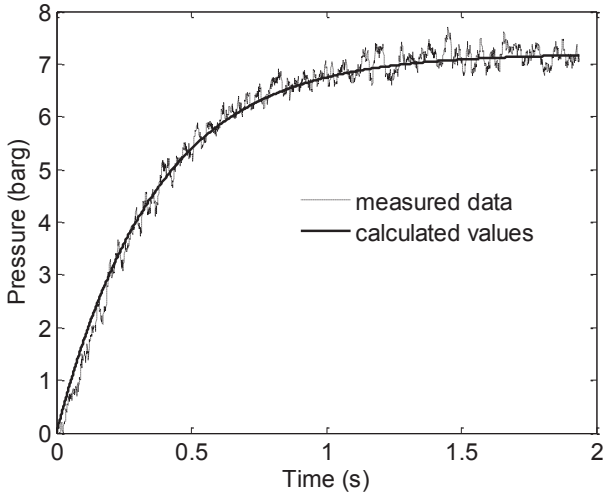

Figure 4-8: Measured pressures at reactor outlet and curve for the response of a first order system to a step change

4.2.1.2 Comparison with Heat of Compression

Figure 4-9 compares the measured pressure response at the reactor outlet with the temperature response in the reactor bed on pressurisation and for the same conditions. The measured temperatures have been corrected using the thermocouple time constant (0.15s). The stabilisation times are coherent and the temperature data supports the measured pressurisation data.

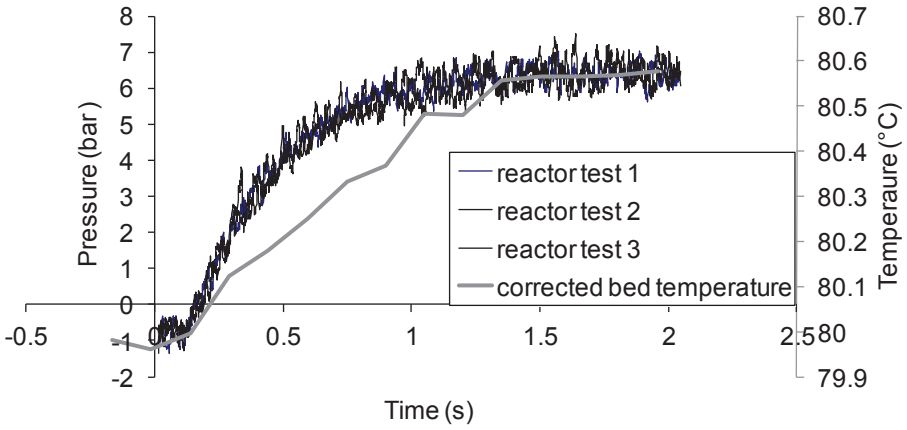

Figure 4-9: Compare measured pressures with corrected bed temperature on reactor pressurisation for the same conditions EXP_48

4.2.1.3 Increased Capacity Pressure Controller

Because of the relatively long pressurisation time of the reactor system, a higher capacity pressure controller was tested. Figure 4-10 compares the response of the two controllers on opening the automatic valve. The pressurisation profiles are measured downstream of the reactor. Use of the higher capacity pressure controller makes very little difference to the measured profile and does not reduce the pressurisation time.

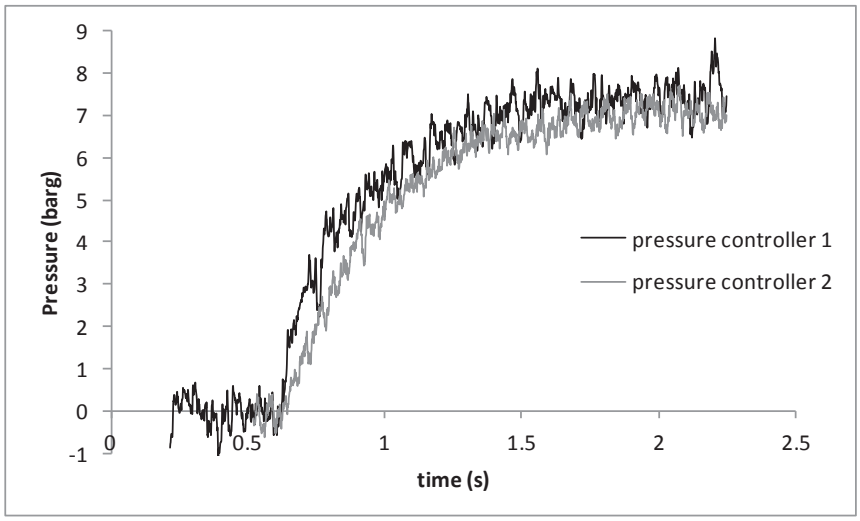

Figure 4-10: Pressurisation of the reactor system with alternative pressure controller as measured at the reactor outlet

4.2.1.4 Reactor Exit Flowrate

To measure the relationship between reaction gas flowrate out of the reactor and reactor pressure, experiments with no catalyst were carried out at 353K with different set pressures. The flow control valve at the reactor outlet was set full open, as per experimental conditions. The flowrate and pressure at the reactor outlet were recorded under steady flow conditions. Figure 4-11 shows that the flowrate is directly proportional to reactor outlet pressure with the relation,

$$Q_m = 48.23\ P_m \qquad \text{4-2}$$

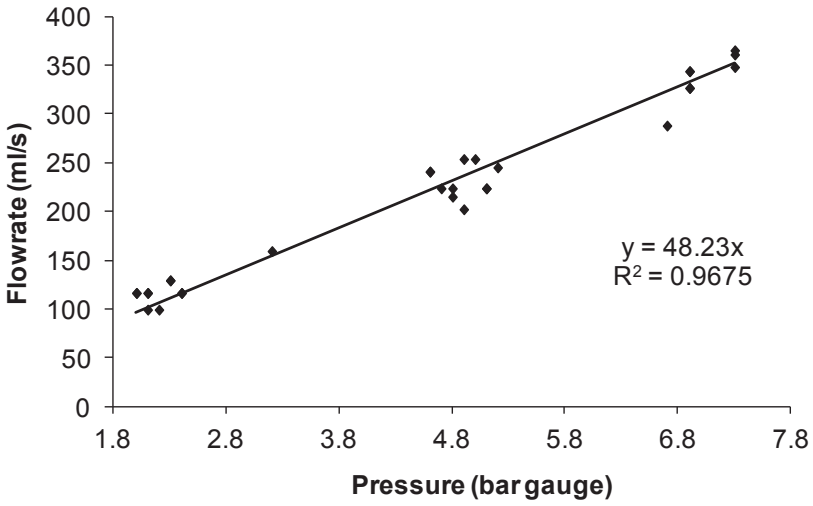

Figure 4-11: Measured flowrates vs measured outlet pressures for several experiments at 353K

4.2.2 Model with Pressurisation

The relations for reactor pressurisation rate and outlet flowrate developed in the previous section were incorporated into the reactor model.

4.2.2.1 Typical Results

Figure 4-12 shows the reactor pressure calculated in the revised version of the model (Run 2) compared with the value used in the previous version of the model (Run 1) for typical experiment, ET_PE_SFG_124, of 15 seconds duration. Figure 4-13 compares the reactor outlet temperatures calculated by the two versions of the model. There is very little difference but a slight delay can be seen when pressurisation is taken into account. Figure 4-14 compares the bed exit temperatures and shows a similar delay when pressurisation is included in the model and a slightly higher peak.

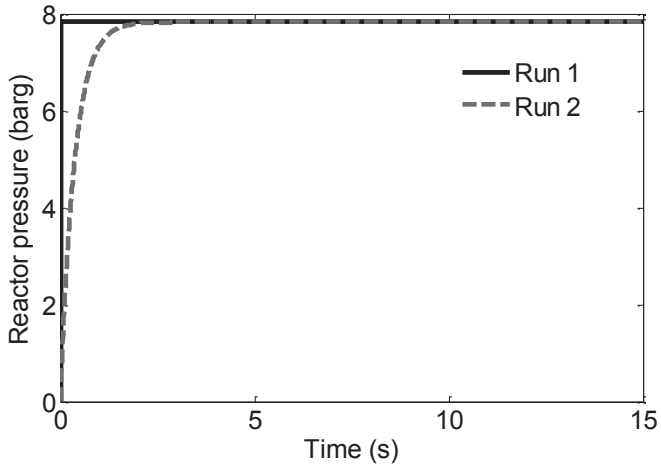

Figure 4-12: Calculated reactor pressure against time for experiment ET_PE_SFG_124 of 15s duration at optimised conditions

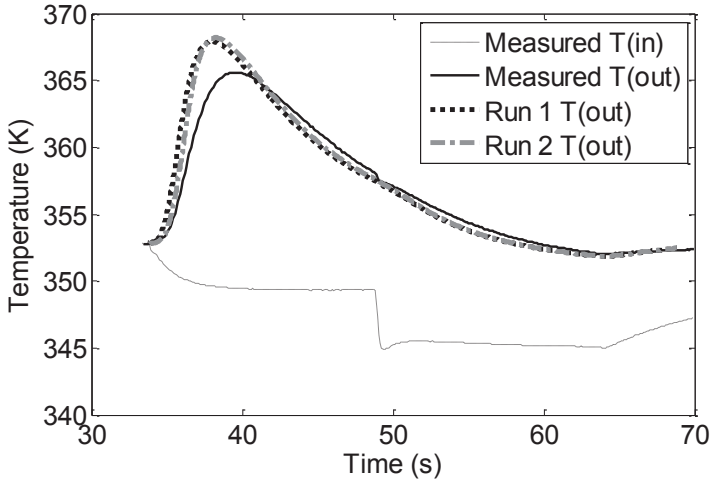

Figure 4-13: Comparison of calculated reactor outlet temperatures for experiment ET_PE_SFG_124 of 15s duration

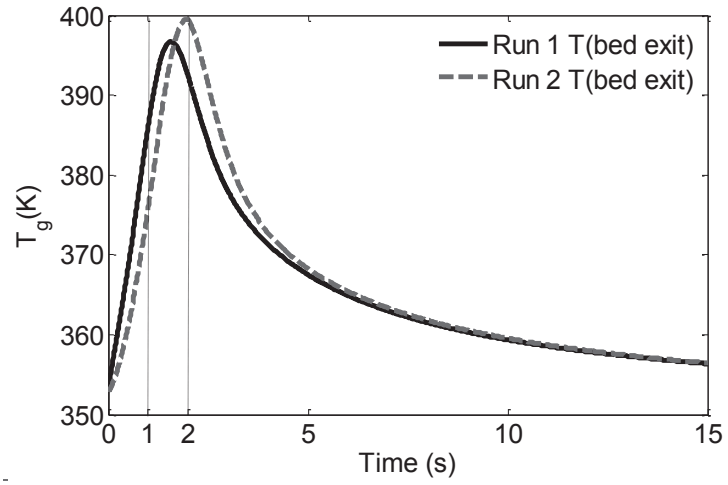

Figure 4-14: Comparison of calculated bed exit temperatures for experiment ET_PE_SFG_124 of 15s duration

4.2.2.2 Observer

At this point it is interesting to return to the discussion of the observer in Chapter 3, section 3.2.4. Figure 4-15 compares the estimates for $kC_{C2}C^*$ based on the reactor bed exit temperatures calculated by the model (i) assuming constant pressure (Run 1) and (ii) with the pressurisation included (Run 2). The observer calculates values which are representative of the kinetics that have been used in the model. The increase in $kC_{C2}C^*$ due to the increasing partial pressure of ethylene is clearly seen for the case where pressurisation has been included. This validates the observer in that it returns the expected profile for $kC_{C2}C^*$. It also shows how sensitive it is to slight changes in input and that it could be an extremely useful tool if better measured data were available.

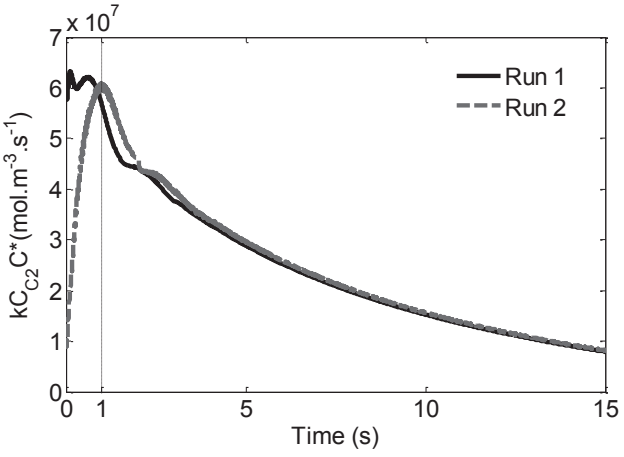

Figure 4-15: Comparison of observer estimates for $kC_{C2}C^*$ using bed exit temperatures from model assuming constant pressure (Run 1) and including pressurisation (Run 2)

4.2.2.3 100ms Experiment

The reactor model assumptions limit the quantity of ethylene entering the reactor. From the mass balances, all the helium entering the reactor must leave in the outlet stream. The outlet stream flowrate is limited by the total reactor pressure and the quantity of ethylene arriving in the reactor is limited because it is in fixed ratio with the helium. So, if the reaction rate is very fast, a concentration gradient develops along the reactor length. If all the ethylene is consumed, the outlet stream is 100% helium.

For the experiment of duration 100 ms the measured mass of polymer formed (7.5mg) is greater than the mass of ethylene able to enter the reactor under the model assumptions and taking pressurisation of the system into account (5.4mg). The shorter the reaction duration, the more significant inaccuracies become which could account for this discrepancy. Possible sources of error are [1].

- weighing of the polymer formed
- timing of the automatic valves
- dead volumes in the lines
- composition of the inlet gas stream.

Figure 4-16 shows the result of running the model with an increased polymerisation rate for this particular 100ms experiment to try to calculate the measured mass of polymer. This is done by setting the lumped reaction constant very high and gives a good fit between the model outputs and measured data. Figure 4-17 shows the calculated ethylene concentration and PE accumulation along the centre line of the reactor for this run. The model calculates that the ethylene is almost all consumed on entering the reactor. So, on this very short time scale, the reaction rate may be limited by the amount of ethylene entering the reactor.

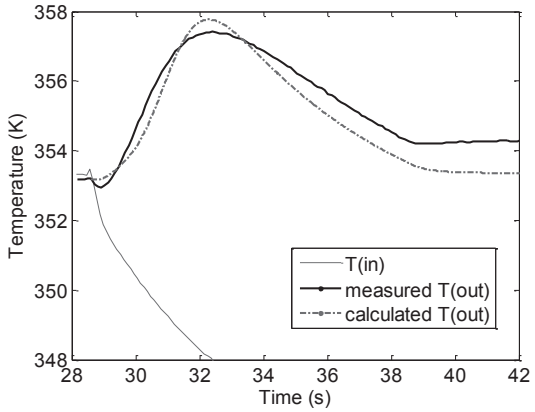

Figure 4-16: Compare Calculated Outlet Temperatures to Measured Values for 100ms Duration Experiment

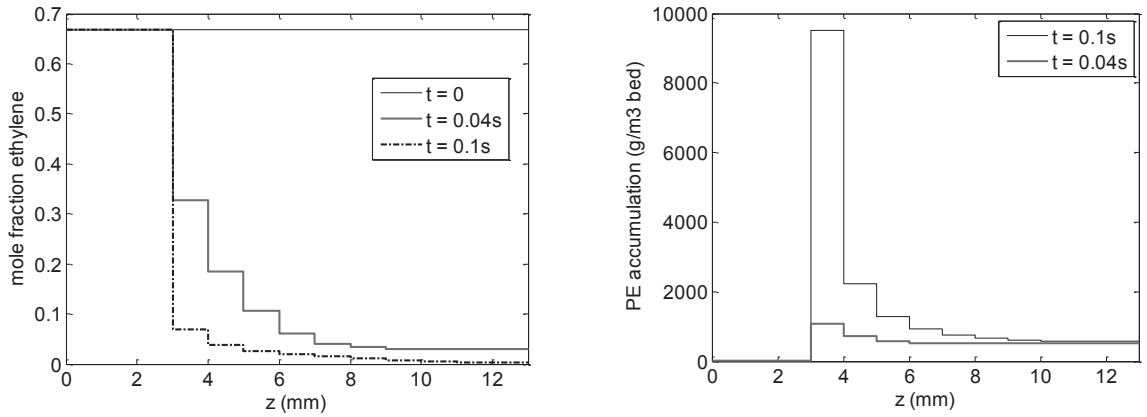

Figure 4-17: Calculated Model Outputs for 100ms Duration Experiment Along the Length of the Reactor Bed (a) Ethylene Mole Fraction (b) PE Accumulation

4.2.2.4 Increased Pressurisation Rate

The reactor set up could be modified to allow a more rapid increase in ethylene partial pressure. For example, the position of the pressure controller could be changed. Alternatively, the reactor could be pressurised with inert gas prior to the passage of the reaction gas. In consideration of this idea, the Peclet number was checked to see whether a clean pulse of ethylene could be transported through the existing system from the pressure controller to the reactor. It was found that dispersion in this section of piping would be negligible. This method would also have the advantage of removing the effect of system compression from the measured temperature profiles.

The effect of instant reactor pressurisation was simulated using the model. Figure 4-18 shows the two pressurisation profiles used in the model to make the comparison. Figure 4-19 shows the results. The model predicts that although the initial reaction rate would be greater for instantaneous reactor pressurisation with ethylene, the higher initial flowrate would compensate and increase heat transfer out of the reactor. This would lead to similar temperature profiles as observed with the current arrangement. However, this simulation should be treated with caution because the initial chemical kinetics of the polymerisation are not certain [2,3].

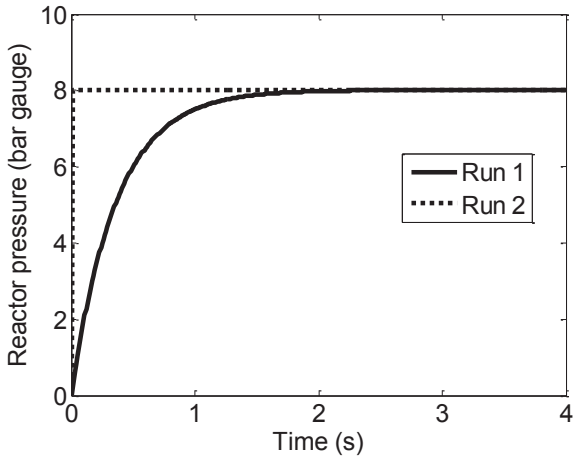

Figure 4-18: Reactor pressurisation profiles for runs 1 & 2

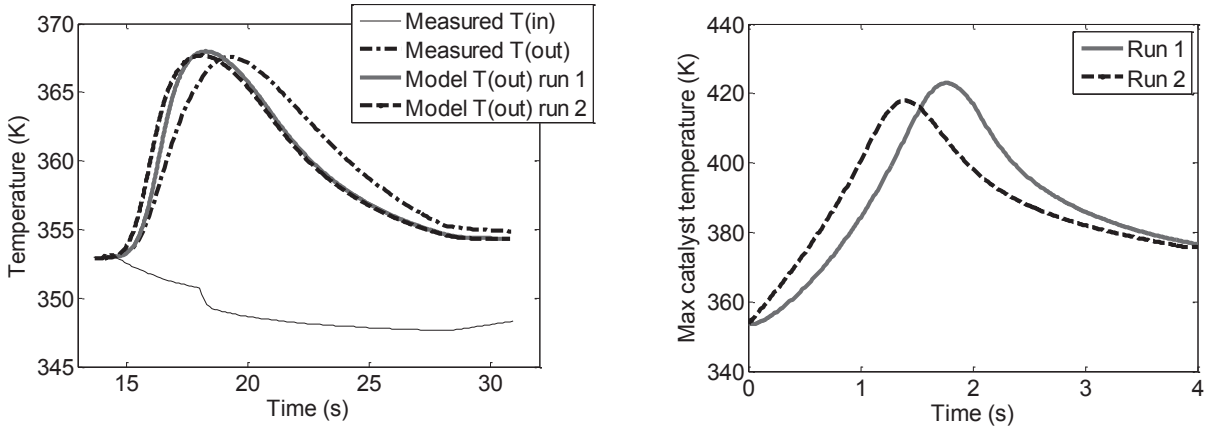

Figure 4-19: Comparison of model outputs for runs 1 & 2 with and without pressurisation time (a) Comparison between measured and calculated temperatures for typical 4s experiment (b) Calculated maximum catalyst temperatures

4.2.3 Activity Profiles

The activity profiles which have been reported for this reactor by Tioni [1] and are mentioned in Chapter 2 section 2.1.3.4 can now be adjusted to take account of the system pressure. The unadjusted profiles are based on the final yield of each experiment and the assumption of constant pressure. The curve can be adjusted to include the measured pressurisation profile as follows:

$$\bar{r}_m' = \bar{r}_m \frac{Pt}{\int_0^t AK_p\left(1 - e^{-\frac{t}{\tau}}\right)}$$

4-3

Where $\bar{r}_m$ represents the average observed reaction rate calculated under the constant pressure assumption and $\bar{r}_m$' includes the effect of pressurisation. This brings the pattern of activity found in this reactor in line with the profiles measured by Silva et al. [2] and by Di Martino et al. [3] with a rapid decrease from time zero.

4.2.3.1 Lower Flowrate

Figure 4-20 shows the change for experiments with nominal gas flowrate of 90 mL.s^{-1} and Figure 4-21 shows the same result plotted on log axes.

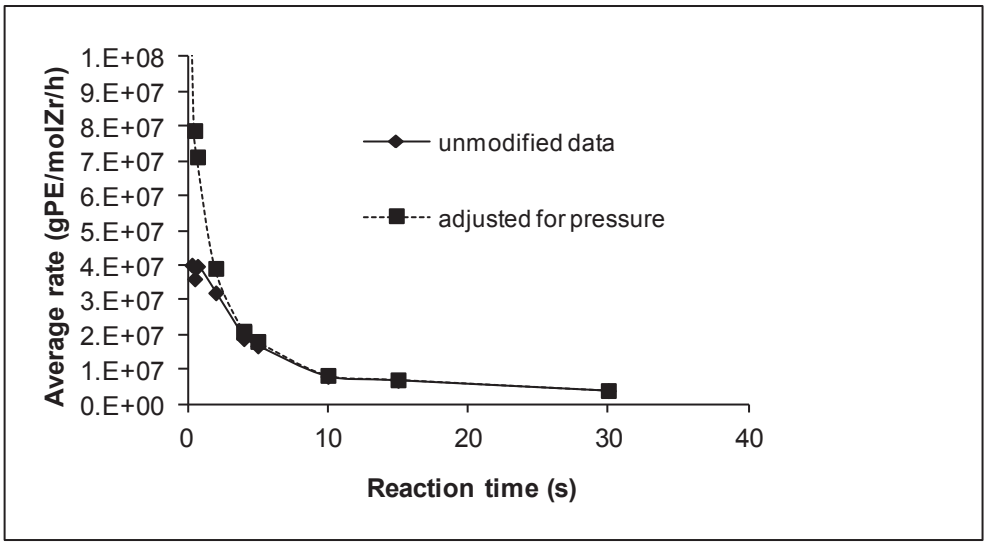

Figure 4-20: Comparison of activity profiles based on constant pressure assumption and adjusted for monomer concentration (ethylene partial pressure) for reaction gas flowrate 90mL.s^{-1}

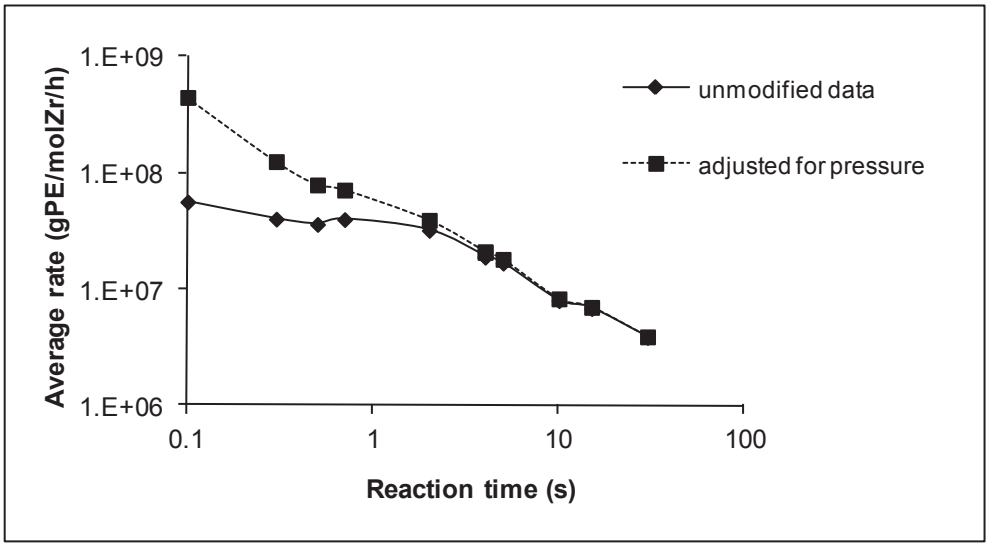

Figure 4-21: Comparison of activity profiles based on constant pressure assumption and adjusted for monomer concentration (ethylene partial pressure) for reaction gas flowrate 90mL.s^{-1}

The amended profile appears as a straight line on log axes and can be represented by the following relation with a R^2 coefficient of 0.989:

$$\ln(\bar{r}_m') = 17.874 - 0.7875\ln(t)$$

$$= \bar{r}_m' = 5.79.10^7 t^{-0.7875}$$

4-4

The effect of the pressurisation time on the instantaneous reaction rates can also be reviewed. The yield of each experiment can be adjusted for pressurisation of the reactor system in the same way as the average activity. Figure 4-22 shows the adjusted yields increasing with reaction duration and the line of best fit through the data:

$$Y = 0.2044ln(t) + 0.6957$$

4-5

So,

$$\frac{dY}{dt} = \frac{0.2044}{t}$$

4-6

Figure 4-23 shows the result of using this linear relationship and its differential to model the yield and the instantaneous reaction rate respectively. The instantaneous reaction rate based on the experimental data is calculated by the difference between reactions of different duration. Because these reaction times are so short and the measured quantities of polymer are so small it is extremely likely that there is some inaccuracy. Variation could also be caused by other physical phenomena which have not been taken into account. Also, because ln(0) does not exist, the yield does not quite go through the origin and calculates zero at about t=0.03s. Despite these factors, the relation gives quite a good match.

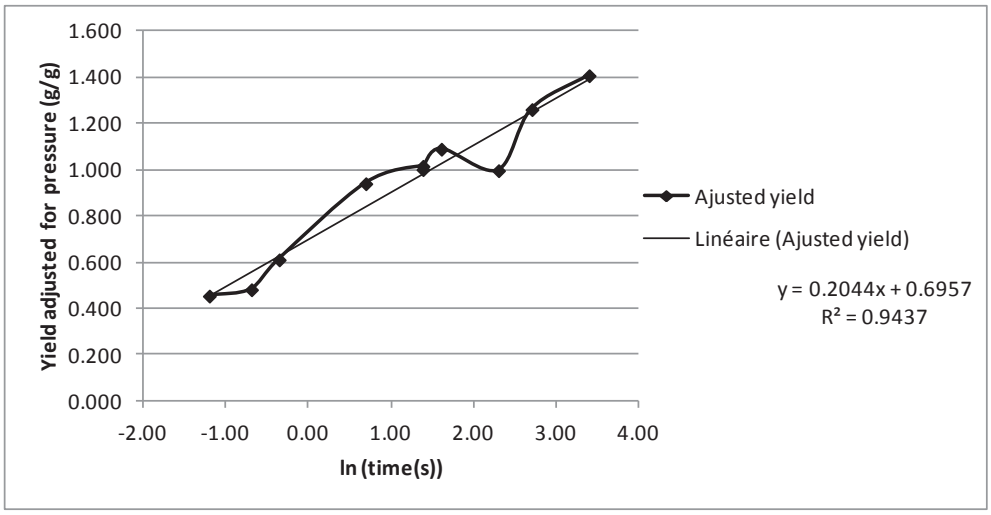

Figure 4-22: Polymerisation yields adjusted for monomer concentration (ethylene partial pressure) for reaction gas flowrate 90mL.s^{-1}

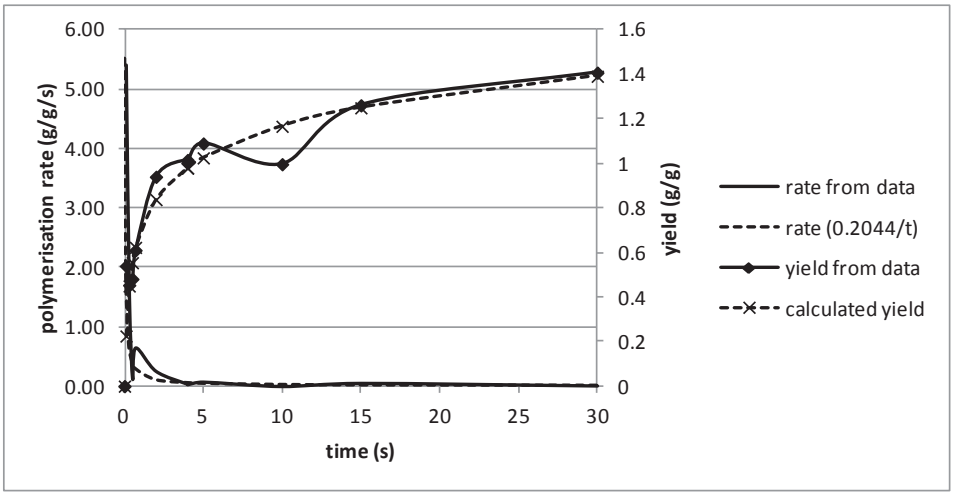

Figure 4-23: Comparison of polymerisation instantaneous reaction rate profile and yield with calculated values for reaction gas flowrate 90mL.s^{-1}

4.2.3.2 Higher Flowrate

Figure 4-24 shows that adjusting the average reaction rate profile for pressure for experiments carried out at the higher flowrate confirms the pattern of rapid decay in reaction rate from time zero.

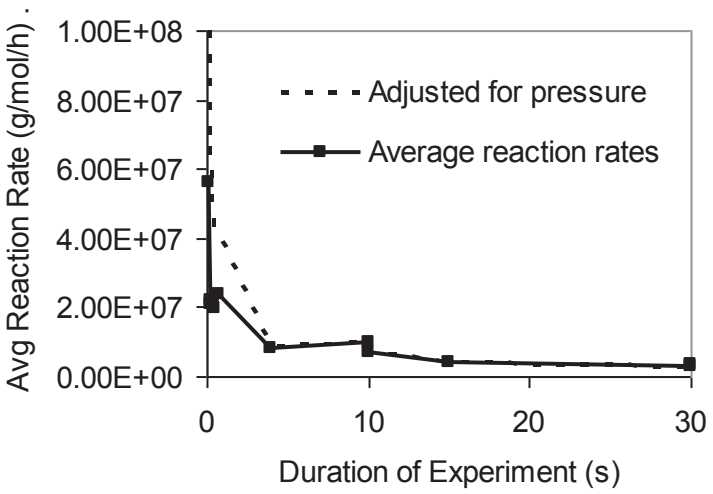

Figure 4-24: Comparison of activity profiles based on constant pressure assumption and adjusted for monomer concentration (ethylene partial pressure) for reaction gas flowrate approx. 300 mL.s^{-1}

There is more scatter in this data than at the lower flowrate and describing the yield only in terms of time is too simplistic. For example, no account is taken of reactor temperature, which depends on the mass of catalyst used. However, this relation could still be useful in conjunction with the activation energy and other physical data for modelling the reactor. The best fit for these experiments is found to be:

$$Y = 0.19\ln(t) + 0.428 \qquad 4\text{-}7$$

Figure 4-25 compares the reaction rate and yield calculated from this relation to the measured data.

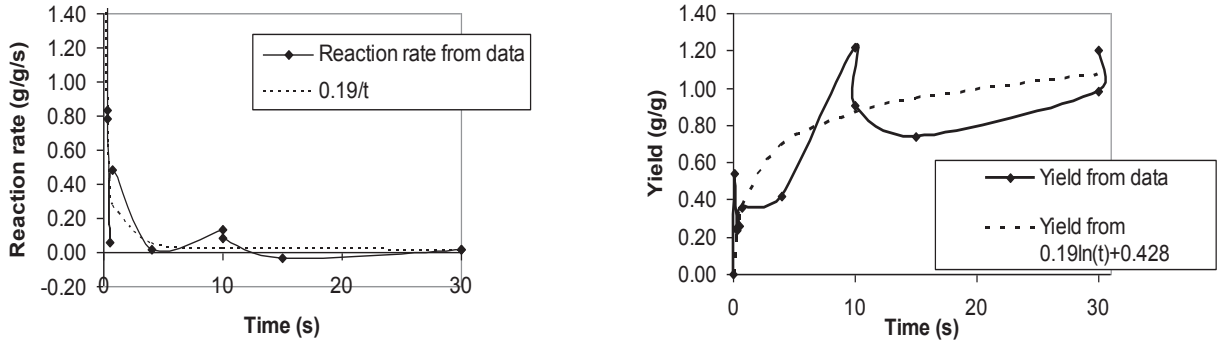

(a) (b)

Figure 4-25: Compare (a) polymerisation instantaneous reaction rate profile and (b) yield with calculated values for reaction gas flowrate approx. 300mL.s-1

4.2.3.3 New Reaction Kinetics

The relation for the decay of reaction rate with time can also be incorporated into the model. Equation 2-46

$$k_{p0} = a - b(M_R)^c$$

which was used previously and where the constants a, b & c were only valid for individual reactions, can be replaced by the equation

$$k_{p0}C^* = \frac{B}{t} \qquad \text{4-8}$$

and,

$$\frac{d\left(k_{p0}C^*\right)}{dt} = -\frac{B}{t^2} \qquad \text{4-9}$$

where B can be used for a series of experiments carried out under the same conditions. Figure 4-26 compares the results of modelling four experiments using the same value of B. They were all carried out at the optimised conditions with the higher flowrate and are of very different durations (0.3s, 4s, 15s and 30s). It can be seen that this relation is able to represent the series of experiments quite well and could be used to give an approximate prediction of the mass of polymer which would be formed in this reactor for experiments of different duration.

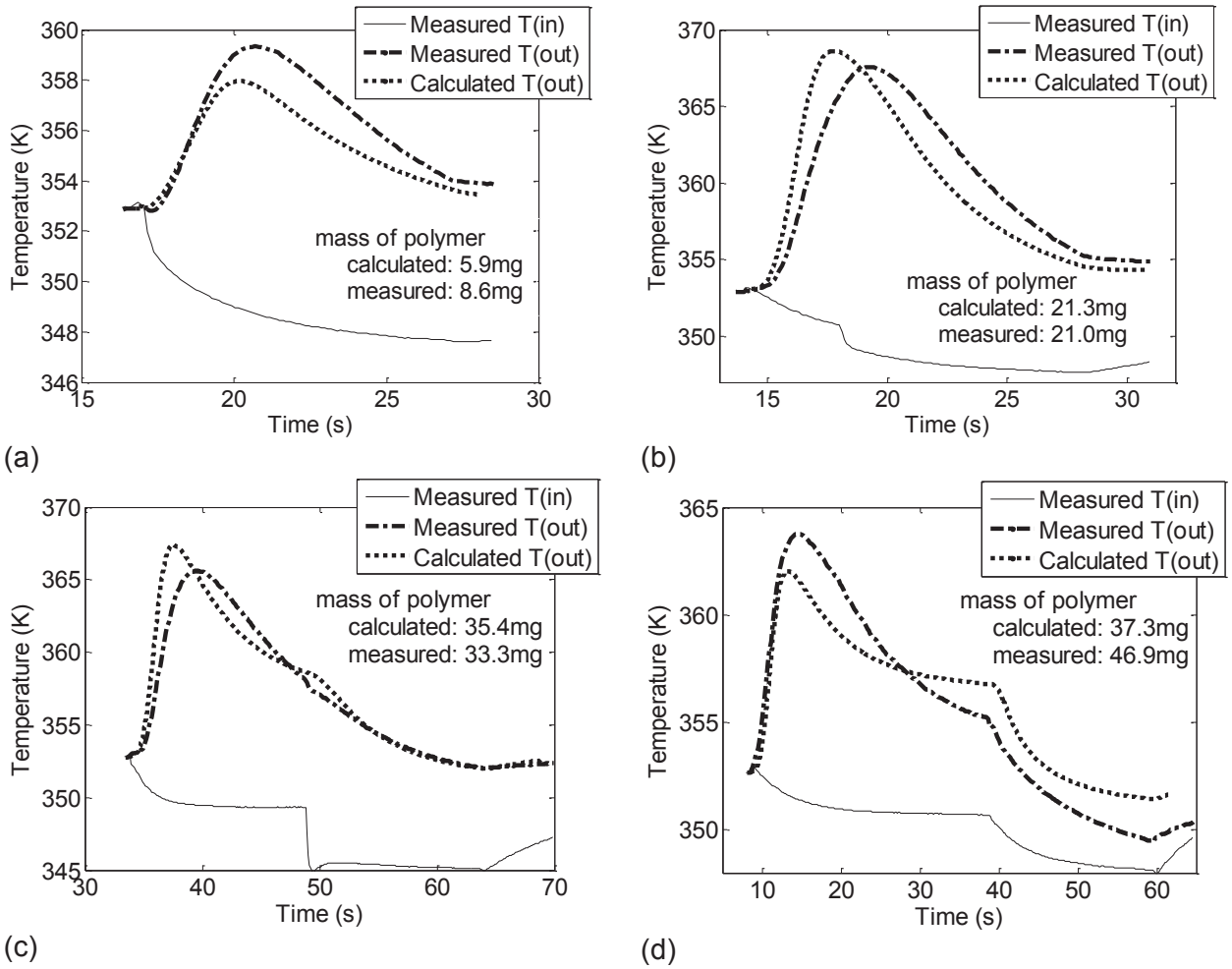

Figure 4-26: Comparison of calculated and measured outlet temperatures using the same model parameters for experiments of different duration (a) ET_PE_SFG_197, 0.3s (b) ET_PE_SFG_122, 4s (c) ET_PE_SFG_118, 15s (d) ET_PE_SFG_338, 30s

The reactor temperatures calculated using this model follow the same trends as in the previous version. Figure 4-27 shows the maximum catalyst temperatures calculated in the reactor for the same 4s experiment used in the previous simulations. The temperature peak appears at almost exactly the same time and position and is of about the same magnitude. Therefore, the new kinetic model does not invalidate the previous simulations.

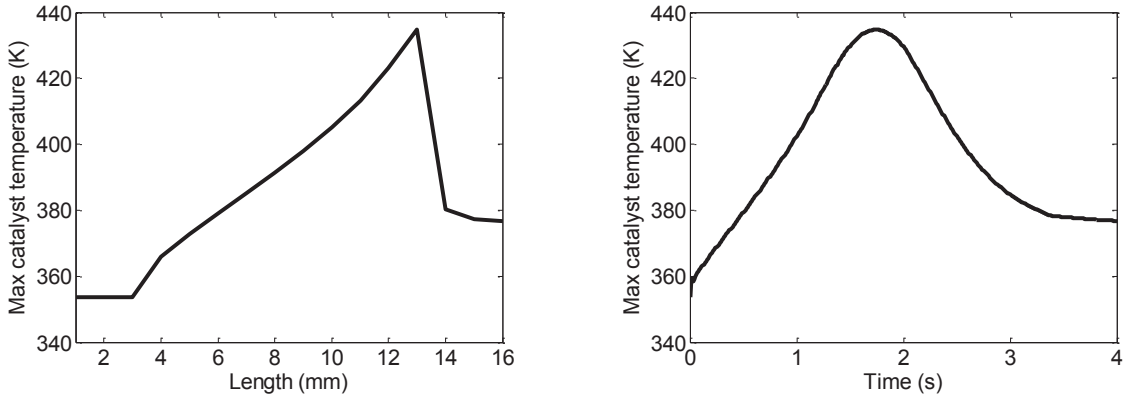

(a) (b)

Figure 4-27: Maximum calculated catalyst temperatures for typical 4s polymerisation experiment, ET_PE_SFG_200, under optimised conditions along the reactor centre-line against (a) position (b) time

However, the same method cannot be applied to the series of experiments carried out at the lower reaction gas flowrate of 90mL.s^{-1} because the model predicts overheating and runaway reaction. This can be demonstrated by running the model with the same value of B in equation 4-9 as used for the series of experiments carried out at optimised conditions. For experiments of 2s duration and less, Figure 4-28 shows the calculated outlet temperatures and masses of polymer are below measured values. This is as would be expected because experiments carried out with low reaction gas flowrate had higher yields. However, for longer duration experiments, the model calculates a hotspot with excessive temperatures and polymer accumulation. The temperatures calculated by the model would certainly deactivate the catalyst causing dead zones in the reactor bed. This can be seen in Figure 4-29 (a) and (b), which shows the maximum catalyst temperature values and position calculated by the model for an experiment of 4s duration, and (c), which shows the predicted axial polymer distribution for the same experiment.

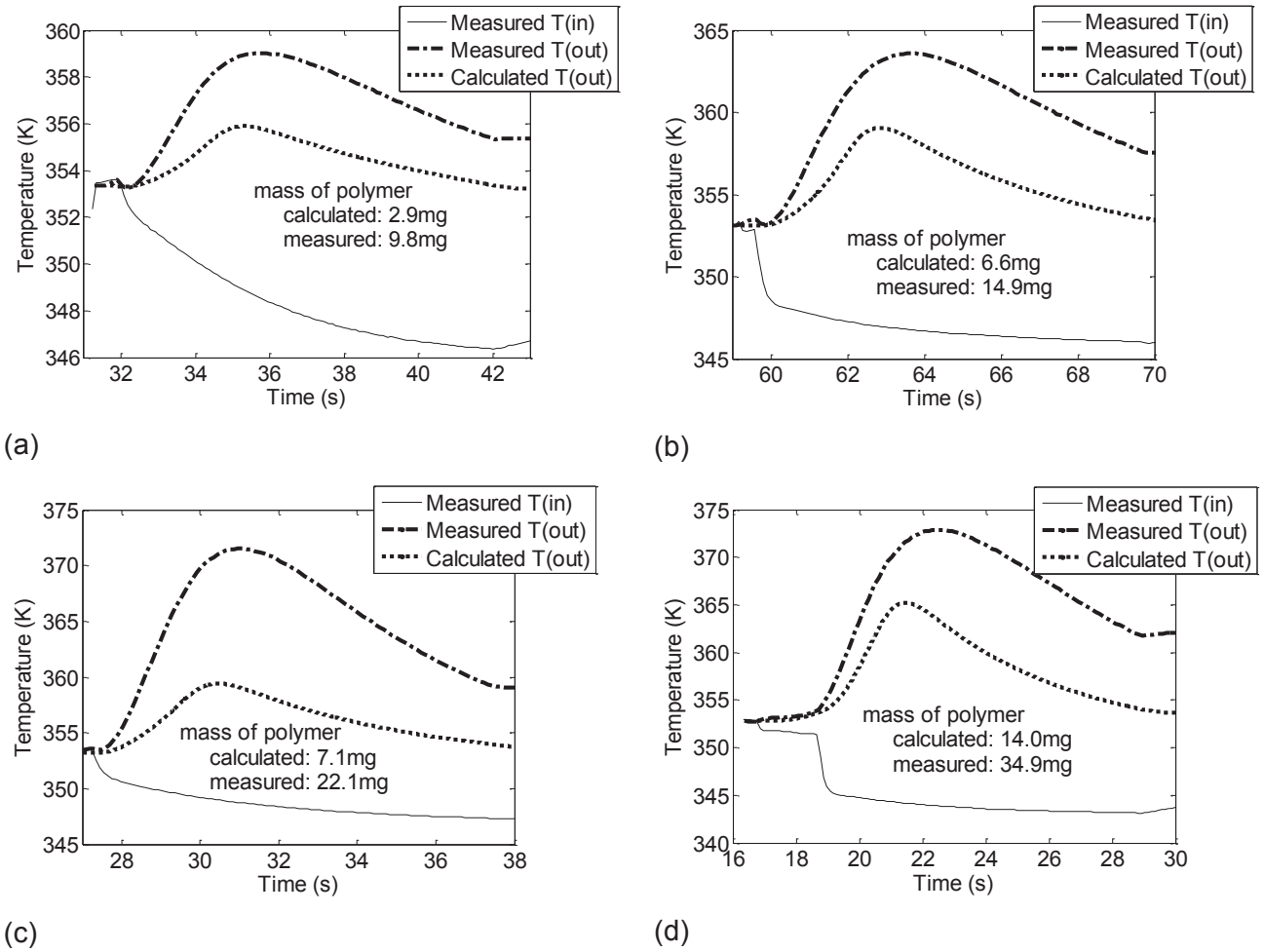

Figure 4-28: Comparison of calculated and measured outlet temperatures using the same model parameters for experiments of different duration (a) ET_PE_SFG_, 0.3s (b) ET_PE_SFG_, 0.5s (c) ET_PE_SFG_, 0.7s (d) ET_PE_SFG_, 2s

Figure 4-29 (d) shows that, for this experiment, the model calculates outlet temperatures in excess of the measured values. This suggests that, for this series of experiments, a local hotspot may develop in the reactor. Thermal deactivation of catalyst would occur at the hot spot and downstream, but activity would remain in cooler parts of the bed near the reactor inlet and walls. This could explain why the catalyst seems to deactivate more quickly in this series of experiments carried out at the lower flowrate.

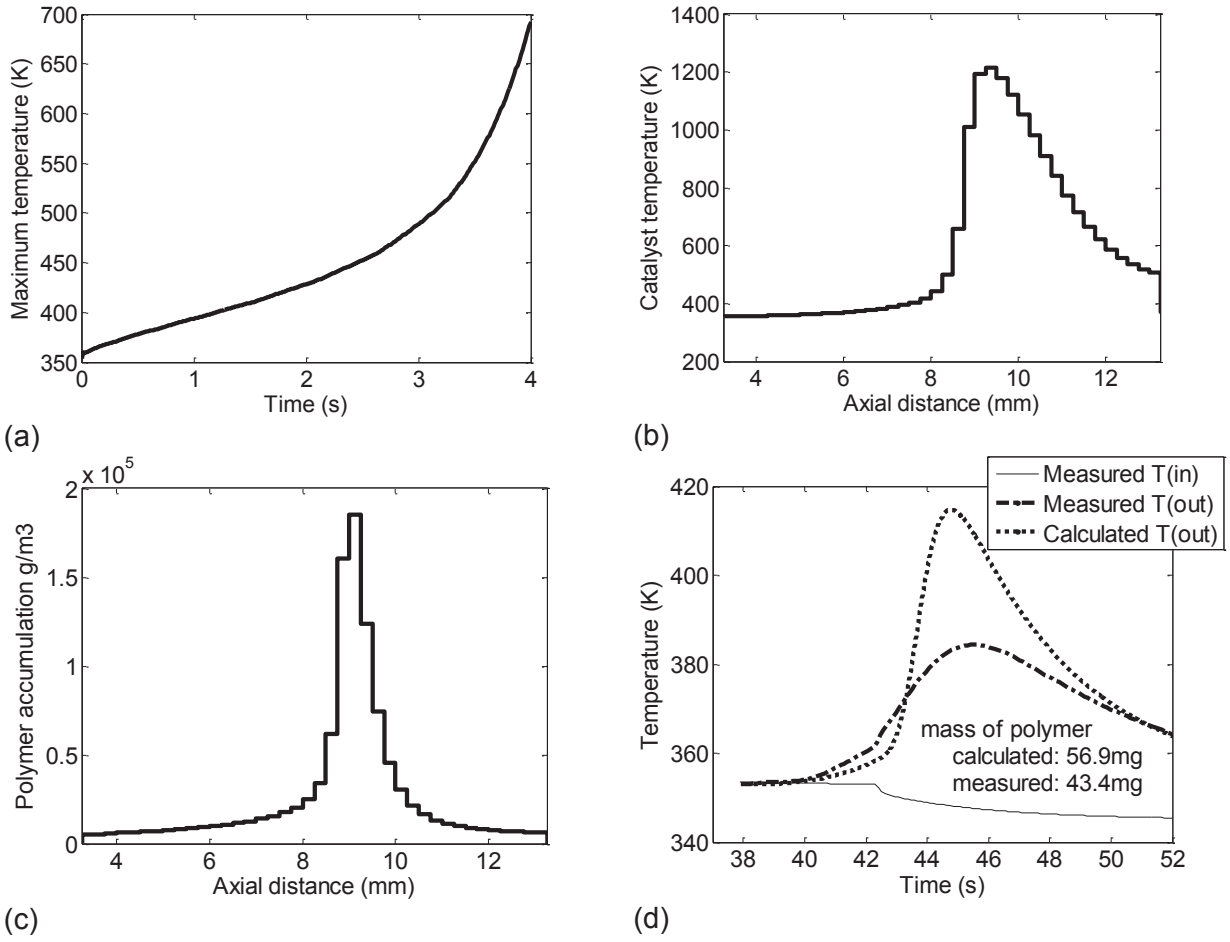

Figure 4-29: Model results for experiment ET_PE_SFG_122 of 4s duration at the lower flowrate of 90 mL.s^{-1} (a) maximum calculated catalyst temperatures (b) calculated catalyst temperatures after 4s along reactor centre line (c) calculated polymer accumulation along the reactor centre line (d) comparison of calculated and measured outlet temperatures

4.2.4 Conclusion

Measurement of the reactor pressurisation rate led to the finding that it could not be neglected. Including the effects of monomer pressure enabled the catalyst activity profiles to be amended and the model to be refined with a single general equation now representing the reaction rate for a series of polymerisation experiments. The reactor temperatures calculated using the revised version of the model are very similar to those found previously for experiments carried out under optimised conditions. For experiments carried out at the lower flowrate of 90 mL.s^{-1} of reaction gas, and of duration longer than 2s, the model predicts development of a hot spot.

4.3 Reaction Kinetic Model with Deactivation

The physical cause behind the initial rapid decrease in reaction rate is unknown. However, one likely possibility is that it is due to a deactivation reaction (possibly because no alkyl aluminium was added to the reactor feed [1]) and the model was amended to incorporate this idea. The pressurisation was included as described in section 4.2.2 and equation 2-46 was removed so that all the decay in the reaction rate would be modelled by the deactivation reaction.

During the initial pressurisation, the monomer concentration has not reached its steady state value and the risk of intraparticle concentration gradients must be re-evaluated. Values for instantaneous reactor pressure and reaction rates were determined in the previous section. From these, and the chart published by Floyd et al. [4] identifying regimes for macroparticle diffusion resistance in olefin polymerisation, it can be calculated that diffusion limitations do exist during the first moments of the reaction as shown in Table 4-2. This is also confirmed by calculation of the Weiss modulus (equation 2-16) which has values of 5.14, 0.27 and 0.03 at 0.1, 0.7 and 4s respectively. This suggests the diffusion limitation lasts only for a short period. If the rapid decay in reaction rate is due to chemical deactivation and the changes in the physical structure of the catalyst support are assumed not to affect diffusion rates, the intrinsic reaction rate would then become controlling. The effects of diffusion limitation are neglected in this version of the model and could be included later if necessary.

Time (s)	0.1	0.3	0.5	0.7	4
Rate ($g.g^{-1}.s^{-1}$)	1.91	0.64	0.38	0.27	0.05
C_{ex} ($mol.L^{-1}$)	0.05	0.08	0.11	0.12	0.19
Weiss modulus	5.14	0.42	0.32	0.27	0.03
	DIFFUSION LIMITED →				OK

Table 4-2: Reaction rate and concentration values used to check for intraparticle concentration gradients

4.3.1 Material Balances

In this version of the model the reaction kinetics are represented by lumped propagation and deactivation reactions:

Propagation: $N(r) + C_2H_4 \rightarrow N(r+1)$

Deactivation: $N(r) \rightarrow N_d + Q(r)$

Where $N(r)$ is a live polymer chain of length r and N_d is a deactivated site and $Q(r)$ is a dead polymer chain of length r. Site formation and initiation are neglected as they are very rapid as discussed in Chapter 1 section 1.3.1.2.1.

The reaction rates are written as:

Propagation: $$r_p = k_{p0} e^{-\frac{Ea_p}{RT}} C_{C2} Y(0)$$ **4-10**

Deactivation: $$r_{ds} = k_{ds0} e^{-\frac{Ea_{ds}}{RT}} Y(0)$$ **4-11**

Where $Y(0)$ is the concentration of live polymer chains.

The material balance for gas phase ethylene and the reactor heat balances remain as equations 2-24, 2-36 and 2-40. The only slight difference being one of terminology, the overall polymerisation rate is now the propagation rate. The heat balance for the cooling period remains unchanged. The method of moments is used to calculate the total mass of polymer formed. The molar balances are as follows:

Concentration of live chains:

$$\frac{dY(0)}{dt} = -k_{ds0} e^{-\frac{Ea_{ds}}{RT_c}} Y(0)$$ **4-12**

The initial value of $Y(0)$ is estimated as 25% of the concentration of zirconium catalyst in the reactor bed (mol m^{-3}).

Concentration of dead chains:

$$\frac{dX(0)}{dt} = k_{ds0} e^{-\frac{Ea_{ds}}{RT_c}} Y(0)$$ **4-13**

The number of dead chains, $X(0)$, is growing at exactly the same rate that the number of live chains is decreasing.

Weight of live chains:

$$\frac{dY(1)}{dt} = k_{p0} e^{-\frac{Ea_p}{RT_c}} C_{C2} Y(0) - k_{ds0} e^{-\frac{Ea_{ds}}{RT_c}} Y(1)$$ **4-14**

The mass of live polymer chains is represented by the first moment of live chains, *Y(1)*, which is equivalent to a mole balance on the monomer units incorporated.

Weight of dead chains:

$$\frac{dX(1)}{dt} = k_{ds0} e^{-\frac{Ea_{ds}}{RT_c}} Y(1)$$

4-15

As for the live chains, the mass of dead polymer chains is represented by the first moment of dead chains, *X(1)*.

The total mass of polymer formed will therefore be the sum of the final values of *X(1)* and *Y(1)* and, including the reactor pressurisation, this model requires eight differential equations for each finite element.

4.3.2 Modelling Results

The model described in the previous section was programmed in MATLAB and the function lsqnonlin was used to estimate the values of the pre-exponential constants and activation energies for propagation and deactivation: k_{p0}, k_{ds0}, Ea_p and Ea_{ds}. Initial guesses are required for the reaction constants and activation energies and as discussed in the literature review, the activation energy for deactivation of metallocenes is known to be higher than the activation energy for propagation. Therefore, an initial estimate of 44 kJ.mol^{-1} was made. In the model the term $e^{-\frac{Ea}{R}\left(\frac{1}{T_c}-\frac{1}{353}\right)}$ is used in place of $e^{-\frac{Ea}{RT_c}}$ to reduce the correlation between reaction parameters.

4.3.2.1 Higher Flowrate

Figure 4-30 shows that this model can fit the measured outlet temperatures well for experiments of different durations carried out under the optimised conditions. Figure 4-30(d) shows that the calculated temperatures in the reactor follow the same pattern with this model as for the previous versions and Figure 4-31 shows the concentration of live chains in the reactor bed decreasing with time and also towards the hot spot at the reactor outlet. This is as expected since the higher the temperature, the faster the deactivation occurs.

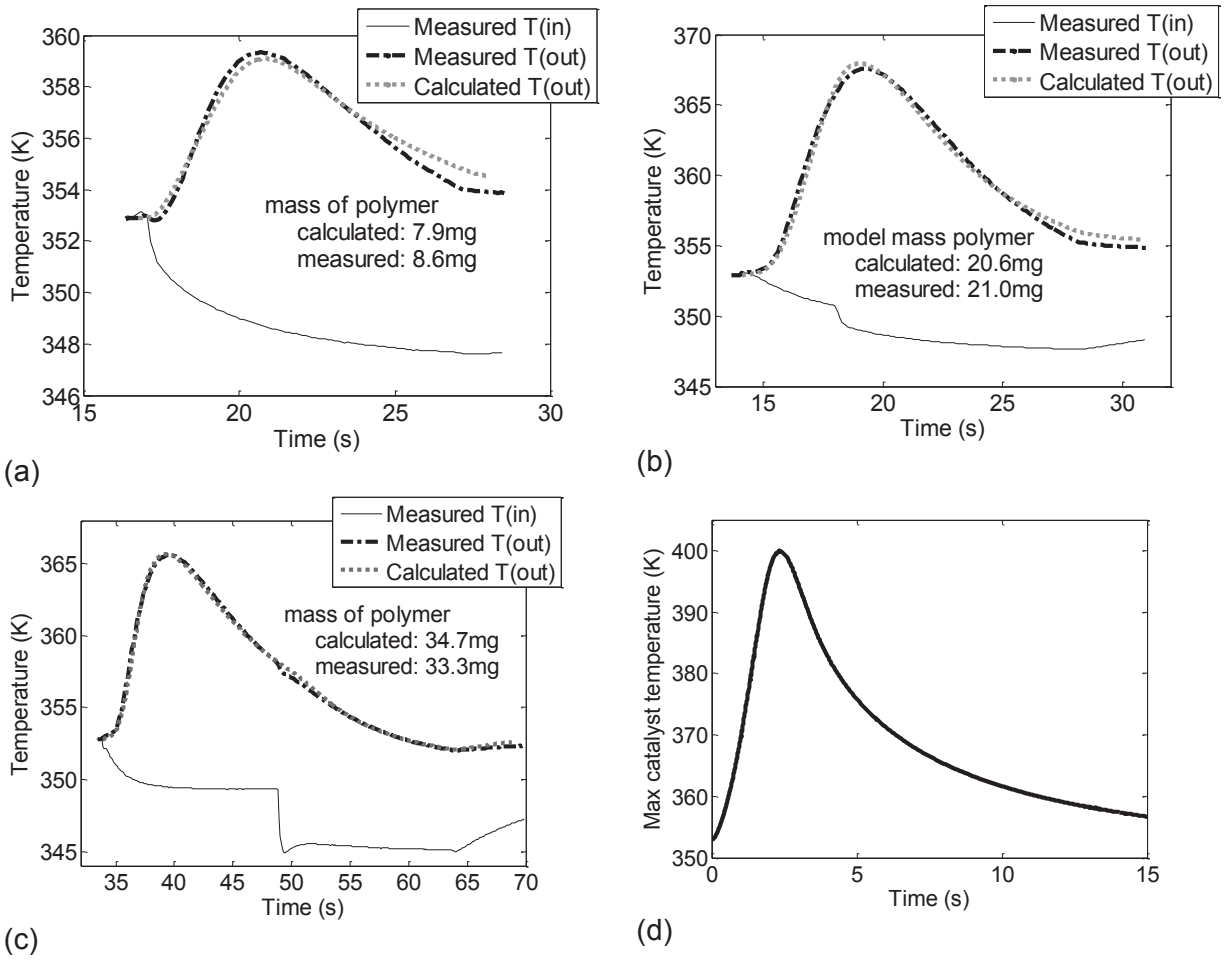

Figure 4-30: Comparison of calculated and measured outlet temperatures for experiments at optimised conditions (a) ET_PE_SFG_197, 0.3s (b) ET_PE_SFG_200, 4s (c) ET_PE_SFG_124, 15s (d), Maximum calculated catalyst temperatures for ET_PE_SFG_124

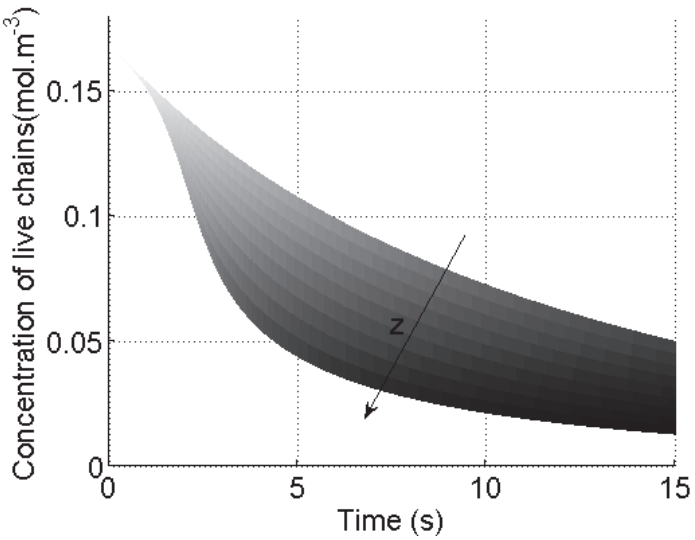

Figure 4-31: Concentration of live chains along reactor centre line for experiment ET_PE_SFG_124, 15s duration, optimised conditions

However, the reaction rate constants found by parameter estimation with this model differ as shown in Table 4-3. So, this model does not seem to give a good representation of the chemical and physical processes occurring in the reactor.

Experiment	Duration (s)	$k_{p\ 353K}$ (s^{-1})	Ea_p ($kJ.mol^{-1}$)	k_{ds} (s^{-1})	$Ea_{ds\ 353K}$ ($kJ.mol^{-1}$)
Optimised Conditions					
ET_PE_SFG_197	0.3	5499	39.88	2.180	44.34
ET_PE_SFG_200	4	478	39.44	0.012	43.85
ET_PE_SFG_124	15	538	39.91	0.080	43.74
Lower Flowrate					
ET_PE_SFG_118	15	236	39.99	0.003	44.00

Table 4-3: Reaction constants and activation energies for propagation and deactivation found by parameter estimation

4.3.2.2 Lower Flowrate

Modelling of experiments carried out at the lower flowrate confirms this. Figure 4-32 (a) compares the calculated outlet temperatures to measured values for experiment ET_PE_SFG_118 (15s duration, 90 $mL.s^{-1}$) after using parameter estimation to find the best fit for the data and Figure 4-32 (b) is a plot of the maximum calculated catalyst temperature against time. The mismatch in the curves shown in Figure 4-32 (a) is not due to different pressurisation dynamics for the different flowrates which is already accounted for in the model. The parameter estimation does not find a good fit between the calculated and measured outlet temperatures because to try and match the calculated temperatures to the measured data it delays the maximum bed temperature. Figure 4-33 shows the decrease in active site concentration at the hot spot. The parameters that give the best fit for this experiment are shown in Table 4-3.

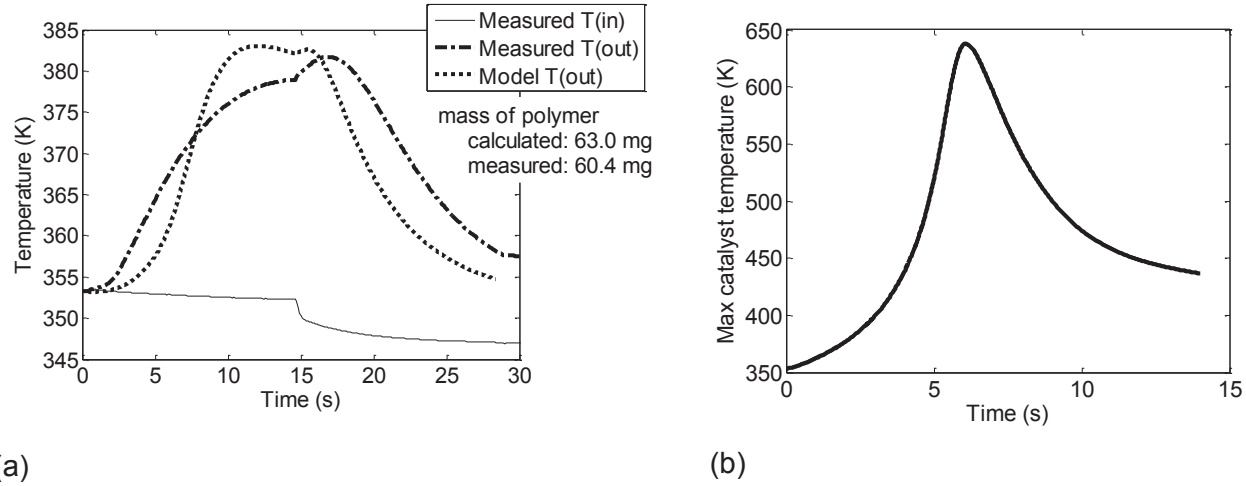

Figure 4-32: Modelling results for experiment ET_PE_SFG_118, 15s duration, 90 $mL.s^{-1}$ (a) Compare calculated and measured outlet temperatures (b) Maximum calculated catalyst temperatures

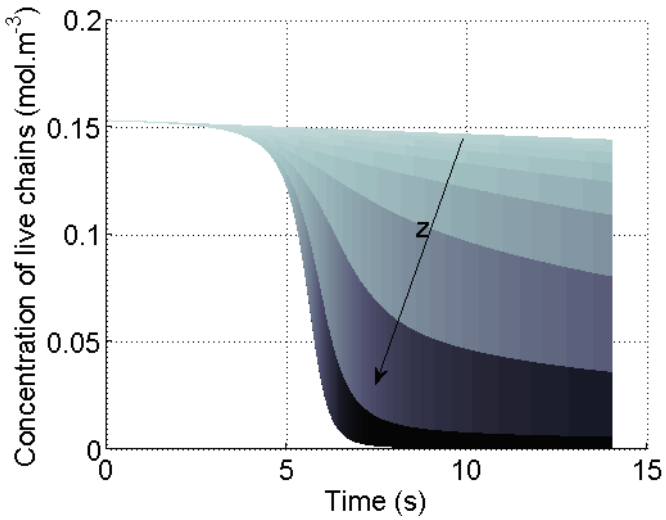

Figure 4-33: Concentration of live chains along reactor centre line for experiment ET_PE_SFG_118, 15s duration, 90 mL.s^{-1}

4.3.3 Conclusion

In conclusion, this form of kinetic model does not provide a good fit for the measured data. This is logical because, although metallocenes are known to be temperature sensitive with deactivation rates increasing with temperature for solution polymerisation, in this fixed bed reactor, the polymerisation rate is observed to decrease sharply when the reactor is at its coolest. A possible cause of this is poisoning of the active sites and there is some evidence for this in the work of Tioni [1] who found that introducing scavenger into the reactor increased the polymer yield. Thermal deactivation almost certainly exists as well since the most stable polymerisation rates are found under the optimised reaction conditions where excessive temperature excursions are avoided.

To represent the polymerisation kinetics more phenomena would therefore have to be taken into account in the reactor model. A lumped propagation reaction with poisoning and spontaneous deactivation is one example of alternative reaction kinetics that could be tested. There is also the effect of adsorption to be considered and diffusion limitations at the start of the polymerisation due to the very high reaction rate. As the polymerisation progresses other factors such as the physical properties of the polymer formed may also influence the polymerisation rate as the ethylene has to diffuse through this to reach the active sites. The ultimate goal would be to integrate a single particle model into the validated reactor model.

4.4 General Conclusions

A reactor fitted with an internal thermocouple to measure polymerisation temperatures directly was tested. However, the results were variable, the catalyst activity in this reactor was below the expected level and channelling was suspected so experiments in this reactor were not pursued.

The pressurisation rate of the system was measured and found not to be negligible on the timescale of the experiments. It can be modelled as the response of a first order system to a step change with the reactor exit flowrate proportional to the pressure. This was incorporated into the model and showed that, in the early stages of the polymerisation, the reaction rate may be limited by the amount of ethylene which can enter the reactor. The effect of potential modifications to eliminate the pressurisation period, allowing the reactor to operate at constant pressure from the start of the experiment, was modelled to check whether this would cause overheating. The model predicts that the increased reaction gas flowrate associated with the higher reactor pressure would provide additional cooling, compensating for the increased heat generation rate.

The new information about the reactor pressure allows the reaction kinetics to be adjusted and the initial polymerisation reaction is shown to be extremely rapid. This brings the results from this reactor into agreement with the slurry phase work of Di Martino et al. [3]. It also allowed a new, more general relation for the reaction rate to be incorporated into the model so that series of experiments can be modelled using the same set of input parameters. The revised model predicts development of a hot spot in the reactor bed for experiments carried out at the lower flowrate of 90 $ml.s^{-1}$.

The in reaction rate has also been modelled as lumped propagation and chemical deactivation reactions. It is shown that the usual parameters for deactivation of metallocene catalyst, with the activation energy for deactivation greater than for propagation, do not fit the initial rapid reduction in polymerisation rate observed in this reactor, so this can be excluded as the cause of the initial sharp decay in polymerisation rate.

4.5 Nomenclature

A	Size of pressure step change	$N.m^{-2}$
B	Constant	-
C_{C2}	Ethylene concentration	$mol.m^{-3}$
C^*	Active site concentration	$mol.m^{-3}$
Ea_{ds}	Activation energy for spontaneous deactivation	$J.mol^{-1}$
Ea_p	Activation energy for propagation	$J.mol^{-1}$
k_{p0}	Pre-exponential reaction constant for propagation	$mol^{-1}.s^{-1}.m^3$
k_{ds0}	Pre-exponential reaction constant for spontaneous deactivation	s^{-1}
K_p	Gain	-
M_R	Mass of PE per uint volume of reactor	$g.m^{-3}$
P	Total pressure	$N.m^{-2}$
P_m	Measured pressure	bar gauge
Q_m	Measured flowrate	$mL.s^{-1}$
R	Ideal Gas Constant	$J.mol^{-1}.K^{-1}$
$\bar{r}_m$	Average observed reaction rate	$g_{PE}.h^{-1}.mol_{Zr}^{-1}$
r_p	Propagation rate	$mol.s^{-1}.m^{-3}$
r_{ds}	Spontaneous deactivation rate	$mol.s^{-1}.m^{-3}$
T	Temperature	K
T_c	Temperature of catalyst/polymer	K
t	Time	s
Y	Yield	$g_{PE}.g_{cat}^{-1}$
$X(0)$	Concentration of dead chains (0th moment)	$mol.m^{-3}$
$X(1)$	First moment of dead chains	$mol.m^{-3}$
$Y(0)$	Concentration of live chains (0th moment)	$mol.m^{-3}$
$Y(1)$	First moment of live chains	$mol.m^{-3}$
τ	Time constant	s

[1] Tioni E., Optimization of a Tool to Study the Start-up of the Gas Phase Olefin Polymerization, Phd thesis, UCBL1

[2] Silva F., Lima E.L., Pinto J.C. & McKenna T.F.L., Investigation of Catalyst Fragmentation in Gas-Phase Olefin Polymerisation: A Novel Short Stop Reactor, Macromol. Rapid Commun. 26 (2005) 1846-1853

[3] Di Martino A., Weickert G. & McKenna T.F.L., Contributions to the Experimental Investigation of the Nascent Polymerisation of Ethylene on Supported Catalysts 1: A Quenched Flow Appartaus for the Study of Particle Morphology and Nascent Polymer Properties, Macromol. React. Eng. 1 (2007) 165-184

[4] Floyd S., Choi K.Y., Taylor T.W. & Ray W.H., Polymerization of Olefins Through Heterogeneous Catalysis III. Polymer Particle Modelling with an Analysis of Intraparticle Heat and Mass Transfer Effects, J. App. Polym. Sci. 32 (1986) 2935-2960

5 Conclusions and Perspectives

The fixed bed reactor and experimental set-up for ethylene polymerisation were reviewed and analysed prior to construction of a reactor model. A main conclusion of this initial study was that measured thermal effects unrelated to the polymerisation exist. Heat released due to the sudden pressurisation of the system at the start of the reaction is observed as a small temperature peak but is slight enough to be neglected. When a raw silica seedbed is used, ethylene adsorption causes a significant temperature increase in the reactor bed. Under the optimised reactor conditions, with the reaction gas flowrate set at its maximum, the reactor and set-up are close to capacity with quite high pressure drops calculated across the reactor bed supports and the heating coils in the hot water bath.

A bi-dimensional, heterogeneous, dynamic, finite element, reactor model has been constructed in MATLAB. The model uses simplified reaction kinetics and assumes constant pressure in the reactor bed. It is able to account for the heat of adsorption where a silica seedbed is used and includes both the reaction and cooling periods of each experiment. Standard correlations for heat transfer in fixed bed reactors were used and the mass and heat balances were integrated using the differential equation solver, ode45, in MATLAB.

This model was validated and provides a good fit with the measured data for individual, short duration experiments. The measured outlet temperature is not very responsive to temperature fluctuations in the reactor due to the high heat capacity of the stainless steel frit bed support. Under optimised experimental conditions, this masks a brief, local excursion above the polymer melting point. Use of the reactor as a calorimeter was evaluated and a state observer for the polymerisation rate in the reactor bed was developed. Because the measured reactor outlet temperature is not very sensitive to the bed temperature, the observer uses bed exit temperature values calculated by the model. The observer is robust and returns logical results. It is very sensitive to the input data and has the potential to deliver interesting and useful information about the polymerisation kinetics if the sensitivity of the reactor could be improved so that true measured data could be used.

Simulations were carried out using the model which showed that very high temperatures can occur in the reactor bed at the lower flowrate. A reactor was fitted with a thermocouple for direct measurement of the reactor bed temperature. However, the results from this reactor were variable. Channelling was suspected and this work was not pursued.

Potential reactor improvements were considered and modelled. The effects of reactor geometry, exit frit material and reaction gas flowrate and composition on reactor bed temperatures were all calculated. It was found that, on the time scale of the temperature excursion, the reactor is adiabatic and thermal gradients can be reduced by changes to the reaction gas flowrate and composition but not by changes to the reactor geometry. The sensitivity of the measured outlet temperature to thermal effects in the bed could be improved by replacing the outlet frit with stainless steel mesh and preliminary tests were carried with a reactor cartridge modified in this way.

The pressurisation rate of the reactor system was found to be significant with respect to the duration of the polymerisation experiments and the reaction rate data was adjusted. A new relation for the decrease in reaction rate with time was determined and incorporated into the reaction model, thereby making it general for series of experiments carried out under the same conditions. Finally, the reactor was modelled with the reaction kinetics represented by lumped propagation and deactivation reactions. It was found that the usual parameters for metallocene catalyst, with activation energy for deactivation greater than for propagation, cannot fit the measured data from the fixed bed reactor, which suggests another mechanism for the early rapid decay in the polymerisation rate.

In terms of perspectives for the future, the first objective of this project, to construct a valid reactor model, has been met. However, there remains much potential work to be done with regard to both modelling and modifications to the reactor and experimental set-up. The first useful piece of work which could be done would be to review other simulations which might be of use in specifying a new reactor. One example could be modelling alternative materials for the inert solid which might improve thermal conditions in the fixed bed. Also, the catalyst used to date in this reactor has very low activity so increased catalyst activity could be simulated to allow an experimental set-up and reactor to be specified for use with other catalyst. The experimental method could also be reviewed, particularly with regard to bed dilution and how the mixing is carried out.

The work to test the new reactor cartridge to increase the sensitivity of the existing reactor could be continued. This could be part of a complete redesign and specification of the reactor and experimental set-up which would allow for increased reaction gas flowrates in the system and take into account other points raised in this thesis. For example, the mass of the reactor cartridge could be reduced and its volume could be increased so long as the reaction gas flowrates were also increased accordingly.

The modelling could also be taken further. It would be interesting to continue the state estimation work to develop a 2D observer which might bring a finer knowledge of the polymerisation kinetics. The version of the model which gives the best fit so far with the measured data uses time dependent kinetics. Whilst this is able to provide a reasonable match between measured and calculated outlet temperatures and can be used to predict the mass of polymer formed in an experiment, it does not relate to any specific physical property. The fundamental aim of research in this area is to gain understanding of the physical and chemical changes occurring during the first instants of the polymerisation. Another avenue which could be pursued is therefore, to replace the time dependent kinetics with something more meaningful. A first step is the work described in Chapter 4, section 4.3, where lumped propagation and deactivation reactions are used. Alternative reaction kinetics could be tested in the model with parameter estimation to identify whether they could be used to give a good representation of the polymerisation.

Finally, if the reactor and experimental set-up were modified to provide more precise bed temperature data, useful information about the early stages of the polymerisation might be provided by incorporating a particle scale model into the current reactor model.

Appendix 1 – List of Experiments

Experiments initially presented for modelling						
Experiment number	duration	mass of catalyst (mg)	mass of inert (g)	reaction gas flowrate ($mL.s^{-1}$)	CO_2 pressure at bottle (bar gauge)	Yield ($g.g^{-1}$)
Silica seedbed						
ET_PE_SFG_184	0.1	119.2	0.446	250	6	0.038
ET_PE_SFG_182	0.3	114.4	0.553	90	6	0.06
ET_PE_SFG_183	0.5	104.4	0.522	90	6	0.16
ET_PE_SFG_185	0.7	98.2		90	6	0.164
ET_PE_SFG_187	4	45.4	0.549	90	6	0.68
ET_PE_SFG_188	10	46.8	0.514	90	6	0.85
Fine NaCl seedbed						
ET_PE_SFG_116	0.1	109.6	0.705	310	6	0.0684
ET_PE_SFG_129	0.3	67.5	0.895	90	6	0.145
ET_PE_SFG_130	0.5	67.9	0.83	90	6	0.22
ET_PE_SFG_120	0.7	64.9	0.87	90	6	0.34
ET_PE_SFG_121	2	45.3	0.88	90	6	0.77
ET_PE_SFG_122	4	47	0.915	90	6	0.924
ET_PE_SFG_123	10	46.4	0.882	90	6	0.96
ET_PE_SFG_118	15	49.1	0.7	90	6	1.23
ET_PE_SFG_117	30	48.1	0.826	90	6	1.39
ET_PE_SFG_197	0.3	114.3	0.808	310	6	0.075
ET_PE_SFG_126	0.3	51.9	0.808	270	6	0.08
ET_PE_SFG_125	0.5	52.1		310	6	0.12
ET_PE_SFG_198	0.7	102.2	0.793	310	6	0.2
ET_PE_SFG_200	4	55.2	0.764	310	6	0.38
ET_PE_SFG_124	15	46.2	0.778	310	6	0.72
Silica						
EXP_1	150	0		90	6	
EXP_2	75	0		90	6	

EXP_2a	75	0		90	6	
EXP_3	75	0		90	6	
EXP_4	75	0		90	6	
EXP_5	2	0		90	6	
EXP_6	2	0		90	6	
EXP_7	1	0		90	6	
EXP_9	75	0		90	6	
EXP_9a	75	0		90	6	
EXP_10	75	0		90	6	
EXP_11	75	0		90	6	
EXP_34	30	0		340	9	
EXP_35	30	0		340	9	
testNaClonly3TC	30	0		270	6 & 9	
ET_PE_SFG_321	30	42.8	0.86	300	9	0.54
ET_PE_SFG_326	30	43.1	0.902	290	9	0.97
ET_PE_SFG_327	30	46.9	1.002	250	9	1.12
ET_PE_SFG_331	30	41.9	0.96	250	9	1.21
ET_PE_SFG_328	30	24.5	0.946	270	9	1.14
ET_PE_SFG_329	30	11	0.846	260	9	0.71
ET_PE_SFG_330	30	4.2	0.836	310	9	0
ET_PE_SFG_338	30	39.4	0.831	250	9	1.19
ET_PE_SFG_383	30	39.4	0.976	230	9	1.76
ET_PE_SFG_386	30	30.4	0.984	320	9	0.92
ET_PE_SFG_388	30	27.8	0.906	340	9	0.51
ET_PE_SFG_397	30	29.7	1.017	340	9	0.31
ET_PE_SFG_462	75	26.1	0.859	340	9	1.18
ET_PE_SFG_466	75	24.5	0.854	340	9	0.65

Appendix 1 –List of Experiments

BAB Experiments							
EXP_36	75	23.4	1.181	344	9	0.752	Pb <45μm NaCl;reactor w/o int.T.C.
EXP_37	75	25.9	1.109	331	9	0.45	Pb <45μm NaCl;reactor w/o int.T.C.
EXP_R1			1.266				Stem effects negligible
EXP_R2-EXP_R7							Need to use 45μm-63μm NaCl
EXP_R8			1.136				Pressurisation rate measurements
EXP_R9			1.078				Check that reactor sealed at TC
EXP_R10			1.029				Bed compression measurement
EXP_R11-13			0.912				Si/NaCl remain evenly distributed
EXP_38	manual	112.2	1.253	-	9	-	Pressurisation effects Si/NaCl bed Inlet TC broken, 353K
EXP_R14			1.133				CO2 flowrate measurement
EXP_39	manual	-	1.185	-	9	-	Pressurisation NaCl bed 293K
EXP_40	manual	-	1.220	-	9	-	Pressurisn NaCl bed 353K (repeat)
EXP_41	manual	-	1.245	-	-	-	Pressurisation NaCl bed/He 353K
EXP_42	manual	-	1.245	-	-	-	Pressurisation NaCl bed 353K
EXP_43	10	38.2	0.584	310	9	0.05	Pb no activity
EXP_44	10	49.4	0.584	296	9	1.176	Test cata in ET reactor, cata OK
EXP_45	10	45.1	0.584	288	9	0.521	
EXP_46	6	44.5	0.529	288	9	0.4?	Pb cuve not weighed; CO2 shut
EXP_47	manual	104.2	0.529	-	9	-	Pressurisation Si/NaCl bed 293K
EXP_48	manual	104.2	1.164	-	9	-	Pressurisation Si/NaCl bed 353K
EXP_49	manual		1.215	-	9	-	Pressurisation Si bed 293K
EXP_50	manual		1.186	-	9	-	Pressurisation Si bed 353K
EXP_51	manual		1.216	-	9	-	Check EXP_49
EXP_52	manual		1.297	-	9	-	Pressurisn Si bed 293K, new P.reg

EXP_53	manual		1.246	-	9	-	Pressurisn Si bed 353K, new P.reg
EXP_54	4	44.6	1.332	353	9	0.27	
EXP_55	2	32.4	1.332	331	9	0.04	
EXP_56	0.7	41.6	1.213	<331	9	-	
EXP_57	0.5	46.8	1.056	<245	9	-	+check max flows @<1s
EXP_58	0.3	58.2	1.278	<245	9	-	
EXP_59	0.1	55.5	1.362	<160	9	-	
EXP_60	0.1-6	-	1.261		9	-	Auto exps no cata (blancs)
EXP_61	manual	-	1.181		9	-	Pressurisation NaCl bed 353K
EXP_62	6	51.5	1.109	331	9		
EXP_63	manual	-	1.266				Not in glove box (inversed reactor)
EXP_64	10	43.3		181	9	0.767	Low flow, blockage at manual flow regulator
EXP_65	10	45.5	1.136	160	9	0.58	Low flow, ditto
EXP_66	10	41.9	1.261	344	9	0.57	
EXP_67	10	38.8	1.260	344	9	0.87	repeat exp44 (ET reactor)

Appendix 2 - Physical Data and Reactor System Measurements

		Helium	Ethylene	CO_2	Argon
Molecular weight	$g.mol^{-1}$	4	28	44	
Critical temperature	K	5.2	283.05	304.21	
Critical pressure	atm	2.26	50.5	7.383E6	
Critical volume	$m^3.kmol^{-1}$	0.058	0.132	0.095	
Crit. compressibility factor	(-)	0.305	0.283	0.277	
Acentric factor	(-)	-0.388	0.086	0.224	
Specific heat capacity	$J.kmol^{-1}.K^{-1}$	0.2079E5			
Joule Thomson coeff, 353K	$K.atm^{-1}$	-0.0636	0.74	0.75	0.27

Table A1.1 Physical Constants of Gases [7]

Catalyst support :amorphous silica Grace 948			
Pore volume	1.7	$ml.g^{-1}$	1
Specific surface	290	$m^2.g^{-1}$	7
Conductivity	1.52	$W.m^{-1}.K^{-1}$	
Emissivity	0.76	(-)	2
d50	58	µm	
Mean pore diameter	232	Å	
Specific heat capacity (dry)	0.8	$J.g^{-1}.K^{-1}$	3
Specific heat capacity (10%volatile)	1.38	$J.g^{-1}.K^{-1}$	4
Density	2.2	$g.mL^{-1}$	5
Inert solid: **fine NaCl bed clusters of cubes of side=5 micron sieve fraction 45-63µm**			
Thermal conductivity	1.15	$W.m^{-1}.K^{-1}$	6
Emissivity	0.34	(-)	7
Density	2170	$Kg.m^{-3}$	7
Specific heat capacity	0.89	$J.g^{-1}.K^{-1}$	7
Polyethylene			
Specific heat capacity	2.15	$J.g^{-1}.K^{-1}$	8
Heat of reaction	3830	$J.g^{-1}$	
Heat of fusion (crystal)	290	$J.g^{-1}$	9
Heat of fusion (equilibrium)	146	$J.g^{-1}$	10
Stainless steel			
Conductivity	17	$W.m^{-1}.K^{-1}$	7
Density	8000	$Kg.m^{-3}$	
Specific heat capacity	0.51	$J.g^{-1}.K^{-1}$	
Zirconium			
Molecular weight	92	$g.mol^{-1}$	7

Table A1.2 Physical Properties of Solids

For the model specific heat capacity of NaCl assumed constant at 0.89 $J.g^{-1}.K^{-1}$ but the actual formula in Perry is 0.779+3.033E-4T.

Physical Property Estimation

Physical properties of the pure gases and the reaction gas mixture are determined as a function of temperature by the following methods. For pure ethylene and CO2 the specific heat capacity is calculated from Perry 7th ed. Table 2-198. The viscosity and thermal conductivity of ethylene and CO2 are determined by the method of Steil and Thodos [Perry 7th ed p2-368]. Helium viscosity and thermal conductivity values are found by interpolation of the data given in Perry 7th ed. Table 2-363.

For the reaction gas mixture, compressibility and density are found using Kay's method of pseudo-critical properties [Perry 7th Ed]; thermal conductivity and viscosity are found using Wilke's method [11].

Calculated values at 353K and 9 bar gauge pressure are:

	ethylene	CO2	helium	C2H4:He 2:1 mixture
Specific heat capacity ($J.g^{-1}.K^{-1}$)	1.732	0.8931	5.198	1.962
Viscosity (cP)	0.0118	0.0176	0.0224	0.0155
Thermal conductivity ($W.m^{-1}.K^{-1}$)	0.0294	0.0212	0.1663	0.0607
Compressibility Factor (-)				0.9865
Density ($kg.m^{-3}$)				6.91

Piping line lengths and volumes

The details of the pipe sizes and lengths used in the reactor system are noted in the following table:

Pipe lengths	length (cm)	porosity	material	i.d. (cm)	Volume (ml)	
Argon valve to						
leg	30		Cu	0.4	3.77	
leg	15		Cu	0.4	1.88	
leg to argon inlet (T)	20		Cu	0.4	2.51	8.16
Pressure regulator to Argon						
inlet	18		Cu	0.4	2.26	
Argon inlet to						
coils	147		Cu	0.4	18.46	
Coils (33cm x 2.5cm dia coils)	259.05		Cu	0.1753	6.25	
Coils to electrovanne	30		Inox	0.4	3.77	
Inlet						
CO2 inlet valve to T	20			0.1753	0.48	
Electrovanne to clip	20		Inox	0.4	2.51	
Clip to reactor	24		Inox	0.4	3.01	
Reactor						
inlet pipe	2.3			0.4	0.29	
inlet chamber	0.1			2	0.31	
frit	0.3	0.4		2	0.38	
bed	1	0.8		2	2.51	
frit	0.3	0.4		2	0.38	
outlet chamber conical	0.38			2	0.40	
outlet pipe	2			0.4	0.25	
						4.52
Outlet						
Reactor to clip	20		Inox	0.4	2.51	
clip to vent valve	30		Cu	0.4	3.77	
clip to flow control valve	45		Cu	0.4	5.65	

Pressure regulator to Reactor	36.87
Pressure regulator to Electrovanne	30.74
Pressure regulator to Electrovanne inc argon section	38.91
Electrovanne to Reactor	6.13
Electrovanne to Flow Control Valve	21.98
Electrovanne to Flow Control Valve 2ml flexi in place of reactor	13.93
Reactor to Flow Control Valve	11.93

[1] Tisse,V. Kinetics and Morphology of Metallocene Catalysts used in Ethylene Polymerisation, PhD Thesis

[2] http://www.monarchinstrument.com/pdfs/TableofEmissivity.pdf)

[3] Horbach, J. Specific Heat of Amorphous Silica within the Harmonic Approximation, J.Phys.Chem. B 1999, 103, 4104-4108

[4] Grace Davison add ref

[5] Bergna H.E., The Colloid Chemistry of Science, American Chemical Society 1994

[6] www.crystran.co.uk

[7] Perry's Chemical Engineers' Handbook, 6th edition McGraw-Hill.

[8] Eriksson,E. Investigation of heat transfer and kinetic mechanisms in olefin polymerization, PhD Thesis

[9] Mandelkern L., Allou A.L. & Gopalan M., The Enthalpy of Fusion of Linear Polyethylene, J. Phys. Chem. 72,1 (1968) 309-318

[10] Wunderlich B. & Czornyl G., A Study of Equilibrium Melting of Polyethylene, Macromol. 10,5 (1977) 906-913

[11] Reid R.C., Prausnitz J.M. & Poling B.E., The Properties of Gases & Liquids, 4th Ed. McGraw-Hill Inc. (1987)

Appendix 3 – State Estimator Calculations

A3.1) Observability of System of Equations, T_g, T_c, r_p

Observability of our system by critère de Kalman, valid for linear systems

Single segment

Start with equation 3-7:

$$\underbrace{\begin{bmatrix}\dot{T}_g\\ \dot{T}_c\\ \dot{\bar{r}}_v\end{bmatrix}}_{\dot{X}} = \underbrace{\begin{bmatrix}0 & \dfrac{S_c h_{cat}}{\sum(\rho c_p)_g} & 0\\ 0 & \dfrac{-S_c h_{cat}}{\sum(\rho c_p)_c} & \dfrac{\Delta H}{\sum(\rho c_p)_c}\\ 0 & 0 & 0\end{bmatrix}}_{A} \cdot \underbrace{\begin{bmatrix}T_g\\ T_c\\ \bar{r}_v\end{bmatrix}}_{X}$$

$$+ \underbrace{\begin{bmatrix}\dfrac{1}{\sum(\rho c_p)_g}\left(-S_c h_{cat} T_g + F_T Mwt_{rg} c_{prg}\dfrac{\left(T_g - T_{g\,in}\right)}{S_r \partial z} + \bar{h}_{\text{int}} A_w\left(T_g - T_w\right)\right)\\ \dfrac{S_c h_{cat}}{\sum(\rho c_p)_c} T_g\\ \varepsilon\end{bmatrix}}_{\phi}$$

The measured output $y = T_g$

$$C = y.X^{-1} = \begin{bmatrix}1 & 0 & 0\end{bmatrix}$$

since

$$X = \begin{bmatrix}T_g\\ T_c\\ r_p\end{bmatrix}$$

For the system to be observable the matrix $\begin{bmatrix}C\\ CA\\ CA^2\\ CA^3\\ \vdots\end{bmatrix}$ must have the same rank as the number of states. For the set of equations for a single segment the number of states is 3.

Let,

$$a = S_c h_{cat},\ b = \left(\rho c_p\right)_g, c = \left(\rho c_p\right)_c$$

$$CA = \begin{bmatrix} 0 & \frac{a}{b} & 0 \end{bmatrix}$$

$$A^2 = \begin{bmatrix} 0 & \frac{a}{b} & 0 \\ 0 & -\frac{a}{c} & \frac{\Delta H}{c} \\ 0 & 0 & 0 \end{bmatrix}\cdot\begin{bmatrix} 0 & \frac{a}{b} & 0 \\ 0 & -\frac{a}{c} & \frac{\Delta H}{c} \\ 0 & 0 & 0 \end{bmatrix} = \begin{bmatrix} 0 & \frac{-a^2}{bc} & \frac{a\Delta H}{bc} \\ 0 & \frac{a^2}{c^2} & \frac{a\Delta H}{c^2} \\ 0 & 0 & 0 \end{bmatrix}$$

$$CA^2 = \begin{bmatrix} 0 & \frac{-a^2}{bc} & \frac{a\Delta H}{bc} \end{bmatrix}$$

$$\begin{bmatrix} C \\ CA \\ CA^2 \end{bmatrix} = \begin{bmatrix} 1 & 0 & 0 \\ 0 & \frac{a}{b} & 0 \\ 0 & -\frac{a^2}{bc} & \frac{a\Delta H}{bc} \end{bmatrix}$$ has rank = 3 so is observable

Two segments

Start with equation 3-7 bis:

$$\underbrace{\begin{bmatrix} \dot{T}_{g2} \\ \dot{T}_{g1} \\ \dot{T}_{c2} \\ \dot{T}_{c1} \\ \dot{r}_{p2} \\ \dot{r}_{p1} \end{bmatrix}}_{\dot{X}} = \underbrace{\begin{bmatrix} 0 & 0 & \frac{a}{b} & 0 & 0 & 0 \\ 0 & 0 & 0 & \frac{a}{b} & 0 & 0 \\ 0 & 0 & -\frac{a}{c} & 0 & \frac{\Delta H}{c} & 0 \\ 0 & 0 & 0 & -\frac{a}{c} & 0 & \frac{\Delta H}{c} \\ 0 & 0 & 0 & 0 & 0 & 0 \\ 0 & 0 & 0 & 0 & 0 & 0 \end{bmatrix}}_{A}\cdot\underbrace{\begin{bmatrix} T_{g2} \\ T_{g1} \\ T_{c2} \\ T_{c1} \\ r_{p2} \\ r_{p1} \end{bmatrix}}_{X} + \phi$$

$$C = y.X^{-1} = \begin{bmatrix} 1 & 0 & 0 & 0 & 0 & 0 \end{bmatrix}$$

$$A^2 = \begin{bmatrix} 0 & 0 & \frac{a}{b} & 0 & 0 & 0 \\ 0 & 0 & 0 & \frac{a}{b} & 0 & 0 \\ 0 & 0 & -\frac{a}{c} & 0 & \frac{\Delta H}{c} & 0 \\ 0 & 0 & 0 & -\frac{a}{c} & 0 & \frac{\Delta H}{c} \\ 0 & 0 & 0 & 0 & 0 & 0 \\ 0 & 0 & 0 & 0 & 0 & 0 \end{bmatrix} \cdot \begin{bmatrix} 0 & 0 & \frac{a}{b} & 0 & 0 & 0 \\ 0 & 0 & 0 & \frac{a}{b} & 0 & 0 \\ 0 & 0 & -\frac{a}{c} & 0 & \frac{\Delta H}{c} & 0 \\ 0 & 0 & 0 & -\frac{a}{c} & 0 & \frac{\Delta H}{c} \\ 0 & 0 & 0 & 0 & 0 & 0 \\ 0 & 0 & 0 & 0 & 0 & 0 \end{bmatrix} = \begin{bmatrix} 0 & 0 & -\frac{a^2}{bc} & 0 & \frac{a\Delta H}{bc} & 0 \\ 0 & 0 & 0 & -\frac{a^2}{bc} & 0 & \frac{a\Delta H}{bc} \\ 0 & 0 & \frac{a^2}{c^2} & 0 & -\frac{a\Delta H}{c^2} & 0 \\ 0 & 0 & 0 & \frac{a^2}{c^2} & 0 & \frac{a\Delta H}{c^2} \\ 0 & 0 & 0 & 0 & 0 & 0 \\ 0 & 0 & 0 & 0 & 0 & 0 \end{bmatrix}$$

$$A^3 = \begin{bmatrix} 0 & 0 & \frac{a}{b} & 0 & 0 & 0 \\ 0 & 0 & 0 & \frac{a}{b} & 0 & 0 \\ 0 & 0 & -\frac{a}{c} & 0 & \frac{\Delta H}{c} & 0 \\ 0 & 0 & 0 & -\frac{a}{c} & 0 & \frac{\Delta H}{c} \\ 0 & 0 & 0 & 0 & 0 & 0 \\ 0 & 0 & 0 & 0 & 0 & 0 \end{bmatrix} \cdot \begin{bmatrix} 0 & 0 & -\frac{a^2}{bc} & 0 & \frac{a\Delta H}{bc} & 0 \\ 0 & 0 & 0 & -\frac{a^2}{bc} & 0 & \frac{a\Delta H}{bc} \\ 0 & 0 & \frac{a^2}{c^2} & 0 & -\frac{a\Delta H}{c^2} & 0 \\ 0 & 0 & 0 & \frac{a^2}{c^2} & 0 & \frac{a\Delta H}{c^2} \\ 0 & 0 & 0 & 0 & 0 & 0 \\ 0 & 0 & 0 & 0 & 0 & 0 \end{bmatrix} = \begin{bmatrix} 0 & 0 & \frac{a^3}{bc^2} & 0 & -\frac{a^2\Delta H}{bc^2} & 0 \\ 0 & 0 & 0 & \frac{a^3}{bc^2} & 0 & -\frac{a^2\Delta H}{bc^2} \\ 0 & 0 & -\frac{a^3}{c^3} & 0 & \frac{a^2\Delta H}{c^3} & 0 \\ 0 & 0 & 0 & -\frac{a^3}{c^3} & 0 & \frac{a^2\Delta H}{c^3} \\ 0 & 0 & 0 & 0 & 0 & 0 \\ 0 & 0 & 0 & 0 & 0 & 0 \end{bmatrix}$$

$$A^4 = \begin{bmatrix} 0 & 0 & \frac{a}{b} & 0 & 0 & 0 \\ 0 & 0 & 0 & \frac{a}{b} & 0 & 0 \\ 0 & 0 & -\frac{a}{c} & 0 & \frac{\Delta H}{c} & 0 \\ 0 & 0 & 0 & -\frac{a}{c} & 0 & \frac{\Delta H}{c} \\ 0 & 0 & 0 & 0 & 0 & 0 \\ 0 & 0 & 0 & 0 & 0 & 0 \end{bmatrix} \cdot \begin{bmatrix} 0 & 0 & \frac{a^3}{bc^2} & 0 & -\frac{a^2\Delta H}{bc^2} & 0 \\ 0 & 0 & 0 & \frac{a^3}{bc^2} & 0 & -\frac{a^2\Delta H}{bc^2} \\ 0 & 0 & -\frac{a^3}{c^3} & 0 & \frac{a^2\Delta H}{c^3} & 0 \\ 0 & 0 & 0 & -\frac{a^3}{c^3} & 0 & \frac{a^2\Delta H}{c^3} \\ 0 & 0 & 0 & 0 & 0 & 0 \\ 0 & 0 & 0 & 0 & 0 & 0 \end{bmatrix} = \begin{bmatrix} 0 & 0 & -\frac{a^4}{bc^3} & 0 & \frac{a^3\Delta H}{bc^3} & 0 \\ 0 & 0 & 0 & -\frac{a^4}{bc^3} & 0 & \frac{a^3\Delta H}{bc^3} \\ 0 & 0 & \frac{a^4}{c^4} & 0 & -\frac{a^3\Delta H}{c^4} & 0 \\ 0 & 0 & 0 & \frac{a^4}{c^4} & 0 & -\frac{a^3\Delta H}{c^4} \\ 0 & 0 & 0 & 0 & 0 & 0 \\ 0 & 0 & 0 & 0 & 0 & 0 \end{bmatrix}$$

$$A^5 = \begin{bmatrix} 0 & 0 & \frac{a}{b} & 0 & 0 & 0 \\ 0 & 0 & 0 & \frac{a}{b} & 0 & 0 \\ 0 & 0 & -\frac{a}{c} & 0 & \frac{\Delta H}{c} & 0 \\ 0 & 0 & 0 & -\frac{a}{c} & 0 & \frac{\Delta H}{c} \\ 0 & 0 & 0 & 0 & 0 & 0 \\ 0 & 0 & 0 & 0 & 0 & 0 \end{bmatrix} \cdot \begin{bmatrix} 0 & 0 & -\frac{a^4}{bc^3} & 0 & \frac{a^3\Delta H}{bc^3} & 0 \\ 0 & 0 & 0 & -\frac{a^4}{bc^3} & 0 & \frac{a^3\Delta H}{bc^3} \\ 0 & 0 & \frac{a^4}{c^4} & 0 & -\frac{a^3\Delta H}{c^4} & 0 \\ 0 & 0 & 0 & \frac{a^4}{c^4} & 0 & -\frac{a^3\Delta H}{c^4} \\ 0 & 0 & 0 & 0 & 0 & 0 \\ 0 & 0 & 0 & 0 & 0 & 0 \end{bmatrix} = \begin{bmatrix} 0 & 0 & \frac{a^5}{bc^4} & 0 & -\frac{a^4\Delta H}{bc^4} & 0 \\ 0 & 0 & 0 & \frac{a^5}{bc^4} & 0 & -\frac{a^4\Delta H}{bc^4} \\ 0 & 0 & -\frac{a^5}{c^5} & 0 & \frac{a^4\Delta H}{c^5} & 0 \\ 0 & 0 & 0 & -\frac{a^5}{c^5} & 0 & \frac{a^4\Delta H}{c^5} \\ 0 & 0 & 0 & 0 & 0 & 0 \\ 0 & 0 & 0 & 0 & 0 & 0 \end{bmatrix}$$

Finally,

$$\begin{bmatrix} C \\ CA \\ CA^2 \\ CA^3 \\ CA^4 \\ CA^5 \end{bmatrix} = \begin{bmatrix} 1 & 0 & 0 & 0 & 0 & 0 \\ 0 & 0 & \frac{a}{b} & 0 & 0 & 0 \\ 0 & 0 & -\frac{a}{bc}^2 & 0 & \frac{a\Delta H}{bc} & 0 \\ 0 & 0 & \frac{a^3}{bc^2} & 0 & -\frac{a^2\Delta H}{bc^2} & 0 \\ 0 & 0 & -\frac{a^4}{bc^3} & 0 & \frac{a^3\Delta H}{bc^3} & 0 \\ 0 & 0 & \frac{a^5}{bc^4} & 0 & -\frac{a^4\Delta H}{bc^4} & 0 \end{bmatrix}$$

Matrix is not of rank 6 so system not observable

A3.2) Change of Variables

To create the observer the matrix A must be canonical, ie of the form: $\begin{bmatrix} 0 & 1 & 0 \\ 0 & 0 & 1 \\ 0 & 0 & 0 \end{bmatrix}$.

For this we carry out a change of variables. The method is to replace X with Z where:

$$Z = \begin{bmatrix} z_1 \\ z_2 \\ z_3 \end{bmatrix} = \begin{bmatrix} y \\ L_f y \\ L_f{}^2 y \end{bmatrix} = \begin{bmatrix} y \\ \frac{dy}{dX} f \\ \frac{d(L_f y)}{dX} f \end{bmatrix} \qquad \text{and} \qquad f = AX .$$

So,

$$f = AX = \begin{bmatrix} 0 & \frac{S_c h_{cat}}{\sum(\rho c_p)_g} & 0 \\ 0 & \frac{-S_c h_{cat}}{\sum(\rho c_p)_c} & \frac{\Delta H}{\sum(\rho c_p)_c} \\ 0 & 0 & 0 \end{bmatrix} . \begin{bmatrix} T_g \\ T_c \\ r_p \end{bmatrix} = \begin{bmatrix} \frac{S_c h_{cat}}{\sum(\rho c_p)_g} . T_c \\ \frac{-S_c h_{cat}}{\sum(\rho c_p)_c} . T_c + \frac{\Delta H}{\sum(\rho c_p)_c} . r_p \\ 0 \end{bmatrix}$$

and

$$\frac{dy}{dX} = \begin{bmatrix} \frac{dT_g}{dT_g} & \frac{dT_g}{dT_c} & \frac{dT_g}{dr_p} \end{bmatrix} = \begin{bmatrix} 1 & 0 & 0 \end{bmatrix}$$

and

$$z_2 = L_f y = \frac{dy}{dX} f = \begin{bmatrix} 1 & 0 & 0 \end{bmatrix} \begin{bmatrix} \dfrac{S_c h_{cat}}{\sum (\rho c_p)_g} . T_c \\ \dfrac{-S_c h_{cat}}{\sum (\rho c_p)_c} . T_c + \dfrac{\Delta H}{\sum (\rho c_p)_c} . r_p \\ 0 \end{bmatrix} = \frac{S_c h_{cat}}{\sum (\rho c_p)_g} . T_c$$

Then

$$\frac{d(L_f y)}{dX} = \begin{bmatrix} 0 & \dfrac{S_c h_{cat}}{\sum (\rho c_p)_g} & 0 \end{bmatrix}$$

and

$$z_3 = L_f{}^2 y = \frac{d(L_f y)}{dX} f = \begin{bmatrix} 0 & \dfrac{S_c h_{cat}}{\sum (\rho c_p)_g} & 0 \end{bmatrix} . \begin{bmatrix} \dfrac{S_c h_{cat}}{\sum (\rho c_p)_g} . T_c \\ \dfrac{-S_c h_{cat}}{\sum (\rho c_p)_c} . T_c + \dfrac{\Delta H}{\sum (\rho c_p)_c} . r_p \\ 0 \end{bmatrix}$$

$$= \frac{S_c h_{cat}}{\sum (\rho c_p)_g \sum (\rho c_p)_c} \left(- S_c h_{cat} . T_c + \Delta H . r_p \right)$$

Finally,

$$Z = \begin{bmatrix} z_1 \\ z_2 \\ z_3 \end{bmatrix} = \begin{bmatrix} T_g \\ \dfrac{S_c h_{cat}}{\sum (\rho c_p)_g} . T_c \\ \dfrac{S_c h_{cat}}{\sum (\rho c_p)_g \sum (\rho c_p)_c} \left(- S_c h_{cat} . T_c + \Delta H . r_p \right) \end{bmatrix}$$

Check Whether Matrix A now has Canonical Form:

So,

$$\dot{Z} = \begin{bmatrix} \dot{z}_1 \\ \dot{z}_2 \\ \dot{z}_3 \end{bmatrix} = \begin{bmatrix} \dot{T}_g \\ \dfrac{S_c h_{cat}}{\sum (\rho c_p)_g} . \dot{T}_c \\ \dfrac{S_c h_{cat}}{\sum (\rho c_p)_g \sum (\rho c_p)_c} \left(- S_c h_{cat} . \dot{T}_c + \Delta H . \dot{r}_p \right) \end{bmatrix}$$

$$= \begin{bmatrix} \dot{T}_g \\ \dfrac{S_c h_{cat}}{\sum (\rho c_p)_g} \dot{T}_c \\ \dfrac{-(S_c h_{cat})^2}{\sum (\rho c_p)_g \sum (\rho c_p)_c} \dot{T}_c \end{bmatrix}$$

so

$$\dot{Z} = \begin{bmatrix} Z_2 \\ \left(\dfrac{S_c h_{cat}}{\sum (\rho c_p)_g} \right) \left(\dfrac{-S_c h_{cat}}{\sum (\rho c_p)_c} T_c + \dfrac{\Delta H}{\sum (\rho c_p)_c} r_p \right) \\ \dfrac{-(S_c h_{cat})^2}{\sum (\rho c_p)_g \sum (\rho c_p)_c} \left(\dfrac{-S_c h_{cat}}{\sum (\rho c_p)_c} T_c + \dfrac{\Delta H}{\sum (\rho c_p)_c} r_p \right) \end{bmatrix}$$

$$= \underbrace{\begin{bmatrix} 0 & 1 & 0 \\ 0 & 0 & 1 \\ 0 & 0 & 0 \end{bmatrix}}_{A} . \underbrace{\begin{bmatrix} Z_1 \\ Z_2 \\ Z_3 \end{bmatrix}}_{Z} + \underbrace{\begin{bmatrix} 0 \\ 0 \\ \varphi(Z) \end{bmatrix}}_{\Phi}$$

Since,

$$\dot{Z}_2 = \left(\frac{S_c h_{cat}}{\sum (\rho c_p)_g} \right) \left(\frac{-S_c h_{cat}}{\sum (\rho c_p)_c} T_c + \frac{\Delta H}{\sum (\rho c_p)_c} r_p \right)$$

$$Z_3 = \frac{S_c h_{cat}}{\sum (\rho c_p)_g \sum (\rho c_p)_c} \left(- S_c h_{cat} . T_c + \Delta H . r_p \right)$$

$$\dot{Z}_2 = Z_3$$

It can be concluded that *Z* has a canonical form and therefore an observer can be developed for *Z*.

A4.3) Find $\frac{dz}{dX}$ for the Observer Correction Term

$$\frac{dz}{dX} = \begin{bmatrix} \frac{dz_1}{dX_1} & \frac{dz_1}{dX_2} & \frac{dz_1}{dX_3} \\ \frac{dz_2}{dX_1} & \frac{dz_2}{dX_2} & \frac{dz_2}{dX_3} \\ \frac{dz_3}{dX_1} & \frac{dz_3}{dX_2} & \frac{dz_3}{dX_3} \end{bmatrix}$$

and

$$X = \begin{bmatrix} T_g \\ T_c \\ r_p \end{bmatrix}; \quad Z = \begin{bmatrix} T_g \\ \frac{S_c h_{cat}}{\sum(\rho c_p)_g}.T_c \\ \frac{S_c h_{cat}}{\sum(\rho c_p)_g \sum(\rho c_p)_c}\left(-S_c h_{cat}.T_c + \Delta H.r_p\right) \end{bmatrix}$$

so

$$\frac{dz}{dX} = \begin{bmatrix} 1 & 0 & 0 \\ 0 & \frac{S_c h_{cat}}{\sum(\rho c_p)_g} & 0 \\ 0 & \frac{-(S_c h_{cat})^2}{\sum(\rho c_p)_g \sum(\rho c_p)_c} & \frac{S_c h_{cat}\Delta H}{\sum(\rho c_p)_g \sum(\rho c_p)_c} \end{bmatrix}$$

The inverse of this is:

$$\frac{dz}{dX}^{-1} = \begin{bmatrix} 1 & 0 & 0 \\ 0 & \frac{\sum(\rho c_p)_g}{S_c h_{cat}} & 0 \\ 0 & \frac{\sum(\rho c_p)_g}{\Delta H} & \frac{\sum(\rho c_p)_g \sum(\rho c_p)_c}{S_c h_{cat}\Delta H} \end{bmatrix}$$

A3.4) Observer for $kC_{C2}C^*$

So, the observer will have 2 states T and $k_{p0}C_{C2}C^*$.

Let $\dot{k}_{\mathrm{p0}}C_{C2}C^* = 0$

Write equations 3-14 and 3-15 in matrix form and separate out measured variables and constants. The system is non-linear so we cannot write the matrix A.

$$\begin{bmatrix} \dot{T} \\ \dot{k}C_{C2}C^* \end{bmatrix} = \begin{bmatrix} \frac{1}{\sum(\rho c_p)}\left(kC_{C2}C^* e^{\frac{-E_a}{RT}}\Delta H + F_{in}Mwt_g cp_g \frac{dT}{S_r dz} - h^{sf}{}_{\mathrm{int}} AT \right) \\ 0 \end{bmatrix} + \begin{bmatrix} h^{sf}{}_{\mathrm{int}} AT_w \\ \varepsilon \end{bmatrix}$$

In order to create the observer we will need a 'corrective term' which includes $\left(\frac{dz}{dX}\right)^{-1}$

$z_1 = y = T$

$$z_2 = \frac{dy}{dX} f = \left[\frac{dT}{dT} f_1 + \frac{dT}{dk} f_2\right] = \left[1.f_1 + 0\right] = \frac{1}{\sum(\rho c_p)}\left(kC_{C2}C^* e^{\frac{-E_a}{RT}}\Delta H + F_{in}Mwt_g cp_g \frac{dT}{S_r dz} - h^{sf}{}_{\mathrm{int}} AT \right)$$

$$\frac{dz_2}{dX} = \left[\frac{-1}{\sum(\rho c_p)}\left(\frac{E_a}{RT^2} kC_{C2}C^* e^{\frac{-E_a}{RT}}\Delta H + \frac{F_{in}Mwt_g cp_g}{S_r dz} + h^{sf}{}_{\mathrm{int}} A \right) \quad \frac{\Delta H e^{\frac{-E_a}{RT}}}{\sum(\rho c_p)} \quad 0 \right]$$